INTERPRETATIVE CHALLENGES AND OPPORTUNITIES IN OXYGEN AND STRONTIUM ISOTOPE COMPOSITIONS OF BIVALVE SHELLS

by

María Carlota Marcano

A dissertation submitted in partial fulfillment
of the requirements for the degree of
Doctor of Philosophy
(Geology)
in The University of Michigan
2010

Doctoral Committee:

Professor Kyger C Lohmann, Chair
Professor Daniel C Fisher
Professor George W Kling II
Professor Samuel B Mukasa
Professor Diarmaid O'Foighil
Professor Bruce H Wilkinson

S. V. M

I dedicate this work to my family. To my mom and my mother–in–law, Berta Alicia and Ligia del Carmen, that helped me in the past when my boys were small. I hope to be now repaying at least in a small measure their dedication with this dedication. I am sorry my dad is no longer with us. Because I married young, still an undergrad, and had my first child right away, he thought I would never graduate. Looking at it now from the perspective of a mom, I am sure the days when I received my previous degrees were among his happiest days. He would have really enjoyed this one.

To my 4 awesome guys, Ricardo, Luis, Manuel and Juan, because watching their beautiful faces gives meaning to my life every day.

To some special friends: Elizabeth, Daniela, Lorena, Marielva, Maria Alejandra, Popi, Miguel, Ana Elisa (my beautiful goddaughter) and Milagros, because between good friends and family there is not much of a difference really.

To my hosts in my alternate office at Morgan and York where much of this dissertation was written.

To all the earth scientists who wrote their dissertations themselves using typewriters.

ACKNOWLEDGEMENTS

In addition to the acknowledgements specific to each chapter, I want to recognize all members of my dissertation committee who have been always diligent and enlightening, in particular, Bruce H. Wilkinson and Samuel B. Mukasa. Bruce and Sam provided not only motivation and encouragement, but also made this pursue genuinely meaningful through a sense of collaboration. Special thanks are due to my advisor, Kacey C. Lohmann, for his support and patience, and for allowing me the freedom to explore and bring to completion this work without compromising other priorities. I would also like to thank Linda Ivany who has been always helpful and generous with her time.

Thanks are due to the staff and faculty of the Department of Geological Sciences at the University of Michigan for their continued support. Lora Wingate, Ted Huston, Alex Andronikov, Jamie Gleason, Sara Worsham, Carl Henderson, Lindsay Shuller and Antek Wong–Foy provided technical support and guidance in the use of the University of Michigan facilities engaged for this dissertation: the Stable Isotope Laboratory, the Keck Elemental Geochemistry Laboratory, the Geochronology and Isotope Geochemistry Laboratory, the Biogeochemistry and Environmental Isotope Geochemistry Laboratory, and the Electron Microbeam Analyses Laboratory in Geological Sciences, and the Matzger Laboratory in Chemistry. I would like to specially thank Jim Hitchcliff, Nancy Kingsbury, Dale Austin, Tom Merline and Bill Wilcox for their kind help and good disposition always. Thanks to all others that in one way or another helped me and shared their expertise and time, specially Franek Hasiuk, Jim Hnat, Christopher Stefano, and Sara Rilling.

Chapter 4 of this dissertation was published in the journal Global and Planetary

Change:

Marcano, M.C., Mukasa, S., Lohmann, K.C, Stefano, C., Taviani, M., and Andronikov, A., 2009. Chronostratigraphic and paleoenvironmental constraints derived from the $^{87}Sr/^{86}Sr$ and $\delta^{18}O$ signal of Miocene bivalves, Southern McMurdo Sound, Antarctica. Global and Planetary Change, (Special Issue: Antarctic Cryosphere).

TABLE OF CONTENTS

LIST OF TABLES

LIST OF FIGURES

LIST OF APPENDICES

CHAPTER 1

Introduction

More than 2 centuries ago, James Hutton defined his principle of uniformitarianism saying, "In examining things present, we have data from which to reason with regard to what has been; and, from what has actually been, we have data for concluding with regard to that which is to happen hereafter"[1]… "with respect to human observation, this world has neither a beginning nor an end"[2]. This idea influenced geological research and still leads modern views regarding the earth's evolution both in its own right and through the realization that such a static approach may not always apply. Since his words were first published, understanding of earth's processes have increased dramatically, in great measure due to geochemical studies. Critical aspects of geology such as paleoenvironmental interpretations, chronostratigraphy and diagenesis rely heavily on stable isotopes, which are fundamental geochemical tools.

The past 200 years have also witnessed the fastest and most intense anthropogenic environmental changes in history. Only recently, the profound effect these changes have had and will continue to have on the climate system have become apparent (IPCC, 2007; Gillett et al., 2008). The potential consequences of imminent climate change have refocused geochemical research toward recognizing modern climate mechanisms in order to procure solutions to practical and urgent concerns. The level of understanding gained from modern processes will, in large part, determine the success of interpreting the geologic record and predicting future behavior, as Hutton envisioned. At the same time,

1 Hutton, J. 1788.
2 ——, J. 1785

research efforts must be focused on climate sensitive areas of the planet, such as the Polar Regions, especially during periods characterized by climate shift to serve as model for future changes.

Modern calcium carbonate secreting marine organisms are an important source of geochemical data that link ancient and modern environments, especially when considering the recent past. The relevance of these organisms is directly related to the fundamental role of the ocean as a climate system component and as a geological archive. Because many marine taxa precipitate shells in equilibrium or close to equilibrium conditions with their environment, they produce a potentially decipherable skeletal geochemical record. Oxygen isotopes from marine biogenic carbonates, for example, have been successfully used as a temperature proxy since Harold Urey established the relation between measured isotope fractionation factors and calculated equilibrium constants for the corresponding isotope exchange reactions in 1947. Foraminiferal $\delta^{18}O$, in particular, has helped develop a record of deep ocean temperature and global ice volume change for the Cenozoic (Zachos et al., 2001; Raymo, 2006). A more detailed record of not only temperature but also seasonality through time can be derived from oxygen isotope compositions of long–lived invertebrates that accrete their shells over time. Molluscs bivalves are of special interest in generating more meaningful paleoenvironmental interpretations and have been successfully used for the past 20 years in concert with independent schlerochronological determinations (Jones et al., 1990; Jones and Quitmyer, 1996).

The interpretation of bivalve $\delta^{18}O$ is not without complications. The $^{18}O/^{16}O$ of $CaCO_3$ precipitating from seawater depends on temperature and on the initial isotopic composition of the fluid. Applying empirically obtained calibrations to calculate temperature from fossil carbonates requires a priori estimates of water $\delta^{18}O$. Reasonable assumptions can be made to produce temperature estimates from fossil organisms known to inhabit relatively stable environments. On the other hand, bivalves are dwellers of

shallow marine and transitional environments, where salinity changes may be large enough to confound the temperature signal. In addition, ecological limitations that shorten their environmental record (i.e., temperature tolerances, spawning or stress–triggered growth cessation) and unknown variations in growth rate contribute to obscure paleoenvironmental interpretations. For these reasons, the study of modern bivalves is critically important. Understanding the limitations and strengths of the modern $\delta^{18}O$ record of individual taxa to reproduce the marine environment at a local and regional scale is relevant information to consider when interpreting the fossil record. Chapters 2 and 3 of this dissertation are dedicated to this purpose.

In chapter 2, the interpretative problem was undertaken at a local scale by the simultaneous analyses of several coexisting taxa. The extent to which the known local temperature and salinity annual variation was represented in the shells was tested. This relation was explored through the construction of time series from $\delta^{18}O$ versus distance profiles, growth rates and fractionation factors calculation. In addition, published temperature thresholds and intra–annual growth rate variability in the bivalves were reassessed. The marine temperature range recorded in the biogenic carbonate extended to lower temperatures than expected and was in its entirety better represented not by a single taxon but by the concurrent use of at least two taxa. Chapter 3 recasts the interpretative problem of modern carbonate $\delta^{18}O$ from a regional perspective. A large temperature–salinity dataset representative of several shallow water marine climates along the North American east coast was used to model bivalve oxygen isotope compositions. Several concrete observations were obtained for the tropical climate regimes while the higher salinity ranges in temperate areas made interpretations more speculative. When compared to measured hard clam $\delta^{18}O$ profiles, discrepancies suggested that seasonal and geographically restricted adjustments of δ_w–salinity relations are necessary. Importantly, the seasonal variability of the modeled hard clams was found relevant to discriminate between broad marine climates. This is a useful tool for paleoenvironmental studies that

exploits the dependence of carbonate $\delta^{18}O$ on salinity instead of merely recognizing it. Results from chapters 2 and 3 are relevant to the reliability of $\delta^{18}O$ paleoenvironmental interpretations from fossil bivalves, which is one fundamental task of stable isotope geochemistry.

The study of the areas most sensitive to climate change is a priority for the geological sciences today because global warming is anticipated to occur sooner and be more intense at higher latitudes. Antarctic ice sheets are the focus of active research due to their control over atmospheric and oceanic circulation and their likely influential response in a warming world. Drilling to recover shelf and slope sedimentary sequences around Antarctica began in 1975 with the Deep Sea Drilling Project (DSDP) leg 35. In 2006, the Antarctic Geological Drilling Program (ANDRILL) set to recover Neogene sediments from McMurdo Sound on the southwest edge of the Ross Sea, with the goal of reconstructing ice sheet variation and clarifying polar climate evolution. Chapters 4 and 5 include the results of chronostratigraphic and paleoenvironmental analyses carried out in bivalve shell fragments from ANDRILL's core AND–2A.

Chapter 4 examines the use of calcite and aragonite shell fragments to provide chronostratigraphic constraints and give initial paleoenvironmental interpretations based on Sr and O isotope compositions. Because Sr isotope composition of seawater is, at any one time, homogeneous and a reflection of the overall proportion and distribution of different lithologies, and because Sr is not fractionated when incorporated into $CaCO_3$, $^{87}Sr/^{86}Sr$ is a powerful tool to discern provenance and age. Producing reliable time datums for stratigraphic sequences is obviously fundamental and can be done by comparison with the well–established curve of secular variation of Sr isotopes in seawater (McArthur et al., 2001). Well–preserved, in situ recovered calcite shells provided Sr ages that helped refine the core's age model. In addition, contrasting calcite $\delta^{18}O$ between late Early Miocene (16.5 – 16.0 Ma) and early Late Miocene (~11 Ma) suggested a possible climate contrast at this age, with global marine climate better represented in Antarctica during

the Burdigalian–Langhian epochs and cooler than global average conditions probably controlling local marine climate during the Serravalian–Tortonian.

In contrast to the calcite fragments, Sr concentrations and isotope compositions of the aragonite shells resulted in older than possibly reasonable ages prompting further research, which resulted in chapter 5. Besides measuring pore water Sr concentrations and $^{87}Sr/^{86}Sr$ compositions, EPMA, PXR microdiffractions and more detailed $\delta^{18}O$ analyses of the shell fragments were carried out. While aragonite was confirmed as the only phase present in the shells, Sr was found to be highly concentrated in the outer layer and along growth bands of the middle layer. Aragonite Sr concentrations and O isotope compositions modeled for modern conditions suggested that, despite their mineralogy and the lack of clear paragenesis, early alteration was probably responsible for the anomalous Sr compositions of these fragments.

Hutton's claim of persistent action is truly applicable to the progress made to understand natural processes rather than to the natural processes themselves. The development of geochemical proxies as applied today, probably unimaginable for pioneers such as James Hutton, has greatly contributed to this steady advance. A modest contribution to such advance is represented by this dissertation that examines oxygen and strontium of bivalve carbonates in various contexts. Together, these four chapters contribute new perspectives to environmental interpretations by exploring the modern environment and by producing new data and relevant interpretations from a climate sensitive region during the Miocene.

References

Gillett, N.P., Stone, D.A., Stott, P.A., Nozawa, T., Karpechko, A.Y., Hegerl, G.C., Wehner, M.F., and Jones, P.D., 2008. Attribution of polar warming to human influence. Nature Geosci, 1 (11): 750-754.

Hutton, J., 1785. Abtract of a dissertation read in the Royal Society of Edinburgh, upon the Seventh of March, and Fourth of April, M,DCC,LXXXV, concerning the system of the Earth, its duration and stability. 30 p.

—, 1788. Theory of the Earth; or an investigation of the laws observable in the composition, dissolution, and restoration of land upon the globe. Transactions of the Royal Society of Edinburgh, I, Part II: 209-304.

IPCC, 2007. Climate Change 2007: The Physical Science Basis. Contribution of Working Group I to the Fourth Assessment Report of the Intergovernmental Panel on Climate Change. Cambridge University Press, Cambridge, United Kingdom and New York, 996 p.

Jones, D.S., and Quitmyer, I.R., 1996. Marking time with bivalve shells; oxygen isotopes and season of annual increment formation. Palaios, 11 (4): 340-346.

Jones, D.S., Quitmyer, I.R., Arnold, W.S., and Marelli, D.C., 1990. Annual shell banding, age, and growth rate of hard clams (*Mercenaria* spp.) from Florida. Journal of Shellfish Research, 9: 215-225.

McArthur, J.M., Howarth, R.J., and Bailey, T.R., 2001. Strontium isotope stratigraphy: LOWESS Version 3. Best-fit line to the marine Sr-isotope curve for 0 to 509 Ma and accompanying look-up table for deriving numerical age. Look-up table Version 4:08/04. Journal of Geology, 109: 155-169.

Raymo, M.E., 2006. Plio-Pleistocene ice volume, Antarctic climate, and the global ^{18}O record. Science, 313: 492.

Urey, H., 1947. The thermodynamic properties of isotopic substances. Journal of the Chemical Society: 562-581.

Zachos, J., Pagani, M., Sloan, L., Thomas, E., Billups, K., Smith, J.(prefacer), and Uppenbrink, J.(prefacer), 2001. Trends, rhythms, and aberrations in global climate 65 Ma to present; Paleoclimate; Earth's variable climatic past. Science, 292 (5517): 686-693.

CHAPTER 2

Using oxygen isotope compositions of skeletal carbonate to evaluate temperature thresholds, equilibria and seasonal rates of precipitation in a modern marine community

Abstract

Modern contemporaneous specimens of the bay scallop (*Argopecten irradians irradians)*, the northern hard clam (*Mercenaria mercenaria)*, the northern stony coral (*Astrangia poculata)*, the purple sea urchin (*Arbacia punctulata)*, the toothed crust bryozoan (*Parasmittina nitida)* and serpulid polychaetes *(Hydroides dianthus)* were retrieved from their shared shallow marine habitat in Vineyard Sound, south of Falmouth, Massachusetts, U.S.A., to evaluate $\delta^{18}O$ in relation to the well constrained temperature and salinity data available for this site. Limited and reasonable assumptions that tie temperature and carbonate $\delta^{18}O$ data were used to assign time to seasonal profiles. The biocenosis was then reassessed in terms of equilibrium precipitation, temperature thresholds of shell precipitation and overall temperature range. Detailed and diverse information about the precipitation process in the study site was produced by the bivalve records. Results indicate that the bay scallop precipitates calcite in equilibrium with local seawater whereas the aragonite shell of the hard clam does not. This departure from equilibrium (~0.9 ‰) appears to be constant but in the opposite direction of the recognized positive fractionation between calcite and aragonite. Average growth rates and optimal growth temperatures are in keeping with field observations. Summer precipitation retardation occurs in both bivalves, and shell precipitation initiation and cessation

appears to take place at temperatures below published thresholds. This temperature difference is greater for the bay scallop, whose $\delta^{18}O$ provides the widest range and lowest values of seawater temperatures. The warmest temperatures appear to be recorded by the purple sea urchin. The bryozoan represents about two years of precipitation, but sample time averaging prevented intra–annual resolution. These tentative results for the bryozoan indicate that growth was more variable during the initial year of colonization and stabilized thereafter. Potential disequilibrium precipitation prevented drawing further insight from the northern stony coral data. Results suggest that environmental characterization may be hindered instead of enhanced by the use of fixed environmental thresholds and that species–specific kinetic effects can influence precipitation and pose interpretative challenges if considered in isolation. In addition, more complete temperature ranges can be obtained if several taxa are used. The results are relevant to paleoenvironmental studies and the improvement of information drawn from fossil shells.

Keywords: shallow–water environment; temperature; salinity; O–18/O–16; biocenoses; bivalvia; growth rates; ecology; Cape Cod.

2.1. Introduction

Oxygen isotope compositions of biogenic carbonates are a powerful tool in paleoenvironmental studies. In deep sea settings, for example, the use of foraminiferal $\delta^{18}O$ has been invaluable in understanding climate variability during the Cenozoic (e.g., Zachos et al., 2001; Lisiecki and Raymo, 2005; Raymo, 2006). The success of this approach to open ocean studies is in part a consequence of the temporal stability of these settings where the oxygen isotope composition of the water can be estimated with a large degree of certainty. On the other hand, in coastal and shallow marine environments where conditions are less stable, the ambiguity introduced by the dependence of carbonate isotopic composition on both temperature and water isotopic composition

is more influential and makes direct interpretations of carbonate oxygen isotope data more problematic. This uncertainty has not prevented productive use of stable isotope geochemistry in such environments (e.g., Ivany et al., 2004), but a strong sense of what the analysis conveys and the limiting constraints on data interpretation must be considered. In this paper, the modern relation between shallow marine environmental parameters and $\delta^{18}O$ is evaluated locally with the goal of illuminating the process of interpreting these parameters from fossil shells.

Many paleoenvironmental studies have focused on one species, usually with the goal of developing or improving empirical calibrations of carbonate $\delta^{18}O$ to environmental conditions (e.g., Jones, 1981; Krantz et al., 1987; Patterson et al., 1993; Leder et al., 1996; Quitmyer et al., 1997). This is a necessary first step to understand the relation between environment and carbonate isotopic composition of marine organisms, but the ecology and ontogenetic growth changes of an individual taxon limits retrieval of environmental change information from its isotopic record (e.g., Goodwin et al., 2003; Ivany et al., 2003). Incorporation of several members of a marine biocenosis has the potential to improve the record of environmental complexity. Schöne et al. (2006), for example, studying two bivalves and one barnacle from a shared recent environment using oxygen isotope compositions deduced that the bivalves were precipitating their shell during the summer while the barnacle precipitated its shell during the winter; the records complemented each other showing the benefit of analyzing several individuals growing under the same environmental conditions.

A modern community of marine invertebrates is used in this study to evaluate the utility of a multitaxon approach to refine environmental reconstructions from isotope geochemical records in biogenic carbonate. Oxygen isotope compositions from the skeletons of several coexisting marine invertebrates and the annual variation of environmental parameters characteristic of the study area were used to evaluate precipitation and individual ecological limitations. Skeletal isotopic composition

variation through time was discernable in some specimens, particularly the bivalve shells. Temperature data were used to produce $\delta^{18}O$ time series, and different estimates of seawater oxygen isotope compositions (δ_w) were then associated with $\delta^{18}O$ compositions through the time series. This information served to determine the best estimate of δ_w and to evaluate the degree of fractionation between seawater and carbonate materials in the study area. Finally, detailed growth rates were calculated to examine growth rate variations and dates of initiation and cessation of carbonate precipitation from the time series. In doing so we: 1) Assess the seasonality of δ_w and the suitability of applying empirically determined paleotemperature equations and fractionation factors to all data; 2) survey the ecological limits of important species in both modern aquaculture and paleoclimatic studies; 3) evaluate potential additional gains from a multispecies approach to reconstruct the range of annual environmental change (summer to winter extremes).

2.2. Seawater variation in Falmouth

This section evaluates temperature, salinity and δ_w data measured close to the sampling location at 20 m depth on the eastern edge of Vineyard Sound, 2 km south of Falmouth, Cape Cod, Massachusetts, U.S.A. (41.50 ºN, 70.55 ºW, Figure 2.1). Following the approach of Wilkinson and Ivany (2002), annual variation of environmental data was characterized with best–fit sinusoids. Although the data sets were fairly complete (see below), best–fit sinusoids are a better choice to characterize the environmental parameters than central tendency and dispersion statistics for several reasons. First, temperature variation on the Earth's surface is a function of solar insolation, which changes annually as a function of the sine of the solar incidence angle. This relation is not equally secure for salinity and δ_w, but still a good proposition given that their variation depends on similar annual seasonal patterns of precipitation and evaporation. Second, the goal was to obtain a single representative profile of environmental variation for the area per parameter. To do this, several individual daily–measured annual profiles were stacked to estimate inter–annual variation. Using a sinusoid fit ensured that this variability was

captured as an unbiased numerical representation by avoiding giving excessive weight to extreme values that may be present in the sample but do not characterize the population. The fit's position is a measure of annual average whereas the amplitude of the sinusoid is representative of the annual seasonality not impacted by extreme values that are inappropriate to describe long term patterns (Wilkinson and Ivany, 2002). Third, residuals to the fit comprise Gaussian distributions, which suggest that, unlike local averages, the fit is an appropriate representation of the data at every point and also that the variation is due solely to random error. Finally, though daily averages are for the most part very close to the best–fit sinusoid for temperature and salinity, these numbers diverged more visibly for δ_w data. Thus, the parameters obtained through the mathematical fits are considered a better approximation.

2.2.1. Seawater temperature variation

Samples were recovered in a single dredge in the fall of 2002. The closest and most complete sources of seawater temperature and salinity data in the study area are Woods Hole Oceanographic Institution (WHOI), Woods Hole, Massachusetts, and Martha's Vineyard Coastal Observatory (MVCO), Edgartown, Massachusetts. Sea surface temperature records from WHOI (41.5 ºN, 70.6 ºW, http://dlaweb.whoi.edu/DIG_RES/ water_temp.php) exist from 1886 to the present as daily measurements or monthly averages. Temperature data from MVCO (http://www.whoi.edu/mvco/data/oceandata.html) are available from 2001 to the present. These data are generated on a 12–meter sea node, a sensor located at a depth of 12 m offshore South Beach in Martha's Vineyard (41.3 ºN, 70.5 ºW), where readings are made every 20 minutes. These data are not as complete as WHOI data. For example, for years 2002 to 2005, MVCO daily averages are about 60% complete compared to 96 to 98% for the WHOI data. It is described here because water temperature is measured at depth in this site.

WHOI data differ very little as far back as 1982. For instance, during years 1987, 1988, 1991, 1994 and 1995, for which both density and temperature data were available

and close to complete, annual averages vary between 11.1 and 12.6 ºC, and the highest and lowest monthly averages are 22.3 and 1.1 ºC measured in August and February, respectively. For years 1997 to 2002, annual averages are between 11.2 ºC to 12.3 ºC and monthly averages extremes are 22.5 ºC and 1.2 ºC also measured in August and February. Average annual temperature from MVCO for years with complete records is also around 11 ºC. Highest average monthly temperature is 20.1 ºC measured in August and lowest is 0.0 ºC measured in February.

Best–fit sinusoids were determined for all these data sets (Figure 2.2). In contrast to SST at WHOI, modeled sine–fit temperatures for MVCO are on average 2 ºC and 0.5 ºC cooler during summer and winter peaks, respectively. The attenuated summer peak and slightly intensified winter peak result in a reduced temperature range. In addition, the sinusoid fit to MVCO seawater temperatures shows a small temporal shift, with season peaks occurring somewhat later. Vineyard Sound's temperature is well represented by WHOI's data because the annual temperatures range of bottom water in Vineyard Sound is reported elsewhere to be similar to that of WHOI's surface waters (Wigley and Theroux, 1981; Theroux and Wigley, 1998). Unlike MVCO, Vineyard Sound is closer to areas of increased summer temperature and temperature range. MVCO is near deeper, colder and less seasonal bottom waters.

WHOI's daily averaged SST from years 1987, 1988, 1991, 1994 and 1995 will be used as a proxy for Vineyard Sound's shallow water average temperature. Given that the residuals between the daily average temperatures and the modeled sinusoid fit produce a normal distribution around a mean of 0.13 ºC ($2\sigma = 2.25$), shallow marine temperature in Vineyard Sound can be predicted by the equation:

$$T = 10.46 \pm 0.07 \times \sin(2\pi/364 \pm 2 \times (X - 131.6 \pm 0.6)) + 11.75 \pm 0.07 \quad (2.1)$$

where X is the day of the year, seasonal amplitude is 20.9 °C, and annual mean temperature is 11.75 °C. Errors are 95% confidence levels.

2.2.2. Seawater salinity variation

Seawater salinity data are less complete than temperature data. The most recent and complete salinities were measured very near Vineyard Sound (41.5 ºN, 70.6 ºW) at 1 m depth as part of a lobster monitoring program and cover only Sep–2001 to Jun–2002 (Manning, 2006). A more complete record exists at WHOI from Nov–1962 to Dec–1971 when salinity at the surface was continuously measured at the Woods Hole Shiplight, about 30 km southeast of Vineyard Sound between Martha's Vineyard and Nantucket islands (41.31 ºN, 70.40 ºW). Recently, another monitoring plan was started to record continuous, high quality salinity data at 1 m depth on the WHOI dock (Schmitt, 2008).

Since 2001, relatively consistent salinity monitoring has existed in MVCO. Unfortunately, the salinity sensors located 12 meters below sea level fail frequently, and the records show large interruptions and sudden drops which are suggestive of large, abrupt freshwater input. In actuality, these drops are likely the result of contamination by sediment or bio–fouling (e.g., Manning, 2006). One indication is that these drops usually occur in a single day and the sensor stops recording shortly after the minimum is reached. Excluding these suspect short–term drops, MVCOs salinity records remain fairly constant around 31.5 psu to 32.5 psu. Both WHOI and the Woods Hole Shiplight records show salinity values higher than 29 psu and lower than 33 psu throughout the year.

For some of WHOI's temperature data, matching water density values were available through the institution's archive. Based on the salinity considerations noted above, the UNESCO seawater equation of state as described in Fofonoff (1985) was used to calculate daily average salinity from density and temperature data for the years with the most complete records: 1987, 1988, 1991, 1994 and 1995. Calculated salinities vary between 31 psu and 32 psu and are likely good estimates of local salinity. One potential source of error is the lack of specific correction for the hydrometer calibration. In general, the difference in density can be on the order of ± 0.0009 units per each 5 ºC departure from 15.56 ºC (Crandall, 1954), which is presumably the calibration temperature.

The described measured and calculated salinities that characterize waters close to

the study area suggest that salinity in Vineyard Sound remains well bracketed between 29 psu and 33 psu year round. In terms of seasonal variation, best–fit sinusoids to the different data sets reveal contrasting seasonal patterns. Both the 2001–2002 record from WHOI and the 2002–2005 from MVCO suggest reduced salinities during the summer months, while the 1962–1971 record of Woods Hole Shiplight and the salinity calculated from temperature and density measured at the WHOI dock for several years between 1987 and 1995 show slightly fresher waters in the spring months (Figure 2.3).

Local precipitation characteristics suggest that among the measured records, the Woods Hole Shiplight data are the most reliable; the apparent summer salinity minima observed in some may in part be the result of monitoring problems explained before, in particular for the MVCO data. Long–term average precipitation in Falmouth exhibits little month–to–month variation, with monthly means between 7.6 mm and 11.4 mm. The highest average precipitation occurs in March or November–December, and the lowest in July (e.g., Falmouth Monthly Climate reports http://cis.whoi.edu/science/PO/climate/index.cfm and NOAA, United States Climate Normals, 1971–2000, Historical Climatography Series 42).

Calculated salinities are considered the best estimates of Vineyard Sound's actual annual salinity variation. These data are derived from samples that are closest to Falmouth Vineyard and conform to the range and seasonal pattern observed in the Woods Hole Shiplight data. They offer the additional benefit of being derived from the same water samples that provide the best temperature estimate. For these data, the distribution of the residuals is very close to normal about a mean of 0.03 psu ($2\sigma = 0.90$ psu). Salinity values through the year can be approximated as:

$$S = 0.49 \pm 0.03 \times \mathit{sin}\ (2\pi/365 \times (X - 157 \pm 4)) + 31.57 \pm 0.02 \qquad (2.2)$$

where amplitude is about 1 psu and the average salinity is 31.57 psu. Errors are 95% confidence levels except for fixed parameter where no error is reported.

2.2.3. Seawater oxygen isotope variation

No data exists on local δ_w values. Worldwide ocean δ_w data (N=696) at similar latitudes (40–45) ºN for depths above 6 km (Schmidt et al., 1999) show a seasonal trend with a range of about 2.5 ‰ and peaks in July (–1.0 ‰) and February (1.5 ‰) . Seasonal δ_w range in Vineyard Sound is probably not as large as the global average for the same latitude because freshwater input varies little. Nevertheless, some seasonality is expected. In this dataset, δ_w values closest to Vineyard Sound come from 31 stations off the coast of Nova Scotia (40–45 ºN, 55–70 ºW, Figure 2.4). Here, waters generally have temperature and salinity similar to those in the study area. Unfortunately, this data subset (N=95, < 50m depth) offers a very limited spread throughout the year. Only values for the months of April, June, July and October are available. The average δ_w for the month of July is –1.4 ‰, and based on the characteristics of the entire δ_w dataset at similar latitudes, this is a reasonable minimum value for the region.

Assuming the seasonal change in the oxygen isotope composition of seawater in this area is sinusoidal, a best–fit to the few available monthly average points suggests that maximum δ_w here is probably close to 0 ‰. δ_w is predicted by:

$$\delta_w = 0.72 \pm 0.71 \times \mathit{sin}\,(2\pi/12 \times (X + 2.98 \pm 1.69)) - 0.72 \pm 0.54 \qquad (2.3)$$

where X is time in months and the errors are 95% confidence levels. Average δ_w is –0.72 ‰, the annual range is ~1.4 ‰, and the minimum is –0.17 ‰.

Estimates of δ_w can also be obtained by applying general δ_w–salinity relations to local salinity values. Using two published equations valid for the mid–latitudes of the North American Atlantic coast (Fairbanks, 1982; Elliot et al., 2003) and two equations calculated here from the available data (Table 2.1), δ_w is estimated to remain between –2.9 ‰ and –0.4 ‰ for the salinity range in Vineyard Sound. However, looking only at the published equations (Table 2.1, equations A and B), the minimum value is no less than –1.7 ‰. The δ_w–salinity relation suggested by Fairbanks (1982), derived from waters of the New York Bight between 39 and 41ºN, is probably the most suitable to use here. Applying it to the best salinity record suggests a slightly more positive minimum of

–1.2 ‰ (Figure 2.5).

Given that none of the estimates suggest that δ_w ever exceeded 0 ‰, it is safe to assume this is a maximum value. Similarly, the minimum value is probably between –1.4 ‰ and –1.2 ‰. Though the timing of the minimum and maximum peaks differ between the sinusoid fits to measured δ_w (δ_w1) and to δ_w based on the best salinity estimates (δ_w2), carbonate $\delta^{18}O$ estimates based on these δ_w compositions will not differ by more than 1‰. Annual variation in temperature exerts the dominant control on carbonate isotopic compositions. Given the scarcity of actual δ_w measurements in the area, calculations based on measured salinity provide a better δ_w estimate for the study area. The residuals for this approach are normally distributed, which is not surprising given the origin of the data (mean ~ 0 ‰; $2\sigma = 0.24$ ‰). δ_w can then be estimated as:

$$\delta_w = 0.13 \pm 0.01 \times sin\,(2\pi/365 \times (X - 157.5 \pm 3.9)) - 0.99 \pm 0.01 \quad (2.4)$$

where X is the day of the year. The average annual variation in δ_w is about 0.3 ‰, and the annual average value is ~ –1 ‰. Errors are 95% confidence levels for all parameters.

Though δ_w2 is the best δ_w estimate, it conveys an additional uncertainty from the use of a δ_w–salinity relation that was not locally determined. Conversely, δ_w1 is based on sparse data and requires an assumption of annual sinusoidal variation of δ_w in Vineyard Sound. Although the available data are sufficient and appropriate to produce an annual sinusoidal, the adequacy of the data to accurately represent local δ_w values remains problematic.

2.3. Materials and methods

2.3.1. Isotope determinations

Living members of a marine community established at a depth of about 20 m were recovered in a single dredge in March of 2002. Samples recovered for this study include several Pectinid and Venerid bivalves, Mucronellid bryozoan spherical colonies (ectoproctaliths of Rider and Enrico, 1979; bryoliths of Reguant et al., 1991), Astrangiid anthozoans, Arbaciid echinoids and associated Serpulid polychaete tubes.

Specimens were eviscerated and all surfaces were cleaned to remove sand and encrusting organisms. Carbonate material was embedded in epoxy resin and/or sectioned and polished when necessary for detailed and bulk sampling. The majority of the sampling was done using a Merchantek MicroMill, a device designed for high resolution sampling that allows precise recovery of very small amounts of powder (i.e., tens of micrograms). This apparatus provides submicron stage resolution and accurate positioning, which makes it ideal for the sampling of growth structures in shells (Dettman and Lohmann, 1995). Some samples were taken using a conventional dental laboratory drill with a sampling burr of approximately 0.5 mm in diameter.

Drilled samples were roasted *in vacuo*, at 200 ºC, to eliminate volatile contaminants. Oxygen and carbon isotope ratios were determined using an automated Kiel device coupled to a triple–collector gas source Finnigan MAT 251 isotope–ratio mass spectrometer and reported against the VPDB standard. Standard deviations for both carbon and oxygen are equal to or better than 0.1 ‰.

2.3.2. Modeling

Time series of $\delta^{18}O$ compositions were constructed for the bivalves and the bryolith, while only the isotope ranges are provided for the other taxa. Given the difficulties associated with time series reconstruction (see below) and the limitations of the data, best–fit sinusoids (Wilkinson and Ivany, 2002) were used to transform shell–length referenced $\delta^{18}O$ profiles into a time domain.

In order to relate shell derived $\delta^{18}O$ profiles and seasons of shell accretion, knowledge of precipitation dates or rate of intra–annual accretion is necessary. Neither of these factors is independently known for the samples used in this study. Placing carbonate hardpart $\delta^{18}O$ values vs. sample distance data into such a temporal framework is not straightforward but clearly a relevant step to produce useful information from environmental archives in this and other contexts. To do so, some sort of assumption is necessary. Depending on the assumptions made, the information obtained from the record

can be potentially biased or simply limited. Numerous methods to produce time–series from proxy vs. distance records have been developed (Jones, 1981; Martinson et al., 1982; Jones, 1983; Paillard et al., 1996; Wilkinson and Ivany, 2002; De Ridder et al., 2004; de Brauwere et al., 2008), but those that strive to minimize assumptions are costly in terms of implementation ease (e.g., de Brauwere et al., 2008; 2009).

In general, the problem of assigning time to proxies such as those considered here has been dealt with in two ways. In the first scenario, data spanning several periods are tuned to another well–dated signal by calculating a mapping function and maximizing the coherence between this mapping function and the original distorted signal. In the second scenario, a function that describes the time distortion affecting the original signal is iteratively calculated to adjust an initial assumption of constant growth rate. In the first type of method, the shape of the resulting function is predetermined. In the second, the function is not prescribed, but rather the record is assumed to be periodic. Periodicity is a very reasonable assumption for shell $\delta^{18}O$ data given that the seasonality expressed by this proxy is mainly a function of temperature, which varies according to annual changes in insolation.

2.3.2.1. Best–fit sinusoid

The periodicity of the seasons expressed in the spatial variation in $\delta^{18}O$ values is an attribute that can be readily exploited. A proxy that mainly reflects temperature is not only periodic, but can also be accurately described by a sinusoidal function, as insolation intensity varies with the sine of the solar incidence angle, which changes periodically through the year. Because this annual variation is the underlying cause of water temperature changes recorded in shell $\delta^{18}O$, and because temperature is highly seasonal while salinity remains relatively stable at the study site, the original data can be fitted successfully with a sinusoid as described in Wilkinson and Ivany (2002) and DeRidder (2007), not unlike the sinusoidal fits applied to the environmental data above. Due to discontinuous and variable growth rates, a realistic estimate of average $\delta^{18}O$ and

its seasonal variation can be obtained through the best-fit sine position and amplitude instead of using arithmetic average and the full range of the $\delta^{18}O$ data. In addition, apparent changes in $\delta^{18}O$ periods can be interpreted as reflecting differences in rate of growth, which in turn can vary in any one taxa due to ecological restrictions and local or short–term environmental variability.

Because the data represent only about a single period (~1 year), no moving window was used when applying the method (see de Brauwere et al., 2009). Instead, the records were divided into sections that could be easily described with different sine curves. Sinusoid fits were calculated applying a non–linear least square method and trust–region algorithm in Matlab® using the equation:

$$Y = amp \times \sin(2\pi/prd \times (X - phs)) + pos \quad (2.5)$$

where *amp*, *prd*, *phs* and *pos* are amplitude, period, phase and position of the sinusoid respectively, and X is the day of the year. The assumption adopted here was that the maximum water temperature corresponds to the minimum carbonate $\delta^{18}O$. This is a reasonable assumption because 1) upper temperature limits for all taxa are > 30 ºC, and 2) slow growth or cessation of growth appears to occur only at high $\delta^{18}O$ (winter) values (Figure 2.7). The published temperature tolerance limits were initially used to reconstruct the possible $\delta^{18}O$ maxima. Because the fitting exercise is mostly concerned with the data distribution along the abscissa (i.e., period and phase) this choice does not control the date assignment in the best–fit sinusoid method. Adjustments to the amplitude at the scale implemented here are not critical. In other words, if different positive limits were to be chosen, the date assignment would not be substantially affected.

Calcification dates were assigned to the best–fit sinusoids under the assumption outlined above. The published temperature tolerances of the different organisms initially helped to set the amplitude of the $\delta^{18}O$ variation. Specifics on the implementation for each data set are provided with the results.

2.3.2.2. Growth rate function

In general, carbonate isotopic compositions calculated from temperature and δ_w annual variation are tied to time and are often used to determine precipitation dates of the sampled material, thus providing an evaluation of precipitation timing and growth rates (Surge et al., 2001; Elliot et al., 2003; Goodwin et al., 2009). In addition to simplicity, the main advantage of comparing measured to modeled compositions is that no *a priori* anchor points along the measured $\delta^{18}O$ profile are needed. Examples of anchor points include temperature–based precipitation limits, or dates of maximum/minimum temperature during the year. Instead, in these studies the environmental parameters of the area are used to provide independent time constraints. However, this method has some important drawbacks. First, there is no unequivocal way to consider the time averaging that some samples necessarily represent, resulting in unrealistic single date assignments to samples that most likely average several days of precipitation. This ultimately introduces distortion to growth rate estimates (see Beelaerts et al., 2009, for an alternative). Second, using average environmental information to be matched by discrete $\delta^{18}O$ values may introduce deviations in time because the local conditions that existed while the sampled specimen lived may have differed from the average environmental signal. Third, the results are a function of the quality of the environmental data and the adequacy of the paleotemperature relations used. The first may not be a major issue, whereas the empirical equations that are constructed in laboratory settings for inorganic material, or for certain species under limited natural conditions, may not be fully applicable to the processes and specimens at hand.

Goodwin et al. (2009) developed a method to explore growth rate variation. Measured shell increments are dated through the $\delta^{18}O$ time series to build a plot of distance vs. time. A shape–preserving curve is then fitted to these data using piecewise cubic hermite interpolation. The resulting function has the advantage of including every point while maintaining a null or positive slope. The derivative to this curve is a profile of changing shell increments through time (i.e., growth rate), which is then smoothed using

a moving average. The result is a growth rate function that describes the magnitude and variation of predicted shell increments. The reader is referred to Goodwin et al. (2009) for a detailed explanation of the method and its rationale.

This approach was applied here with several modifications. First, Goodwin et al. (2009) use temperatures calculated from measured carbonate $\delta^{18}O$ and local δ_w to assign dates to shell increments by comparing their results to a known local average temperature profile. Here, the dates from the best–fit sinusoid are translated to the shell increments by comparing the best–fit sinusoid results to the measured $\delta^{18}O$ values. While it may appear equally arbitrary to relate the best–fit dates back to the data, the fundamental goal here is to further describe a time series already constructed from limited assumptions. The limitations introduced by adjusting measured to modeled data are not compounded by this strategy. Quite the opposite, relating the best–fit dates back to the data ensures that the growth rates produced from the dated increments are pertinent to the best–fit data and that no further assumptions are made about the timing of precipitation. In other words, several fundamental assumptions are implicitly made when measured data are directly related to modeled data. This is not the case here.

Second, a number of synthetic random $\delta^{18}O$ vs. distance profiles were generated in Goodwin et al. (2009) using the experimental error of the isotopic determinations to produce a confidence boundary in the final growth rate prediction. Because the average of all these random profiles converges to the original one, and because the main purpose of this exercise is to further evaluate the date assignment method rather than estimate the variation limits of the growth rates, this step was not implemented. Third, the resulting predicted increment widths (PIW) in Goodwin et al. (2009) are calculated for one calendar year using $\delta^{18}O$ data averaged to a single monotonic decrease/increase profile. Here, the assigned dates preserved the original time frame of the data (as suggested by the shape of the $\delta^{18}O$ profiles), revealing growth changes from one season to the next. Though limited, this is a very simple way to revisit both probable precipitation dates and

growth rates previously determined by the best–fit approach.

2.4 Results

$\delta^{18}O$ extremes in the shell carbonate are recorded by the bivalves; 2.3 ‰ for the bay scallop and –4.4 ‰ for the hard clam. The most positive $\delta^{13}C$ also belongs to the hard clam (2.4 ‰), and the most negative to the coral (–5.1 ‰). Maximum spread of the oxygen and carbon data is shown by the pecten and the hard clam, respectively. The bryozoan data has the minimum range for both carbon and oxygen (Figure 2.6). The greatest variation in aragonite $\delta^{18}O$ is in the hard clam *M. mercenaria* (–4.4 to 0.2 ‰). The stony coral compositions vary from –3.8 ‰ to –1.4 ‰ and the bryozoan's $\delta^{18}O$ varies from –2.2 ‰ to –0.9 ‰. Calcite $\delta^{18}O$ varies from –3.6 ‰ to 2.4 ‰. The bivalve is, once again, the only taxon exhibiting the entire isotopic range. The purple sea urchin varies from –3.1 ‰ to –1.2 ‰. Aragonite $\delta^{13}C$ varies from –3.8 ‰ to 2.1 ‰ in the hard clam, from –5.1 ‰ to 0.2 ‰ in the stony coral, and from 0.9 ‰ to 1.7 ‰ in the bryolith. Calcite $\delta^{13}C$ varies from –0.5 ‰ to 1.5 ‰ in the pecten, and from –2.2 ‰ to 1.5 ‰ in the echinoid.

2.4.1. Bay scallop (*Argopecten irradians irradians*)

The valves of *Argopecten* are composed of foliated calcite with aragonite only in the inner myostracal layer (Bathurst, 1972). Sampling was carried out directly from the external surface along the 80.4 mm–height left (exposed) valve where the growth increments are well defined and there is no risk of mixing aragonite and calcite during sampling. 33 samples were taken at a period (i.e., spacing) of about 2.2 mm in the adult scallop. The juvenile bay scallop was sampled at higher resolution with 12 samples in its ~16 mm shell height (Figure 2.7A). Growth bands at this early life stage are difficult to resolve, and the length of the shell is too small to procure enough material for analysis from a single growth band.

Bay scallops rarely live into the winter of their second year (Blake and Shumway, 2006). In the northeastern U. S., normal life span is between 18 and 22 months

(Estabrooks, 2007) or up to 26 months according to Belding (1910). The sampled bay scallop hatched sometime during the summer or early fall, grew until winter shutdown, and then resumed growth in the spring. The cuspate shape of the $\delta^{18}O$ profile is a probable indicator of growth cessation (though see Goodwin et al., 2003).

The highest oxygen isotope value occurs right after the bay scallop's "growth ring" a brake developed in the shell by cessation or slow growth during the winter (Belding, 1910, 1931; Tettelbach, 1991). Samples between the growth ring and the ventral edge were taken from the vertical ridge of single growth bands. These samples from the younger bay scallop average shorter periods of time than samples taken close to the umbo.

The bay scallop data was divided in 4 sections for mathematical analysis. These include: 1) first late summer–fall, samples 1 to 14, 2) spring–early summer, samples 13 to 21, 3) summer, samples 21 to 34, and 4) second late summer–fall, samples 34 to 45. If the fits were to be performed independently of one another, results would imply differing controlling conditions because multiple sinusoid fits can satisfy each group of samples. Some limitations can be imposed to the fits based on the fundamental dependence of calcite $\delta^{18}O$ compositions on the local temperature profile. Therefore, position and amplitude of all the fits must be the same (Table 2.2).

The amplitude was initially set to the range between the data minimum and the data maximum plus 1.1 ‰ and the position to the average of the range limits. These coefficients were permitted very little variation (i.e., ~ 1%). The 1.1 ‰ increment used to estimate the heaviest $\delta^{18}O$ is based on the published temperature tolerance of the species (Sastry, 1961, 1966; Castagna and Duggan, 1971). If the most positive $\delta^{18}O$ of the bay scallop precipitated in 7 to 8 ºC waters, the calcite compositions missing from its record correspond to about 5.7 ºC.

Once the best–fit parameters were determined for each sample group, the best–fit periods (shell–length) were used to calculate the number of days represented by each

precipitation, given that each period is a measure of the distance in mm that would be deposited during an interval of the total accretion period of the shell, which is one year. This ratio was then transferred to the actual distance measured in each fitted section. With the number of days determined for all the fits, the curves were recalculated using the appropriate abscissa lengths. Finally, a date was assigned to each one of the days starting with the anchor point (i.e., Aug–11 corresponds to the day with the minimum summer $\delta^{18}O$). This anchor point choice assumes that the bay scallop is effectively calcifying during the hottest days of the summer months. The day of the year obtained for the first material precipitated in spring was then used to date the last $\delta^{18}O$ value recorded in the first fall section using the temperature profile (Figure 2.8–A1).

The initial precipitation date turned out to be October 19 and growth continued until January 6 when the bay scallop shutdown for winter. Growth resumed on March 26 and continued uninterrupted until October 26. Because the data is limited and a moving window was not implemented, the method calculates only a few discrete periods. Growth rates of the four individually fitted intervals are 0.17, 0.17, 0.29 and 0.64 mm/day for summer–fall, spring–summer, summer and following summer–fall respectively (Table 2.2). Constant growth rates effective for the duration of the segments chosen are not realistic. An alternative is to fit a curve to the growth rates to produce a rough estimate of change in shell accretion with time (Figure 2.8–A2). Cessation is known to occur between the first and second segments, so a shape–preserving hermite interpolation was applied using only the spring, summer and second fall growth rates.

To further explore these results, a growth rate function was calculated as described in the preceding section. A total of 31 points were selected to produce the monotonic profile. The final growth rate function was produced applying a running average of 27 days to the derivative curve, similar to the filter used by Goodwin et al. (2009) (Figure 2.8–A2).

As explained earlier, the basic information needed to construct the growth

function was taken from the best–fit sinusoid data. Precipitation start/shutdown dates should not be read from the function, which is a running average. This function effectively shows the bay scallop's growth variation. Growth was ~0.3 mm/day initially and began to decline pronouncedly by the end of November. Very slow precipitation took place up to early January (<0.08 mm/day). Growth practically ceased until the end of March, when a gradual increase to a rate of ~0.25 mm/day took place until mid–April. Faster growth occurred from mid–June to early August (~0.5 mm/day). Conspicuous mid–summer growth retardation took place, for the most part, in August with rates of about 0.15 mm/day. Growth accelerated again in September to about 0.5 mm/day towards the end of the record.

2.4.2. Hard clam (*Mercenaria mercenaria*)

Samples analyzed belong to one of several large, 17 to 20–year–old individuals based on obvious growth bands (Figure 2.7–B). The selected shell was sampled on the hinge plate of the right valve sectioned along the maximum growth axis. The outer and middle layers of the hard clam show a pattern of consecutive dark and light layers. Each major pair presumably reflects growth (light and opaque–fast, dark and translucent–slow) in a single year (Panella and MacClintock, 1968; Kennish, 1980). Growth bands in the hinge or dental plate tend to be better expressed and are easier to follow and to sample in detail, and they record the same isotopic composition of the middle layer (Ivany et al., 2004). A factor of 8.84 ($2\sigma = 0.02$) was used to estimate shell height from hinge plate distance. This factor was obtained from the average shell height to average dental plate length ratio of all hard clams recovered in the study area.

The crystalline structure of the light and dark bands has been previoulsy studied in an effort to correlate crystal arrangement with seasonal growth and ontogenesis (Kennish, 1980; Fritz, 2001). Jones and Quitmyer (1996), based on data from specimens recovered from Rhode Island and Florida, suggest that there is a latitudinal control in the occurrence of dark or light bands product of water temperature extremes. Because the hard clam is

widely distributed along the entire North American East Coast, the dark (translucent) bands are associated with slow growth in the south during the summer months and in the north during the winter months. In consequence, northern hard clam's dark areas are expected to show the highest isotopic composition. Dark, translucent bands in the analyzed sample, however, appear to correlate with both maxima and minima. Band recognition is complex for the final years of the hard clam.

As was observed in the bay scallop, the cuspate shape of the hard clam's profile indicates absence of the highest $\delta^{18}O$ values in all years due to slowing or cessation of shell accretion during the winter and seemingly also during the summer after the second year (Figure 2.7–B). Because maximum growth is experienced during the first year or two of the hard clam, samples from the shell precipitated by the young hard clam were used. The hard clam's first year of growth was re–sampled at higher resolution and these data were further analyzed. This record starts before the summer peak, appears to be continuous until the winter break and ends in the middle of the following summer season.

Disadvantages of sampling from the mature parts of the hard clam (i.e., after the second year) include the increased likelihood of calcification interruptions during spawning (Carriker, 1961) and the resulting decrease in the $\delta^{18}O$ range. Both of these reduce the environmental information that can be extracted from the hard clam's shell carbonate record. In the first case, growth cessation during spawning cannot be easily assessed, since changes in temperature rather than a certain temperature threshold seem to be the trigger; the actual spawning temperature varies geographically and among individuals (Eversole, 2001). In the second case, for the low resolution record of the analyzed hard clam, the ontogenetic decrease in winter minima is greater than 2 ‰, a failure to record some 10 ºC in temperature change.

Sinusoid fits were determined for two distinct sections of the higher resolution data: 1) summer–fall, samples 1 to 20, and 2) spring–summer, samples 20 to 40. Again, position and amplitude were fixed beforehand, so that only phase and period were

calculated for the data segments. Other than spawning after the second year, cessation of shell calcification occurs only below 9 and above 31 ºC (Ansell, 1968). A minimum precipitation temperature of 9 ºC would imply 7.7 ºC not represented in the shell in the study area. As a consequence, the amplitude and the position of the fit were initialized to the data range plus 1.5 ‰ and to the average of the extremes, respectively (Table 2.2). These values were not allowed to vary more than 1 % while the fits were calculated.

Consistent with the previous calculations, the number of days of precipitation in each segment was estimated using each section's period, the sampled distance, and the overall 365–day period of the $\delta^{18}O$ profile. The fit was then recalculated to the number of growing days, and dates were assigned by fixing the day of minimum $\delta^{18}O$ as August 11 in both sections (Figure 2.8–B1).

The first segment (summer–fall) records precipitation between June 8 and December 3. After the winter, shell growth restarted on April 23, and the record ended in August 11, during the warmest days of the year. Because the two sections of data that were used to fit sinusoids are separated by a period of growth cessation, no interpolation was attempted. Results are equivalent to average growth rates for each segment. Growth rates are 0.09 mm/day and 0.16 mm/day for summer–fall and spring summer, respectively.

A growth rate function for the data was calculated fitting a curve by cubic hermite interpolation to the distance vs. time scatter, the derivative of which was smoothed using a 27–day running average (Figure 2.8–B2). Initial rates of ~ 0.15 mm/day dropped in the middle of the summer, chiefly mid–August, to about 0.04 mm/day. Growth increased again to values between 0.14 mm/day and 0.17 mm/day before declining between mid–November and mid–April when shell growth ceased. Growth resumed and then increased rapidly in spring. Final growth rates were again around 0.15 mm/day and a growth peak occurred at the end of June characterized by the highest rates of the profile (~0.19 mm/day). Another brief retardation appeared in the second summer, with an immediate

rebound that was cut by the profile's termination.

2.4.3. Bryozoan (*Parasmittina nitida*)

Two spherical colonies (circumrotatory colonies and macroids of Kissling, 1973 and Hottinger, 1983, respectively) of encrusting bryozoans were also analyzed. Several organisms, such as red algae and corals also develop this morphology (Rider and Enrico, 1979; Kidwell and Gyllenhaal, 1998). Concentric growth can develop in areas of sufficient energy to feed the organism and free it from sediment, at least intermittently, and this is probably the case in Vineyard Sound. Conditions that are sometimes considered essential for this type of colony, such as slow growth and low sedimentation rate, may not necessarily occur in the study area (Kidwell and Gyllenhaal, 1998). Bryozoa commonly precipitates calcite with up to 14 mol % $MgCO_3$, but some species precipitate aragonite or variable mixtures of the two (Smith et al., 2006). The ones studied here are aragonitic, composed exclusively of the toothed crust bryozoan *Parasmittina nitida* (Verrill, 1875).

The largest available colony was sectioned and sampled from the center to the outer surface.One sample per approximately 3 layers of zooids (~25 zooid layers total) was retrieved to procure enough material for analysis. Research has shown that zooid size and $\delta^{18}O$ variation are both related to temperature changes in other bryozoan species (O'Dea, 2005). The $\delta^{18}O$ profile suggests a possible seasonal control on the isotopic composition of the colony (Figure 2.7–C). The samples obtained, however, are insufficient to interpret the nature of growth or of growth cessation. While growth rates in other bryozoans vary greatly (e.g., from 4.7 mm to 32 mm per year in branching bryozoa, Stebbing, 1971; Pätzold et al., 1987; Brey et al., 1998; Bader and Schafer, 2005), no specific information exists on this species.

Rider and Enrico (1979) assumed that growth rate in this type of colony amounts to some 8 to 10 zooid layers per year. This growth pattern was assumed to be valid for the analyzed colony, which means 3 to 4 samples represent a year's worth of carbonate

precipitation. Growth was assumed to be continuous because no obvious interruptions, incorporated sediment or check lines could be detected between the zooid layers in thin section, and also because other bryozoa species are known to grow continuously even in colder climates (Brey et al., 1998).

Because each sample potentially averages about 3 to 4 months of growth, the best–fit sinusoid could not be constrained beforehand as was done for the bivalves. No $\delta^{18}O$ range limitation was imposed to the fit. Instead, the algorithm was permitted to vary assuming that these data were complete. The uncertainty of this fit is obviously large, which results in inferior goodness–of–fit values (Table 2.2). The result suggests the bryolith represent a total of 2.2 years of precipitation (Figure 2.8–C1). One representative year cycle, recalculated to 365 days, was dated assuming that the hottest day of the year was coincident with the lowest $\delta^{18}O$. Because the data are fitted as a single window, no estimate of variable growth can be assessed, but only an overall average growth rate of 0.007 mm/day or 2.802 mm/year is suggested by the period.

Because each sample averages several months, assigning a date from the best–fit sinusoid back to the original $\delta^{18}O$ measurements was not attempted. However, this $\delta^{18}O$ profile has at least 2 periods, and the algorithm provided by De Ridder et al. (2007) was tested to further refine the average growth rate obtained with the fit (Figure 2.8–C2). Results suggest that yearly growth rates could have varied from 1.85 mm/year to 3.01 mm/year (average 2.8 mm/year ±0.4 mm/year) or 0.005 mm/day to 0.008 mm/day (average 0.007 mm/day ±0.001 mm/day). Results also suggest that accretion rates may have been more variable during the precipitation of the earlier colonies. Most of the variation in the growth rates comes from the initial 2 mm of the bryolith.

2.4.4. Northern stony coral (*Astrangia poculata*)

The corals recovered for this study had only the outermost dissepiments and corallites, probably of the living polyps, available to sample. Six corallites were sampled longitudinally and across, resulting in no particular isotopic pattern associated to

morphology. In consequence, no attempt was made to construct a time series of any sort with these data.

A. poculata is a facultative symbiotic coral, developing zooxanthellate as well as azooxanthellate colonies (Dimond and Carrington, 2007). In this case, carbon and oxygen isotope data exhibit both, the strong positive correlation characteristic of ahermatypic corals and the lowest carbon–oxygen isotopic composition of the entire dataset (Figure 2.6–B). The average and range of oxygen isotope compositions comprise all the information that can be deducted from this species, assuming the range obtained here is a representative sample of the coral's $\delta^{18}O$.

2.4.5. Purple sea urchin (*Arbacia punctulata*)

Growth in echinoids takes place by both increasing plate size and incorporating new plates onto the aboral end of the corona. Age determination based on growth bands potentially indicates *A. punctulata* can live for about 7 years (Hill et al., 2004). However, producing time series for *Arbacia* is at present problematic given the uncertainties in the nature of its growth bands and also the known occurrence of resorption of carbonate throughout ontogeny (Ebert, 1985, 1986, 2007).

All parts of the skeleton were sampled, and isotopic compositions were found to correlate with morphology as was observed before (Weber and Raup, 1966; Ebert, 2007). With the exception of one sample, calcite $\delta^{18}O$ from the spines is noticeably heavier. Samples from the poriferous zone of the ambulacra are somewhat heavier than samples from the interporiferous zone. This subtle trend in $\delta^{18}O$ is also observed in the pyramids, where samples taken transversally show an increase in oxygen isotopic signature from the smooth to the toothed edge.

Isotope composition contrast is also apparent in carbon. The ambulacral material shows a general increase in $\delta^{13}C$ from the oral to the aboral end of the corona. Heavier $\delta^{13}C$ toward the aboral end of the corona is also observed in the mamelon and interambulacral plates in general, which may indicate ontogenetic changes in carbon

incorporation to the plates. A better assessment of new plate addition and calcite accretion to existing plates is necessary before attempting to develop time series from equinoid $\delta^{18}O$ data. As for the coral, only average and range $\delta^{18}O$ compositions can be considered.

2.4.6. Serpulid tubes (*Hydroides dianthus*)

Serpulid tubes, mostly *Hydroides dianthus* (Verrill, 1873) a common tube–builder polychaete in this area, were attached to several of the other individuals and were also sampled. Their $\delta^{18}O$ varied between –1.6 ‰ and –1.3 ‰ and $\delta^{13}C$ from –4.7 ‰ to –1.8 ‰.

Serpulids are thought to deposit their shells in oxygen isotopic equilibrium with ambient water (Epstein et al., 1953; Lowenstam and Epstein, 1957; Bathurst, 1975). In temperate climates, they live from early spring to early winter, which makes them good candidates to provide an uninterrupted record of summer temperatures. However, according to Milliman (1974), *H. dianthus* exhibits mixed mineralogy. Aragonite is precipitated from the calcium–secreting glands and calcite is thought to be produced from the worm's ventral shield epithelium. Specimens of this species collected from the Woods Hole area for other studies vary in composition from less than 5% to more than 42% aragonite. $MgCO_3$ increases in the calcite fraction of the tube as the proportion of calcite itself decreases (Bornhold and Milliman, 1973), probably as a function of temperature.

The mixed mineralogy suggested in the literature was confirmed through X–ray diffraction, and serpulids were not examined further due to the complications associated with and the time necessary to produce good enough mineral separation. Nevertheless, this taxon may be deserving of more attention. Their widespread distribution and visible growth structures make them potentially useful as environmental indicators, a possible valuable source of isotopic composition profiles of co–precipitating calcite and aragonite.

2.5. Discussion

The analysis above provides the temporal framework to relate specific parts of the shell records to environmental parameters. It is now possible to evaluate equilibrium

precipitation and ecological implications derived from the time–series and growth rate functions.

2.5.1. Fractionation factors

Applying commonly used carbonate–water fractionation factors to model the carbonate oxygen isotope compositions, the range of calculated calcite $\delta^{18}O$, based on observed temperature and estimated δ_w, is found to be close to the range of measured calcite compositions, while only a fraction of the calculated aragonite $\delta^{18}O$ compositions overlap with the measured ones (Figure 2.9). Modeled and measured minima $\delta^{18}O$ are expected to coincide or to be very close in magnitude because growth is presumably continuous during the summer at these latitudes. Yet, there is about 0.3 ‰ to 0.6 ‰ and 1.0 ‰ to 1.4 ‰ discrepancy between measured and modeled calcite and aragonite isotopic minima, respectively. This calculation also highlights the effect of the different δ_w estimates in the resulting carbonate composition (i.e., using δ_w1 increases this difference).

To evaluate whether bivalves precipitated carbonate in equilibrium, and to finally judge which δ_w estimate is more appropriate, each temperature–$\delta^{18}O$ pair obtained from the best–fit exercise was assigned a value of δ_w1 and δ_w2 using the date. Calcite–water and aragonite–water fractionation factors were calculated for both δ_w estimates using the relation $\alpha = (1000 + \delta^{18}O)/(1000 + \delta_w)$. Results were plotted as $10^3\ln\alpha$ vs. $10^3/T$, and the temperature dependence of the fractionation factor was determined by fitting the data with a linear least square method (Figure 2.10).

The fit for calcite–water fractionation factors calculated using δ_w2 diverges very little from the relation published by O'Neil et al. (1969) (Figure 2.10–A). The minimal discrepancy can be attributed to the original equation being developed as a function of T^2 instead of T. In contrast, the fit for δ_w1 is at an angle to the experimentally determined equations. The equation for the fit using δ_w2 with 95% confidence levels is:

$$10^3\ln\alpha_{calcite\text{-}water} = 19.64 \pm 0.08 \times (10^3/T) - 37.53 \pm 0.26 \qquad R^2 = 0.99 \qquad (2.6)$$

This result is a strong indication that $\delta_w 2$ is the better choice, and that the bay scallop is precipitating its shell in equilibrium with seawater. Conversely, it also suggests that O'Neil et al. (1969) provide the correct expression of equilibrium between calcite and water at the local temperature range.

Aragonite–water fractionation factors calculated with either δ_w show a considerable departure from known equilibrium fractionation (Figure 2.10–B). Both lines have a reduced intercept compared to the published equations. However, the equation based on $\delta_w 2$ has a slope comparable to Grossman and Ku (1986), while the relation based on $\delta_w 1$ does not. The resulting equation using $\delta_w 2$ with 95 % confidence boundaries is:

$$10^3 \ln\alpha_{\text{aragonite-water}} = 17.35 \pm 0.28 \times (10^3/T) - 30.17 \pm 0.97 \qquad R^2 = 0.89 \qquad (2.7)$$

The uncertainty of the linear coefficients is greater in this fit.

These results show that the hard clam is precipitating aragonite at a considerable though constant departure from equilibrium. Hard clams are thought to precipitate aragonite in or close to equilibrium at all latitudes (see for example Veizer, 1983 for mollusk in general, and Elliot et al., 2003, for the hard clam in particular). The divergence from expected oxygen isotope values reported here, however, is not a unique occurrence. A similar deviation was obtained by Elliot et al. (2003), where the minimum forecasted aragonite $\delta^{18}O$ at about 41º N was heavier than the *Mercenaria* measured values by ~ 1.6 ‰.

Difficulties modeling recent precipitation with the widely accepted equilibrium conditions, as established by Grossman and Ku's (1986) paleotemperature equation, have also been reported in other settings. For example, Owen et al. (2008) found a depletion of up to 2 ‰ in some of the aragonite shells precipitated by sea scallop larvae reared in controlled conditions, while Carré et al. (2005) found between 0.4 ‰ and 0.7 ‰ depletion in the samples with respect to equilibrium calculations in *Mesodesma donacium* off the Peruvian coast.

For the most part, however, field calibration experiments have lent support to the results of Grossman and Ku's (1986) fractionation relation for mollusks (e.g., White et al., 1999; Böehm et al., 2000). While there are some contentious results that point towards a negative aragonite–calcite fractionation (Zhou and Zheng, 2000; Zhou and Zheng, 2003; Zheng and Zhou, 2007), recent experimental and theoretical calculations of equilibrium fractionation between aragonite and water, and in carbonate systems in general, continue to support a positive aragonite–calcite fractionation (Kim et al., 2007; Chacko and Deines, 2008). Aragonite precipitated in accordance with the equation presented here is 0.8 ‰ to 0.9 ‰ lighter than $\delta^{18}O$ compositions expected using Grossman and Ku (1986). Results indicate a local negative fractionation between calcite and aragonite that is difficult to disregard in light of the calcite results.

2.5.2. Rates and timing of precipitation

Three aspects of the bivalve's results are relevant and should be considered in more detail: first, the overall pattern of increasing growth–rate; second, the occurrence of a period of growth retardation in the middle of the summer, and third, the start/shutdown precipitation dates obtained from the fit, some of which are surprising, particularly for the bay scallop. On the other hand, the magnitude and possible cause of the growth rate changes, although relevant from a biological standpoint, are not assessed here. In general, drops in $\delta^{13}C$ of different magnitudes appear to be concomitant to the major episodes of enhanced growth rate in both the scallop and the hard clam, which suggest contemporaneous productivity increases.

2.5.2.1. Bay scallop

The overall growth rate increases from about 0.2 mm/day to a maximum of ~0.5 mm/day. This result contradicts the usual growth rate functions produced for most bivalves, including *Argopecten irradians*, where initial growth is very rapid and turns asymptotic with time (Blake and Shumway, 2006).

The overall rate of calcite precipitation before and after the bivalves' first winter

was calculated here using *Argopecten* shell height values recorded through time in studies done in areas relatively close to Falmouth (i.e., Niantic and Poquonock Rivers, CT, ~125 Km west of Falmouth) and around Cape Cod (Nantucket, Edgartown, Chatham, Monomoy, and Buzzards Bay; see Appendix). Juvenile precipitation varies between 0.17 mm/day and 0.37 mm/day, with short term growth rates as low as 0.11 mm/day and as high as 0.62 mm/day. Generally, these numbers are in good agreement with the rates given by the models.

The juvenile bay scallop grew at a rate comparable to the lowest growth rate in the range suggested by the empirically–determined shell height vs. time relation. In effect, by the end of their first year, most of these measured bay scallops (tens to hundreds per sample) were on average about 4 cm in height (Appendix). Tettelbach (1991), for example, reports that more than 95% of the 47 young bay scallops he measured in December of 1983 were larger than about 3.2 cm. The bay scallop in the present study was only about 16 mm in height by winter, as revealed by the location of the annual growth line. This observation not only supports, but also requires an early slow growth rate.

Bay scallops with a growth ring very close (2 mm to 7 mm) to the dorsal edge are known as "ring at hinge" and have been reported close to the study area. During 1980, for example, in Pleasant Bay, Massachusetts, about 9% of the bay scallop population developed an annual growth line very close to the umbo (MacFarlane, 1991, 1999). These specimens are the result of late spawning and may live to develop a second ring and spawn the following spring, dying shortly after. The majority of broods are produced in early summer, but spawning can continue into August and even September (Sastry, 1966; Taylor and Capuzzo, 1983; MacFarlane, 1991).

Although the analyzed bay scallop is not an example of a "ring at hinge" individual, it was considerably smaller than the reported average at the time of winter shutdown, and the October date obtained for its initial precipitation is in agreement with a

rather late spawning. The composition of the very first precipitated growth layers is most likely averaged or missing from the record. Interestingly, MacFarlane (1991) showed that by the following summer, these "ring at hinge" bay scallops were not smaller than regular ring size bay scallops, which may explain the accelerated growth rate of the sampled bay scallop after spring in contrast to those calculated from published shell height data.

A more recent study indicates that bay scallops attain at least 20 mm to 25 mm by early spring. In the summer, shell height is 40 mm to 50 mm and reaches 60 mm to 90 mm at the beginning of the next winter (Blake and Shumway, 2006). These ranges translate approximately into initial rates between 0.22 mm/day and 0.27 mm/day, with spring growth between 0.16 mm/day and 0.22 mm/day and a highly variable final rate anywhere between 0.11 mm/day and 0.55 mm/day. These estimates indicate that, in general, growth rates estimates are reasonable.

The total number and width of growth bands could be used to try to independently assess growth rate. *Argopecten irradians* develop very clear growth bands that end in a vertical ridge and can be distinguished in the exterior of both valves. Helm and Malouf (1983) observed that only during peak growing season, 90% of the bay scallops they analyzed added growth bands and their associated vertical ridges daily. At other times, the growth band–ridge structure required more than one day to form. In their analyses, average growth rates were 0.55 mm/day and 0.15 mm/day (N=20), during stages of rapid and slow growth respectively. They concluded that a minimum distance, in opposition to a determined length of time, was required to develop the ridge that marks the end of the growth band. As a result, the ridges observed in the bay scallop cannot be confidently associated with age.

The second observation, that growth retardation occurs in mid–summer, is counterintuitive, particularly on the grounds of bay scallops' observed lethal temperatures of ~32 ºC and optimal growth above 10 ºC (Sastry, 1961, 1966; Castagna and Duggan, 1971). Maximum temperatures in the study during the summer are well below 32 ºC, and

temperatures above 10 ºC occur between early May and mid November. However, this growth rate drop coincides with major spawning reported for *Argopecten irradians* along the coast of Massachusetts, Rhode Island, Connecticut and New York (Barber and Blake, 2006, and references within). Massachusetts populations are said to spawn mostly from May to July (Taylor and Capuzzo, 1983), but spawning can occur any time from May to October and has been reported most significantly in June, July and August for the study area. Differences are somewhat controlled by latitude, and there is a direct correlation between latitude and energy apportion to reproduction. As a consequence, precipitation retardation in Falmouth during the summer is a very reasonable proposition.

Early observations by Belding (1910) on Massachusetts' bay scallops indicate that the lowest percentages of total shell growth, besides that which represents the winter months, occurred in June and July. Bricelk et al. (1987) and Bricelj and Krause (1992) confirmed slow or no growth during gonadal production and spawning in the bay scallop. This is most likely the reason for growth retardation in the bay scallop examined in this study.

Growth (i.e., positive growth) occurs when the energy balance from essential physiological processes allows further energy expenditure and is influenced by several variables, particularly temperature and food supply (MacDonald et al., 2006). Stress factors can impact this balance. For example, prolonged exposure to low salinity has been repeatedly documented as detrimental and even lethal to bay scallops especially at warm temperatures (Mercaldo and Rhodes, 1982; Tettelbach et al., 1985; Dame, 1996). Even short term salinity drops triggered by storm events affect spawning in adults (Bologna, 1998). Low salinity, however, is not a concern in this study, and growth interruptions are probably safely attributed solely to low temperature.

Results indicate that initial precipitation occurs in October and stops in early January. Growth restarts in late March and ends again in October (Table 2.3). Tettelbach (1991) and Barber and Davis (1997) indicate that growth in adult bay scallops declines

in November and virtually stops in December, with no growth between December and May, or while temperatures remain below 7 ºC or 8 ºC. According to the water temperature record representative of the study area, 7 ºC to 8 ºC temperatures occur between approximately Apr–12 and Apr–23 and again from Nov–30 to Dec–11. Best–fit results suggest that precipitation starts and ends about a month earlier and later than these published limits respectively, with temperatures between 3.2 ºC and 4.2 ºC.

The growth rate function, however, suggests that the magnitude of the growth during this extended period is much reduced. From the end of November to the end of December, the growth rate drops from 0.3 mm/day to 0.06 mm/day. Similarly, growth at the end of March is ~0.03 mm/day and by April 15 is 0.2 mm/day. In other words, the model suggests that growth occurs at these low temperatures but at an exceedingly slow rate.

The bay scallop has developed several subspecies that are characteristic of different latitudinal ranges, *A. irradians irradians* being the northernmost one. This differentiation suggests a probable adaptation to specific, possibly narrow environmental conditions. However, for other functions, such as spawning, acclimation is relevant to temperature limits in *Argopecten* (Sastry, 1961). This means that rather than a fixed threshold, critical temperatures are dependant on the specific environmental conditions affecting the bay scallop. Acclimation can probably control other physiological responses too. It is possible that bay scallops accustomed to colder or warmer waters may start and stop precipitating respectively at lower or higher temperatures, though at a slower rate.

High mortality rates, however, have been associated with temperatures below 5 ºC in river cultures in Maine and Canada, although not always conclusively (Couturier et al., 1995; Barber and Davis, 1997). Interestingly, bay scallops are normally exposed to temperatures well below 5 ºC along their northern geographical range. Moreover, they have been observed to tolerate temperature < –2 ºC for short periods (Couturier et al., 1995). Thus, it is unclear why cold temperatures commonly experienced by bay

scallop populations would be lethal per se. The aforementioned temperature tolerance of 7 ºC to 8 ºC may not constitute a firm threshold for this species. Unfortunately, other environmental elements that are correlated to high bay scallop mortality, such as winter tides or salinity drops were not explored in the referenced studies. Precipitation at normal rates is not likely to occur in very cold waters, but the high $\delta^{18}O$ values indicate that some ultra–slow rates of accretion must be taking place in winter and are otherwise difficult to explain.

Some additional information can be derived from the growth rate function. As described by Goodwin et al. (2009), the highest growth rates can be associated with optimal growth temperature without previous knowledge of growth pattern. This is valuable information because periods of fast or slow growth in the bay scallops are not necessarily ontogenetically determined. According to the growth rate function, these optimal temperatures vary between 14 ºC and 18 ºC in the study area. This range is reasonable given that temperatures above 10 ºC to 15 ºC are considered optimal for bay scallop growth (Castagna and Duggan, 1971; Tettelbach, 1991).

2.5.2.2. Hard clam

In Narragansett Bay, Rhode Island, 70 km west of Vineyard Sound, average growth rates calculated from shell heights of 2–year–old hard clams vary between 9.5 mm/year and 17.6 mm/year (Henry and Nixon, 2008). While working with hard clams in the same area, Jones et al. (1989) found that the main growing season was from April–May to October–November, 6 to 7 months. These combined data result in average daily growth rates from 0.04 mm/day to 0.13 mm/day considering an active growing period between 153 and 215 days. Growth rates calculated here are comparable to the published ones when averaged (i.e., ~0.11 mm/day).

Modeled growth rates in the second season (spring–summer) are greater than rates from the previous summer–fall season. Although annual growth rates in the hard clam decrease with time (Jones et al., 1989; Malouf and Bricelj, 1989; Appleyard

and Dealteris, 2001), it is not clear that this pattern applies to intra annual variability. Most importantly, these seasons are not perfectly complete, and an entire single record could provide a different average growth rate and trend. Also, a margin of error may be attributed to the conversion to shell height from hinge plate distance. Nevertheless, obtained growth rates are within reasonable ranges.

The initial and final dates of the hard clam's $\delta^{18}O$ time series do not represent natural limits of shell accretion. With certainty, the relevant dates the model provides in terms of precipitation temperature constraints are the first fall shutdown (December 3) and the spring precipitation restart (April 23). These dates indicate fall shutdown and spring restart temperatures of 7.6 ºC and 8.4 ºC, respectively (Table 2.3). Adult hard clams can survive temperatures from below freezing up to 35 °C (Stanley and DeWitt, 1983). According to Ansell (1968), optimum growth occurs between 15 ºC and 25 ºC, with cessation starting at about 9 ºC. Jones et al (1990) found that growth was negligible below 10 ºC. Temperatures at the maximum growth rate (end of June and mid–October) are in good agreement with the temperatures associated with optimum growth from the literature. Initial and final precipitation temperatures from the best–fit sinusoid are slightly below the published threshold.

However, as was the case with the bay scallop, a closer examination of the growth rate variation calculation requires growth rates to drop rapidly after mid–November. By November 20, the growth rate has decreased to 0.03 mm/day. Similarly, the spring precipitation growth rate starts to increase by mid April, and the rate does not reach a maximum until early May. In other words, the limits predicted by the fit represent the latest and earliest dates of precipitation shutdown and restart respectively and a period of slow growth follows and antecedes these extreme dates.

In addition, the observed latitudinal dependence of the growth band pattern in the hard clam (Jones and Quitmyer, 1996) suggests that marine climate exerts control over the hard clam's shell configuration. As is the case with growth cessation due to spawning

(Jones et al., 1990), precipitation temperature limits may also vary geographically. Although temperature is a dominant factor along the latitudinal range, other factors such as food supply and substrate may also be important or even determinant to growth patterns in some individuals (Jones et al., 1990). Thus, growth limits that are always attributed to temperature may, in reality, be a response to another factor or combination of factors.

For example, part of the difficulty encountered by Henry and Nixon (2008) in establishing a clear correlation between growth rate changes and the variety of environmental parameters they examined may hinge on the assumption of an invariant temperature threshold. They found that the greater temperature seasonality in the upper reaches of Narragansett Bay did not result in a change in growth rate. The implication is that the hard clams adjust their growth rate in shorter seasons. Alternatively, it is possible that acclimation plays a role and that precipitation of the shell may also occur at slightly lower temperatures. The lack of correlation is probably the result of comparing yearly shell accretion widths while assuming equivalent yearly length of precipitation. Published precipitation temperature thresholds may not be applicable in all settings.

It is tempting to consider published temperature tolerance limits to be general and invariant because this offers additional anchor points to date or limit $\delta^{18}O$ profiles and to calculate annual growth rates. Nevertheless, it frustrates the opportunity to explore these limits in greater detail and predetermines the resulting $\delta^{18}O$ time frame, while perpetuating discrepancies that may be created by this assumption.

Summer slow growth is also exhibited in the growth rate function of the hard clam. Growth retardation occurs after the hard clam reaches reproductive maturity, usually after the second year. The drop in growth rate is apparent in both seasons of the record, though the second season is incomplete. It is possible that the material did not belong to the first year of shell precipitation. Instead, the profile may represent the end of the second year and the beginning of the third. Sample collection started right where the

first layer could be distinguished on the dental plate. Thus, it is possible very early growth may not develop obvious bands.

2.5.3. Bryozoan, northern stony coral and purple sea urchin

Even though the best–fit produced a reasonable age for the bryolith, and compatible with published growth rate estimates, these results remain rather speculative. The measured $\delta^{18}O$ range is too narrow and the average too low to convincingly represent year–long precipitation. It is possible that much faster or denser summer growth biases the isotopic record. However, to further the interpretations offered here, more refined sampling strategies need to be implemented (e.g., one sample per zooid layer would produce an almost monthly record), which is not a straightforward task in this type of skeletal structure.

The northern stony coral *Astrangia poculata* (Ellis and Solander, 1786) (junior synonym *A. danae*), is the only one found in this area, which represents the northern extreme of its geographical range (http://www.mbl.edu/). Growth is positively correlated to temperature. Observations indicate it ceases during the 3 – 4 coldest months of the year (Dimond and Carrington, 2007). According to Jacques et al. (1983), the temperature threshold for precipitation lies around 6.5 ºC, and at 15 ºC, the presence of zooxanthellae begins to enhance calcification (i.e., it grows faster above 15 ºC).

If this is the case in the study area, using the fractionation factor obtained from equation (2.6) at 6.5 ºC ($\alpha_{aragonite\text{-}water}$ = 1.03238) and $\delta_w 2$ between 0 ‰ and –0.1 ‰, the maximum $\delta^{18}O$ should be ~0.4 ‰. Instead, the highest $\delta^{18}O$ measure in the coral is –1.4 ‰. This measured $\delta^{18}O$ is within the rather large 95 % confidence boundaries of the calculated $10^3 \ln\alpha_{aragonite\text{-}water}$ vs. $10^3/T$ relationship (±1.9 ‰), but the expectation is that the coral starts precipitation in colder temperatures. This result, the reduced $\delta^{18}O$ values compared to the hard clam data, and the high correlation with $\delta^{13}C$ are likely indicators of carbon and oxygen isotopic disequilibrium. These vital effects are due to both CO_2 incorporation from respiration, which is in agreement with the absence of *zooxanthellae*

in the coral, and kinetic effects, which are probably attributable to faster growth during the warm season. The summer increase in growth rate occurs even in the absence of a symbiont (Keith and Weber, 1965; Swart, 1983).

Arbacia punctulata (Lamarck, 1816), is a common purple sea urchin species on the Atlantic coast and is variably abundant south of Cape Cod, which is the northern extreme of its geographic range. It inhabits the lower intertidal zone to a depth in excess of 200m, preferably on sandy or rocky bottoms (Myers et al., 2006).

Echinoids precipitate a highly porous high–magnesian calcite endoskeleton at a growth rate of 10 mm/day to 20 mm/year. This rate increases with increasing temperature (Milliman, 1974; Bathurst, 1975). In other words, a larger fraction of the echinoid test is probably precipitated during the summer months. According to Hill and Lawrence (2006), the purple sea urchin occupies areas where temperatures range between 9 ºC and 31 ºC. Temperatures above 30 ºC can affect growth and other metabolic rates, but its geographical range suggests it can adapt to higher temperatures, at least for short periods. Acclimation is also very relevant to echinoid survival and ecology. For example, Moore (1966) reports one particular cold spell that caused a kill of *Lytechinus* at 16 ºC in Miami and at 9 ºC in Cedar Key, Florida. All echinoderms, echinoids in particular, are intolerant of low salinities. The established minimum salinity for the purple sea urchin is 19 (Moore 1966).

The maximum $\delta^{18}O$ measured in the echinoid was –1.2 ‰, compared to ~0.6 ‰, which is the expected composition at its minimum temperature for precipitation. Conversely, minimum oxygen isotope composition is closer to the minimum $\delta^{18}O$ expected from the highest local temperatures. According to Weber and Raup (1966), only the spines of echinoids precipitate in equilibrium with seawater, while other ossicles precipitate at partially predictable departures from equilibrium. Ebert (2007) summarized data indicating that spines also discriminate more efficiently against Mg incorporation in the carbonate structure. These are also composed of high–Mg calcite, and Mg content

induces further oxygen fractionation at a rate of 0.06 ‰ per mol–percent $MgCO_3$ (Tarutani et al., 1969).

In the samples analyzed, the highest oxygen isotopic compositions come from the spines (between ~ –1 ‰ and –2 ‰). Correction for Mg content would reduce these values somewhat. These $\delta^{18}O$ compositions may represent average preferred precipitation temperature or be an indication of a higher temperature threshold for this species, but it is difficult to evaluate. No particular trend was discernable within the spines. On the other hand, the lower values are much closer to what can be predicted from equilibrium (–3.1 ‰ measured; –2.4 ‰ predicted), even more when considering the correction for Mg content. All measured values < –2 ‰ come from skeletal structures that allegedly precipitate out of equilibrium, but out results do not support this observation. Instead, the purple sea urchin appears to be recording the warmest temperatures registered in the area.

2.6. Conclusion

This study demonstrates the ability of a limited number of samples from several taxa (in contrast to many specimens of one taxon) to reproduce average environmental parameters and alert about taxon specific deviations through their oxygen isotopic composition. Using oxygen isotope records from several modern coexisting carbonate–precipitating invertebrates to evaluate general environmental conditions proved useful to test equilibrium condition and reconsider ecological limitations. Although the use of a single taxon is a reasonable and necessary first step, the use of several taxa can reveal a more complex assemblage of marine interactions as they are imprinted on a variety of calcareous skeletons. When translated to the fossil record, results presented here suggest that paleoenviromental interpretations would benefit from a multiple taxa approach. A richer past environmental signal can be obtained from coexisting fossils using different $\delta^{18}O$ profiles, growth rates analyses and, when appropriate, $\delta^{18}O$ ranges.

Both magnitude and variation of δ_w were found to be relevant. Even though the difference in magnitude and variation between the two δ_w estimates was not very large,

it introduced appreciable discrepancies when testing their relation to the carbonates. This observation is of particular interest because research is often fairly unconcerned with the magnitude and in particular with variation of δ_w. In Vineyard Sound, Massachusetts, U.S.A., where the annual temperature range is ~20 ºC and salinity remains above 30 and varies annually < ~2, calcite–water fractionation factors calculated for the bay scallop are in agreement with equilibrium precipitation. Aragonite–water fractionation factors associated with the hard clam, on the other hand, are not. Although there is greater uncertainty in the $T–\alpha_{aragonite–water}$ relation, aragonite precipitation appears to proceed at a constant departure from equilibrium (~ –0.9 ‰). This discrepancy suggests a negative fractionation between calcite and aragonite, opposite to the accepted equilibrium relation. Although some experiments have supported such reverse fractionation, this observation likely reflects changes in the hard clam's precipitation process. A further insight from this result is that the assumption of equilibrium precipitation in mollusks may not always be appropriate, and that departures from it can be considerable. Similar to the potential influence of acclimation in the precipitation initiation temperatures, constant departures from equilibrium may occur locally. On the other hand, it can be speculated that this 'equilibrium shift' may not only be a species specific condition, but also an environmentally controlled equilibrium adjustment, given the constant departure from accepted equilibrium relations and the coincidence in the $\delta^{18}O$ ranges of the hard clam and the bryozoa.

Though at a differing scale, both the bay scallop and the northern hard clam appear to start and stop precipitation at colder temperatures than the established thresholds. Further analyses of growth rates suggest that the bivalves continue precipitating into colder days at a much reduced rate, and normal pace precipitation is closer to published temperature limits. While effective growth is not detected in regular catch–release experiments, winter temperatures appear to be partially recorded in the bay scallop's $\delta^{18}O$, contrary to what can be anticipated based solely on ecological limitations.

In addition, both bivalves' growth rate functions indicate some precipitation retardation during the summer, which has been amply documented but is not otherwise obvious in oxygen isotope profiles.

Age estimate and growth rate determination for the bryolith coincide with the literature estimates, but results are considered only tentative. *Parasmittina nitida* shows the potential to reflect seasonality. More information about ectoprotalith's growth and a reduced sampling period are necessary to corroborate and improve the outcome. The northern stony coral is probably precipitating aragonite in at least partial disequilibrium with seawater. The high–Mg calcite of the purple sea urchin's spines has the heaviest $\delta^{18}O$ of all analyzed ossicles and probably represents equilibrium conditions. Maximum $\delta^{18}O$, however, is below what would be expected from the published temperature threshold for precipitation. These compositions may represent average or preferred growth temperatures. But because no other constraint can be used to estimate a time of precipitation, interpretations based solely on the $\delta^{18}O$ range or value are somewhat speculative. The Mg concentration of the calcite was not measured, and this represents an additional uncertainty over the potential equilibrium compositions. Nevertheless, isotopic disequilibrium is not evident from these data, and the purple sea urchin may be completing the higher temperatures of the year. Given the strong morphological control echinoids exert over oxygen isotopes incorporation, this taxon is potentially important to better understand fractionation processes.

Acknowledgements

We are deeply grateful to Bruce Wilkinson for significant input on earlier versions of this paper and for his insightful comments to later ones. Many thanks to Fjo DeRidder for sharing his knowledge (and algorithms!) and for his input on some sections of the paper. Thanks to JoAnn Sanner and Judith Winston for identification of the bryozoa, and to Daniel Miller for his initial help with this specimen. Salinity and density data was kindly shared by James Manning and Melissa Lamont. Thanks also to Lora Wingate, Frank Dehairs, David Gillikin, Juske Horita, Rene Schlitzer, Ray Schmitt, Christopher Stefano, Aaron O'Dea and Harry Sargous for sharing their expertise. And to Dottie Rogers for going out there every day of every month of every year.

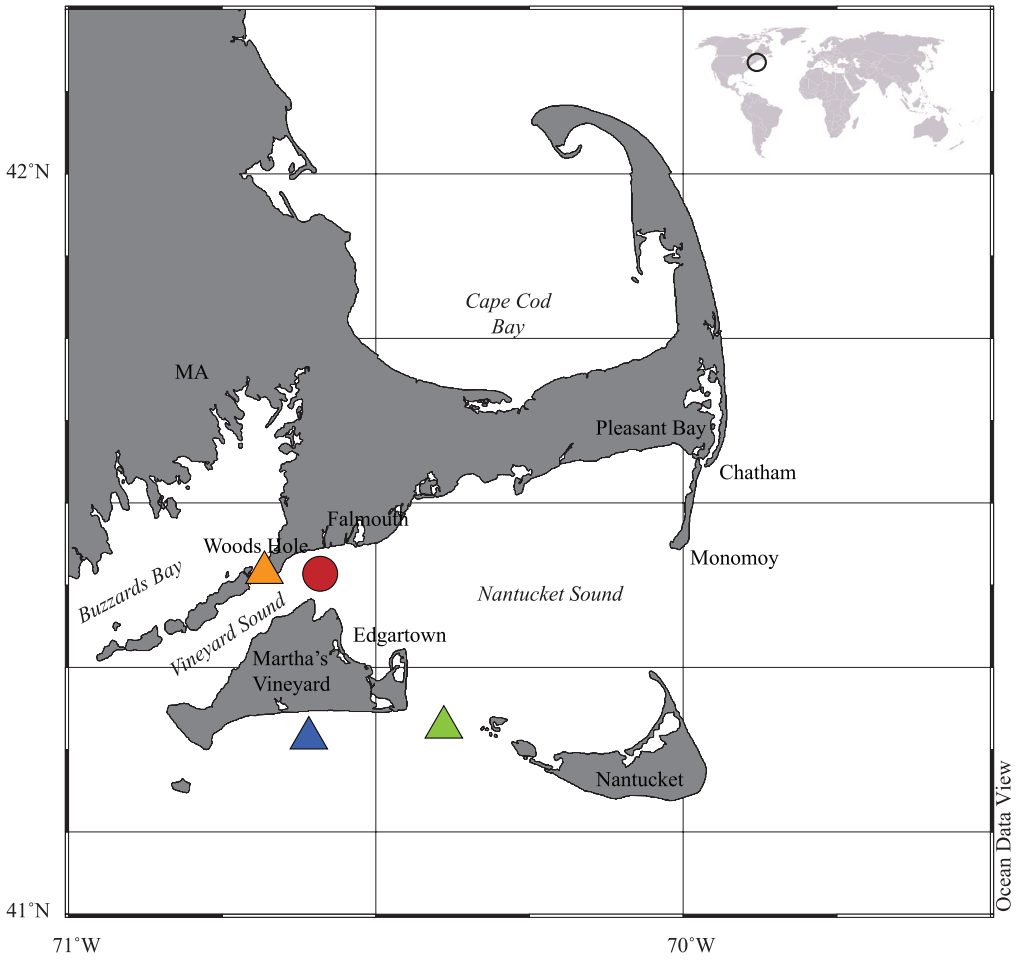

Figure 2.1. Location Map showing sampling area south of Falmouth (circle) and temperature and salinity sample sites (WHOI – yellow triangle, MVCO – blue triangle, Woods Hole Shiplight – green triangle).

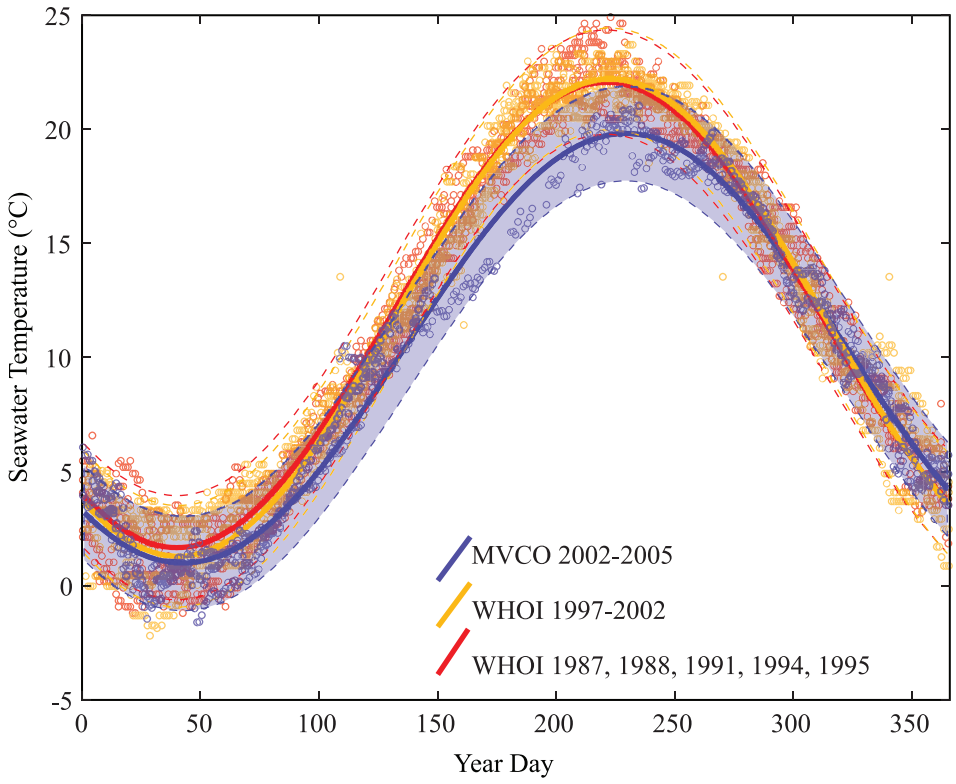

Figure 2.2. Daily average sea surface temperature from the WHOI dock for years 1987, 1988, 1991, 1994, 1995 (orange data points) and from 1997 to 2002 (yellow data points). Daily average seawater temperature from 2002 to 2005 recorded in MVCOs 12–m sea node (blue data points). Continuous lines are best–fit sinusoids to each data set, and dashed lines are 95% prediction bounds for new observations. The confidence area has been highlighted for the MVCO data (light purple). Sinusoid fits are calculated applying a non–linear least square method and trust-region algorithm in Matlab® using the equation:

$$Y = amp \times \sin(2\pi/prd \times (X–phs)) + pos$$

with amp–amplitude, prd–period, phs–phase and pos–position of the sinusoid. X is the day of the year. The residuals to the fits (not shown) are normally distributed about 0, which means the fit values represent the best daily temperature estimates.

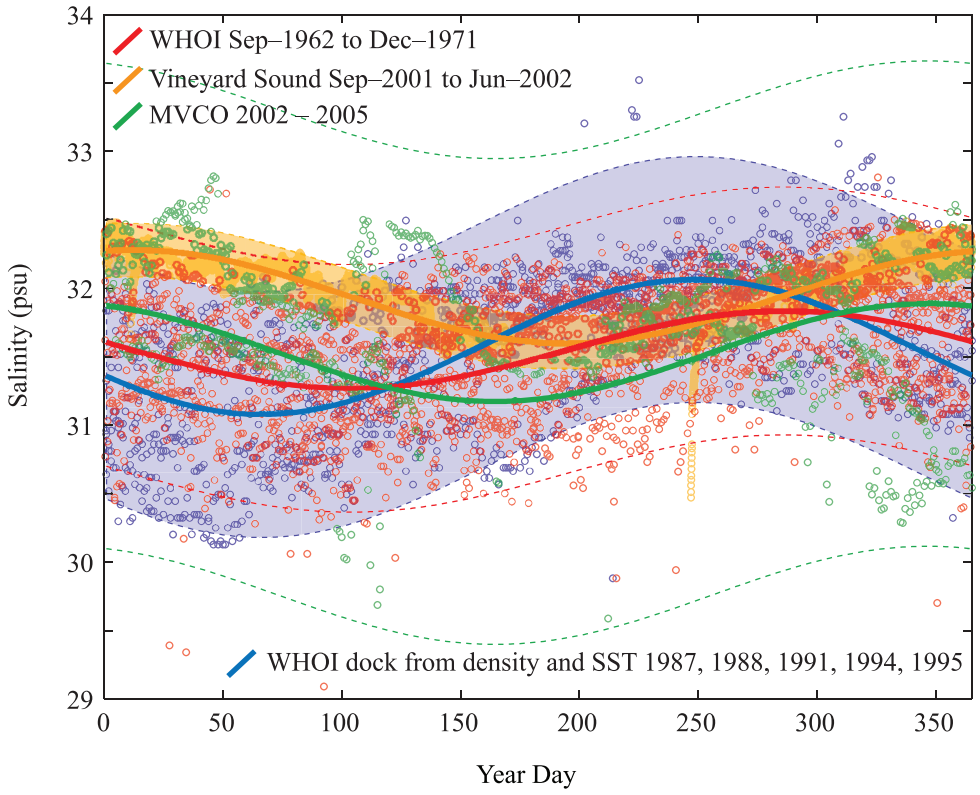

Figure 2.3. Salinity records from WHOI dock Sep–1962 to Dec–1971 (red). Recent salinity record from Vineyard Sound, Falmouth, Sep–2001 to Jun–2002 (yellow). Daily average salinity from MVCO between 2002 and 2005 (green). Calculated salinity for WHOI dock surface waters based on density and SST data for years 1987, 1988, 1991, 1994 and 1995 (blue). A single outlier was excluded from the 1962–1971 data. Continuous lines are best–fit sinusoids to each data set, and dashed lines are 95% prediction bounds for new observations. The confidence areas have been highlighted for the 2001–2002 salinity from Vineyard Sound (yellow), and for the calculated salinity from WHOI's seawater data (light purple).

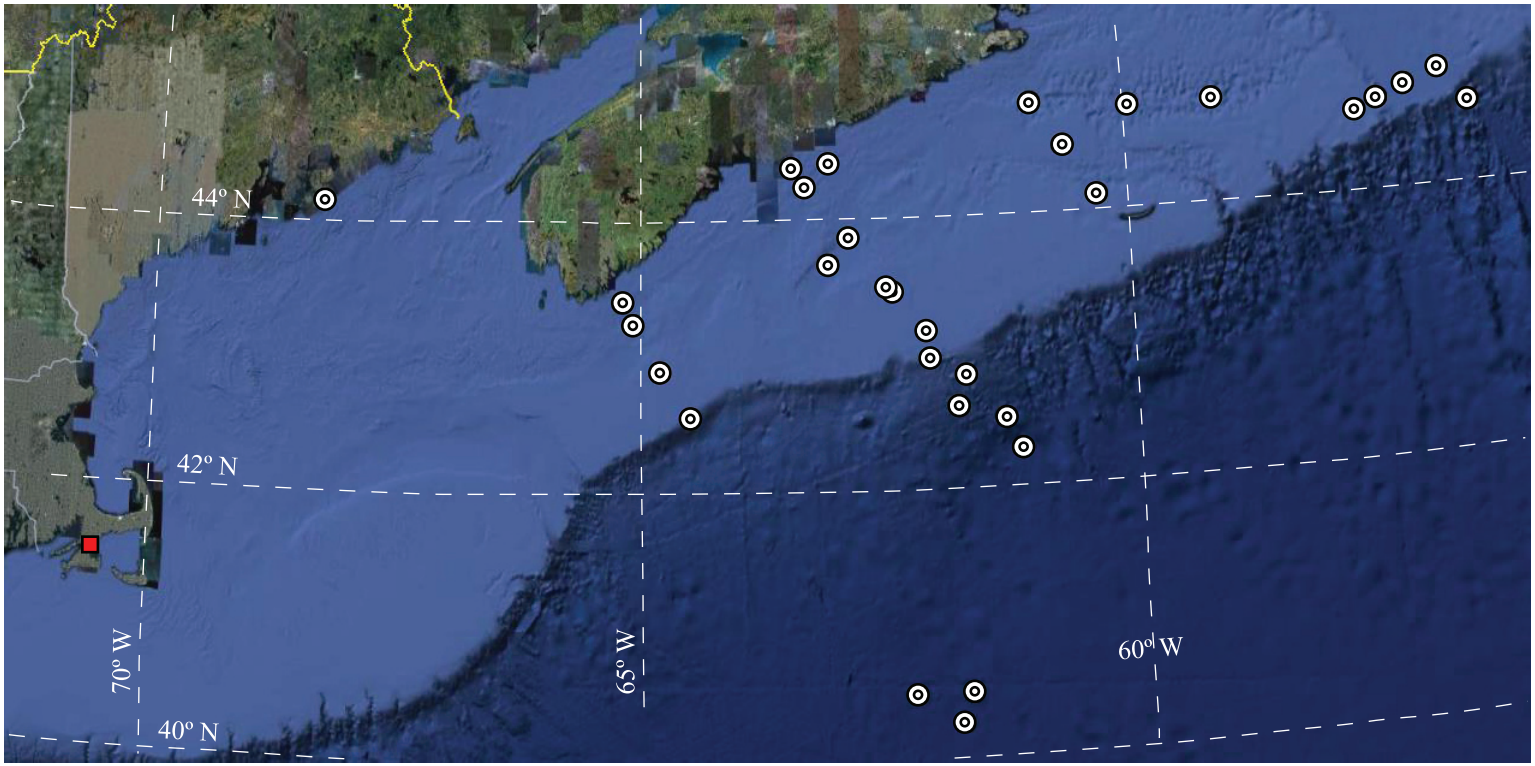

Figure 2.4. Closest available δ_w measurements to the study site (square) from 31 stations at 50 m depth or less (white circles, Schmidt et al., 1999). 83 km per longitude degree at 42 ºN.

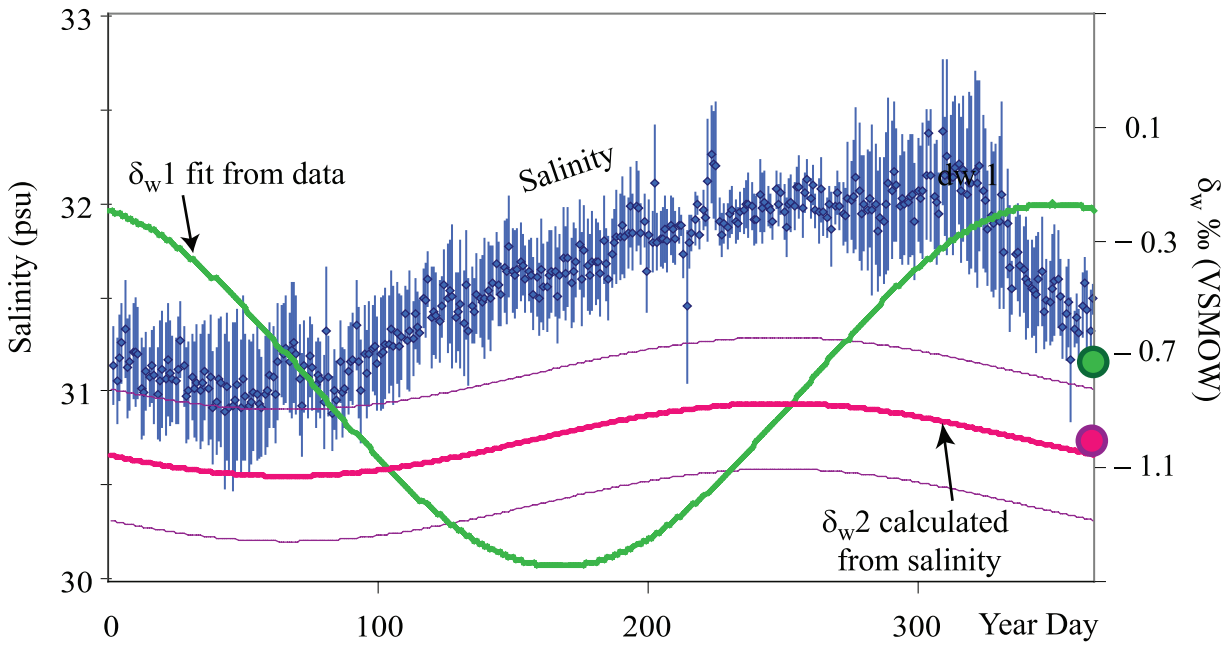

Figure 2.5. δ_w estimates. $\delta_w 1$, Best–fit sinusoid to the monthly δ_w averages from the closest available measured data. The maximum is about –0.17 ‰. $\delta_w 2$, best–fit sinusoid to δ_w calculated from salinity using $0.258 \times Salinity - 9.41$ (Fairbanks, 1982). This salinity was calculated from temperature and density data from WHOIs 1987, 1988, 1991, 1994, and 1995 data, applying the UNESCO seawater equation of state as described in Fofonoff (1985). $\delta_w 2$ daily averages are also shown (purple line). Blue diamonds and vertical lines are daily salinity averages and range of the data used to calculate $\delta_w 2$. Maximum difference between the 2 calculations (i.e., blue and pink curves) is about 1.1 ‰. Averages of the fits are shown as cirles on the right–side axis.

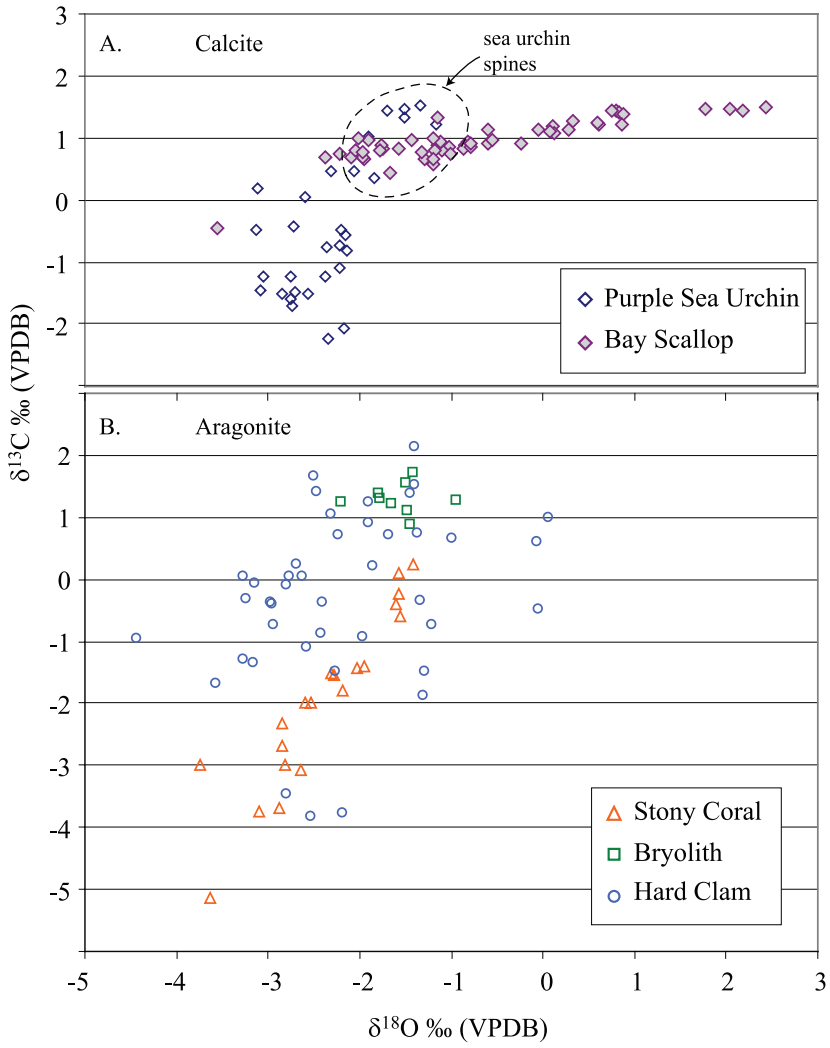

Figure 2.6. Isotopic composition of the biocenosis, $\delta^{13}C$ vs. $\delta^{18}O$ (‰VPDB). Maximum ranges correspond to the bivalves. Note the highly correlated data from the northern stony coral. $\delta^{13}C$ is particularly narrow in the bay scallop. The most positive $\delta^{18}O$ values from the purple sea urchin correspond to calcite taken from the spines.

Figure 2.7. Oxygen and Carbon isotopes compositions vs. distance. Blue diamonds are $\delta^{13}C$, white diamonds are $\delta^{18}O$. The distance is measured in mm from the umbo for the bivalves and from the nucleus for the bryolith. A. Bay scallop isotope record. B. Northern hard clam isotope record. The vertical bands correspond to opaque (white) and translucent (grey) growth bands. The distance is shown as it was measured on the hinge plate. C. Bryozoan isotope record. Each sample represents 3 to 4 zooid layers.

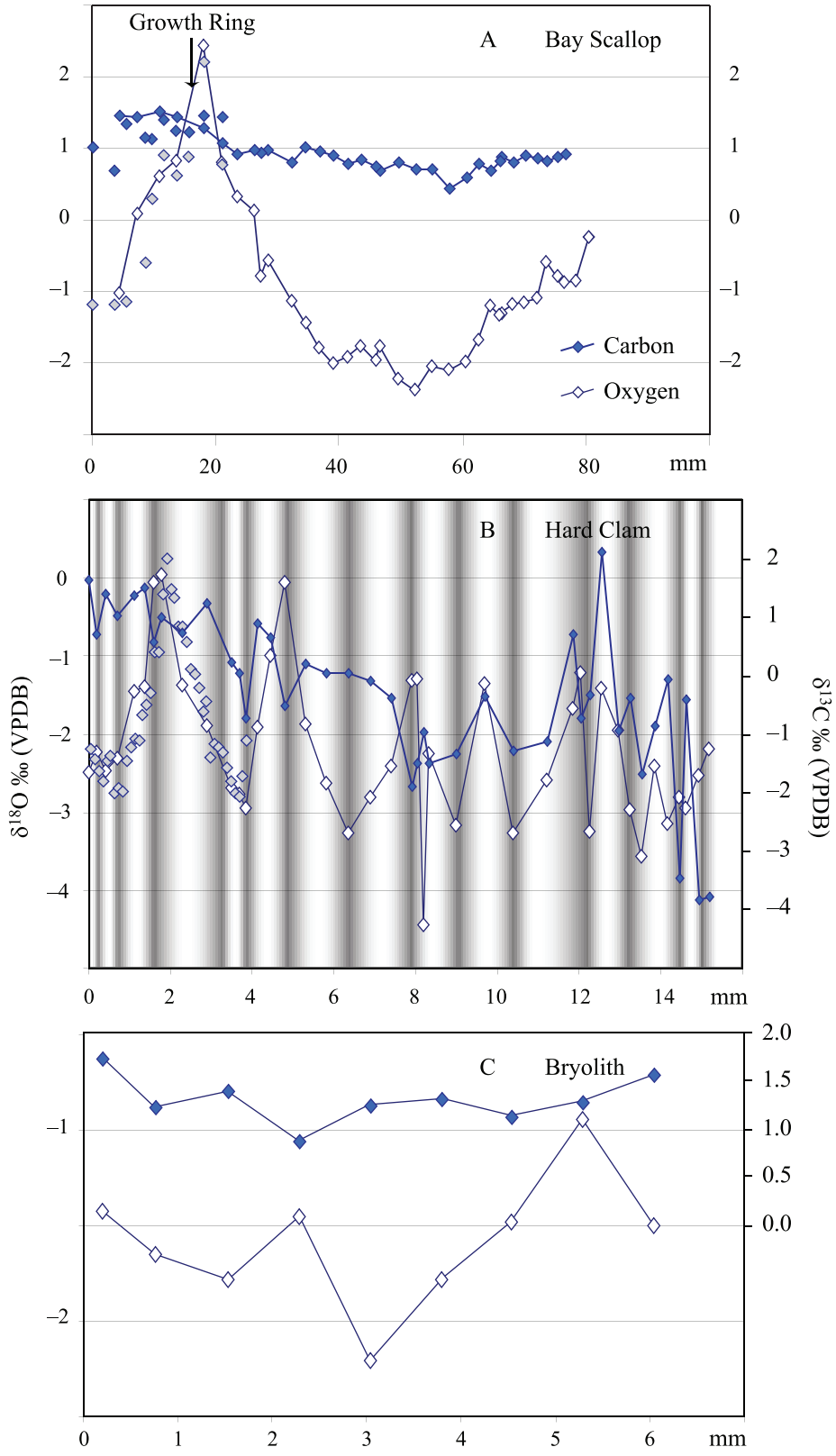
Growth Ring
A Bay Scallop
Carbon
Oxygen
mm
B Hard Clam
δ18O ‰ (VPDB)
δ13C ‰ (VPDB)
mm
C Bryolith
mm

Figure 2.8. Time series (A1, B1, C1) and growth rate functions (A2, B2, C2). A1 and A2 Bay scallop. Each diamond represents one day of precipitation. Time–series assigned using Wilkinson and Ivany (2003) best–fit sinusoid approach. Growth rates (mm/day) are interpolated from the best–fit sinusoids periods (purple line) and calculated using Goodwind et al., (2009) modified approach (blue line). B1 and B2 Hard clam. Horizontal lines are growth rates from best–fit sinusoid periods. The blue curve is the growth rate function. C1 and C2 Bryozoan. Growth is presumably continuous through the year. Growth rates were calculated using De Ridder et al., (2004) algorithm. Rate is in mm/year.

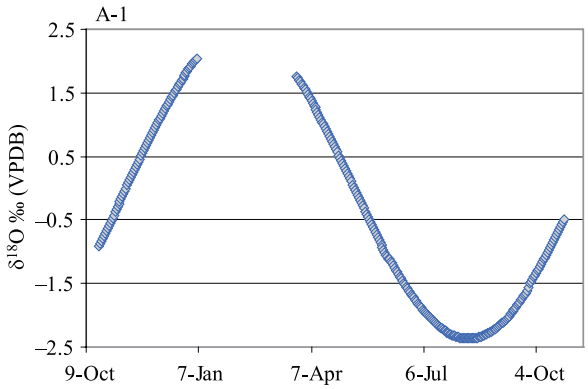
A-1
2.5
1.5
0.5
–0.5
–1.5
–2.5
δ18O ‰ (VPDB)
9-Oct
7-Jan
7-Apr
6-Jul
4-Oct

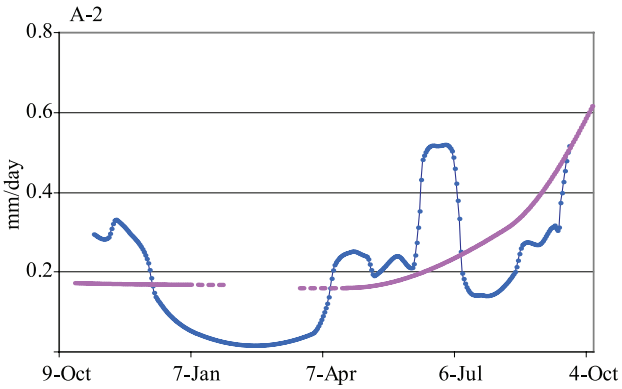
A-2
0.8
0.6
0.4
0.2
mm/day
9-Oct
7-Jan
7-Apr
6-Jul
4-Oct

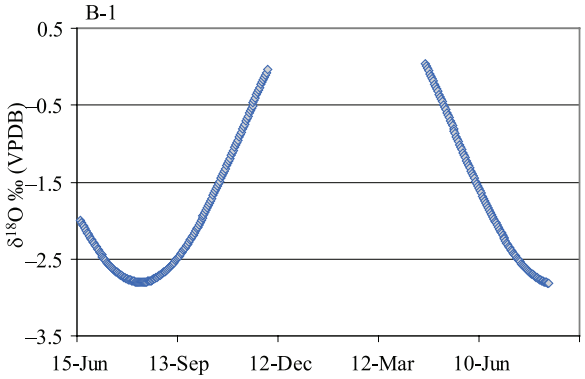
B-1
0.5
–0.5
–1.5
–2.5
–3.5
δ18O ‰ (VPDB)
15-Jun
13-Sep
12-Dec
12-Mar
10-Jun

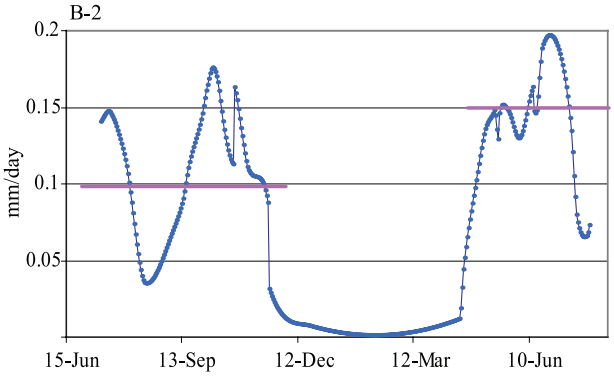
B-2
0.2
0.15
0.1
0.05
mm/day
15-Jun
13-Sep
12-Dec
12-Mar
10-Jun

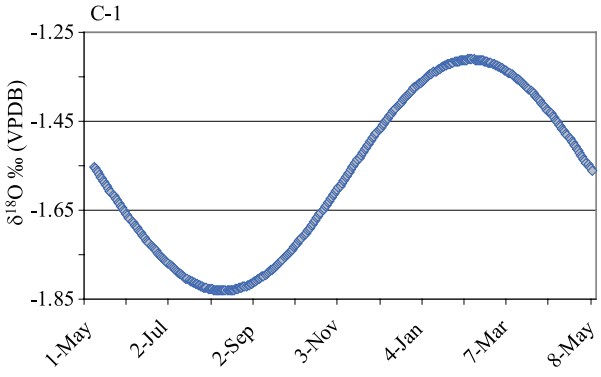
C-1
-1.25
-1.45
-1.65
-1.85
δ18O ‰ (VPDB)
1-May
2-Jul
2-Sep
3-Nov
4-Jan
7-Mar
8-May

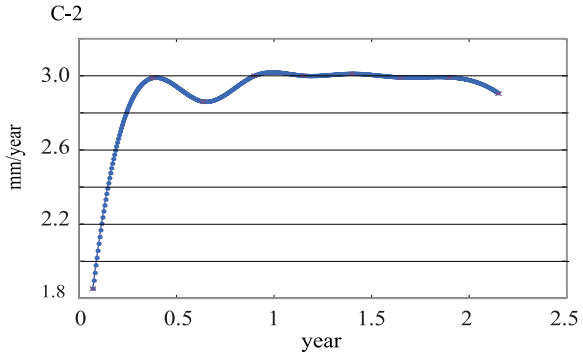
C-2
3.0
2.6
2.2
1.8
mm/year
0
0.5
1
1.5
2
2.5
year

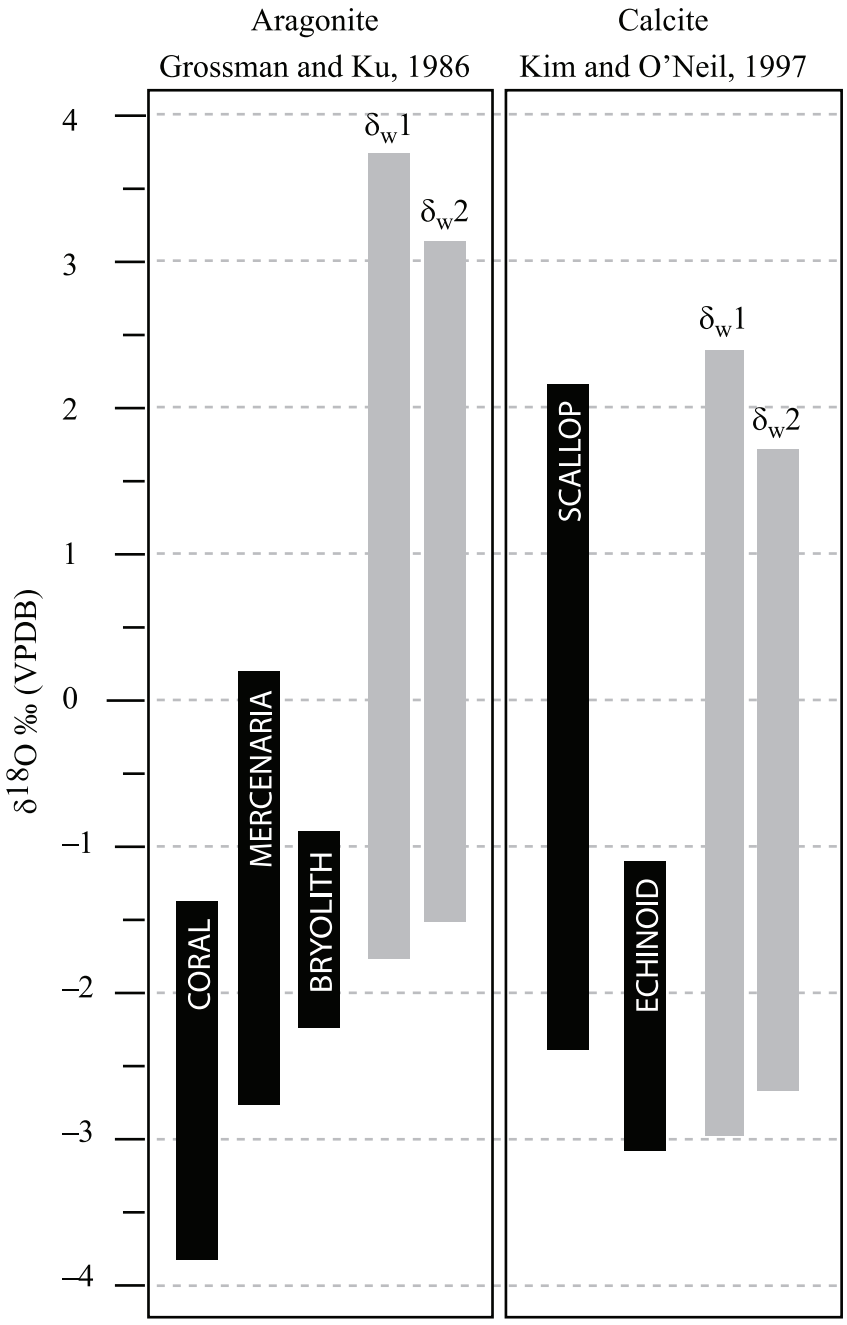

Figure 2.9. Oxygen isotope compositions of calcite and aragonite calculated using Grossman and Ku (1986) paleotemperature equation and Kim and O'Neil (1997) fractionation factors and the two δ_w estimates (from measured data ($\delta_w 1$) and from salinity data ($\delta_w 2$)) compared to the $\delta^{18}O$ ranges of the samples.

Figure 2.10. Carbonate–water fractionation factors calculated using the two δ_w estimates plotted vs. temperature and compared to published equations. A Calcite fractionation from the bay scallop data. The relationship obtained using $\delta_w 2$ has a slope comparable to other relationships and is very close to O'Neil (1969) equation, while the line based on $\delta_w 1$ diverges from all others. B Aragonite fractionation from the northern hard clam data. The line calculated using $\delta_w 2$ has a slope similar to other published equations, but is shifted to more negative $\delta^{18}O$ in the solid.

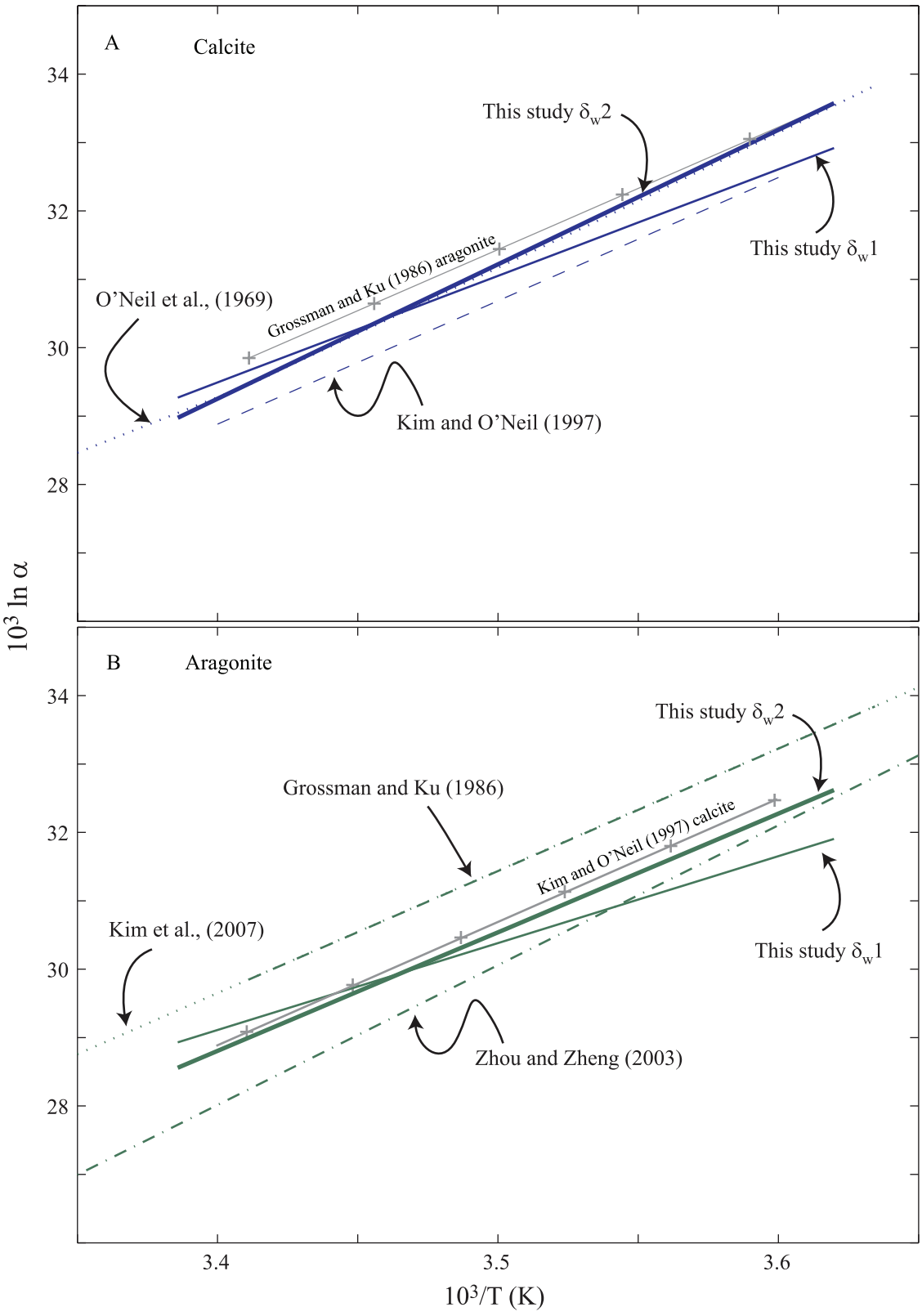
A
Calcite
This study δw2
This study δw1
Grossman and Ku (1986) aragonite
O'Neil et al., (1969)
Kim and O'Neil (1997)
B
Aragonite
This study δw2
Grossman and Ku (1986)
Kim and O'Neil (1997) calcite
Kim et al., (2007)
This study δw1
Zhou and Zheng (2003)
34
32
30
28
3.4
3.5
3.6
10³ ln α
10³/T (K)

Table 2.1. Published and estimated δ_w–salinity relations for the study site

	Reference	$\delta_w = f$(salinity)	δ_w range (‰ VSMOW) For 29 < Salinity < 33
A	In Elliot et al. (2003), from Fairbanks, reported as personal communication, 2001.	$\delta_w = 0.16 \times Salinity - 6.31$	–1.67 to –1.03
B	Fairbanks (1982). New York Bight equation from 39 °N to 41 °N, surface water and cool pool.	$\delta_w = 0.258 \times Salinity - 9.14$	–1.69 to –0.63
C	Caculated using NASA δ_w database. Schmidt et al. (1999), 40 °N–45 °N, 55 °W–70 °W, <50m depth.	$\delta_w = 0.532 \times Salinity - 18.32$	–2.89 to –0.76
D	Calculated using a freshwater end–member of –9‰ (from Kendall and Coplen, 2001), and a marine end–member of –0.5‰ and salinity 35 psu.	$\delta_w = 0.26 \times Salinity - 9.0$	–1.46 to –0.42

Table 2.2. Sinusoid fit parameters, days of precipitation, and growth rate per season for the bay scallop, the hard clam, and the bryozoan

Bay Scallop (*Argopecten irradians irradians*)

	Season[a]	2xAmplitude	Position	Phase	Period	Days of Precipitation	Growth Rate (mm/day)
1	Fall	4.82	0.03	66.7	62.4	80	0.17
2	Spring			52.1	61.3	85	0.17
3	Summer			72.3	105.4	112	0.29
4	Next Fall			83.5	235.1	28	0.64
						Total: 305, ~10 mo	

Hard Clam (*Mercenaria mercenaria)*

	Season[b]	2xAmplitude	Position	Phase	Period	Days of Precipitation	Growth Rate (mm/day)
1	Summer-Fall	4.04	-0.803	1603.0	4028.0	169	0.10
2	Spring-Summer			5548.0	6486.0	105	0.16
						Total: 274, ~ 9 mo	

Bryolith (*Parasmittina nitida*)

	Season[c]	2xAmplitude	Position	Phase	Period	Days of Precipitation	Growth Rate (mm/day)
1	One year	0.520	-1.571	1.6	2.8	365	0.01
						Total: 365, ~12 mo	

a Goodness of fit, fall R^2 =0.93; spring R^2 =0.88; summer R^2 =0.43; next fall R^2 =0.79.

b Goodness of fit, summer-fall R^2 =0.93; spring-summer R^2 =0.95.

c R^2 =0.28.

Table 2.3. Precipitation initiation and cessation dates and temperatures

Bay Scallop	Growth Function				Best-fit
Season	Precipitation Starts	T (°C)	Precipitation Stops	T (°C)	Growth Rate (mm/day)
Fall	19-Oct	15.6	6-Jan	3.1	0.171
Spring	26-Mar	4.2	----		0.368*
Next Fall	-----		26-Oct	14.4	

Hard Clam	Growth Function				Best-fit
Season	Precipitation Starts	T (°C)	Precipitation Stops	T (°C)	Growth Rate (mm/day)
Summer-Fall	8-Jun	16.5	3-Dec	7.6	0.10
Spring-Summer	23-Apr	8.4	11-Aug	22.2	0.16

* Average of the spring, summer and fall rates shown in Table 2.2.

Appendix - *Argopecten irradians* measured heights and calculated growth rates

Author	Date	Shell Height (mm)	+/-	YearDay	Growth rate[a] (mm/day)	Approximate Season Growth (mm/day)	Overall Growth (mm/day)
[b] Bricelj and Krause (1992)	15-Aug	0.43		227			
					0.62		
	15-Sep	19.67		258		0.37	
					0.27		
	5-Dec	41.51		339			
	15-Apr	43.24		470			
					0.08		0.10
	25-May	46.57		510		0.08	
					0.04		
	20-Jul	48.74		566			
					0.11		
	30-Oct	59.73		668			
	25-Apr	63.49		845			
[c] Tettelbach (1991)	7-Aug	4.70		219			
					0.24		
	15-Sep	14.10	4	258			
					0.36		
	20-Oct	26.63	5	293		0.26	
					0.33		
	22-Nov	37.38	5	326			
					0.11		
	20-Dec	40.40	4	354			
	10-Feb	41.75	4	406			
					0.00		
	17-Mar	40.16	4	441			
					0.00		
	2-May	39.85	4	487			
					0.02		0.13
	20-May	40.25	4	505			
					0.05		
	20-Jun	41.94	4	536			
					0.10	0.07	
	25-Jul	45.36	4	571			
					0.08		
	15-Aug	47.11	3	592			
					0.16		
	5-Oct	55.18	4	643			
					0.00		
	1-Nov	55.22	6	670			
					0.28		
	1-Dec	63.71	9	700			
					0.04		
	31-Dec	64.87	7	730			

Appendix - *Argopecten irradians* measured heights and calculated growth rates (Continued)

Author	Date	Shell Height (mm)	+/-	YearDay	Growth rate[a] (mm/day)	Approximate Season Growth (mm/day)	Overall Growth (mm/day)
	2-Oct	23.29		275			
					0.17	0.17	
	4-Dec	34.24		338			
	11-Jan	34.24		376			
					0.00		
	20-Mar	34.24		444			
					0.00		
	21-Apr	34.24		476			
					0.14		
	30-May	39.51		515			
					0.07		
[d] Belding (1910, 1931)	1-Jul	41.77		547			0.13
					0.09	0.08	
	1-Aug	44.57		578			
					0.18		
	18-Sep	53.42		626			
					0.17		
	16-Oct	58.11		654			
					0.09		
	16-Nov	60.98		685			
					0.02		
	3-Dec	61.27		702			
	11-Jan	61.27		741			

[a] Calculated here.

[b] 1986 cohort of *A. irradians irradians* followed from Aug. 1986 to Apr. 1988. in the Niantic River, CT. 200 to 300 individuals per sampling date.

[c] 1983 cohort of *A. irradians irradians* followed from Aug. 1983 to Dec. 1984 in the Poquonock River, CT. Sample size varied from 4 to 127 individuals per sampling date.

[d] Average from several hundred scallops measured in years 1904, 1905 and 1906 in Nantucket, Edgartown, Chatham, Monomoy, North Falmouth and Marion.

References

Ansell, A.D., 1968. The rate of growth of the hard clam *Mercenaria mercenaria* (L.) throughout the geographical range. Conseil Permanent International pour l'Exploration de la Mer, Journal du Conseil, 31 (3): 364-409.

Appleyard, C., and Dealteris, J.T., 2001. Modeling growth of the northern quahog, *Mercenaria mercenaria*. Journal of Shellfish Research, 20 (3): 1117-1125.

Bader, B., and Schafer, P., 2005. Impact of environmental seasonality of stable isotope composition of skeletons of the temperate bryozoan *Cellaria sinuosa*. Palaeogeography, Palaeoclimatology, Palaeoecology, 226: 58-71.

Barber, B.J., and Blake, N.J., 2006. Reproductive Physiology. *In* Shumway, S., and Parsons, G.J., eds., Scallops: Biology, Ecology and Aquaculture, Developments in aquaculture and fisheries science, 35, Elsevier, Amsterdam: 357-416.

Barber, B.J., and Davis, C., 1997. Growth and mortality of cultured bay scallops in the Damariscotte River, Maine (USA). Aquaculture International, 5: 451-460.

Bathurst, R.G.C., 1975. Carbonate sediments and their diagenesis. Elsevier, Amsterdam, 593 p.

Beelaerts, V., De Ridder, F., Schmitz, N., Bauwens, M., Dehairs, F., Schoukens, J., and Pintelon, R., 2009. On the elimination of bias averaging-errors in proxy records. Mathematical Geosciences, 41 (2): 129-144.

Belding, D., 1910. A report upon the scallop fishery of Massachusetts, including the habits, life history of *Pecten irradians*, its rate of growth, and other facts of economic value. The Massachusetts commission on fisheries and game, 150 p.

—, 1931. The scallop fishery of Massachusetts, including an account of the natural history of the common scallop. The Commonwealth of Massachusetts, Department of conservation, Marine Fisheries Series, No. 3, 51 p.

Blake, N.J., and Shumway, S., 2006. Bay Scallop and Calico Scallop fisheries, culture and enhancement in eastern North America. *In* Shumway, S., and Parsons, G.J., eds., Scallops: Biology, Ecology and Aquaculture, Developments in aquaculture and fisheries science, 35, Elsevier, Amsterdam: 945-964.

Böehm, F., Joachimski, M.M., Dullo, W.-C., Eisenhauer, A., Lehnert, H., Reitner, J., and Woerheide, G., 2000. Oxygen isotope fractionation in marine aragonite of coralline sponges. Geochimica et Cosmochimica Acta, 64 (10): 1695-1703.

Bologna, P., 1998. Growth, production and reproduction in bay scallops *Argopecten i. concentricus* (Say) from the northern gulf of Mexico. Journal of Shellfish Research, 17 (4): 911-917.

Bornhold, B.D., and Milliman, J.D., 1973. Generic and environmental control of carbonate mineralogy in serpulid (Polychaete) tubes. The Journal of Geology, 81: 363-373.

Brey, T., Gutt, J., Mackensen, A., and Starmans, A., 1998. Growth and productivity of the high Antarctic bryozoan *Melicerita obliqua*. Marine Biology, 132: 327-333.

Bricelj, V.M., Epp, J., and Malouf, R., 1987. Intraspecific variation in reproductive and somatic growth cycles of bay scallops *Argopecten irradians*. Mar. Ecol. Prog. Ser., 36: 123-137.

Bricelj, V.M., and Krause, M.K., 1992. Resource allocation and population genetics of the bay scallop, *Argopecten irradians irradians*: effects of age and allozyme

heterozygosity on reproductive output. Marine Biology, 113: 253-261.
Carré, M., Bentaleb, I., Blamart, D., Ogle, N., Cardenas, F., Zevallos, S., Kalin, R.M., Ortilieb, L., and Fontugne, M., 2005. Stable isotopes and sclerochronology of the bivalve *Mesodesma donacium*: potential application to Peruvian paleoceanographic reconstructions. Palaeogeography, Palaeoclimatology, Palaeoecology, 228: 4-25.
Carriker, M.R., 1961. Interrelation of functional morphology, behavior, and autoecology in early stages of the bivalve Mercenaria mercenaria. Journal of the Elishe Mitchell Scientific Society, 77: 168-241.
Castagna, M., and Duggan, W., 1971. Rearing the bay scallop, *Aequipected irradians*. Proceedings of the National Shellfisheries Association, 61: 80-85.
Chacko, T., and Deines, P., 2008. Theoretical calculation of oxygen isotope fractionation factors in carbonate systems. Geochimica et Cosmochimica Acta, 72: 3642-3660.
Couturier, C., Dabinett, P., and Lantelgne, M., 1995. Scallop culture in Atlantic Canada. *In* Boghen, A.D., ed., Cold-water aquaculture in Atlantic Canada, Canadian Institute for Research on Regional Development, Moncton: 297-340.
Crandall, E.R., 1954. Hydrometers and hydrometry. Detroit, 94 p.
Dame, R.F., 1996. Ecology of marine bivalves: an ecosystem approach. CRC Press, Boca Raton, 245 p.
de Brauwere, A., De Ridder, F., Pintelon, R., Meersmans, J., Schoukens, J., and Dehairs, F., 2008. Identification of a periodic time series from an environmental proxy record. Computers and Geosciences, 34: 1781-1790.
de Brauwere, A., De Ridder, F., Pintelon, R., Schoukens, J., and Dehairs, F., 2009. A comparative study of methods to reconstruct a periodic time series from an environmental proxy record. Earth-Science Reviews, in press.
De Ridder, F., de Brauwere, A., Pintelon, R., Schoukens, J., Dehairs, F., Baeyens, W., and Wilkinson, B.H., 2007. Comment on: Paleoclimatic inference from stable isotope profiles of accretionary biogenic harparts-a quantitative approach to the evaluation of incomplete data, by Wilkinson, B. H., Ivany, L. C., 2002. Palaeogeogr. Palaeocl. Palaeoecol. 185, 95-114. Palaeogeography, Palaeoclimatology, Palaeoecology, 248: 473-476.
De Ridder, F., Pintelon, R., Schoukens, J., Gillikin, D.P., Andre, L., Baeyens, W., de Brauwere, A., and Dehairs, F., 2004. Decoding nonlinear growth rates in biogenic environmental archives. Geochem., Geophys. Geosyst., 5 (12).
Dettman, D.L., and Lohmann, K.C., 1995. Microsampling carbonates for stable isotope and minor element analysis; physical separation of samples on a 20 micrometer scale. Journal of Sedimentary Research, (65): 566-569.
Dimond, J., and Carrington, E., 2007. Temporal variation in the symbiosis and growth of the temperate scleractinian coral *Astrangia poculata*. Mar. Ecol. Prog. Ser., 348: 161-172.
Ebert, T.A., 1985. The non-periodic nature of growth rings in echinoid spines, *in* Keegan, B.F., and O'Connor, B.D.S., eds. Fifth international echinoderm conference, Galway, Ireland: 261-268 p.
—, 1986. A new theory to explain the origin of growth lines in sea urchin spines. Mar. Ecol. Prog. Ser., 34: 197-199.

—, 2007. Growth and survival of postsettlement sea urchins. *In* Lawrence, J.M., ed., Edible Sea Urchins: Biology and Ecology, Developments in aquaculture and fisheries science, 37, Elsevier Science: 95-134.

Elliot, M.B., deMenocal, B.K.L., and Howe, S.S., 2003. Environmental controls on the stable isotopic composition of *Mercenaria mercenaria*. Potential application to paleoenvironmental studies. Geochem., Geophys. Geosyst., 4 (7): 1056.

Epstein, S., Buchsbaum, R., Lowenstam, H.A., and Urey, H.C., 1953. Revised carbonate-water isotopic temperature scale. Geological Society of America Bulletin, 64 (11): 1316-1326.

Estabrooks, S.L., 2007. The possible role of telomeres in the short life span of the bay scallop, *Argopecten irradians irradians* (Lamarck 1819). Journal of Shellfish Research, 26 (2): 307-313.

Eversole, A., 2001. Reproduction in *Mercenaria mercenaria*. *In* Kraeuter, J.N., and Castagna, M., eds., Biology of the Hard Clam, Developments in aquaculture and fisheries science, 31, Elsevier, Amsterdam: 221-256.

Fairbanks, R.G., 1982. The origin of continental shelf and slope water in the New York Bight and Gulf of Maine; evidence from $H_2{}^{18}O/H_2{}^{16}O$ ratio measurements. Journal of Geophysical Research. C. Oceans and Atmospheres, 87 (8): 5796-5808.

Fofonoff, N.P., 1985. Physical properties of seawater: a new salinity scale and equation of state for seawater. Journal of Geophysical Research. C. Oceans and Atmospheres, 90 (4): 3332-3342.

Fritz, L.W., 2001. Shell struture and age determination. *In* Kraeuter, J.N., and Castagna, M., eds., Biology of the Hard Clam, Developments in aquaculture and fisheries science, 31, Elsevier, Amsterdam: 53-74.

Goodwin, D.H., Prabasaj, P., and Wissink, C., 2009. MoGroFunGen: a numerical model for reconstructing intra-annual growth rates of bivalve molluscs. Palaeogeography, Palaeoclimatology, Palaeoecology, 276: 47-55.

Goodwin, D.H., Schöne, B.R., and Dettman, D.L., 2003. Resolution and fidelity of oxygne isotopes as paleotemperature proxies in bivalve mollusk shells: models and observations. Palaios, 18: 110-125.

Grossman, E.L., and Ku, T.-L., 1986. Oxygen and carbon isotope fractionation in biogenic aragonite; temperature effects. Chemical Geology; Isotope Geoscience Section, 59 (1): 59-74.

Helm, N.E., and Malouf, R.E., 1983. Rate of production of external ridges in the bay scallop, *Argopecten irradians*. American Zoologist, 23 (4): 1024.

Henry, K.M., and Nixon, S.W., 2008. A half century assessment of hard clam, *Mercenaria mercenaria*, growth in Narragansett Bay, Rhode Island. Estuaries and Coasts, 31: 755-766.

Hill, S.K., Aragona, J.B., and Lawrence, J.M., 2004. Growth bands in test plates of the sea urchins *Arbacia punctulata* and *Lytechinus variegatus* (Echinodermata) on the Central Florida Gulf Coast Shelf. Gulf of Mexico Science, 22 (1): 96-100.

Hill, S.K., and Lawrence, J.M., 2006. Interactive effects of temperature and nutritional condition on the energy budgets of the sea urchins *Arbacia punctulata* and *Lytechinus variegatus* (Echinodermata: Echinoidea). Journal of the Marine Biological Association of the United Kingdom, 86 (4): 783-790.

Hottinger, L., 1983. Neritic macroid genesis, an ecological approach. *In* Peryt, T.M., ed., Coated Grains, Springer, Berlin: 38-55.

Ivany, L.C., Wilkinson, B.H., and Jones, D.S., 2003. Using stable isotopic data to resolve rate and duration of growth throughout ontogeny: and example from the surf clam *Spisula solidissima*. Palaios, 18: 126-137.

Ivany, L.C., Wilkinson, B.H., Lohmann, K.C., Johnson, E.R., McElroy, B., and Cohen, G.J., 2004. Intra-annual isotopic variation in *Venericardia* bivalves: implications for Early Eocene temperature, seasonality, and salinity on the U. S. Gulf Coast. Journal of Sedimentary Research, 74 (1): 7-19.

Jacques, T.G., Marshall, N., and Pilson, M.E.Q., 1983. Experimental ecology of the temperate scleractinian coral *Astrangia danae*. II. Effect of temperature, light intensity and symbiosis with *zooxanthellae* on metabolic rate and calcification. Marine Biology, 76: 135-148.

Jones, D.S., 1981. Annual growth increments in shells of *Spisula solidissima* record marine temperature variability. Science, 211 (4478): 165-167.

—, 1983. Sclerochronology: reading the record of the molluscan shell. American Scientist, 71: 384-391.

Jones, D.S., Arthur, M.A., and Allard, D.J., 1989. Sclerochronological records of temperature and growth from shells of *Mercenaria mercenaria* from Narragansett Bay, Rhode Island. Marine Biology, 102: 225-234.

Jones, D.S., and Quitmyer, I.R., 1996. Marking time with bivalve shells; oxygen isotopes and season of annual increment formation. Palaios, 11 (4): 340-346.

Jones, D.S., Quitmyer, I.R., Arnold, W.S., and Marelli, D.C., 1990. Annual shell banding, age, and growth rate of hard clams (*Mercenaria* spp.) from Florida. Journal of Shellfish Research, 9: 215-225.

Keith, M.L., and Weber, J.N., 1965. Systematic relationships between carbon and oxygen isotopes in carbonates deposited by modern corals and algae. Science, 150 (3695): 498-501.

Kendall, C., and Coplen, T.B., 2001. Distribution of oxygen-18 and deuterium in river waters across the United States. Hydrological Processes, 15 (7): 1363-1393.

Kennish, M.J., 1980. Shell microgrowth analysis: *Mercenaria mercenaria* as type example for research in population dynamics. *In* Rhoads, D.C.L., Richard A, ed., Skeletal growth of aquatic organisms, Plenum Press, NY: 255-292.

Kidwell, S.M., and Gyllenhaal, E.D., 1998. Symbiosis, competition, and physical disturbance in the growth histories of Pliocene cheilostome bryoliths. Lethaia, 31: 221-239.

Kim, S.-T., O'Neil, J.R., Hillaire-Marcel, C., and Mucci, A., 2007. Oxygen isotope fractionation between synthetic aragonite and water: influence of temperature and Mg^{+2} concentration. Geochimica et Cosmochimica Acta, 71: 4704-4715.

Kissling, D.L., 1973. Circumrotatory growth form in Recent and Silurian corals. *In* Boardman, R.S., Cheetham, A.H.*, et al.*, eds., Animal Colonies, Dowden, Hutchinson & Ross, Stroudsburg.

Krantz, D.E., Williams, D.F., and Jones, D.S., 1987. Ecological and paleoenvironmental information using stable isotope profiles from living and fossil molluscs. Palaeogeography, Palaeoclimatology, Palaeoecology, 58 (3-4): 249-266.

Leder, J.J., Swart, P.K., Szmant, A.M., and Dodge, R.E., 1996. The origin of variations in the isotopic record of scleractinian corals: I. Oxygen. Geochimica et Cosmochimica Acta, 60 (15): 2857-2870.

Lisiecki, L.E., and Raymo, M.E., 2005. A Pliocene-Pleistocene stack of 57 globally distributed benthic $\delta^{18}O$ records. Palaeogeoceanography, 20: 1003.

Lowenstam, H.A. and Epstein, S., 1957. On the origin of sedimentary aragonite needles of the Great Bahama Bank. California Institute of Technology, Contribution No. 810.

MacDonald, B.A., Bricelj, V.M., and Shumway, S., 2006. Physiology: energy acquisition and utilisation. *In* Shumway, S., and Parsons, G.J., eds., Scallops: Biology, Ecology and Aquaculture, Developments in aquaculture and fisheries science, 35, Elsevier, Amsterdam: 417-477.

MacFarlane, S.L., 1991. Managing scallops *Argopecten irradians irrandias* (Lamarck 1819) in Pleasant Bay, Massachusetts; large is not always legal. *In* Shumway, S., and Sandifer, P.A., eds., An international compendium of scallop biology and culture, Baton Rouge: 264-272.

—, 1999. Bay scallops in Massachusetts waters: a review of the fishery and prospects for future enhancement and aquaculture. Barnstable County's Cape Cod Cooperative Extension, SEMAC, http://www.ci.chilmark.ma.us/Pages/ChilmarkMA_BBoard/Archived%20News/FinalScallopReport.pdf.

Malouf, R., and Bricelj, V.M., 1989. Comparative biology of clams: environmental tolerances, feeding, and growth. *In* Manzi, J.J., and Castagna, M., eds., Clam Manriculture in North America, Developments in aquaculture and fisheries science, 19, Elsevier, Amsterdam: 23-73.

Manning, J., 2006. Environmental monitors on lobster traps. Phase II: Salinity. National Oceanic Atmospheric Administration, Northeast Fisheries Science Center, http://www.nefsc.noaa.gov/epd/ocean/MainPage/lob/saltfinal.pdf.

Martinson, D.G., Menke, W., and Stoffa, P., 1982. An inversal approach to signal correlation. Journal of Geophysical Research. B., 87 (B6): 4807-4818.

Mercaldo, R.S., and Rhodes, E.W., 1982. Influence of reduced salinity on the Atlantic bay scallop *Argopecten irradians* (Lamarck) at various temperatures. Journal of Shellfish Research, 2 (2): 177-181.

Milliman, J.D., 1974. Marine Carbonates, Recent Sedimentary Carbonates, Volume 1, Springer-Verlag, Berlin: 375.

Moore, H., 1966. Ecology of Echinoids. *In* Boolootian, R.A., ed., Physiology of echinodermata; a collective effort by a group of experts, Interscience Publishers - John Wiley & Sons, New York: 73-86.

Myers, P., Espinosa, R., Parr, C.S., Jones, T., Hammond, G.S., and Dewey, T.A., 2006. The Animal Diversity Web (online), http://animaldiversity.org.

O'Dea, A., 2005. Zooid size parallels contemporaneous oxygen isotopes in a large colony of *Pentapora foliacea* (Bryozoa). Marine Biology, 146 (5): 1075-1081.

Paillard, D., Labeyrie, L., and Yiou, P., 1996. Macintosh program performs time-series analysis. EOS, Transaction, American Geophysical Union, 77 (39): 379.

Panella, G., and MacClintock, C., 1968. Biological and environmental rhythms reflected in molluscan shell growth. Journal of Paleontology, 42: 64-80.

Patterson, W.P., Smith, G.R., and Lohmann, K.C., 1993. Continental paleothermometry and seasonality using the isotopic composition of aragonitic otoliths of freshwater fishes. *In* Swart, P.K., Lohmann, K.C.*, et al.*, eds., Climate change in continental isotopic records, Geophysical Monograph, 48, American Geophysical Union, Washington, DC.

Pätzold, J., Ristedt, H., and Wefer, G., 1987. Rate of growth and longevity of a large colony of *Pentapora foliacea* (Bryozoa) recorded in their oxygen isotope profiles. Marine Biology, 96: 535-538.

Quitmyer, I.R., Jones, D.S., and Arnold, W.S., 1997. The sclerochronology of hard clams, *Mercenaria spp*., from the south-eastern USA: A method of elucidating the zooarchaeological records of seasonal resource procurement and seasonality in prehistoric shell middens. Journal of Archaeological Science, 24 (9): 825-840.

Raymo, M.E., 2006. Plio-Pleistocene ice volume, Antarctic climate, and the global $\delta^{18}O$ record. Science, 313: 492.

Reguant, S., Fernandez, J., Rodriguez-Fernandez, J., and Serra-Keil, J., 1991. Bryozoan biofacies, zoarial forms and sedimentary environments in the Tertiary of Spain, *in* Bigey, F.P., ed. Bryozoa living and fossil; 8th International conference on Bryozoa, Bulletin de la Societe des Sciences Naturelles de l'Ouest de la France, Paris: 361-370 p.

Rider, J., and Enrico, R., 1979. Structural and functional adaptations of mobile anascan ectoproct colonies (ectoproctaliths). *In* Larwood, G.P., and Abbott, M.B., eds., Advances in Bryozoology, Systematics Association, 13, Academic Press, London: 297-319.

Sastry, A.N., 1961. Studies on the bay scallop, *Aequipecten irradians concentricus* Say, in Alligator Harbor, Florida, Ph.D. thesis, Florida State University. 125 p.

—, 1966. Temperature effects in reproduction of the bay scallop, *Aequipecten irradians* Lamarck. Biological Bulletin, 130 (1): 118-134.

Schmidt, G.A., Bigg, G.R., and Rohling, E.J., 1999. Global seawater oxygen-18 database, http://data.giss.nasa.gov/o18data/

Schmitt, R., 2008. Salinity at the Dock, http://www.whoi.edu/science/po/people/rschmitt/

Schöne, B.R., Rodland, D.L., Fiebig, J., Oschmann, W., Goodwin, D.H., Flessa, K.W., and Dettman, D.L., 2006. Reliability of multitaxon, multiproxy reconstructions of environmental conditions from accretionary biogenic skeletons. The Journal of Geology, 114: 267-285.

Smith, A.M., Key Jr., M.M., and Gordon, D.P., 2006. Skeletal mineralogy of bryozoans: Taxonomic and temporal patterns. Earth-Science Reviews, 78: 287-306.

Stanley, J.G., and DeWitt, R., 1983. Species profiles: life histories and environmental requirements of coastal fishes and invertebrates (North Atlantic)-Hard Clam. TR EL-82-4, U. S. Fish and Wildl. Serv., FWS/OBS-82/11.18, 35 p.

Stebbing, A.R.D., 1971. Growth of *Flustra foliacea* (Bryozoa). Marine Biology, 9: 267-273.

Surge, D., Lohmann, K.C., and Dettman, D.L., 2001. Controls on isotopic chemistry of the American oyster, *Crassostrea virginica*; implications for growth patterns. Palaeogeography, Palaeoclimatology, Palaeoecology, 172 (3-4): 283-296.

Swart, P.K., 1983. Scleractinian corals, a review. Earth-Science Reviews, 19: 51-80.

Tarutani, T., Clayton, R.N., and Mayeda, T.K., 1969. The effect of polymorphism and magnesium substitution on oxygen isotope fractionation between calcium carbonate and water. Geochimica et Cosmochimica Acta, 33: 987-996.

Taylor, R., and Capuzzo, J., 1983. The reproductive cycle of the bay scallop, *Argopecten irradians irradians* (Lamarck), in a small coastal embayment on Cape Cod, Massachusetts. Estuaries, 6 (4): 431-435.

Tettelbach, S.T., 1991. Seasonal changes in a population of northern bay scallops, *Argopecten irradians irradians* (Lamarck, 1819). World Aquaculture Workshops, 1: 164-175.

Tettelbach, S.T., Auster, P.J., Rhodes, E.W., and Widman, J.C., 1985. A mass mortality of northern bay scallops, *Argopecten irradians irradians*, following a severe spring rainstorm. The Veliger, 27 (4): 381-385.

Theroux, R.B., and Wigley, R.L., 1998. Quantitative composition and distribution of the macrobenthic invertebrate fauna of the continental shelf ecosystems of the northeastern United States. NOAA, NMFS -140, 240 p.

Veizer, J., 1983. Trace elements and isotopes in sedimentary carbonates. Reviews in Mineralogy, 11: 265-299.

Weber, J.N., and Raup, D.M., 1966. Fractionation of the stable isotopes of carbon and oxygen in marine calcareous organisms - the Echinoidea. Part I. Variation of C^{13} and O^{18} content within individuals. Geochimica et Cosmochimica Acta, 30: 681-703.

White, R.M.P., Dennis, P.F., and Atkinson, T.C., 1999. Experimental calibration and field investigation of the oxygen isotopic fractionation between biogenic aragointe and water. Rapid communications in mass spectrometry, 13: 1242-1247.

Wigley, R.L., and Theroux, R.B., 1981. Atlantic continental shelf and slope of the United States; macrobenthic invertebrate fauna of the Middle Atlantic Bight region; faunal composition and quantitative distribution. U.S. Geological Survey, 529-N, 197 p.

Wilkinson, B.H., and Ivany, L., 2002. Paleoclimatic inference from stable isotope profiles of accretionary biogenic hardparts - a quatitative approach to the evaluation of incomplete data. Palaeogeography, Palaeoclimatology, Palaeoecology, 185: 95-114.

Zachos, J., Pagani, M., Sloan, L., Thomas, E., Billups, K., Smith, J. (prefacer), and Uppenbrink, J. (prefacer), 2001. Trends, rhythms, and aberrations in global climate 65 Ma to present; Paleoclimate; Earth's variable climatic past. Science, 292 (5517): 686-693.

Zheng, Y.-F., and Zhou, G.-T., 2007. Response to the comment by J. Horita and R. N. Clayton on "The studies of oxygen isotope fractonation between calcium carbonates and water at low temperatures". Geochimica et Cosmochimica Acta, 71: 3136-3143.

Zhou, G.-T., and Zheng, Y.-F., 2003. An experimental study of oxygen isotope fractionation between inorganically precipitated aragonite and water at low temperatures. Geochimica et Cosmochimica Acta, 67 (3): 387-399.

Zhou, G., and Zheng, Y., 2000. Experimental studies of oxygen isotope fractionation between $CaCO_3$ and H_2O at low temperatures. Dixue Qianyuan - Earth Science Frontiers, 7 (2): 321-338.

CHAPTER 3

Evaluation of the environmental signal in modern *Mercenaria sp.* from temperature and salinity data along the U. S. east coast. Implications for paleoenvironmental interpretations from fossil clams

Abstract

Aragonite $\delta^{18}O$ compositions were modeled from a large temperature and salinity database along the U.S. east coast, from 25 ºN to 45 ºN, to evaluate and characterize salinity influence in modern shell $\delta^{18}O$ at a regional level. This exercise is relevant to paleoenvironmental interpretations from oxygen isotope compositions of shallow marine fossil bivalves which were typically modified by salinity influences at the time of shell precipitation. Such influences are poorly constrained through simplistic approximations to past seawater $\delta^{18}O$ values. A good example is the interpretation of published $\delta^{18}O$ data from modern marine hard clams along the North American coast assuming only temperature influence, which results in a complete reversal of their geographical distribution. In this study, seawater oxygen isotope compositions (δ_w) were calculated using δ_w–salinity relations characteristic of the four latitudinal zones used, which were defined in agreement with modern shallow marine water environments. Results indicate that salinity is an important modifier of aragonite $\delta^{18}O$ compositions for regions north of ~35 ºN (temperate regions). While some predictions about the influence of salinity are possible south of this latitude (tropical regions), inferences are highly speculative for the temperate zones. Analysis of the modeled hard clam data suggests that seasonal variation is useful to distinguish between the two main marine climates without the need

of assessing the salinity influence separately. Mean winter $\delta^{18}O$ is more variable that summer $\delta^{18}O$ in tropical climates while the opposite is true for the temperate zones.

Keywords: Bivalvia; *Mercenaria*; O–16/O–18; Paleoenvironment; Modern; Shallow–water environment.

3.1. Introduction

Mollusks generally incorporate oxygen into their shells in isotopic equilibrium with ambient seawater, or at a constant deviation from equilibrium (Wefer and Berger, 1991). The use of bivalves as environmental archives of recent and past climate has produced interesting but mostly local results in spite of its potential as a source of climate information (Krantz et al., 1987; Jones and Quitmyer, 1996; Dettman et al., 1999; Surge et al., 2001; Goodwin et al., 2003; Schöne et al., 2004; Schöne et al., 2006; Surge and Walker, 2006; Walker and Surge, 2006; Ivany et al., 2008; Versteegh et al., 2009). Several limitations prevent more productive use of bivalve shells in paleoclimate studies. Restrictions include discontinuous precipitation of the shell during a full year, the need of time–consuming high–resolution sampling, and the need to assume some environmental parameters, which can render regional or long–term interpretations unconvincing. Nevertheless, schlerochronology and schlerochemistry are areas of intense current research (Gröcke and Gillikin, 2008). Furthermore, confidence in paleoenvironmental applications relies in large measure on our understanding of modern analogs.

Although many $\delta^{18}O$–temperature calibrations exists and have been in use for decades (Epstein et al., 1953; Grossman and Ku, 1986; Böehm et al., 2000), the ambiguity imposed by the dependence of oxygen isotope compositions on both temperature and water salinity rarely lead to unambiguous environmental interpretation of fossil carbonate. The development of new techniques based only on the temperature information associated with the C–O chemical bond is promising (Ghosh et al., 2006;

Eiler, 2007), but the resolution necessary to produce data detailed enough for seasonal interpretations is yet to be developed. In the mean time, efforts must focus on improving understanding of the environmental data produced by bivalve $\delta^{18}O$.

Therefore, the goal of this study is to model bivalve carbonate $\delta^{18}O$ from geographically and temporally averaged environmental parameters to find significant connections between shell and marine climate, and in doing so, transcend the shortcomings derived from the $\delta^{18}O$ dependence on salinity and temperature, and benefit from this relation instead. Because modern temperature and salinity variations are well known (these are measured variables), this exercise offers a regional assessment of the environmental information derived from widely used $\delta^{18}O$–water–temperature calibrations. Although this approach does not help to amend any of the setbacks mentioned earlier, it highlights the geographical and temporal average environmental information that can be expected from oxygen isotope profiles of fossil bivalves, thus providing context to paleoenvironmental interpretations. In other words, this exercise tests the extent to which individual $\delta^{18}O$ profiles can be used to represent environmental variability and also the accuracy of common $\delta^{18}O$–water–temperature relations to describe this proxy. Recognizing what characteristics of the modern marine environment become apparent in individual and composite oxygen isotope profiles of bivalves at the resolution commonly used for sampling is important to allow more meaningful and unambiguous marine climate interpretations from $\delta^{18}O$ profiles of ancient shells.

The North American east coast was chosen for this study. It has shallow marine environments that vary both in average value and seasonal amplitude of temperature and salinity with latitude. Data with adequate temporal resolution and spatial distribution from the North American east coast are available. In addition, bivalve taxa that span the entire latitudinal range exist, allowing the use of $\delta^{18}O$ from a single genus and avoiding complications associated with different taxon specific corrections from biological (i.e., vital) effects or differences related to calcite versus aragonite skeletal mineralogies.

Coastal bivalves in general are eurythermal, tolerating a wide temperature range, broadly between –3 ºC and 44 ºC. While temperature is undoubtedly the dominant control on distribution at a biogeographic scale, salinity is the main limiting environmental factor within temperature regions dictating distribution of coastal and estuarine bivalves. Both temperature and salinity influence physiological rates and calcification (Dame, 1996) and the east coast of North America exhibits a broad range in both of these parameters making it ideal for this modeling study.

Here, the aragonitic hard clam, *Mercenaria sp.* (Linné, 1758), which can be found from Prince Edward Island to the Yucatán Peninsula, was used as the modeled bivalve. This choice is appropriate because the hard clam appears to closely record seasonality and has been used repeatedly in paleoenvironmental and paleoclimate studies (Jones et al., 1989; Jones and Quitmyer, 1996; Elliot et al., 2003; Surge and Walker, 2006). Consequently, a number of published detailed $\delta^{18}O$ profiles of the hard clam are available, which complement the analysis of this study by serving as an empirical record for comparison of measured versus modeled results.

Ansell (1968) recognized that optimum growth in the hard clam occurred between 15 ºC and 25 ºC, and that shell precipitation appeared to stop below 9 ºC and above 31 ºC or during spawning after the second year. Maximum growth is experienced during the first year or two of the clam. They grow quickly and live 20–25 years. Hard clams are euryhaline and can be found occupying variable habitats in estuarine and proper marine environments alike, usually in intertidal to subtidal zones to about 20 m depth, chiefly areas where the salinities do not fall below 15 psu (Dame, 1996). In response to short periods of adverse conditions, such as sudden drops in salinity, hard clams have the ability to isolate temporarily from the environment by closing their valves and slowing their metabolism. Shell growth may stop and some dissolution may take place as a result of acid production in anaerobiosis during such temporal stress–triggered valve closures (Crenshaw, 1980). Together, these observations suggest that hard clams probably do not

precipitate any shell aragonite when temperature is above 31 ºC, below 9 ºC, or during ephemeral but significant salinity changes.

3.2. Environmental parameters dataset

An extensive dataset of marine environmental parameters along the North American east coast was obtained from the National Oceanographic Data Center (NODC) of the National Oceanographic and Atmospheric Administration (NOAA – http://www.nodc.noaa.gov/). The complete dataset included a total of 2,384,848 measurements of temperature and/or salinity, from 213,286 stations collected by 3,905 cruises and fixed observatories from July 9, 1912 to June 14, 2006. Data were obtained from the following sources: 1) the World Ocean Circulation Experiment (WOCE), 2) atlases constructed based on WOCE data, 3) the Global Temperature–Salinity Profile Project (GTSPP), 4) the Atlantic Upper Ocean Thermal Program (uot–Atlantic), and 5) the United States Global Ocean Data Assimilation Experiment (USGODAE) data browser, in particular the Argo Profiling Temperature–Salinity floats (http://www.usgodae.org/index.html). Local data from Martha's Vineyard Coastal Observatory ascribed to Woods Hole Oceanographic Institution (WHOI – http://mvcodata.whoi.edu/cgi–bin/mvco/mvco.cgi) are also included. All the data were checked for redundancies, and measurements were kept only if they comply with the following criteria: 1) quality flag 'good' or better, 2) record of both temperature and salinity, 3) depth <50 m, 4) maximum distance offshore ~300 km measured approximately perpendicular to the coast line (distance varies from ~50 km to ~300 km), and 5) no continental stations (no river or spring water measurements). A total of 33,287 data points fulfilled all 5 criteria. Because temperature is commonly reported alone, the requirement of having both temperature and salinity considerably reduced the number of data points available. Most samples are surface water samples (mean depth 0.79 m), and 95% of the measurements are from 2 m depth or less. The filtered dataset basically represents near shore marine environments seasonally affected by low salinity spikes related to storms and continental fresh water input. Examination

of shallow to intermediate depth shelf waters is the intention of this study as most fossil molluscan assemblages are collected from sedimentary sequences representative of this environmental setting.

The area considered extends from 25 ºN to 45 ºN and was subdivided in 4 latitudinal zones of 5 degrees each, a meridional distance of ~556 km. The zones were labeled from South to North as Zone 1, 2, 3 and 4 and will be referred to hereafter using these labels (Figure 3.1). This division is not arbitrary. Broad differences between zones exist based on shallow water marine climates as defined by Hall (1964) based on molluscan distribution. Molluscan provinces are defined using near–shore mollusk communities. These communities maintain a definite makeup that characterizes and distinguishes them from each other. Molluscan provinces are chiefly controlled by temperature and agree with the limits of shallow water marine climates (Figure 3.2). According to Hall (1964), the crucial factor that defines these limits appears not to be a low temperature threshold but rather the number of consecutive days when water temperature is at the appropriate temperature for gametogenesis and reproduction.

Zone 1 includes the platform of the Florida peninsula, 25 ºN to 30 ºN and 78 ºW to 84 ºW. A total of 3,444 data points were selected from this area after applying the restrictions referred above. Zone 2 comprises the area between 30 ºN and 35 ºN, and from 75 ºW to 82 ºW, offshore Northeast Florida, Georgia, South Carolina, and North Carolina extending up to Cape Hatteras. For this area, 5,814 datapoints were chosen. Zones 1 and 2 belong to the inner and outer tropical marine climate provinces respectively (Caribbean and Carolinian molluscan provinces). The inner–tropical climate is characterized at its northern range (~30 ºN) by 9 months with water temperature monthly averages at about 20 ºC and no monthly average below 18 ºC (Hall, 1964). At 35 ºN, the outer–tropical zone is characterized by approximately 4 months at 20 ºC monthly average water temperatures and no month cooler than 10 ºC. It should be noted that the Gulf Stream is influential in controlling the temperature and salinity of these coastal waters. Zone 3

extends 35 ºN to 40 ºN and 72 ºW to 78 ºW, from Cape Hatteras, North Carolina, to Point Pleasant, New Jersey. From this zone 10,734 data points were selected. In this area, both Chesapeake and Delaware Bays impact the intra–annual salinity variation. A total of 13,305 data points were chosen from Zone 4, which extends along the shelf from central New Jersey to Maine from 40 ºN to 45 ºN and 66 ºW to 75 ºW. The marine climate in Zone 3 and in the southernmost part of Zone 4 is mild–temperate (Virginian molluscan province) where the water temperature monthly averages are ~10 ºC for 6 months and ~15 ºC for 5 months. The rest of Zone 4, from about 41 ºN to 45 ºN, belongs to the cool–temperate marine climate (Nova Scotian molluscan province), with less than 4 months averaging water temperatures higher than 10 ºC. The Saint Lawrence River influences the salinity of shelf waters in Zones 3 and 4.

3.3. Methods and model results

3.3.1. Temperature and salinity

Individual annual records would require extensive interpolation to be treated as time series; consequently, all valid data points in each zone were combined across the years by date, thus capturing the overall variability of shallow water along the North American east coast per latitudinal zone during the past century. Treating all records as a single year with the purpose of representing variability in time and space is justifiable as long as no major trend in temperature and salinity exists through time. This assumption is reasonable considering the relative long–term stability of the air temperature and precipitation records during the 20th century in these regions (Gleason, 2010), which in great measure determines marine conditions. The large scale multi–decadal fluctuations (50 to 80 years) that have been described for the North Atlantic in the past century are relevant at the scale of thermohaline circulation (Polyakov et al., 2005). Deeper water layers display more stable temperature and salinity characteristics and small scale trends are recognizable, whereas coastal water variability is much greater with no apparent trends.

Basic descriptive statistics for both temperature and salinity were calculated for each zone (Table 3.1). As expected, average temperature decreases with increasing latitude, from close to 26 °C for Zone 1 to 11 °C for Zone 4, with standard deviations varying between ~ 3 ºC and 8 °C. Temperature differences between overall maximum and minimum vary between 33 ºC (Zone 3) and 28 ºC (Zone 1). Seasonal variability also changes with latitude. Zones 1 and 2 show increased temperature variability during the winter months with relatively well–defined upper limits. Zone 3 exhibits more variability during the winter as well but less scatter occurs in the temperature minima. Zone 4 has more variable summer temperatures. An obvious contrast in salinity exists between Zones 1 and 2 relative to Zones 3 and 4. Modes are around 36 psu for Zones 1 and 2 and closer to 32 psu for Zones 3 and 4. Average salinity is lowest in Zone 3 (~ 29 psu) where many data points come from estuarine settings, resulting in the highest standard deviation in salinity (~7 psu). The highest mean salinity and lowest standard deviation correspond to Zone 1 (~35.9 psu and 0.7 psu, respectively).

Temperature distributions are approximately bimodal, in some instances polymodal, while salinity records resemble extreme value distributions in Zones 1 and 2. Salinity distributions in Zones 3 and 4 are more complex. Above 28 psu, salinities have a distribution close to normal, while salinities below that limit are not easily described (Figure 3.3). Lower salinity incursions are broadly seasonal. Given the frequency distributions, any assumption based on normality is for the most part inapplicable.

Seawater temperature is closely sinusoidal because it is a function of the insolation, which varies with the sine of the solar incidence angle. In contrast, as described above, salinity variations are large and any fit to the data will have a low coefficient of multiple determination (R^2) and limited predictive use. Nevertheless, best–fit sinusoids (Wilkinson and Ivany, 2002) were calculated for each latitudinal zone for temperature and salinity data using the equation:

$$Y = amp \times \sin(2\pi/prd \times (X - phs)) + pos \quad (3.1)$$

with a non–linear least square method and a trust–region algorithm in Matlab®. The coefficients approximated by the fit are the amplitude (*amp*), period (*prd*), phase (*phs*) and position (*pos*) of the sinusoid, and X is the day of the year. The amplitude can be directly related to seasonality, and the position is a measure of the mean annual value. For salinity, the phase is an indication of the season of freshwater input which differs distinctly between Zone 1 (mostly late summer–early fall) and Zones 2 to 4 (mostly spring). The residual to the temperature fits are approximately normally distributed which implies the fit is appropriate to describe the data, and daily temperature values could be estimated as samples from a normal distribution about the best–fit value (Wilkinson and Ivany, 2002) using the 95% confidence bounds ($\sim \pm 2\sigma$) of the fit. On the other hand, salinity variation is too large to use this fit confidently for prediction (Figure 3.4). Nevertheless, the inflections in the sinusoid curves fitted to the salinity data are real and provide a sense of geographical change.

3.3.2. Oxygen isotope compositions

Given the large scatter that characterizes salinity along the North American east coast, each temperature–salinity pair was used to calculate expected aragonite $\delta^{18}O$ directly instead of modeling the populations as random numbers from ideal probability density functions. Oxygen isotope compositions of seawater (δ_w) were first calculated using salinity values and published δ_w–salinity relations. These are dependent on hydrological conditions and vary with latitude. Several δ_w–salinity equations have been applied and the relation can be readily calculated from available local data. The most general and commonly used relation was chosen for each zone (Table 3.2).

Many empirical equations that relate δ_w, aragonite $\delta^{18}O$ and temperature exist (Table 3.3). Grossman and Ku (1986) produced a paleotemperature equation that has been used extensively based on molluscan shells. Their aragonite data were used here to recalculate the temperature dependence of the fractionation factor between aragonite and seawater to the form of $10^3 \times \ln\alpha$:

$$10^3 \times \ln\alpha = 18.01 \times 10^3 \times T^{-1} - 30.49 \quad (3.2)$$

where α is the fractionation factor between aragonite and water and T is temperature in Kelvin. Unlike Grossman and Ku's (1986) original relation, this equation establishes non–linear relations among δ_w, aragonite $\delta^{18}O$, and temperature. Temperature differences between the Grossman and Ku (1986) paleotemperature equation and the relation calculated here are less than ~ ±0.1 ºC for temperatures between ~ 0 ºC and 20 ºC for all combinations of δ_w between –10 ‰ and 5 ‰ and aragonite $\delta^{18}O$ between –5 ‰ and 5 ‰ (Figure 3.5). While the variance in the data is well addressed by the resulting fit ($R^2 = 0.94$), the random errors are not insignificant (RMSE = 0.32). Coefficients calculated here are within the error of those reported by Kim et al. (2007) from their laboratory determined relation, which is similar to the Grossman and Ku (1986) equation for $10^3 \times T^{-1}$ values between 3.4 and 3.6 (~ 4 ºC and 21 ºC). Although both equations are basically equivalent for a wide range of conditions, all calculations presented here are based on the original corrected Grossman and Ku (1986) equation (Kobashi and Grossman, 2003) to avoid large differences arising from salinity extremes, and to be consistent and facilitate comparisons with the large body of literature that uses this relation.

The oxygen isotope composition of aragonite precipitating in equilibrium with seawater at each temperature–salinity data point was calculated using the above equation and δ_w estimates based on measured salinity. Resulting values represent the possible variability of aragonite $\delta^{18}O$ for each zone in any given year. Data from the shallowest available depths were used to produce seasonal aragonite $\delta^{18}O$ isomaps. Although not all points used to produce the zones exist at unique depths, these figures are useful tools to visualize $\delta^{18}O$ seasonal and geographic contrasts. Seasonal bathymetric profiles representative of all data in each zone were also done to complement the surface view with a perspective of variation at depth. These cross sections average all the available data per zone, which are abundant in shallow waters but not at depth. Despite the

limitations imposed by the averaging and non–uniform distribution of the data, aragonite $\delta^{18}O$ is an obvious function of temperature in Zones 1 and 2, while salinity influences become apparent in Zones 3 and 4. These calculations were done using equation 3.2 (Appendix 3).

Isotopic compositions of aragonite modeled from the database in its entirety vary from –8.4 ‰ to 5.6 ‰ for both summer values (JJA) from Zones 3 and 2, respectively. Winter (DJF) extremes are –4.2 ‰ and 4.0 ‰ again from Zones 3 and 2, respectively (Table 4A). These values represent temperature ranges that presumably preclude shell precipitation in hard clams, i.e., temperatures either too high or too low for shell growth. The overall minimum does not change for Zones 2 to 4 if aragonite $\delta^{18}O$ is calculated using only data with temperatures between 9 ºC and 31 ºC, the generally accepted temperature tolerance range of the hard clams (Ansell, 1968). On the other hand, maxima in these zones are reduced by 1.3 ‰ to 2.2 ‰ (Table 3.4B – marine and estuarine hard clams). A third calculation was done excluding data points with salinities below 28 psu, which appears to be a natural boundary based on the data frequency distributions, in particular for Zones 3 and 4 (Table 3.4C – marine only hard clams). In this case minima were reduced to between 0.4 ‰ and 4.5 ‰, and this change affected all zones albeit to different degrees.

For this study, 100 modeled clams per zone were created by subsampling the calculated hard clam $\delta^{18}O$ data from 15–day windows moved 1 day at a time through the year. The choice of this window width assumes that typical sampling of the growth band structure of the hard clam would provide a temporal resolution of about 15 days. The random point selected from the first 15–day window (January 1 to 15) was assigned to January 8, the second (January 2 to 16) to January 9, and so forth. A total of 350 points were obtained this way. The remaining 15 days were calculated using the data from the initial 7 and final 8 days of the year. This method allows the extent of environmental variability to be incorporated into the subsampled data. One disadvantage to this

approach is that the correlation among contiguous days is lost when the data are randomly subsampled instead of averaged. Finally, from the resulting individual, hypothetical clam $\delta^{18}O$ data, a mean value was calculated using a 15–day running average (starting January 1st) to produce profiles that mimic $\delta^{18}O$ averaging and consequent temporal smearing due to sampling (Figure 3.6).

3.4. Discussion

Because the possible combinations of temperature and salinity are geographically constrained by the environmental data, the modeled $\delta^{18}O$ can be used to describe the dependence of carbonate extreme values on temperature and salinity. Exclusion of outlying temperature and salinity values affects zones differently. For example, low salinity data (i.e., below 28 psu) represent less than 2% of the data in Zones 1 and 2 but as much as 35 and 43% of the data in Zones 3 and 4, respectively. In the first section of the discussion, the interpretations are based on $\delta^{18}O$ calculations from the entire dataset. When restrictions such as temperature or salinity thresholds were applied, all resulting points were considered. The second section discusses the modeled clams calculated as running averages applied to random subsamples of the dataset.

3.4.1. Averages and ranges

For Zone 1, the differences between the $\delta^{18}O$ calculated from the entire dataset and that from the hypothetical estuarine–marine clams and marine–only clams suggest that $\delta^{18}O$ minimum value is not uniquely associated to the highest temperature (Table 3.4). Distribution of the calculated $\delta^{18}O$ data by temperature categories shows how salinity influences the oxygen isotope calculations (Figure 3.7). For example, salinities as high as 27 psu in Zone 1 are enough to produce a minimum $\delta^{18}O$ that is not the product of maximum temperature. This is true for the dataset overall and also for summer values. On the other hand, as a consequence of the rather sharp upper limit that characterizes salinity in all Zones (Figure 3.3), aragonite $\delta^{18}O$ maxima changes close to monotonically with temperature. Consequently, maxima $\delta^{18}O$ are less scattered by salinity, correlate

better to temperature, and higher values overall are probably better predictors of winter temperatures. Based on the available data for Zone 1 and assuming the temperature thresholds for the hard clam are reliable and fixed, aragonite $\delta^{18}O$ values lower than ~ –2.5 ‰ are likely to represent local salinity drops.

The overall minimum and maximum in Zone 2 correspond to spring and summer data points of shells that would form at a salinity of ~10 psu and temperature of 0 ºC, respectively. Average and standard deviation of salinity and temperature for this region indicate that considering these data points as outliers is probably reasonable, in particular the 0 ºC summer value (Table 3.1). If both values are ignored, the overall minimum (–1.97 ‰) does not change when temperature and salinity restrictions are applied to the $\delta^{18}O$ calculations. As occurred in Zone 1, salinity scatter is large enough to produce aragonite $\delta^{18}O$ minima that should not be associated with the temperature maximum, for example, values ~25 psu produce a minimum $\delta^{18}O$ at ~24 ºC while the temperature maximum is ~30 ºC (Figure 3.7). Summer minimum and maximum of Zone 2 are also invariant when temperature and salinity restrictions are applied. There is no criterion to decide what parameter is more likely to produce $\delta^{18}O$ values more negative than ~ –2.0 ‰. Winter $\delta^{18}O$ maximum for the entire dataset represents temperature below the hard clam lower temperature threshold. As occurred in Zone 1, $\delta^{18}O$ maxima may be a better temperature predictor. Consequently, aragonite $\delta^{18}O$ above ~3.4 ‰ may indicate salinity greater than ~34 psu.

Zone 3 has the highest salinity variability by temperature range among the 4 zones (Figure 3.7). As in Zones 1 and 2, minimum $\delta^{18}O$ is not associated with temperature maximum and aragonite $\delta^{18}O$ values below ~ –7.5 ‰ are indicative of freshwater (i.e., ~0 psu). This freshwater signal, however, is unlikely to be recorded by clams because shell formation will be greatly reduced or halted under these extreme low–salinity conditions. Considering the minima and maxima of the calculated $\delta^{18}O$, aragonite $\delta^{18}O$ values more negative than~ –3.9 ‰ and greater than ~ 2.2 ‰ are more likely to be caused by salinity

changes in Zone 3 marine environments. Zone 4 has the lowest temperature averages of all the zones. $\delta^{18}O$ values above ~ 1.6 ‰ are a probable indication of increased salinity while $\delta^{18}O$ below ~ –2.8 ‰ may indicate local increased temperatures.

The above conclusions are based on the changes that must take place in salinity so that more positive or more negative aragonite $\delta^{18}O$ will result (Figure 3.7). For example, the $\delta^{18}O$ minimum for marine clams (i.e., salinity ≥ 28 psu and 9 ºC≤ temperature ≤31 ºC) in Zone 3 is –3.9 ‰. $\delta^{18}O$ values below this limit require reduced salinity. Consequently, if measured in a clam from a region with marine climate similar to Zone 3, $\delta^{18}O$ values below –3.9 ‰ could be influenced by increased temperature, but they must be the product of salinity values below 29 psu; increasing temperature is not enough, the salinity must also be reduced. The availability of salinity values in the dataset to produce the predicted changes is also relevant. For instance, it is not possible to assert the probable cause of $\delta^{18}O$ values below –2.0 ‰ in Zone 2 because this is an absolute $\delta^{18}O$ minimum; neither higher temperature nor lower salinities exist in the database. All the limits determined here are of course not absolute, but they need to be considered in the temporal and stratigraphic context provided by the hard clam sample, i.e., they would require a correction for continental ice volume changes for Pleistocene and older samples. For example, according to Lisiecki and Raymo (2005), the average benthic $\delta^{18}O$ range of the last 7 glacial terminations is (1.6 ± 0.1) ‰, and this is presumably mostly due to ice volume changes.

As mentioned before, minima and maxima do not always coincide with the temperature seasonal extremes, which suggest the influence of salinity may locally override temperature control during the spring and fall (Table 3.4). If this is the case, relating the δ_w maxima to the bivalve's low temperature threshold may not be appropriate. Similarly, the adoption of fossil bivalve $\delta^{18}O$ minimum as an anchor point to produce $\delta^{18}O$ time series from the shell's distance profiles (e.g., Gillikin et al., 2005a; Goodwin et al., 2009) may introduce interpretative errors. Nevertheless, the phase shift

difference between the best–fit sinusoids calculated earlier to the temperature data and similar best–fit sinusoids calculated to the modeled aragonite $\delta^{18}O$ is very close to 180 degrees (179±3)º for all zones. This suggests that the phase of the $\delta^{18}O$ signal responds to temperature; while the influence of salinity increases the variation of shell $\delta^{18}O$, it does not affect the $\delta^{18}O$ phase. Consequently, average minimum $\delta^{18}O$ can be confidently associated with average maximum temperature.

Mean and extreme values from published hard clam $\delta^{18}O$ data along the North American East Coast were compared to the modeled clams (Figure 3.8). The contrast between the calculated $\delta^{18}O$ from the entire dataset and subsets of it gives reasonable indications of what the clams' $\delta^{18}O$ values represent at the extremes. In Zone 1, the measured hard clam data are basically within the limits of the modeled marine hard clam $\delta^{18}O$ assuming only temperature limitations. This suggests that clams in inner–tropical marine climates effectively stop shell formation in temperature above ~31 ºC, and salinity variations are of little influence. Outer tropical hard clams (Zone 2) appear not to be affected by salinities below ~28 psu at the southern edge of the climate zone (Table 3.4, and data 'b' in Figure 3.8). However, at the northern limit of Zone 2, salinity seems to be causing the more negative $\delta^{18}O$. It is unlikely that these samples are the result of Zone 3 conditions because the northern limit of Zone 2 is well defined by the Gulf Stream, which creates a stark contrast between coastal waters north and south of Cape Hatteras. Samples from the outer tropical marine climate are reflecting salinity and temperature outside the ranges suggested by the clam data from Zone 2. Reconsideration of the 10 psu salinity outlier mentioned earlier would bring the data within limits; this data point may be significant. A somewhat similar observation can be made about samples in Zone 4. However, the southern limit of the cool temperate marine climate is closer to 41 ºN, so in this case the discrepancy may be a function of the location of the marine climate limit. Samples from the mild temperate zone (Zone 3) are well within the range of calculated $\delta^{18}O$ and may show limited influence from low salinities.

The attempt to relate measured clam $\delta^{18}O$ data to $\delta^{18}O$ values modeled from temperature and salinity data confirms that climate variability greatly influences the information that can be derived from individual $\delta^{18}O$ profiles. Only for the area of limited salinity variation (Zone 1) are the measured clams providing temperature information of the regional marine climate successfully. For all other zones, predictions made from the clams would result in partial correlations that imply either environmental information loss or bias. Measured clam data are consistently shifted to lower salinity and higher temperatures than those predicted by the dataset. The difference between measured clam maxima and the predicted aragonite $\delta^{18}O$ precipitated at ~9 ºC is anywhere between ~0.5 ‰ to ~1.5 ‰, which represents a considerable loss of environmental information. Clams from Zones 2 and 4 have $\delta^{18}O$ minima that suggest higher temperatures and lower salinities than those derived from the database.

There are several possible causes for the lack of correlation between the hard clam $\delta^{18}O$ and the modeled data, but the most likely reason is the seasonal variation of the δ_w–salinity relations (Elliot et al., 2003; Gillikin et al., 2005a). The choice of the δ_w–water relation is not critical when salinity ranges are limited, but it has greater influence in areas of large salinity range. The difficulty is not only the use of one equation over another but also the inadequacy of applying the same relation to large regions characterized by a highly variable hydrographic regime both in time and space. In other words, δ_w changes locally and seasonally as does its relation to salinity. Prediction of δ_w is as important for modeling modern hard clams from environmental parameters as it is to accurately interpret temperature from fossil $\delta^{18}O$.

In addition to the δ_w–salinity relations, $\delta^{18}O$–temperature calibrations may not be universally applicable either. Some organisms precipitate at a constant departure from equilibrium and there are some indications that this may be the case for hard clams at high latitudes (Chapter 2, this volume). It is also unclear that the temperature thresholds in bivalves should function as absolute limits, which may explain part of the discrepancy.

Acclimation is an important process that changes numerous biological processes in bivalves, and shell precipitation thresholds may be locally modified.

3.4.2. Seasonal variability

Unless temperature calculations from fossil $\delta^{18}O$ result in unreasonable values, considerations of salinity changes are usually disregarded. Interestingly, if the collection of modern hard clams used here for comparison purposes (Figure 3.8) was instead a collection of fossil samples, interpreting their $\delta^{18}O$ signal largely as the product of changes in temperature would suggest the existence of a reversed latitudinal thermal gradient. It is not uncommon to assume a unique δ_w and ascribe all $\delta^{18}O$ variation to temperature changes. Isotopic composition of the water can be used instead of oversimplified. It is suggested here that characteristics intrinsic to the carbonate $\delta^{18}O$ should help discern climate contrasts from the $\delta^{18}O$ profiles.

While the scatter in the environmental parameters is too high to establish comparisons directly from the $\delta^{18}O$ calculations beyond what was discussed in the previous section, contrasts can be distinguished in the seasonal variability within each zone and among different zones using the modeled clams (i.e., running averages from the random sub–samples). In this context, examination of the inter–annual seasonal variability observed in $\delta^{18}O$ time series of fossil bivalves may be more useful in defining the climatic zone where the population grew than measures of central tendency (e.g., mean, median) or dispersion (i.e., range, standard deviation) of the entire dataset.

Seasonal averages calculated from the modeled clams show that ^{18}O incorporation into hard clam shells is more variable during the winter than during the summer in Zones 1 and 2 whereas the opposite is true for Zones 3 and 4 (Figure 3.9). Significantly, rather than providing estimates of intra–annual or mean annual temperatures, the seasonal averages of the shell carbonate are dramatically controlled by the integrated variation of temperature and salinity effects per zone. Examination of the intrinsic variability of seasonal values may provide an essential first step to discriminate between general

temperature–salinity regimes of sampled fossil populations. Areas with reduced temperature amplitude and limited salinity variation have higher winter variability whereas areas with high temperature and salinity ranges have stronger variability during the summer months. Further distinction between Zones 1 and 2 on the basis of inter–annual variability is not so obvious. Variation both in summer and winter is higher in Zone 2 than in Zone 1. On the other hand, winter variability may help discern between Zones 3 and 4. While summer variability is only slightly higher in Zone 3 than in Zone 4, winter $\delta^{18}O$ variation is considerably greater in Zone 3.

Note that on the basis of summer and winter average $\delta^{18}O$ values it is not possible to distinguish contrasting climatic zones. For example, modeled clams from zones 1 and 3 have similar summer means while winter averages of Zones 2 and 3 are basically the same. Once broad climatic zones are recognized based on inter–annual variation of winter and summer seasons, it is then possible to constrain the interpretations of absolute $\delta^{18}O$ values with regard to temperature variation. In effect, the role of salinity as it contributes to the shell carbonate $\delta^{18}O$ can be determined through this analysis of variation, which allows further refinements of temperature estimates from the fossil record.

3.5. Conclusion

Hard clam $\delta^{18}O$ modeled from a large temperature and salinity database of shallow water marine environments along the North American east coast were used to define $\delta^{18}O$ characteristics that can be recognized in fossil clams and interpreted in the context of paleoenvironmental reconstructions. The variable contribution of δ_w (salinity) and temperature to the final $\delta^{18}O$ of shell carbonate introduces a persistent, interpretative ambiguity. Because the same uncertainties exist when environmental interpretations are produced from fossil bivalve $\delta^{18}O$ profiles, this study is particularly relevant for constraining the regional paleoenvironmental interpretations made from $\delta^{18}O$ of fossil clams.

Results from the expected aragonite $\delta^{18}O$ modeled from the temperature and

salinity database indicate that regional temperature interpretations can be severely complicated by salinity variations. The $\delta^{18}O$ minimum value observed in the modeled clam carbonate is not always uniquely associated to the highest temperature. In many coastal settings, salinity variation commonly biases the $\delta^{18}O$ such that excessively high annual maximum temperatures can be estimated. This may, in some cases, have implications on the selection of anchor points to assign time to $\delta^{18}O$ vs. distance profiles. On the other hand, as a consequence of the nearly monotonic change of $\delta^{18}O$ maxima with lower temperature, where salinity influences are minimized, winter values are more reliably represented and serve as an identifiable annual benchmark. Consequently, if bivalves temperature thresholds are truly invariant geographically, maximum $\delta^{18}O$ should be a good predictor of such low temperature threshold. In general, $\delta^{18}O$ values below ~ –2.5 ‰ from hard clams of inner tropical marine climates (Zone 1) most likely reflect salinities below ~27, while values above ~3.4 ‰ may indicate salinities greater than about 34 in outer tropical shallow marine climates (Zone 2). These values are not applicable to fossil hard clams without considering paleogeographic differences. Mild and cool temperate regions (Zones 3 and 4) produced shell carbonate $\delta^{18}O$ records that are highly variable due to the effect of large salinity range in combinations with temperature. As a result, interpretation of these records for temperature reconstruction remains highly speculative in the absence of independent salinity and $\delta^{18}O$ estimates.

The $\delta^{18}O$ average and range from modeled clams were compared to measured modern hard clam data. Only where the variation of temperature and salinity was minimal did the modeled clam $\delta^{18}O$ values correlated well with the measured $\delta^{18}O$. The main uncertainty associated with the construction of the modeled clams is the δ_w–water relation, which changes locally and seasonally. In addition, shallow marine environments are in great measure determined by continental influences and this relation should be also considered when interpreting ancient coastal marine environments. The incorporation of paleogeographic constraints associated to coastal marine units is necessary in ancient

marine climate interpretations.

Finally, seasonal variability was shown to be useful for discrimination between the broad shallow water marine climate regions. Areas with reduced temperature amplitude and limited salinity variation have higher winter variability than areas with high temperature and salinity ranges which have stronger variability during the summer months. This observation can be used to distinguish contrasting marine climates from large datasets of co–occurring fossils without the need of assessing salinity influences independently. In combination with seasonal mean values, analysis of variability within seasons is a practical and valuable interpretative tool.

Acknowledgements

We thank Ed Rothman and Beth Crane for their help with visualization and statistical treatment of the data. This chapter benefited greatly from discussions with and input from George Kling.

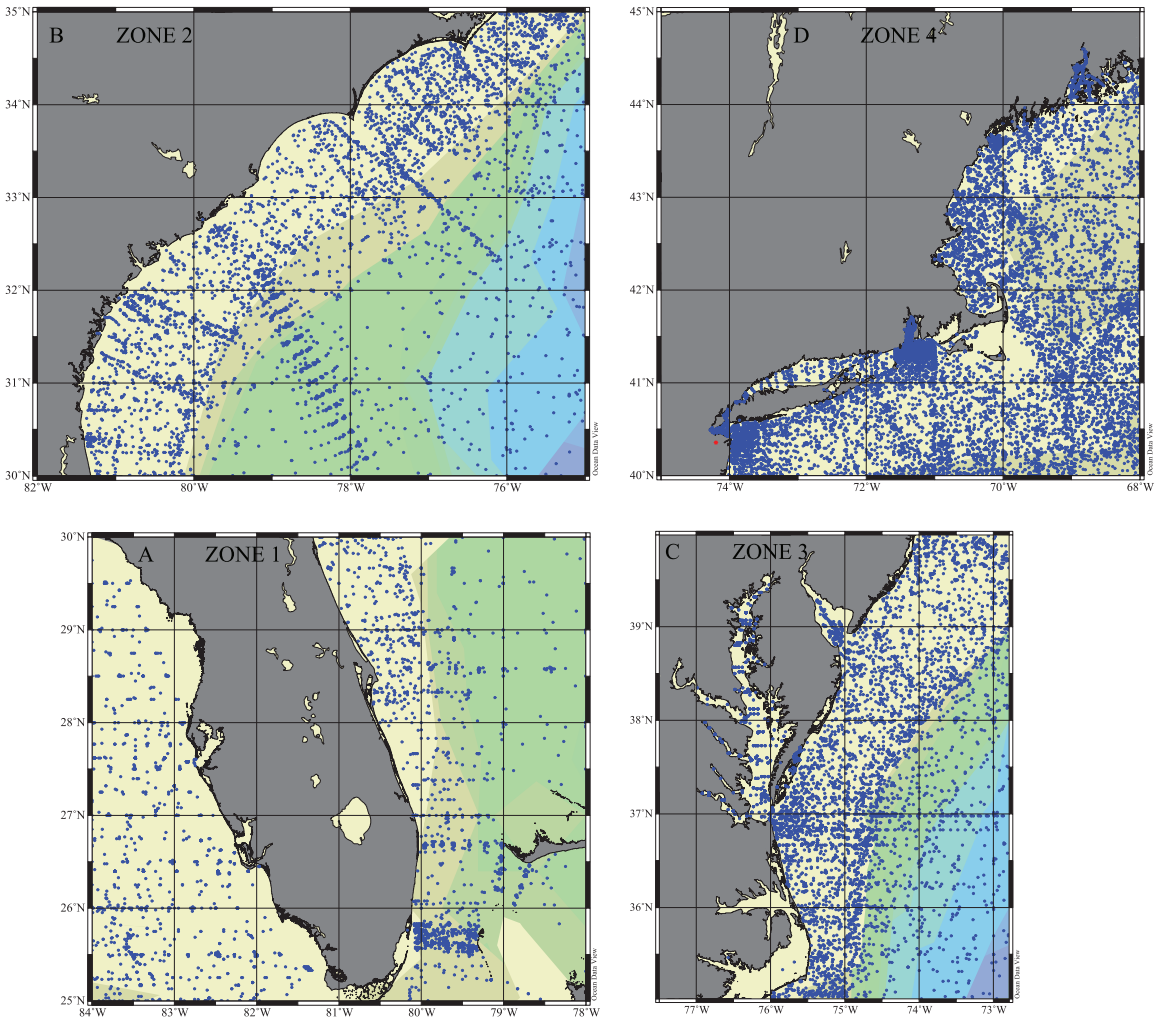

Figure 3.1. Zones 1, 2, 3 and 4 as defined here showing bathymetry and sample station location. Each dot may represent one or multiple data points. Map construction and initial gathering and management of the data was done using Ocean Data View (Schlitzer, 2010).

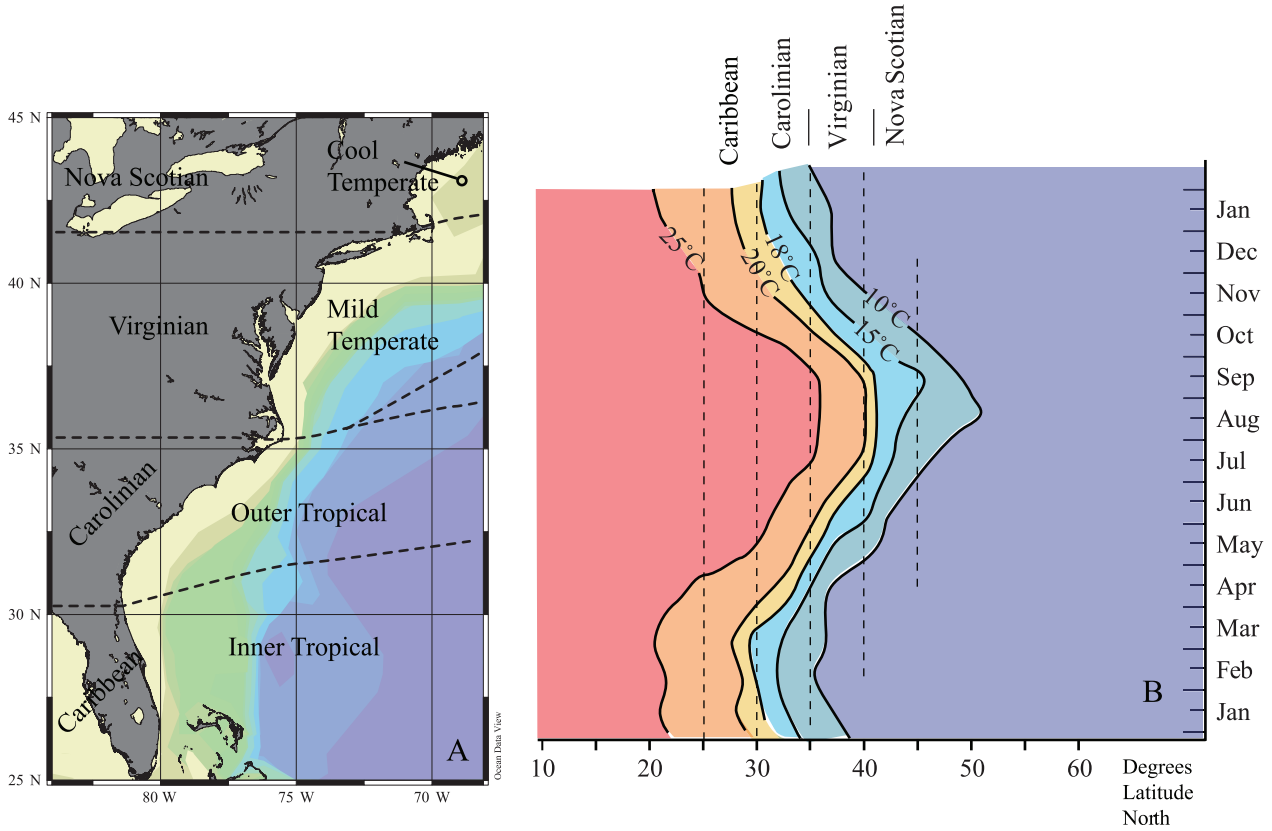

Figure 3.2. A. Shallow water marine climates and molluscan provinces in the study area. B. Approximate annual temperature changes along the Western Atlantic shallow marine waters, which is the basis of the provinces definition. Modified from Hall (1964).

Figure 3.3. Temperature and salinity temporal distribution with best–fit sinusoids. A1, B1, C1, D1. Temperature profiles for zones 1, 2, 3 and 4, respectively. A2, B2, C2, D2. Salinity distribution for zones 1, 2, 3, and 4, respectively.

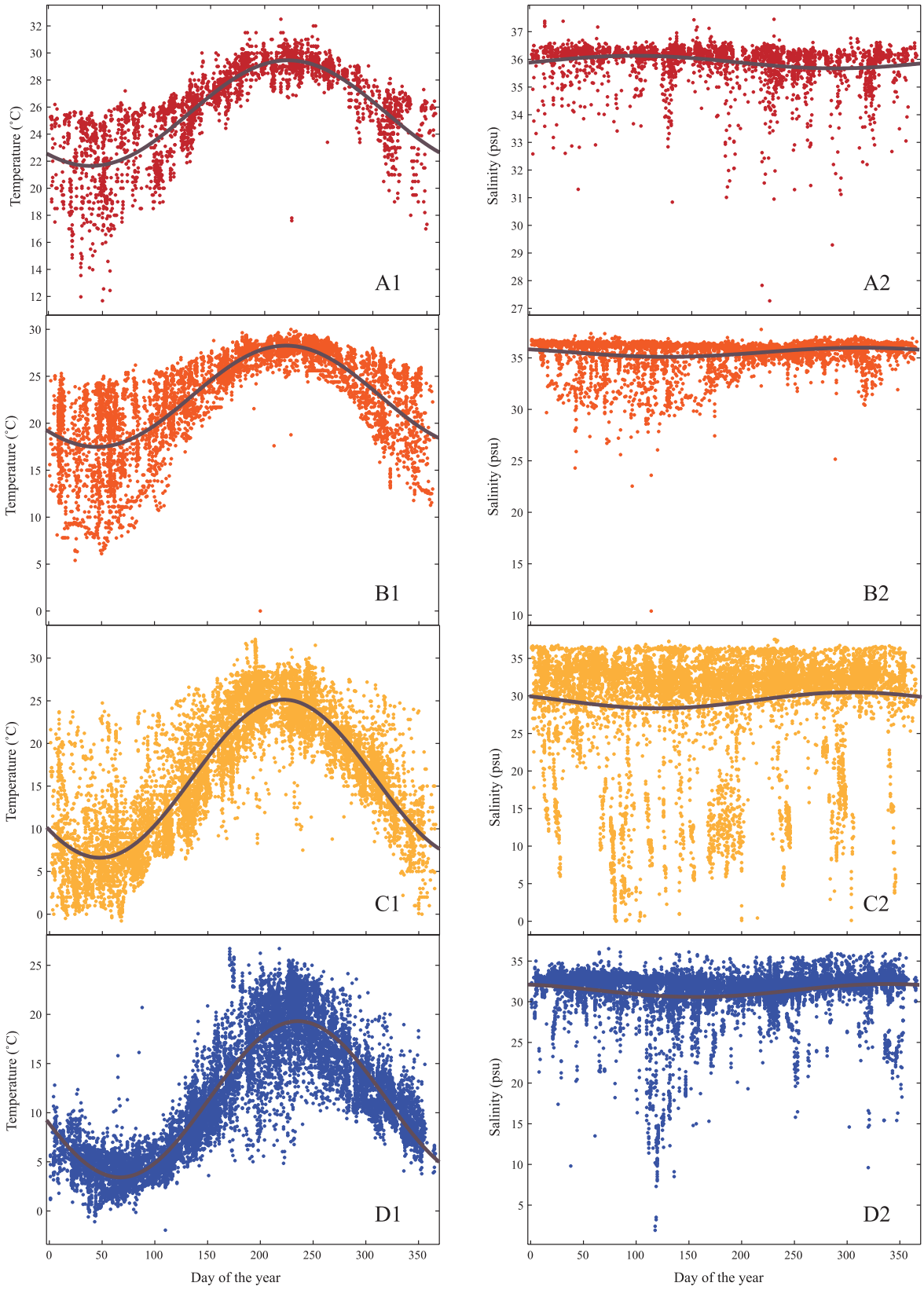
Temperature (°C)
Salinity (psu)
A1
A2
B1
B2
C1
C2
D1
D2
Day of the year
Day of the year

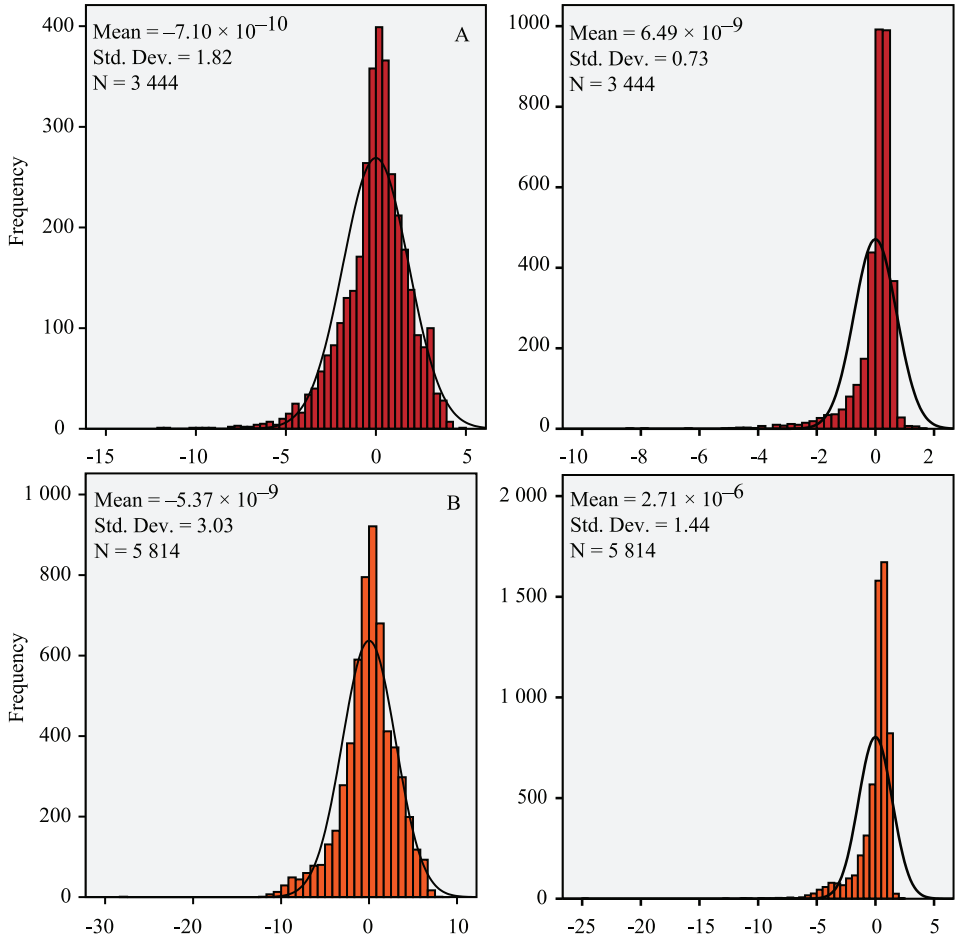

f(x) = amp×sin(2×π/prd×(x−phs))+pos
Coefficients (with 95% confidence bounds):

	Temperature	Salinity
amp	3.903 (3.815, 3.99)	0.2276 (0.194, 0.2613)
phs	130.3 (128.3, 131.8)	1.863 (−7.658, 11.38)
pos	25.55 (25.51, 25.64)	35.88 (35.85, 35.9)
prd	365 (363.3, 366.7)	370 (fixed at bound)
R^2	0.69	0.049

f(x) = amp×sin(2×π/prd×(x−phs))+pos
Coefficients (with 95% confidence bounds):

	Temperature	Salinity
amp	5.389 (5.313, 5.464)	0.447 (0.4083, 0.4858)
phs	133.7 (132.8, 134.5)	221.1 (216.4, 225.7)
pos	22.8 (22.74, 22.86)	35.52 (35.5, 35.55)
prd	364.9 (fixed at bound)	364.9 (fixed at bound)
R^2	0.63	0.043

Figure 3.4. Frequency distributions of temperature and salinity, and parameters of the best–fit sinusoids. A1, B1. Frequency distribution of temperature residuals to best sinusoid fit for Zones 1 and 2, respectively. An ideal normal distribution with the mean and standard deviation from the data is shown over the residuals histogram. A2, B2. Frequency distribution of salinity residuals to best sinusoid fit for Zones 1 and 2, respectively. A3, B3. Model, parameters and coefficients of multiple determination (R^2) of the best–fit sinusoids to temperature and salinity data for Zones 1 and 2, respectively,

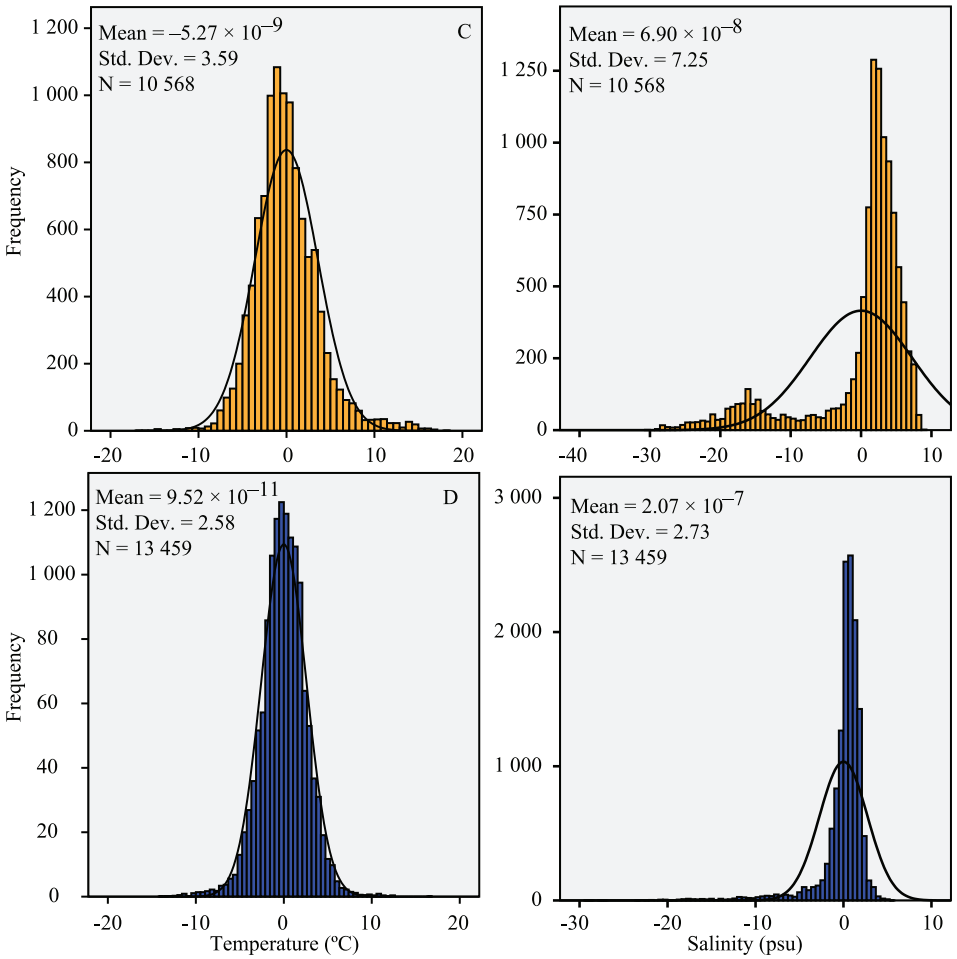

f(x) = amp×sin(2×π/prd×(x−phs))+pos

Coefficients (with 95% confidence bounds):

	Temperature	Salinity
amp	9.286 (9.217, 9.356)	1.07 (0.9318, 1.208)
phs	131.3 (130.9, 131.8)	211 (202.1, 219.9)
pos	15.56 (15.51, 15.61)	29.43 (29.33, 29.53)
prd	364.9 (fixed at bound)	365.1 (351.3, 378.9)
R^2	0.77	0.011

f(x) = amp×sin(2×π/prd×(x−phs))+pos

Coefficients (with 95% confidence bounds):

	Temperature	Salinity
amp	7.911 (7.884, 8.006)	0.7988 (0.751, 0.8466)
phs	146.1 (145.7, 146.4)	247.7 (244.4, 251)
pos	10.97 (10.94, 11.00)	31.5 (31.47, 31.54)
prd	364.9 (fixed at bound)	364.9 (fixed at bound)
R^2	0.82	0.039

Figure 3.4. Continued. Frequency distributions of temperature and salinity, and parameters of the best–fit sinusoids. C1, D1. Frequency distribution of temperature residuals to best sinusoid fit for Zones 3 and 4, respectively. An ideal normal distribution with the mean and standard deviation from the data is shown over the residuals histogram. C2, D2. Frequency distribution of salinity residuals to best sinusoid fit for Zones 3 and 4, respectively. C3, D4. Model, parameters and coefficients of multiple determination (R2) of the best–fit sinusoids to temperature and salinity data for Zones 3 and 4, respectively.

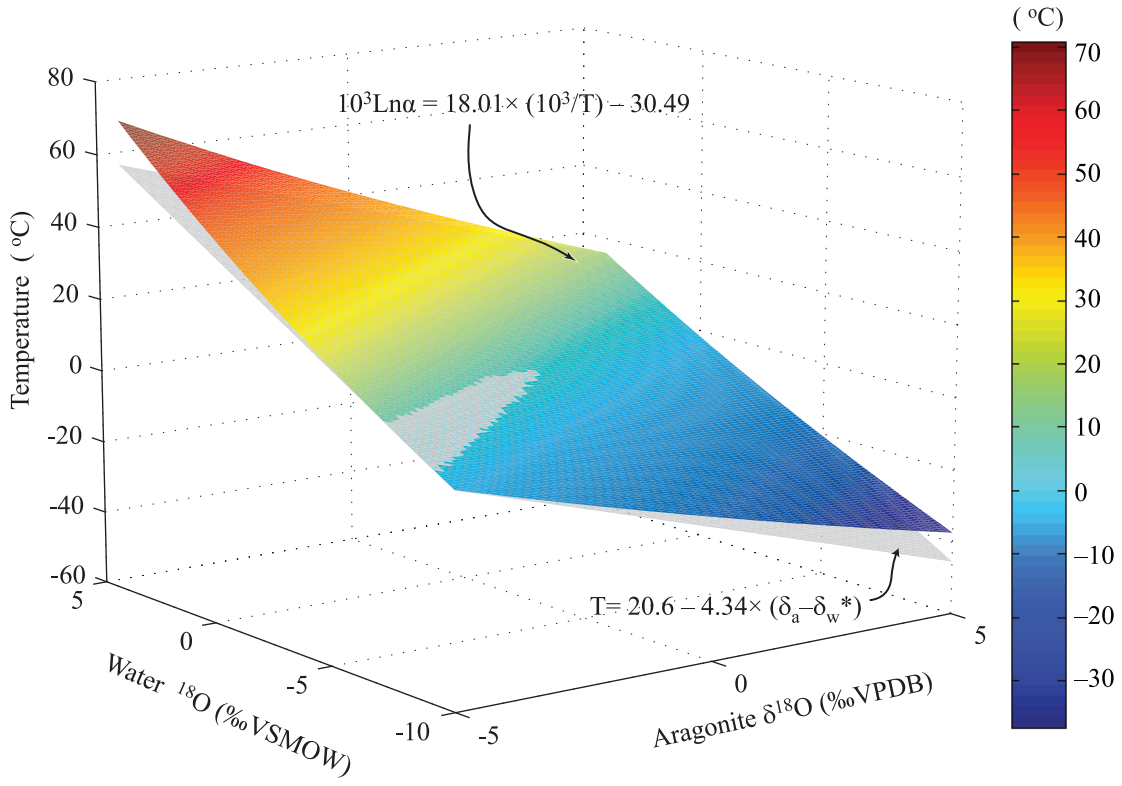

Figure 3.5. Grossman and Ku (1986) corrected ($\delta_w^* = \delta_w - 0.2$) paelotemperature equation in its original form and recalculated to $10^3 \times \ln\alpha = 18.01 \times 10^3 \times T^{-1} - 30.49$ using their aragonite $\delta^{18}O$ and δ_w data.

Figure 3.6. Modeled hard clam aragonite $\delta^{18}O$ precipitating in temperature and salinity conditions as established by the dataset but considering ecological limitations known to affect hard clams (temperature ≥9 ºC and ≤31 ºC). Data points were randomly drawn from a 15–day moving window (colored symbols) and averaged using a 15–day running average (black symbols). A. Zone 1. B. Zone 2. C. Zone 3. D. Zone 4.

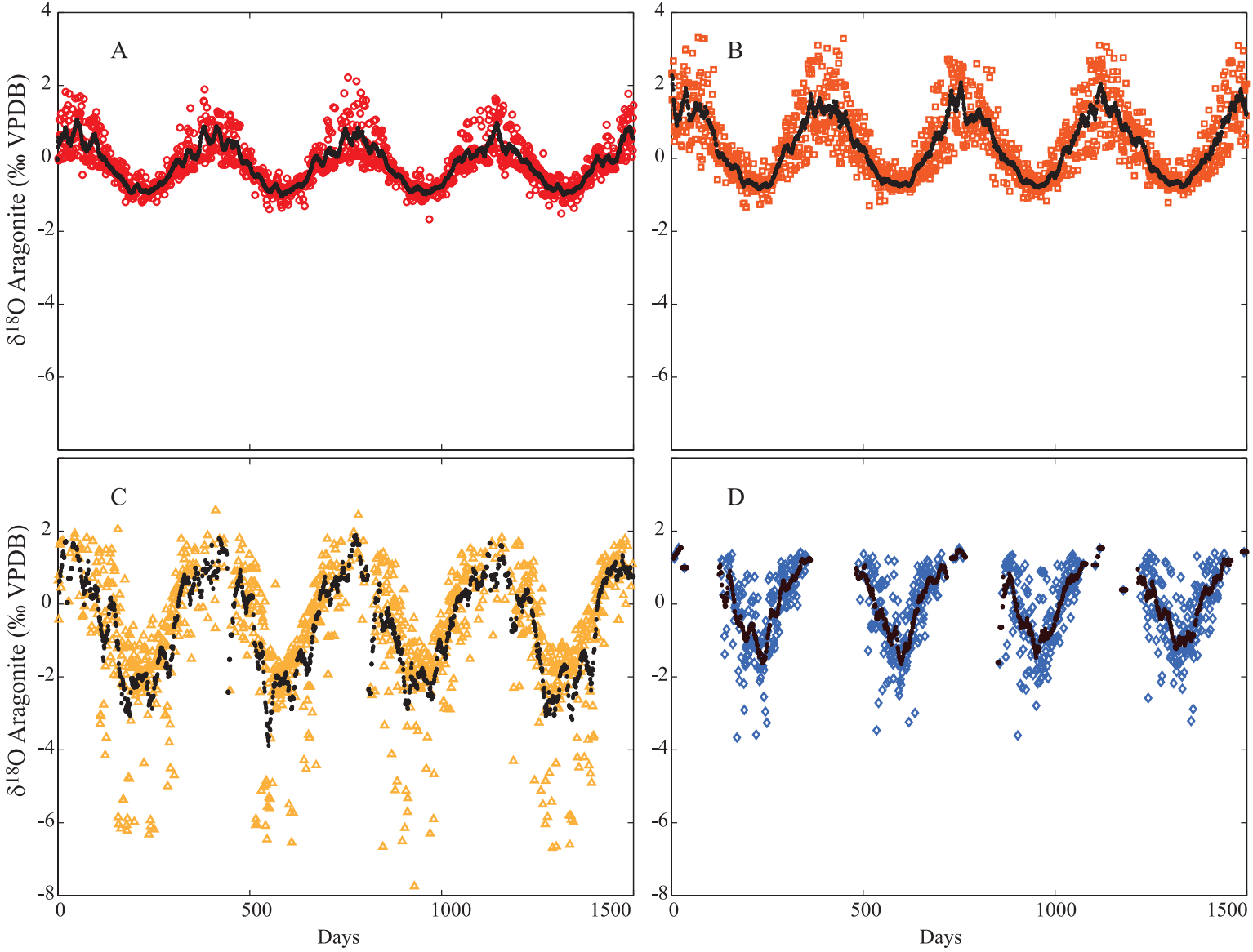
A
B
C
D
δ18O Aragonite (‰ VPDB)
δ18O Aragonite (‰ VPDB)
Days
Days
4
2
0
-2
-4
-6
-8
0
500
1000
1500

Figure 3.7. Box plots of aragonite $\delta^{18}O$ by temperature range. Scales of the ordinate axes differ. The aragonite $\delta^{18}O$ variation in each temperature category, including outliers (open circles) and extreme values (stars), are the result of salinity variations. Some salinity values discussed in the text are included. In each temperature category high salinity values correspond to more positive aragonite $\delta^{18}O$ and low salinity values produce the lowest aragonite $\delta^{18}O$ values. The box lengths are the interquartile ranges (25th to 75th percentile). Outliers are samples within 1.5 and 3 times the interquartile range away from the upper or lower edge of the box, while extreme values are more than 3 interquartile ranges away from the box edges. The line on the box is the median.

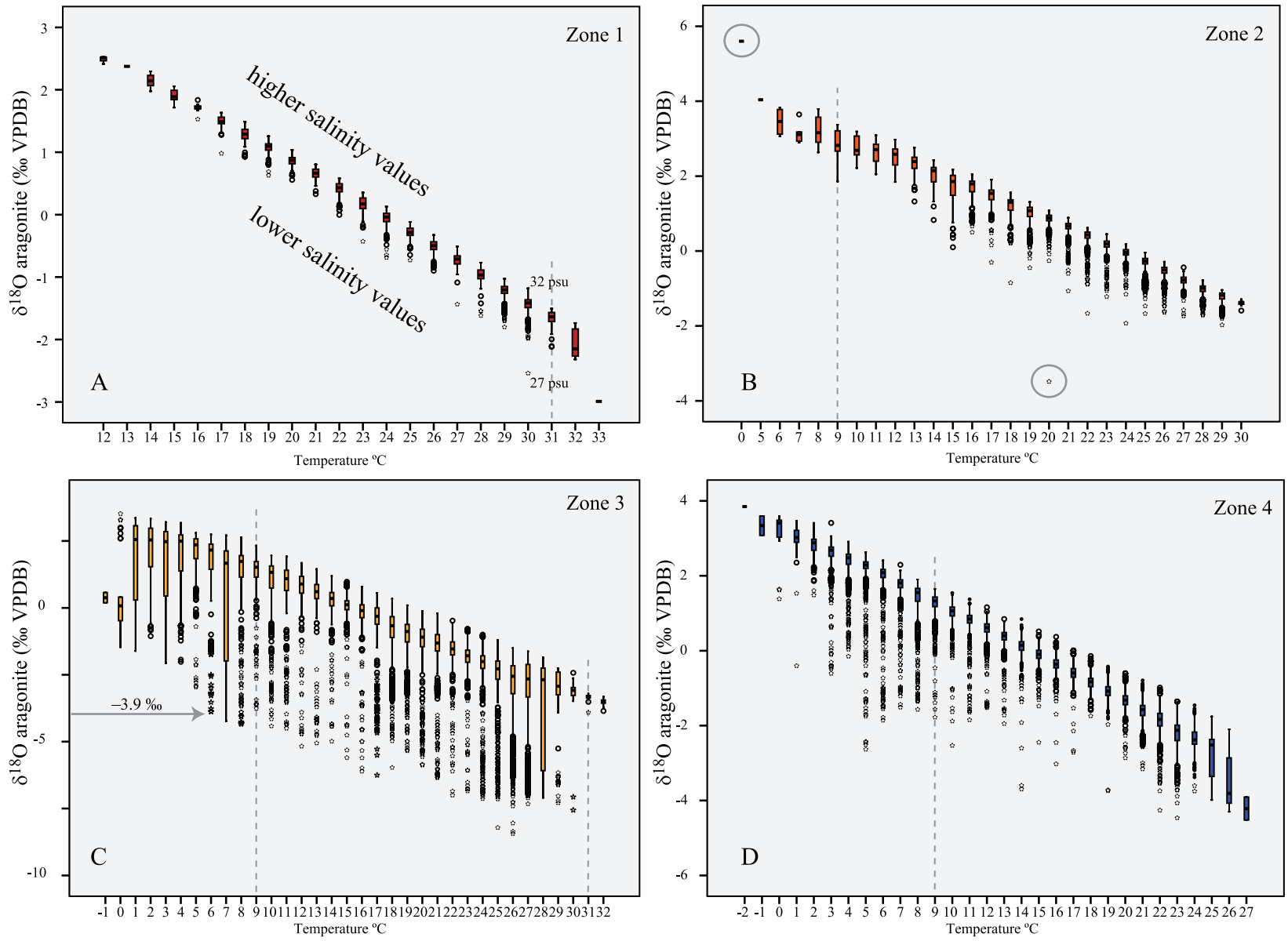
Zone 1
higher salinity values
lower salinity values
32 psu
27 psu
A
δ18O aragonite (‰ VPDB)
Temperature ºC
Zone 2
B
Zone 3
–3.9 ‰
C
Zone 4
D

Figure 3.8. Aragonite $\delta^{18}O$ average and range values from published measured hard clams (colored squares) and calculated in this study from temperature and salinity data (open squares and blue crosses) for Zone 1 (25 ºN to 30 ºN), Zone 2 (30 ºN to 35 ºN), Zone 3 (35 ºN to 40 ºN) and Zone 4 (40 ºN to 45 ºN). Modeled aragonite $\delta^{18}O$ average and range values were calculated per zone as inorganic precipitates from the entire dataset (open squares) and as marine hard clams (salinity ≥28 psu and 9 ºC≤ temperature ≤31 ºC, blue crosses). Latitudinal location of the published data is accurate whereas calculated values are representative of the entire zones. Minimum $\delta^{18}O$ calculated by applying only temperature restrictions differs from $\delta^{18}O$ minimum from the entire dataset only in zone 1 (red circle). Sources are: a–this study; b–Jones et al. (1989); Jones and Quitmyer (1996); c–O'Donell (2002); d–Elliot et al. (2003); e–Potts (2004); f–Stecher et al. (1996); g–Trumbore (1981); h–Surge and Walker (2006).

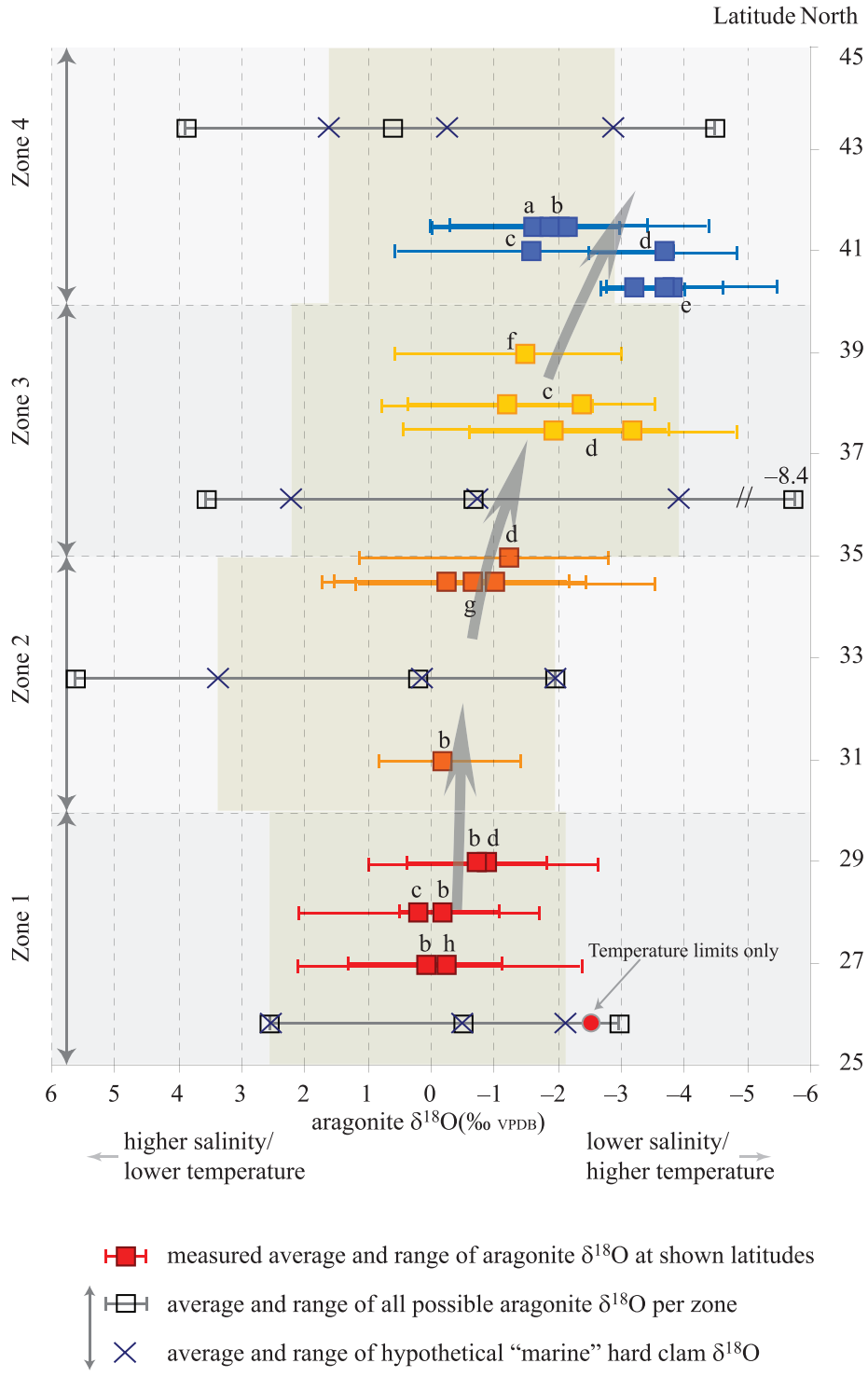
Latitude North
45
43
41
39
37
35
33
31
29
27
25
Zone 4
Zone 3
Zone 2
Zone 1
a b
c
d
e
f
c
d
–8.4
d
g
b
b d
c b
b h
Temperature limits only
6 5 4 3 2 1 0 –1 –2 –3 –4 –5 –6
aragonite δ18O(‰ VPDB)
higher salinity/
lower temperature
lower salinity/
higher temperature
measured average and range of aragonite δ18O at shown latitudes
average and range of all possible aragonite δ18O per zone
average and range of hypothetical “marine” hard clam δ18O

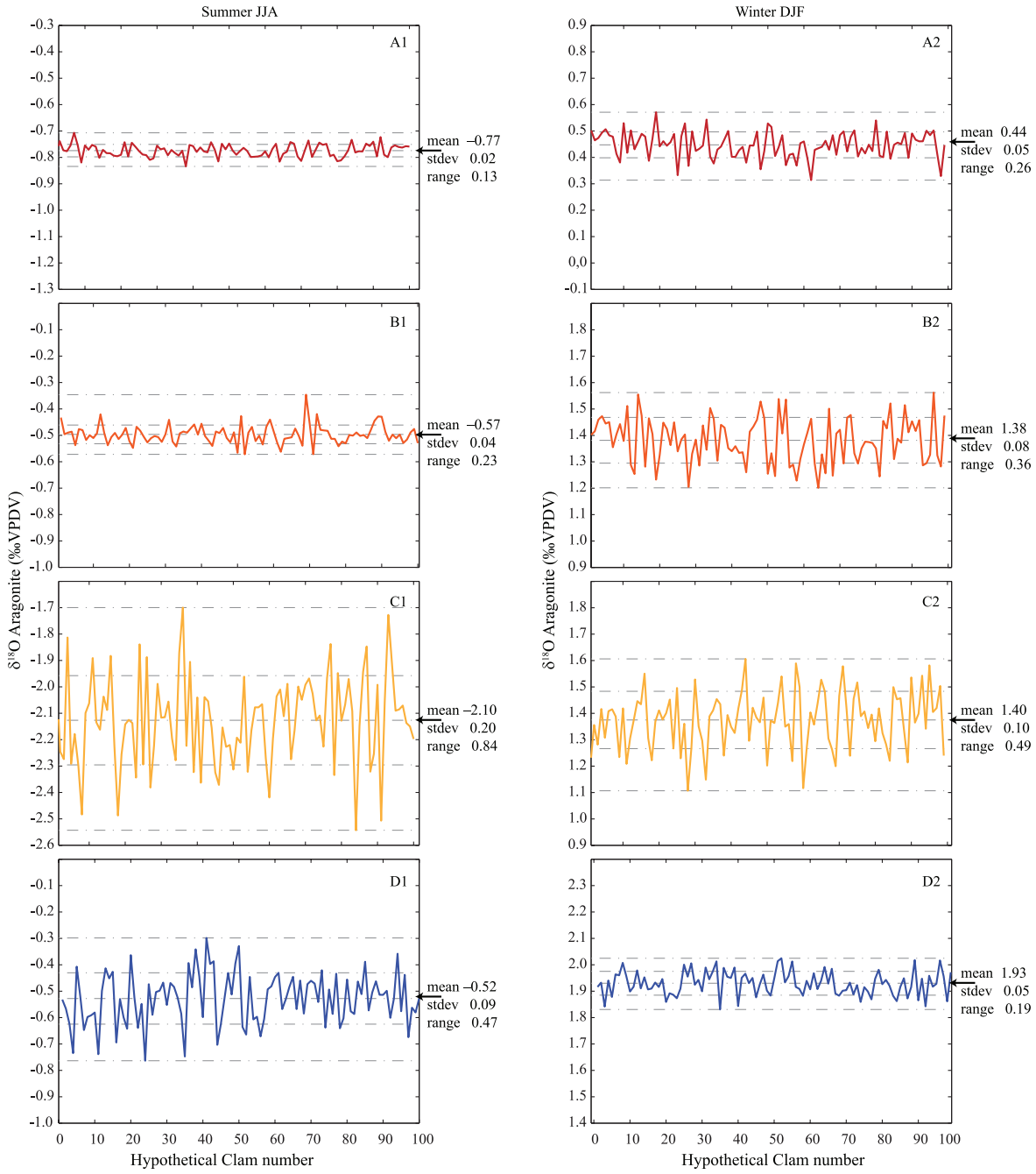

Figure 3.9. Variability of seasonal means from modeled hard clams. Hard clams were modeled as running averages of random subsamples taken from 15–day windows across all possible clam compositions. Y–axis scale is 1 ‰ in all frames. A1–A2. Zone 1 summer and winter variability. B1–B2. Zone 2 summer and winter variability. C1–C2. Zone 3 summer and winter variability. D1–D2. Zone 4 summer and winter variability. Winter variability is greater than summer variability in Zones 1 and 2 while the opposite is true for Zones 3 and 4.

Table 3.1. Temperature and salinity descriptive statistics

Zone	N	Temperature (°C)				Salinity (psu)			
		Average	Standard Deviation	Minimum	Maximum	Average	Standard Deviation	Minimum	Maximum
1	3 444	25.91	3.30	11.68	32.50	35.89	0.74	27.27	37.45
2	5 814	22.66	4.99	0.00	30.00	35.51	1.47	10.4	37.77
3	10 734	16.25	7.49	–0.80	32.20	29.43	7.25	0.02	37.52
4	13 305	11.60	6.23	–1.96	26.70	31.4	2.79	1.9	36.52

Table 3.2. $\delta^{18}O$ **– salinity relations**

Location	Description	Equation
Zone 1 25 to 30° N 78 to 84° W	In Elliot et al. (2003) from Yobbi (1992) who conducted a hydrographic survey 36 Km South of Cedar Key	$\delta_w = \mathbf{0.12}\times \boldsymbol{Salinity} - \mathbf{3.39}$ [a]
	Using data from Schmidt et al. (1999)	$\delta_w = 0.12 \times Salinity - 2.67$
	Using a freshwater end-member of –2.0 ‰ (approximate value from Kendall and Coplen, 2001), and a marine end-member of 0.5‰ and 36 psu	$\delta_w = 0.056\times Salinity - 2.03$
Zone 2 30 to 35° N 75 to 82° W	From Elliot et al. (2003) estimated assuming a linear mixture between a river water end-member from Coplen and Kendall (2000) and an ocean end-member taken from the GISS database	$\delta_w = \mathbf{0.17}\times \boldsymbol{Salinity} - \mathbf{5.19}$ [a]
	From Gillkin, unpublished data around Cape Look Out, North Carolina. For samples with salinities above 24 psu, plus a single point from the GISS database	$\delta_w = 0.14 \times Salinity - 3.17$
	Using a freshwater end-member of –5‰ (approximate from Kendall and Coplen, 2001), and a marine end–member 0.5‰ and 35 psu	$\delta_w = 0.14\times Salinity - 5.07$
Zone 3 34 to 40° N 72 to 78° W	In Elliot et al. (2003), from Khim and Krantz (1996) who did a hydrographic survey on the inner shelf between 10 and 20 m depth, from southern Delaware Bay to the mouth of the Chesapeake Bay	$\delta_w = \mathbf{0.19}\times \boldsymbol{Salinity} - \mathbf{7.08}$ [a]
	Using data from Schmidt et al. (1999)	$\delta_w = 0.13\times Salinity - 5.35$
	Using a freshwater end–member of –7‰ (approximate from Kendall and Coplen, 2001), and a marine end-member 0‰ and 35 psu	$\delta_w = 0.2 \times Salinity - 7.0$
Zone 4 40 to 45° N 66 to 75° W	In Elliot et al. (2003), from Fairbanks, personal communication, 2001.	$\delta_w = \mathbf{0.16}\times \boldsymbol{Salinity} - \mathbf{6.31}$ [a]
	Fairbanks (1982).New York Bight equation from 39 to 41°N, surface water and cool pool.	$\delta_w = 0.258\times Salinity - 9.14$
	Using a freshwater end–member of –9‰ (approximate from Kendall and Coplen, 2001), and a marine end–member –0.5‰ and 35 psu	$\delta_w = 0.26\times Salinity - 9.0$

[a] Relation used in this study

Table 3.3. Temperature dependence relations of the aragonite–water fractionation factor.

Reference	Experiment	Temperature (°C)	Relation
McCrea, 1950	Inorganic synthesis	−1.2 to 31.8	$10^3 \ln \alpha = 16.26 \times 10^3 T^{-1} - 26.01$
Grossman and Ku, 1986[a]	Gastropods, scaphopods, and forams	2.6 to 22	$10^3 \ln \alpha = 18.07 \times 10^3 T^{-1} - 31.08$
Patterson, 1993	Lake fish otoliths	3.2 to 30.3	$10^3 \ln \alpha = 18.56 \times 10^3 T^{-1} - 33.49$
Leder et al., 1996	Corals	23.2 to 30.7	$10^3 \ln \alpha = 17.93 \times 10^3 T^{-1} - 34.12$
Thorrold et al., 1997	Tank fish otoliths	18.2 to 25	$10^3 \ln \alpha = 18.56 \times 10^3 T^{-1} - 32.54$
White et al., 1999	Tank mollusc (*L. peregra*)	8 to 24	$10^3 \ln \alpha = 16.74 \times 10^3 T^{-1} - 26.39$
Böhm et al., 2000	Sclerosponges, forams, molluscs	3 to 28	$10^3 \ln \alpha = 18.45 \times 10^3 T^{-1} - 32.54$
Zhou and Zheng, 2003	Inorganic synthesis	0 to 70	$10^3 \ln \alpha = 20.44 \times 10^3 T^{-1} - 41.48$

[a] As recalculated by Shanahan et al., (2005)

Table 3.4-A. Statistics from expected aragonite $\delta^{18}O$ from all data (‰ VPDB)

Map	Overall			Summer (JJA)			Winter (DJF)			Winter	Summer	N
	Mean	Min	Max	Mean	Min	Max	Mean	Min	Max	N	N	
1	–0.51	–2.99	2.53	–1.13	–2.99	1.40	0.45	–0.80	2.53	645	1043	3444
2	0.17	*–3.48* (–1.97)	*5.60* (4.04)	–0.82	–1.77	*5.60* (1.50)	1.21	–0.51	4.04	1547	1324	5814
3	–0.68	–8.44	3.52	–2.44	–8.44	1.66	1.37	–4.15	3.52	1939	3109	10724
4	0.59	–4.52	3.85	–0.81	–4.52	2.12	1.88	–1.21	3.59	2362	4045	13305

Table 3.4-B. Statistics of expected aragonite $\delta^{18}O$ of estuarine-marine hard clams (‰ vpdb)*

Map	Overall			Summer (JJA)			Winter (DJF)			Winter	Summer	N
	Mean	Min	Max	Mean	Min	Max	Mean	Min	Max	N	N	
1	–0.50	–2.54	2.53	–1.13	–2.54	1.40	0.45	–0.80	2.53	645	1035	3433
2	0.14	*–3.48* (–1.97)	3.37	–0.82	–1.77	1.50	1.14	–0.51	3.37	1494	1323	5751
3	–1.25	–8.44	2.22	–2.44	–8.44	1.42	0.73	–4.15	2.22	651	3086	8368
4	–0.35	–4.52	1.64	–0.90	–4.52	1.45	1.07	0.02	1.64	371	3889	7994

Table 3.4-C. Statistics of expected aragonite $\delta^{18}O$ of marine hard clams (‰ vpdb)**

Map	Overall			Summer (JJA)			Winter (DJF)			Winter	Summer	N
	Mean	Min	Max	Mean	Min	Max	Mean	Min	Max	N	N	
1	–0.50	–2.12	2.53	–1.13	–2.00	1.40	0.45	–0.80	2.53	645	1034	3432
2	0.14	–1.97	3.37	–0.82	–1.77	1.50	1.14	–0.51	3.37	1490	1322	5732
3	–0.71	–3.91	2.22	–1.79	–3.91	1.42	0.83	–1.36	2.22	616	2496	7006
4	–0.26	–2.87	1.64	–0.83	–2.87	1.45	1.09	0.09	1.64	363	3708	7570

* Considering only data with temperature ≥9ºC and ≤31ºC.

** Considering only data with temperature ≥9ºC and ≤31ºC and salinities ≥ 28 psu.

Outliers in italics. Best value in parenthesis.

Table 3.5. Published hard clam $\delta^{18}O$ average, minimum and maximum values along the North American east coast

Reference	Latitude	Locality	$\delta^{18}O$ aragonite (‰ VPDB)		Salinity Min	Salinity Max
25-30 lat N Zone 1 - Florida, East Coast and Gulf of Mexico						
Elliot et al., 2003	29	Cedar Key, FL	average min max	-0.89 -2.71 1.02	11	30
Jones and Quitmyer, 1996	29	Suwannee Reef, Cedar Key, FL	average min max	-0.74 -1.85 0.38	13.9	26
Surge and Walker, 2006	27	Pine Island, FL	average min max	-0.25 -2.44 2.10	23	35
Jones and Quitmyer, 1996	27	Charlotte Harbor, FL	average min max	0.06 -1.08 1.29	11	29.5
Jones and Quitmyer, 1996	28	Mosquito Lagoon, FL	average min max	-0.19 -1.10 0.51		
O'Donnell, 2002	28	Indian River Lagoon, FL	average min max	0.20 -1.70 2.10		
30-35 lat N Zone 2 - Georgia, S.Carolina and SE N.Carolina						
Jones and Quitmyer, 1996	31	Kings'sBay, GA	average min max	-0.21 -1.43 0.82	16.5	29
Elliot et al., 2003	35	Hatteras inlet, NC	average min max	-1.25 -2.75 1.20	15	30
Gillikin et al., 2005	34.5	Jarret Bay (Cape Lookout), NC	average min max	-0.27 -2.21 1.55	23	37
Gillikin et al., 2005	34.5	Wade Creek (Cape Lookout), NC	average min max	-1.01 -3.67 1.23	23	37
Gillikin et al., 2005	34.5	Back Sound (Cape Lookout), NC	average min max	-0.68 -2.48 1.80	28	34
Trumbore, 1981	33		average min max	-0.66 -0.79 -0.42		

Table 3.5. Continued

35-40 lat N Zone 3 - E N.Carolina, Virginia, Maryland, Delaware, S New Jersey						
Stecher et al., 1996	39	Cape Henlopen, Lewes, DW	average min max	-1.50 -3.02 0.68		
O'Donnell, 2002	38	Assateague Channel, Chincoteague, VA	average min max	-2.40 -3.50 0.30		
O'Donnell, 2002	38	Assateague Channel, Chincoteague, VA	average min max	-1.20 -2.50 0.80		
Elliot et al., 2003	37.5	Tom's Cove, MD	average min max	-1.93 -3.85 0.53	28	34
Elliot et al., 2003	37.5	Cherrystone, MD	average min max	-3.20 -4.82 -0.70	20	27
40-45 lat N Zone 4 - N New Jersey, New York, Connecticut, Massachussets, New Hampshire, Main, Rhode Island						
O'Donnell, 2002	41	Long Island Sound, CT	average min max	-1.60 -3.80 0.60		
Jones et al., 1989	41.5	Narragansett Bay, RI	average min max	-2.06 -3.17 -0.30		
Elliot et al., 2003	41	Oyster Bay, NY	average min max	-3.70 -4.84 -2.48	24	28
This study	41.5	Vineyard Sound, MA	average min max	-2.18 -4.44 0.05	29	33
This study	41.5	Vineyard Sound, MA	average min max	-1.62 -3.04 -0.05	29	33
This study	41.5	Vineyard Sound, MA	average min max	-1.87 -3.35 -0.35	29	33
Potts, 2004	40.3	Raritan Bay, New York Harbor, NY	average min max	-3.83 -5.51 -2.89		
Potts, 2004	40.3	Raritan Bay, New York Harbor, NY	average min max	-3.69 -4.70 -2.63		
Potts, 2004	40.4	Islip, NY	average min max	-3.22 -4.06 -2.65		

Appendix

The following pages show seasonal maps of Zones 1, 2, 3 and 4.The first four figures represent summer; the last four figure represent winter. Temperature values were interpolated to create the colored surface. Temperatures were taken from the shallowest available data per station. Aragonite $\delta^{18}O$ calculated from equation 3.2 was used to generate the isolines. The color bar applies to all maps but it is only shown in Zone 1. These figures were generated using ODV (Schlitzer, 2010).

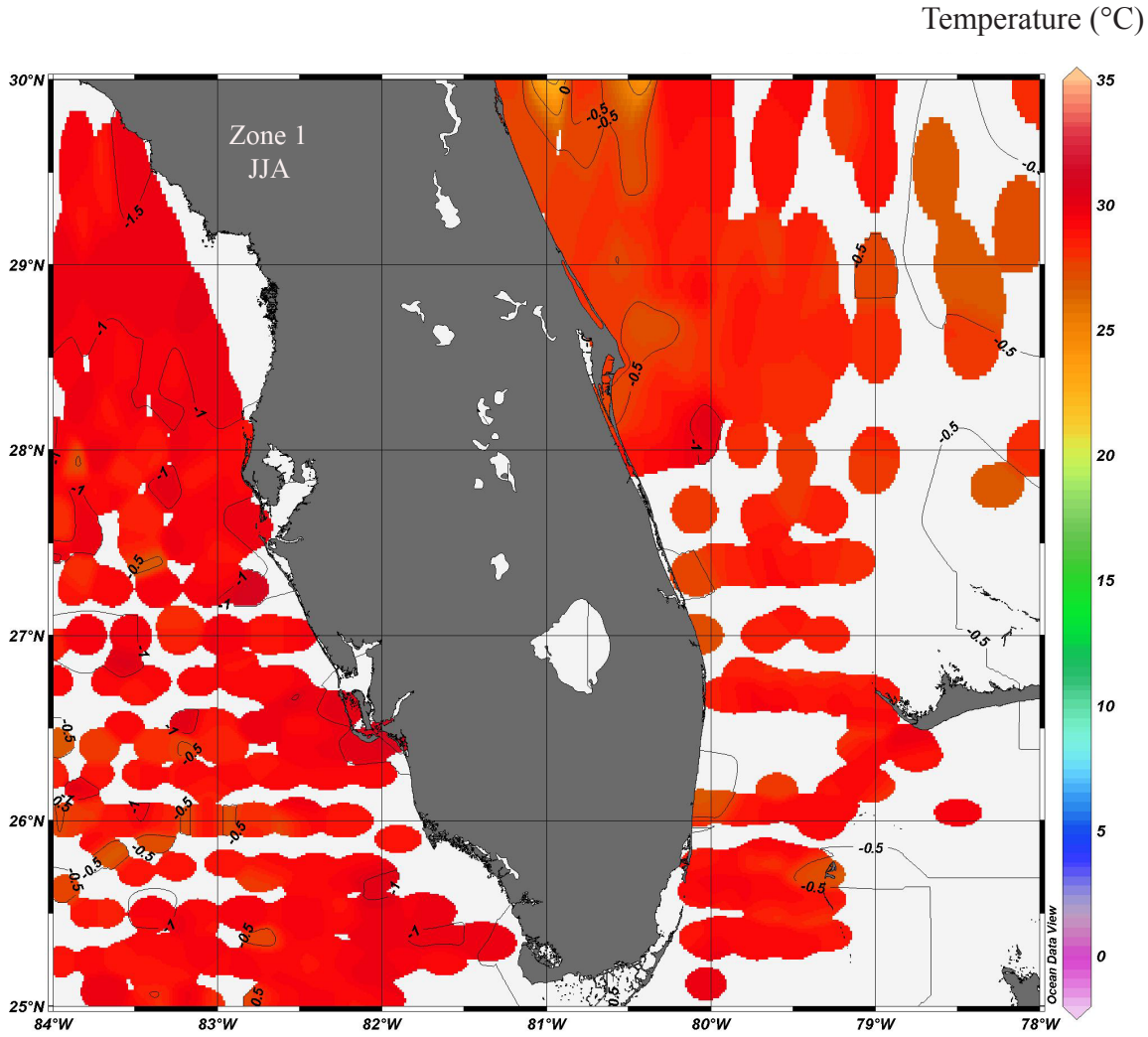

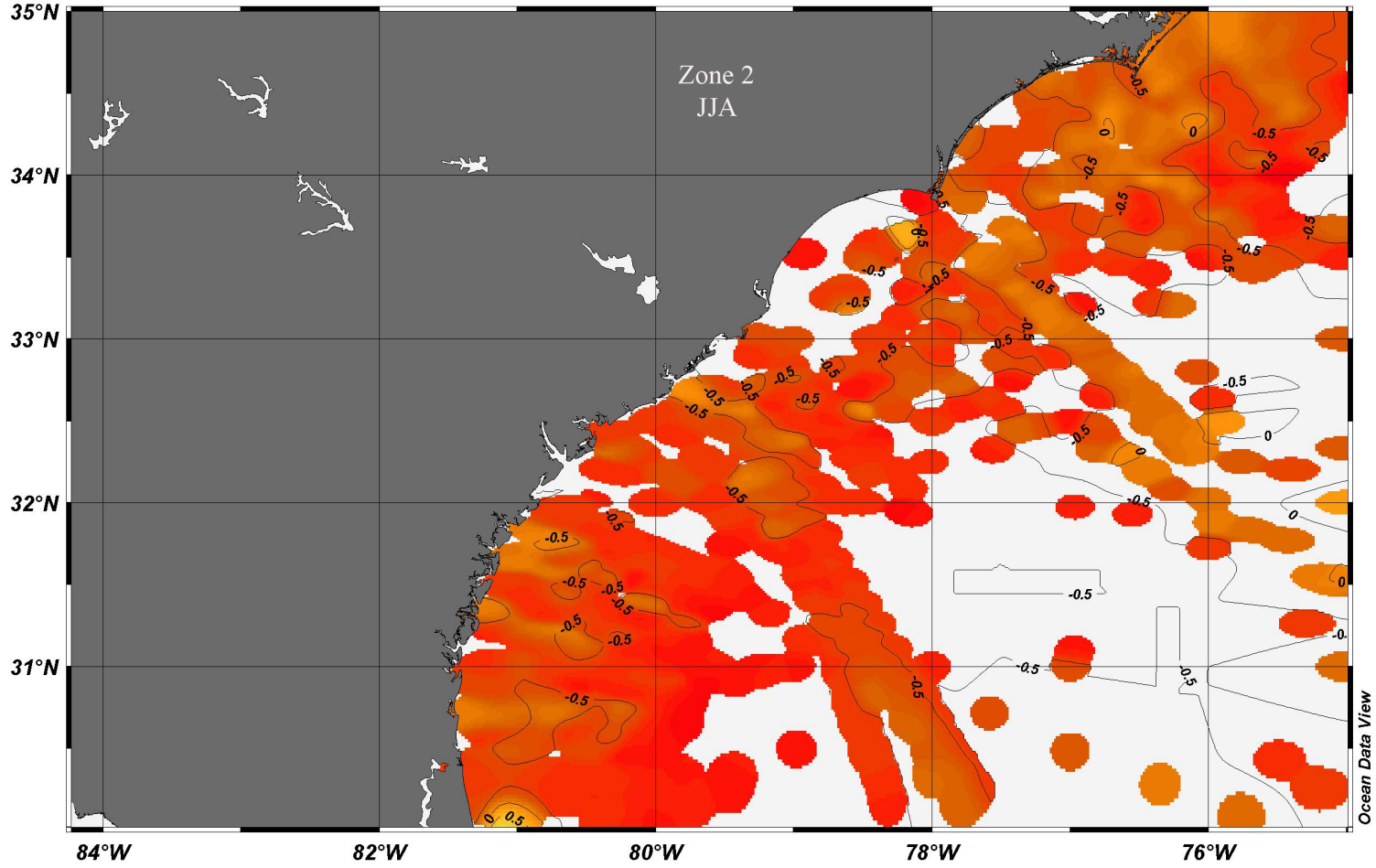
Zone 2
JJA
35°N
34°N
33°N
32°N
31°N
84°W
82°W
80°W
78°W
76°W
Ocean Data View

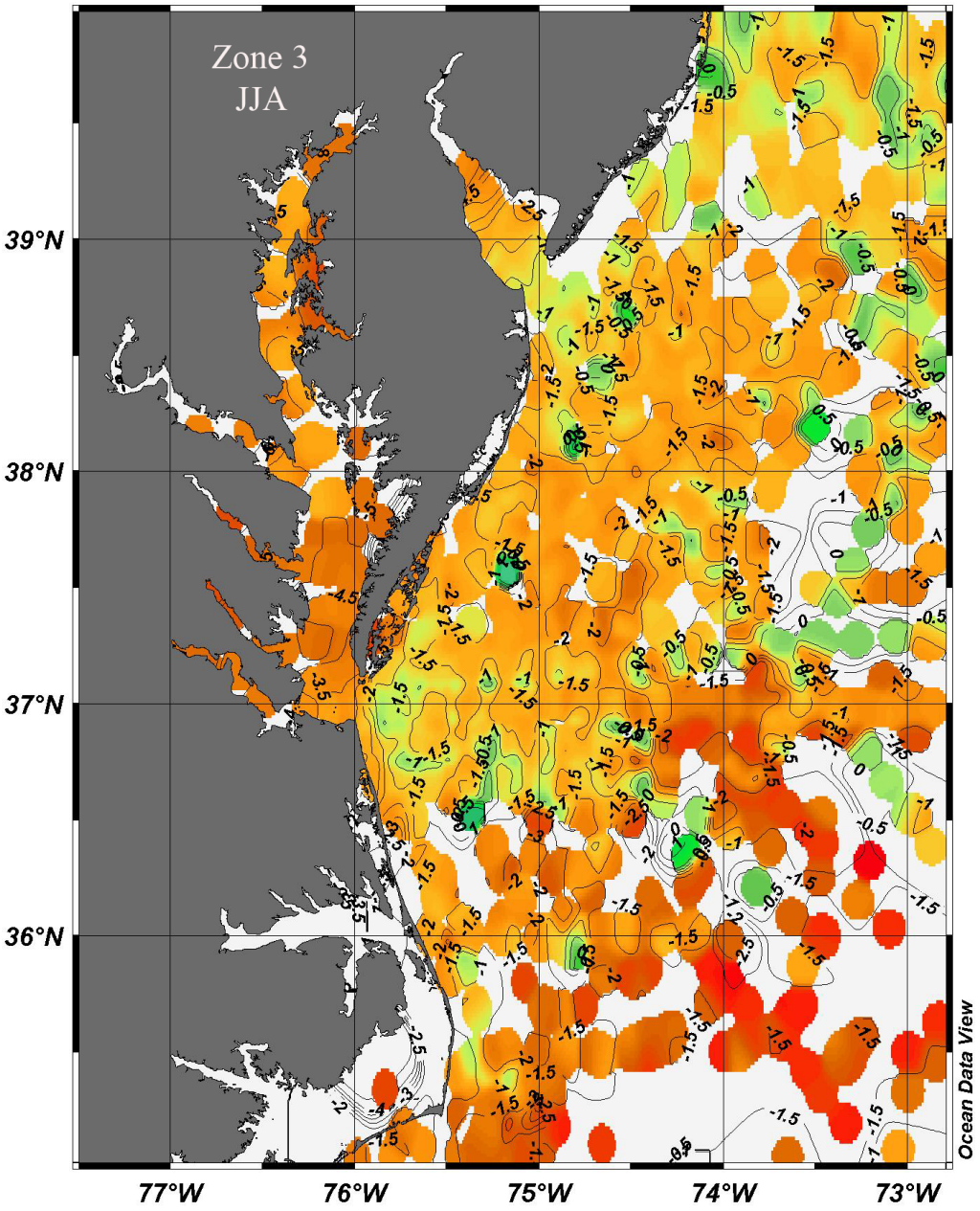
Zone 3
JJA
39°N
38°N
37°N
36°N
77°W
76°W
75°W
74°W
73°W
Ocean Data View

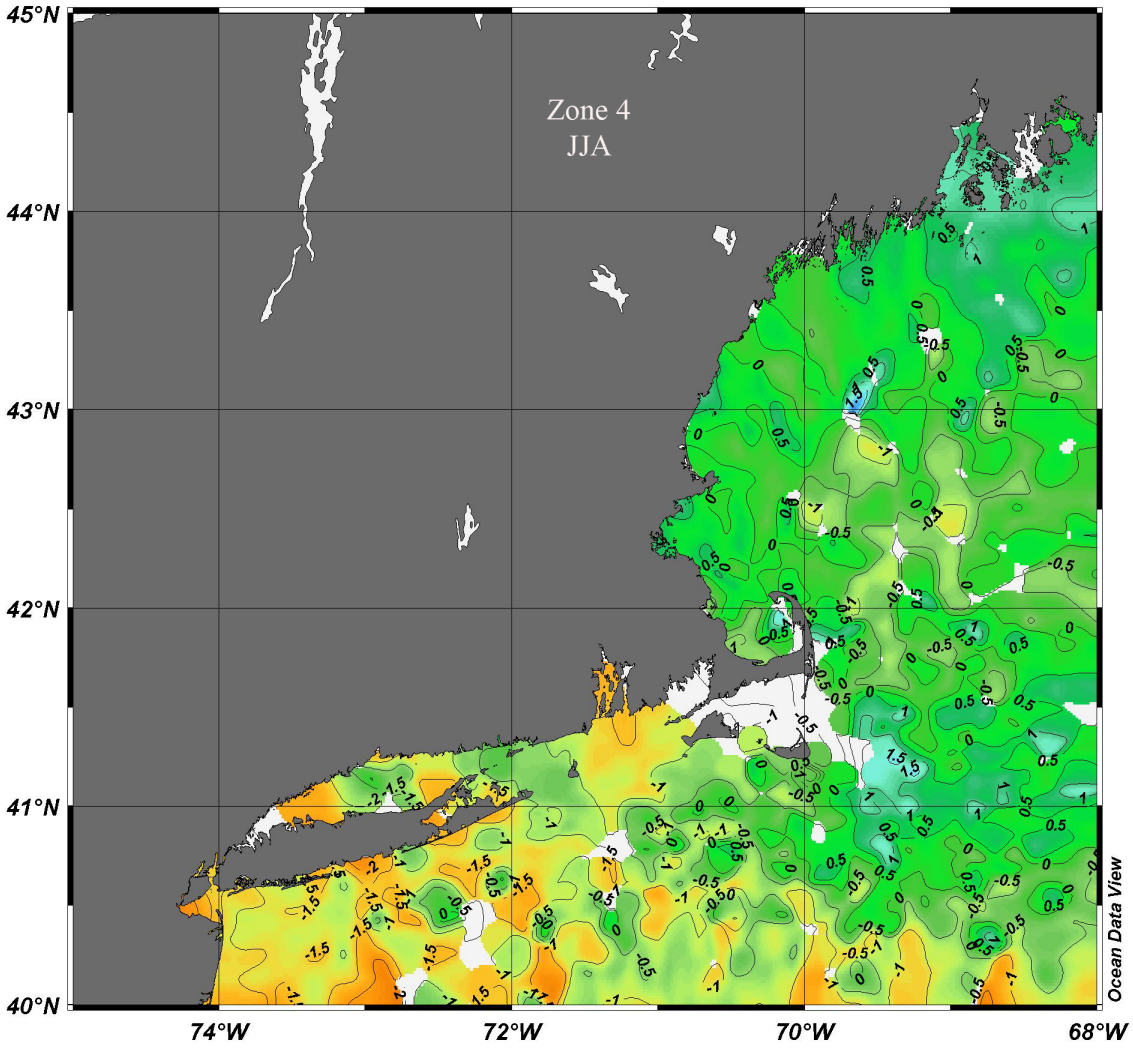
Zone 4
JJA
45°N
44°N
43°N
42°N
41°N
40°N
74°W
72°W
70°W
68°W
Ocean Data View

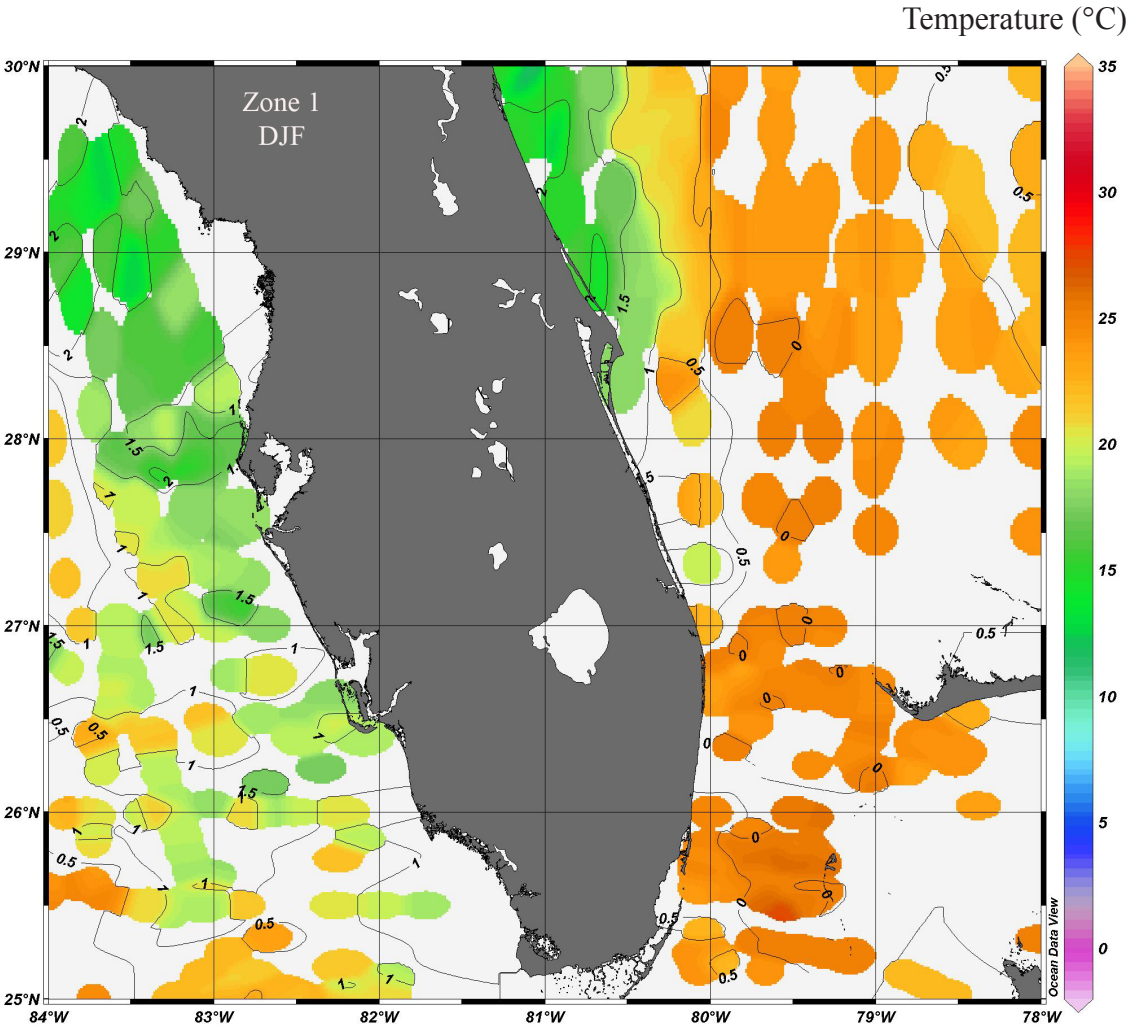
Temperature (°C)
Zone 1
DJF
30°N
29°N
28°N
27°N
26°N
25°N
84°W
83°W
82°W
81°W
80°W
79°W
78°W
35
30
25
20
15
10
5
0
Ocean Data View

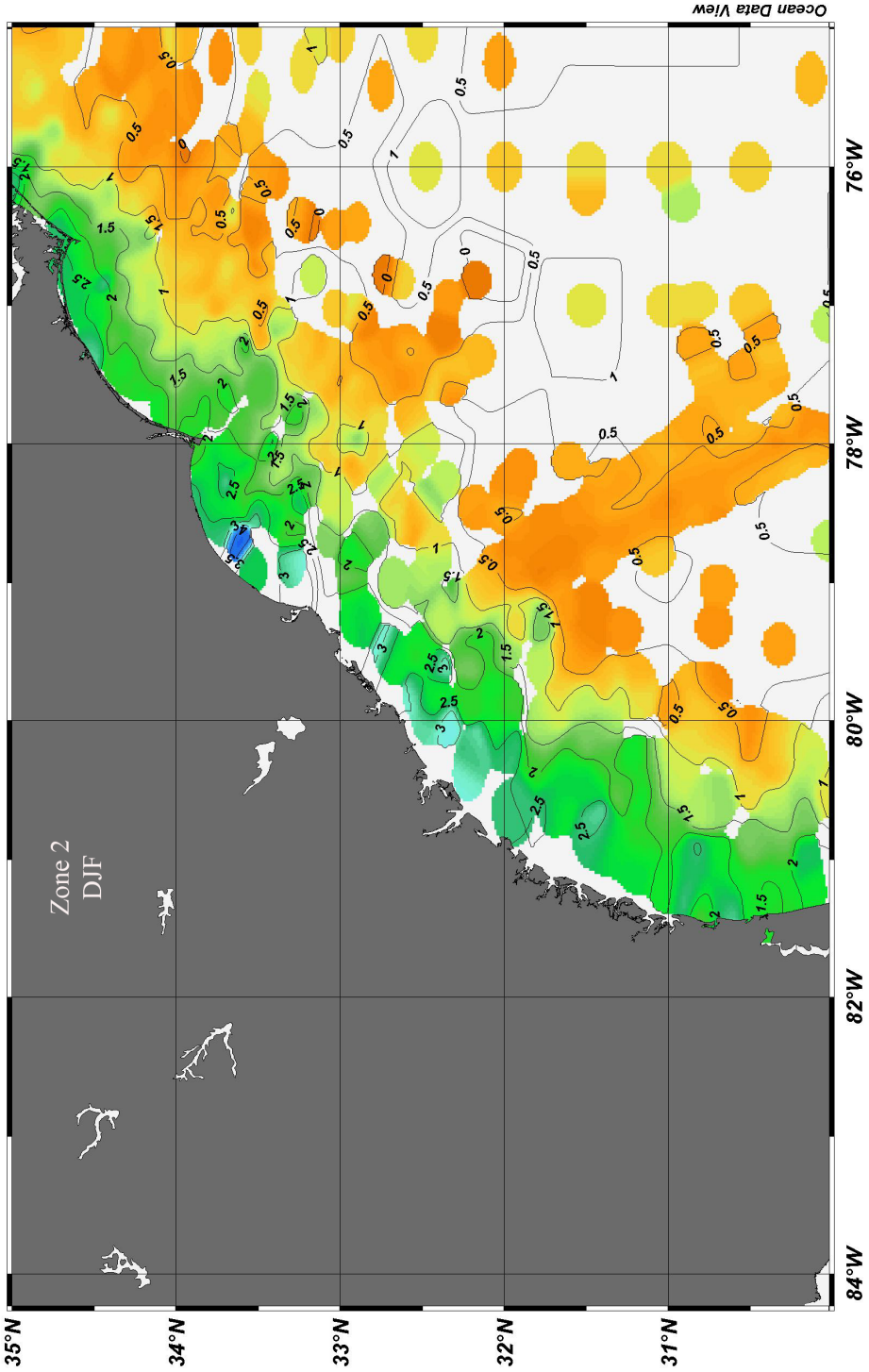
Ocean Data View
Zone 2
DJF
35°N
34°N
33°N
32°N
31°N
84°W
82°W
80°W
78°W
76°W

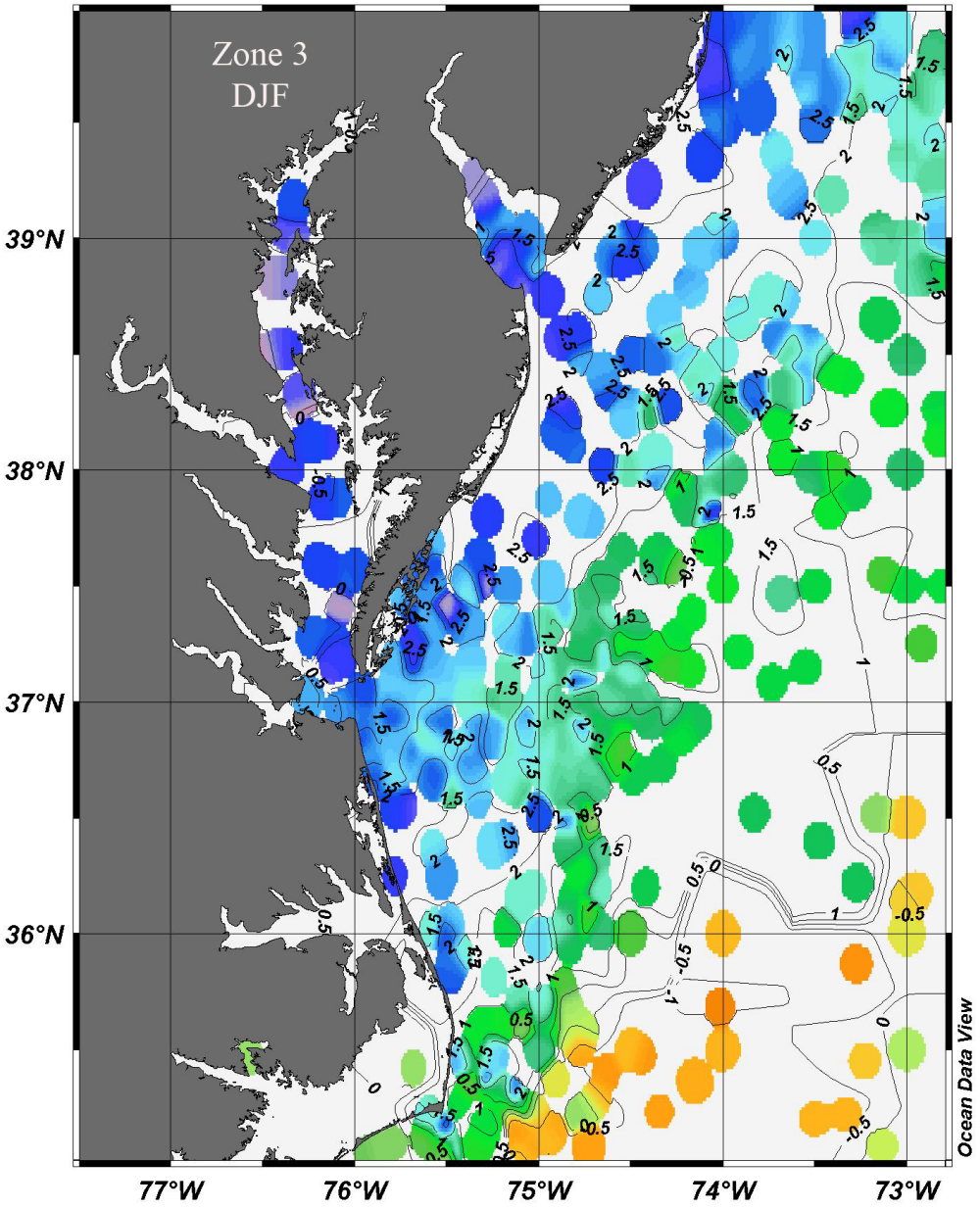
Zone 3
DJF
39°N
38°N
37°N
36°N
77°W
76°W
75°W
74°W
73°W
Ocean Data View

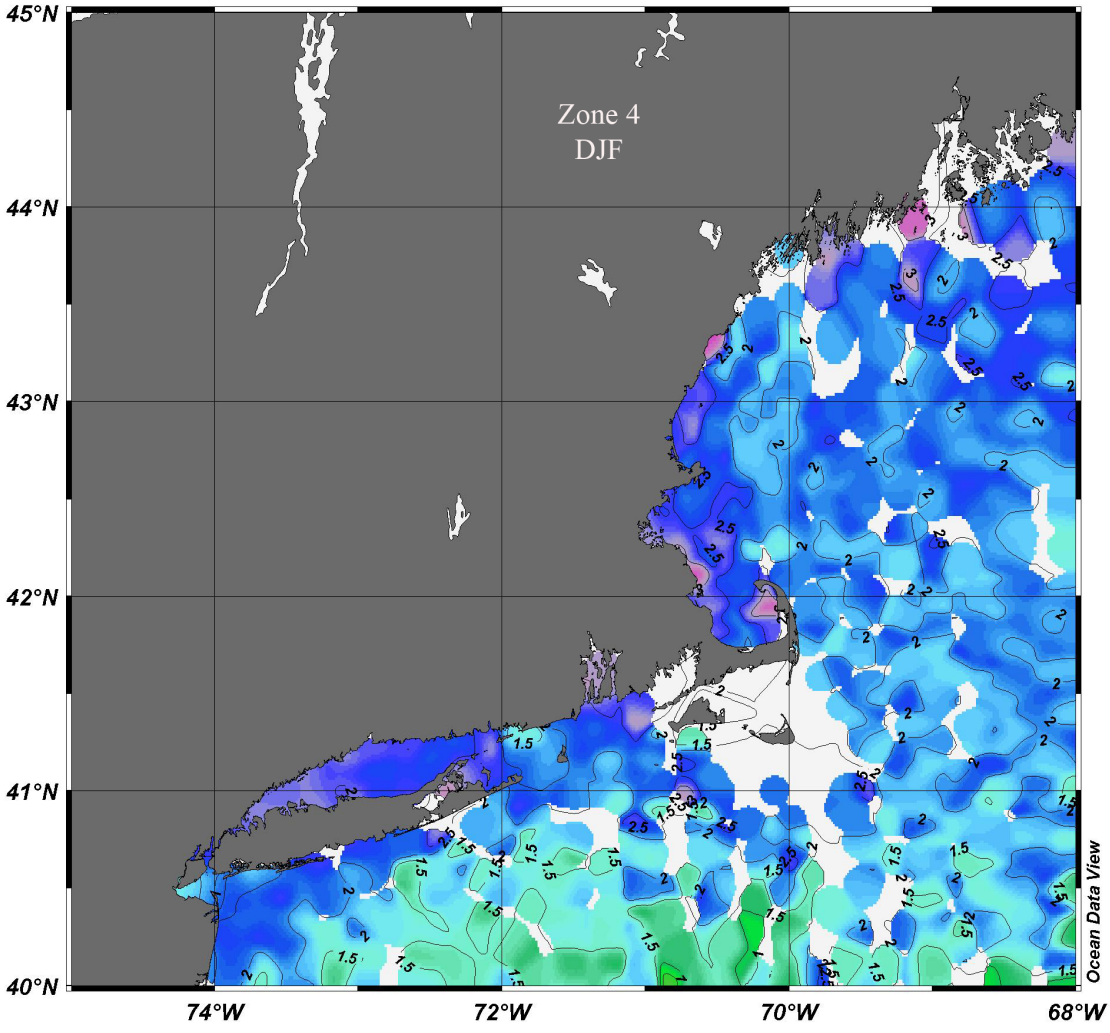
Zone 4
DJF
45°N
44°N
43°N
42°N
41°N
40°N
74°W
72°W
70°W
68°W
Ocean Data View

References

Ansell, A.D., 1968. The rate of growth of the hard clam *Mercenaria mercenaria* (L.) throughout the geographical range. Conseil Permanent International pour l'Exploration de la Mer, Journal du Conseil, 31 (3): 364-409.

Böehm, F., Joachimski, M.M., Dullo, W.-C., Eisenhauer, A., Lehnert, H., Reitner, J., and Woerheide, G., 2000. Oxygen isotope fractionation in marine aragonite of coralline sponges. Geochimica et Cosmochimica Acta, 64 (10): 1695-1703.

Coplen, T.B., and Kendall, C., 2000. Stable hydrogen and oxygen isotope ratios for selected sites of the U. S. Geological Survery's NASQAN and Benchmark surface-water networks. Open-File Report, U. S. Geological Survey, 00-160.

Crenshaw, M.A., 1980. Mechanism of shell formation and dissolution. *In* Rhoads, D.C., and Lutz, R.A., eds., Skeletal growth of aquatic organisms, Plenum Press, NY: 115-128.

Dame, R.F., 1996. Ecology of marine bivalves: an ecosystem approach. CRC Press, Boca Raton, 245 p.

Dettman, D.L., Reische, A.K., and Lohmann, K.C., 1999. Controls on the stable isotope composition of seasonal growth bands in aragonitic fresh-water bivalves (unionidae). Geochimica et Cosmochimica Acta, 63 (7-8): 1049-1057.

Eiler, J.M., 2007. "Clumped-isotope" geochemistry - The study of naturally-occurring, multiply-substituted isotopologues. Earth and Planetary Science Letters, 262: 309-327.

Elliot, M.B., deMenocal, B.K.L., and Howe, S.S., 2003. Environmental controls on the stable isotopic composition of *Mercenaria mercenaria*. Potential application to paleoenvironmental studies. Geochem., Geophys. Geosyst., 4 (7): 1056.

Epstein, S., Buchsbaum, R., Lowenstam, H.A., and Urey, H.C., 1953. Revised carbonate-water isotopic temperature scale. Geological Society of America Bulletin, 64 (11): 1316-1326.

Fairbanks, R.G., 1982. The origin of continental shelf and slope water in the New York Bight and Gulf of Maine; evidence from $H_2{}^{18}O/H_2{}^{16}O$ ratio measurements. Journal of Geophysical Research. C. Oceans and Atmospheres, 87 (8): 5796-5808.

Ghosh, P., Adkins, J., Affek, H., Balta, B., Guo, W., Schauble, E.A., Scharg, D., and Eiler, J.M., 2006. ^{13}C-^{18}O bonds in carbonate minerals: a new kind of paleothermometer. Geochemica et Cosmochimica Acta, 70: 1439-1456.

Gillikin, D.P., De Ridder, F., Ulens, H., Elskens, M., Keppens, E., Baeyens, W., and Dehairs, F., 2005a. Assessing the reproducibility and reliability of estuarine bivalve shells (*Saxidomus giganteus*) for sea surface temperature reconstruction: Implications for paleoclimate studies. Palaeogeography, Palaeoclimatology, Palaeoecology, 228: 70-85.

Gillikin, D.P., Lorrain, A., Navez, J., Taylor, J.W., André, L., Keppens, E., Baeyens, W., and Dehairs, F., 2005b. Strong biological controls on Sr/Ca rations in aragonitic marine bivalve shells. Geochemistry, Geophysics, Geosystems, 6 (5): 16 p.

Gleason, K., 2010. NOAA, National Climate Data Center, http://lwf.ncdc.noaa.gov/oa/climate/research/cag3/cag3.html

Goodwin, D.H., Prabasaj, P., and Wissink, C., 2009. MoGroFunGen: a numerical model for reconstructing intra-annual growth rates of bivalve molluscs.

Palaeogeography, Palaeoclimatology, Palaeoecology, 276: 47-55.
Goodwin, D.H., Schöne, B.R., and Dettman, D.L., 2003. Resolution and fidelity of oxygne isotopes as paleotemperature proxies in bivalve mollusk shells: models and observations. Palaios, 18: 110-125.
Gröcke, D., and Gillikin, D.P., 2008. Advances in mollusc sclerochronology and sclerochemistry: tools for understanding climate and environment. Geo-Marine Letters, 28: 265-268.
Grossman, E.L., and Ku, T.-L., 1986. Oxygen and carbon isotope fractionation in biogenic aragonite; temperature effects. Chemical Geology; Isotope Geoscience Section, 59 (1): 59-74.
Hall, C., 1964. Shallow-Water Marine Climates and Molluscan Provinces Shallow-Water Marine Climates and Molluscan Provinces. Ecology, 45 (2): 226-234.
Ivany, L., Lohmann, K.C., Hasiuk, F., Aronson, R., and Moody, R., 2008. Eocene climate record of a high southern latitude continental shelf: Seymor Island, Antarctica. Geological Society of America Bulletin, 120 (5/6): 659-678.
Jones, D.S., Arthur, M.A., and Allard, D.J., 1989. Sclerochronological records of temperature and growth from shells of *Mercenaria mercenaria* from Narragansett Bay, Rhode Island. Marine Biology, 102: 225-234.
Jones, D.S., and Quitmyer, I.R., 1996. Marking time with bivalve shells; oxygen isotopes and season of annual increment formation. Palaios, 11 (4): 340-346.
Khim, B.-K., and Krantz, D.E., 1996. Oxygen isotopic identity of the Delaware coastal current. Journal of Geophysical Research, 101 (C7): 16,509-16,514.
Kobashi, T., and Grossman, E.L., 2003. The oxygen isotopic record of seasonality in Conus shells and its application to understanding late middle Eocene (38 Ma) climate. Paleontological Research, 7 (4): 343-355.
Krantz, D.E., Williams, D.F., and Jones, D.S., 1987. Ecological and paleoenvironmental information using stable isotope profiles from living and fossil molluscs. Palaeogeography, Palaeoclimatology, Palaeoecology, 58 (3-4): 249-266.
Leder, J.J., Swart, P.K., Szmant, A.M., and Dodge, R.E., 1996. The origin of variations in the isotopic record of scleractinian corals: I. Oxygen. Geochimica et Cosmochimica Acta, 60 (15): 2857-2870.
Lisiecki, L.E., and Raymo, M.E, 2005. A Pliocene–Pleistocene stack of 57 globally distributed benthic $\delta^{18}O$ records. Paleoceanography, 20: 1003.
McCrea, J.M., 1950. On the isotopic chemistry of carbonates and a paleotemperature scale. The journal of chemical sciences, 18 (6): 849-857.
O'Donnell, T.H., 2002. Stable isotope compositions and aminoacid preservation in *Mercenaria* shells, Ph.D. thesis, University of Virginia. 247 p.
Patterson, W.P., Smith, G.R., and Lohmann, K.C., 1993. Continental paleothermometry and seasonality using the isotopic composition of aragonitic otoliths of freshwater fishes. *In* Swart, P.K., Lohmann, K.C.*, et al.*, eds., Climate change in continental isotopic records, Geophysical Monograph, 48, American Geophysical Union, Washington, DC.
Polyakov, I.V., Bhatt, U.S., Simmons, H.L., Walsh, D., Walsh, J.E., and Zhang, X., 2005. Multidecadal variability on North Atlantic temperature and salinity during the twentieth century. Journal of Climate, 18: 4562-4581.

Potts, D.C., 2004. Growth of Hard Clams (*Mercenaria mercenaria*) under brown tide conditions using mark-recovery and stable isotope analysis, Ph.D. thesis, Stony Brook University.

Schlitzer, R., 2010. Ocean Data View, http://odv.awi.de.

Schmidt, G.A., Bigg, G.R., and Rohling, E.J., 1999. Global seawater oxygen-18 database, http://data.giss.nasa.gov/o18data/

Schöne, B.R., Freyre Castro, A.D., Fiebig, J., Houk, S.D., Oschmann, W., and Kroncke, I., 2004. Sea surface water temperatures over the period 1884-1983 reconstructed from oxygen isotope ratios of a bivalve mollusk shell (Arctica islandica, southern North Sea). Palaeogeography, Palaeoclimatology, Palaeoecology, 212 (3-4): 215-232.

Schöne, B.R., Rodland, D.L., Fiebig, J., Oschmann, W., Goodwin, D.H., Flessa, K.W., and Dettman, D.L., 2006. Reliability of multitaxon, multiproxy reconstructions of environmental conditions from accretionary biogenic skeletons. The Journal of Geology, 114: 267-285.

Shanahan, T.M., Pigati, J.S., Dettman, D.L., and Quade, J., 2005. Isotopic variability in the aragonite shells of freshwater gastropods living in springs with nearly constant temperature and isotopic composition. Geochimica et Cosmochimica Acta, 69 (16): 3949-3966.

Stecher, H.A., III, Krantz, D.E., Lord, C.J., III, Luther, G.W., III, and Bock, K.W., 1996. Profiles of strontium and barium in *Mercenaria mercenaria* and *Spisula solidissima* shells. Geochimica et Cosmochimica Acta, 60 (18): 3445-3456.

Surge, D., Lohmann, K.C., and Dettman, D.L., 2001. Controls on isotopic chemistry of the American oyster, *Crassostrea virginica*; implications for growth patterns. Palaeogeography, Palaeoclimatology, Palaeoecology, 172 (3-4): 283-296.

Surge, D., and Walker, K.J., 2006. Geochemical variation in microstructural shell layers of the southern quahog (*Mercenaria campechiensis*): implications for reconstructing seasonality. Palaeogeography, Palaeoclimatology, Palaeoecology, 237: 182-190.

Thorrold, S.R., Campana, S.E., Jones, C.M., and Swart, P.K., 1997. Factors determinign $\delta^{13}C$ and $\delta^{18}O$ fractionation in aragonitic otoliths of marine fish. Geochimica et Cosmochimica Acta, 61 (14): 2909-2919.

Trumbore, S.E., 1981. Oxygen and carbon isotope ratios in modern and pleistocene *Mercenaria*, B.Sc. thesis, University of Delaware.

Versteegh, E., Troelstra, S., Vonhof, H., and Kroon, D., 2009. Oxygen isotope compositions of bivalve seasonal growth increments and ambient water in the rivers Rhine and Meuse. Palaios, 24: 497-504.

Walker, K.J., and Surge, D., 2006. Developing oxygen isotope proxies from archaeological sources for the study of Late Holocene human-climate interactions in coastal southwest Florida. Quaternary International, 150 (1): 3-11.

Wefer, G., and Berger, W.H., 1991. Isotope paleontology: growth and composition of extant calcareous species. Marine Geology, 100 (1-4): 207-248.

White, R.M.P., Dennis, P.F., and Atkinson, T.C., 1999. Experimental calibration and field investigation of the oxygen isotopic fractionation between biogenic aragonite and water. Rapid communications in mass spectrometry, 13: 1242-1247.

Yobbi, D.K., 1992. Effects of tidal stage and ground-water levels on the discharge and water quality of springs in coastal Citrus and Hernando counties, Florida. Water-Resources Investigations, U. S. Geological Survey, WRI 92-4069, 44 p.

Zhou, G.-T., and Zheng, Y.-F., 2003. An experimental study of oxygen isotope fractionation between inorganically precipitated aragonite and water at low temperatures. Geochimica et Cosmochimica Acta, 67 (3): 387-399.

CHAPTER 4

Chronostratigraphic and paleoenvironmental constraints derived from the $^{87}Sr/^{86}Sr$ and $\delta^{18}O$ signal of Miocene bivalves, Southern McMurdo Sound, Antarctica

Abstract

$^{87}Sr/^{86}Sr$ on samples of various macrofossil taxa recovered from the SMS AND–2A core were carried out with the main goal of improving age control of the core, and provide insight on marine climate at the time of carbonate precipitation. Shell material was carefully screened using cathodoluminescence (CL) to discern optimum areas for microdrilling. Powders thus obtained were in addition analyzed for Ca, Mg, Sr, Mn, and Fe contents to further evaluate the possibility of diagenetic alteration of the skeletal carbonate before measuring their Sr isotope compositions. Bivalves turned out to be the best candidates for isotopic determinations. Unaltered calcitic bivalves produced reliable $^{87}Sr/^{86}Sr$ age ranges. Aragonitic material, on the other hand, produced less radiogenic $^{87}Sr/^{86}Sr$ than anticipated, an unexpected result. Preliminary oxygen isotope determinations in calcite samples confirm contrasting marine climate conditions between the late Early Miocene (16.5 – 16.0 Ma), and the early Late Miocene (~11 Ma).

Keywords: McMurdo Sound; Paleoclimatology; Venerida; Aragonite; Sr–87/Sr–86; O–18/O–16.

4.1. Introduction

Interactions among the various components of the climate system are diverse and complex. While definite climate variability has been captured within historical boundaries, this timeframe is insufficient to recognize, evaluate, or predict changes. The modern cryosphere offers the opportunity to study direct climate records at a longer time scale. For example, examining the overall 10^5 ka record of the Vostok and Dome C ice–cores from East Antarctica (Barnola et al., 1987; Petit et al., 1999; Augustin et al., 2004), the potential effects of the remarkable increase in anthropogenic CO_2 occurred during the last century become apparent. Even though some research suggests decoupling between global temperature trends and atmospheric greenhouse gas concentrations at longer time scales (Veizer et al., 2000), the Vostok and similar ice–core records leave no question about the covariant behavior of these two factors in the short run, and the immediacy of future climate warming (see Crowley and Berner, 2001; IPCC, 2001, 2007).

The extent of warming and its effect on other climate components, however, remains unclear. A better understanding of future climate comes only from the deeper geologic past, where a wider range of possible behaviors can place present–day perturbations into context. A sense of urgency stems from the global temperature increase predicted for this century (Cubasch et al., 2001; Meehl et al., 2007), the much faster reduction in the past few years of Arctic sea ice (Parkinson and Cavalieri, 2008), and the recent evidence contradicting the assumption that Antarctica was somewhat insensitive to the recent global temperature change (Gillett et al., 2008).

Computer modeling has become a powerful predictive tool for climate. A complete understanding of forcing, feedback and thresholds is necessary to produce accurate predictions. Two types of models are typically built in climate studies: parameterized models, such as the widely used global circulation models (GCM), apply initial and boundary conditions to produce a temperature outline that represents climate conditions (e.g., DeConto and Pollard, 2003b, 2003a; Pekar and DeConto, 2006);

statistical models, on the other hand, extract and constrain the periodic or non–periodic nature of climate response from temperature records in search of pairing evidence with forcing (e.g., Alley et al., 2001). Success of either one depends on the accuracy of the data feeding the models or against which results are compared. Therefore, continued research to improve and expand proxies' accuracy and reliability is critical to climate understanding and eventual prediction.

Climate proxies in the sedimentary record are abundant and have helped piece together a geologic history of climate change (e.g., Zachos et al., 2001; Lear et al., 2002; Billups and Schrag, 2003). However, the many unanswered questions that remain require focusing research effort on critical areas and time intervals. Antarctica's ice sheets have played a preponderant role on climate through changes in albedo, sea level, and oceanic and atmospheric circulation, among others, and are often called upon to explain remote evidence of climate change (e.g., Harwood et al., 2005). Yet, their behavior under unprecedented rapid global warming is unknown, and sedimentary records from this area during critical intervals are fundamental. Antarctica's climate evidence from the Neogene is particularly important. At this time, the overall Cenozoic cooling trend culminates with the apparent consolidation of both East and West Antarctica ice sheets in the southern hemisphere and the development of permanent ice caps in the northern hemisphere. Understanding the responses and feedbacks established during these events is critical to calibrate climate models and to strengthen their predictive power.

The nature and timing of the change to frigid polar condition in Antarctica during the Miocene is a persistent problem. Global deep–sea $\delta^{18}O$ records indicate a transition from a climatic optimum at 17 to 15 Ma, to perennial ice at about 10 Ma (Zachos et al., 2001), while evidence from other sources suggests that this transition occurred later during the Pliocene (Webb and Harwood, 1991; Harwood and Webb, 1998; Murphy et al., 2002). This latter view is supported by evidence from the northern hemisphere that indicates a mid–Pliocene climatic optimum at about 3 Ma, requiring higher sea–levels

by up to 50 m shortly before the onset of the northern hemisphere glaciations (Haq et al., 1987; Crowley, 1991; Cronin and Dowsett, 1993; Dowsett et al., 1999). This scenario, which requires substantial melting of Antarctica's ice sheets at the time (e.g., Webb et al., 1984; Raymo et al., 2006), is not without controversy (Kennett and Hodell, 1995; Miller and Mabin, 1998; McKay et al., 2008). Understanding these transitions and assessing climate stability during the past 20 Ma from the Antarctica perspective is relevant to estimate future climate response.

In this paper, $^{87}Sr/^{86}Sr$ and $\delta^{18}O$ from selected Miocene to Pleistocene fossil material recovered by ANDRILL from Antarctica's continental shelf are used to pursue two main goals: first, to contribute to the critical chronostratigraphic control of the section through Sr–isotope ages of unaltered samples; and second, to provide insight on local climate based on the environmental limitations imposed by preliminary oxygen isotope data and Sr isotopic composition and concentration in the samples analyzed. Establishing a valid chronostratigraphic framework is critical to enhance interpretations based on this newly retrieved sequence, and thought not providing a complete stratigraphy, Sr isotope control can be critical to corroborate results from other dating methods. Similarly, incipient results based on limited oxygen and strontium isotopic composition serve to confirm environmental variability during the Miocene and to provide some rough estimates of departures from global averages.

4.2. Regional setting – core AND–2A

The Antarctic Geological Drilling (ANDRILL) program is an ongoing multinational collaborative effort to drill Antarctica's margin (Florindo et al., 2008). ANDRILL's goal is to recover complete enough stratigraphic records to help understand the history of glaciations and environmental change in the Victoria Land Basin region (Figure 4.1). This pursuit started with the completion in 2006 of core MIS AND–1B drilled over McMurdo Ice Shelf, and followed in 2007 by the recovery of core AND–2A.

Macrofossil samples analyzed in this study were selected from core AND–2A

located over the sea–ice platform in southern McMurdo Sound. The core recovered 1138 m of Early Miocene to Pleistocene sediments (Fielding et al., 2008; Taviani et al., 2008). The relatively rapid sedimentation rate (an average of 18 cm/ky for most of the core, Acton et al.(2008)) secured improved chronostratigraphic control in this critical area of the continental shelf within the West Antarctic Rift System, flanked by the Transantarctic Mountains and the Erebus volcanic province. These tectonic features created the necessary accommodation space to preserve the thick silici– and volcani–clastic fill that records the interaction among the bodies of ice present in the region (the Ross Ice Shelf, the East Antarctic Ice Sheet and the West Antarctic Ice Sheet) as they responded to climate evolution (Harwood et al., 2005).

Fourteen lithostratigraphic units (LSU) were defined in AND–2A. The top 37 m (LSU 1) are composed chiefly of volcanic and sedimentary rocks. From this depth to the end of the core, with a few exceptions (i.e., LSU 3, 9, 11, 13 and parts of 8), diamictite is the dominant lithology. Between about 40 m and 300 m below sea floor (mbsf) (LSU 2–6) conglomerate, sandstone and claystone appear subordinate to the diamictite. Volcanic debris reappears in LSU 7, at about 340 mbsf, and persists to about 780 mbsf (LSU 10). Macrofossils are present from LSU 2 to the end of the core in variable abundance and preservation. Serpulid tubes are the most abundant form followed by bivalves, gastropods, bryozoans, echinoids, cirripeds, sponges, brachiopods and fish fragments. LSU 7, roughly from 340 to 440 mbsf, has the most remarkable mollusk fossil content. Bivalves are particularly abundant at this level, resulting sometimes in cm–thick mollusk coquina–like layers. Preservation of LSU 7 is also better. Dissolution occurs in shallow units (e.g., LSU 2, 37.1 to 98.5 m), and recrystallization is observed above and below LSU 7 (e.g., LSU 5 – 6, 122.9 to 339.9 m, and 10 – 12, 648.7 to 996.7 m). Local high organic carbon content resulted in some pyritization observed in units 8 and 12. Transport cannot be entirely ruled out in LSU 4 to 6 and probably 12 (Fielding et al., 2008).

4.3. Materials and methods

A total of 19 samples were analyzed for this study. Table 4.1 provides depth and a brief field description of the samples and of the 31 sub–samples that produced $^{87}Sr/^{86}Sr$ results. Sr isotope values are also shown. These 19 samples were carefully selected from the AND–2A units with the best fossil content and preservation potential. All fragments, bivalves from LSU 7 in particular, showed no signs of significant transport.

Samples were screened using cathodoluminescence (CL) to evaluate the possibility of diagenetic alteration of the skeletal carbonate and microsampled powders were analyzed to determine Mg, Sr, Mn, and Fe to Ca ratios before measuring Sr isotope composition. A few of the bivalves were selected for preliminary oxygen isotope analyses. The goal of this multi–analytical approach is to establish stronger quantitative criteria to assess the fidelity of Sr isotope values for age determinations and, at the same time, obtain paleoenvironmental and diagenetic evidence to further understand syn– and post–depositional conditions in McMurdo Sound during the Miocene.

All analyses were carried out at the University of Michigan. The sampling was in part done using a Merchantek MicroMill, a device designed for high resolution sampling that allows precise recovery of very small amounts of powder (i.e., tens of micrograms). Elemental ratios (Mg/Ca, Sr/Ca, Mn/Ca and Fe/Ca) were acquired using a ThermoFisherFinnigan Element inductively coupled plasma–mass spectrometer (ICP–MS). The method was modified from that used by (Rosenthal et al., 1999). Analytical precision was better than 2% for Ca, 1% for Sr and 5% for Mn and Fe relative standard deviation (%RSD) based on check standards, laboratory reference material, and sample replicates.

For the Sr isotope investigations, the extra solution from ICP–MS measurements was left to evaporate before being redissolved in 2.5N HCl. Separation of Sr from the other elements by column chromatography followed the procedures outlined by (Mukasa et al., 1991). Each sample was dried to a solid, treated with a drop of 14N HNO_3, redried,

and then loaded with 0.1% H_3PO_4 and $TaCl_5$ solution on a single rhenium filament. These samples were run on a multi–collector TIMS "VG Sector". Strontium isotope composition was corrected for mass–fractionation using $^{86}Sr/^{88}Sr=0.1194$. The repeated analyses of NBS–987 standard gave average ratio of $^{87}Sr/^{86}Sr=0.710251\pm10$ (n=5). Total blanks averaged 0.35 ng for Sr, which are negligible. Ages were obtained as described in Howarth and McArthur (1997) and McArthur et al. (2001) applying the Look–up Tables Version 4:08/04. Error bars include uncertainty from both the isotope determinations and the 95% confidence levels on the age curve.

To determine oxygen isotope composition, a few selected samples were re–drilled, and roasted in vacuo, at 200 ºC, to eliminate volatile contaminants. Oxygen and Carbon isotope ratios were determined using an automated Kiel IV device coupled to a triple–collector gas source Finnigan MAT 253 isotope–ratio mass spectrometer and reported against the VPDB standard. Standard deviations for both carbon and oxygen are equal to or better than 0.1 ‰.

4.4. Results

Cathodoluminescence and chemical analysis showed that alteration, though notable in several intervals, is not a pervasive problem throughout the core. Table 4.1 shows the metal to Ca ratios for all sub–samples and a letter to qualify CL as bright (B), dull (D) or non–luminescent (N). Uncharacteristic luminescence is described with X. Bold text indicates values within range of comparable modern unaltered material. Concentrations are reported using millimoles of metal to moles of Ca. This makes comparisons more meaningful and reliable, though absolute concentrations are still used in the text.

Luminescence in carbonates is mainly associated with the incorporation of Mn^{2+} within the crystalline structure of diagenetic calcite. In a similar fashion, diagenesis typically results in a decrease in Mg and Sr contents and may be indicated by elevated Fe concentration (e.g., Veizer, 1983; Popp et al., 1986). All Veneridae and most *Adamussium*

sp. and costate pectinid bivalve fragments showed localized, dull or no luminescence. The 2 exceptions are sample 4, of uncertain affinity, possibly another bivalve, and sample 19–2, from a fractured surface of a cirriped fragment. The rest of the fragments of uncertain affinity are brightly luminescent and so are all serpulid tubes. Echinoid fragments vary from non– to brightly luminescent. They appear to have pristine and diagenetic calcite that could be potentially sampled separately but was not the goal of the present study.

Mn concentration of unaltered modern venerids and pectinids is less than about 130 ppm, usually less than 100 ppm, and Fe varies from 30 to 1600 ppm. Recent echinoids show similar Mn but lower Fe concentration (up to about 620 ppm), and unaltered cirripeds are slightly lower in both Mn and Fe (Milliman 1974) (about 0.5 mmol/mol for Mn/Ca and 1 mmol/mol for Fe/Ca). Polychaete annelids show a somewhat higher minimum Fe concentration (Milliman, 1974; Brand and Veizer, 1980). In general Mn/Ca and Fe/Ca of pristine samples is expected to be ≤ 1 and ≤ 3 mmol/mol, respectively. All venerids and pectinid samples 11 and 14 fall in this category, while samples 7 and 17 have slightly higher Fe content. Cirriped and echinoid fragments have high concentrations of both Mn and Fe compared to modern unaltered counterparts (see Table 4.1).

As shown by this sample set, the presence or absence of luminescence alone may not be a good enough measure of diagenetic alteration (e.g., Barbin, 2000; Machel, 2000). Carbonate may not luminesce despite an increase in Mn content in samples where Fe concentration is sufficiently high. All low Fe–high Mn samples in this study are luminescent whereas samples that contain high concentrations of both Fe and Mn show dull or no luminescence despite clear chemical evidence of diagenetic alteration (e.g., samples 4–3, 6 and 19–2). Thus, the application of CL may be an appropriate initial assessment in many instances, but inadequate to uniquely discern altered from unaltered materials and should be paired with elemental analyses to affirm the preservation of

primary composition.

Measured Sr/Ca varies between 0.7 mmol/mol and 6.6 mmol/mol, with a few extreme values between 10.3 mmol/mol and 18.1 mmol/mol in the Veneridae specimens. About 80% of the samples have Sr/Ca between 0.7 mmol/mol and 3.95 mmol/mol, and the rest is entirely above this range. In recent calcitic bivalves, Sr/Ca averages about 1.2 mmol/mol; in aragonitic modern bivalves, it averages 1.6 mmol/mol (Morse and Mackenzie, 1990). In echinoids the maximum ratio is about 2.7 mmol/mol, and in cirripeda the Sr varies between 700 ppm and 6,000 ppm in calcitic plates (between about 0.8 mmol/mol and 6.8 mmol/mol) and up to 8,400 ppm (~ 9.6 mmol/mol) in their aragonite components (Milliman, 1974). The same can be said about the Sr incorporation in serpulid tubes: it depends on the mineralogy and can be as high as 9,300 ppm in aragonitic species. The commonly calcitic tubes show a maximum of about 3,700 ppm (Milliman 1974). Sr concentration within and above the range observed in modern unaltered taxa occurs in both Mn–Fe enriched and Mn–Fe depleted samples. Figure 4.2 shows the Sr to Mn relationship for samples with a Mn/Ca $\leq$ 20 mmol/mol. Note that very high Sr content in venerid shells is associated with undetectable Mn levels. X–ray diffraction corroborated that venerid skeletal composition is aragonite.

Mg/Ca in recent bivalves is typically less than 44 mmol/mol (Morse & MacKenzie, 1990) and 63 mmol/mol in Serpula (Bornhold and Milliman, 1973). Echinoids precipitate high Mg calcite stereoms and pristine Mg to Ca ratios can be as high as 166 mmol/mol (Carpenter and Lohmann, 1992). The measured Mg/Ca falls within this range for most samples. Samples 12 and 13 have Mg/Ca values close to 1 (0.7 to 1.4 mol/mol), a composition similar to that of dolomite. Indeed X–ray diffraction analysis showed dolomite as a major component of sample 13, which in addition displayed an uncharacteristic blue luminescence. Echinoid Mg content is within the normal range for pristine shells except in sample 16–3, taken from the outer surface of a coronal echinoid plate, which has a Mg to Ca ratio that corresponds to about 24 mol %

$MgCO_3$; higher than the normal 10–15 mol % (roughly 100 mmol/mol to 180 mmol/mol) typical of unaltered recent echinoids (e.g., Mackenzie et al., 1983). Highly luminescent secondary calcite fills the pores of the duller, potentially unaltered echinoid plates analyzed. The less porous mamela also produce duller luminescence under CL.

Selected venerid and pectinid individuals were again micro–sampled to measure oxygen isotopes. Results are shown in figure 4.4. $\delta^{18}O$ was determined for shells considered pristine and also for sample 13. Venerids and pectinids show a clear contrast in stable isotopic composition. $\delta^{18}O$ of samples 9 and 10 (i.e., aragonite) ranges from –5.3 to –3.3 ‰, and $\delta^{13}C$ between –3.1 and –2.3 ‰. Calcite, on the other hand, is in average 6 to 7 ‰ heavier than the aragonite in both oxygen and carbon. Dolomitic samples have the most negative compositions. Modern mollusks representing average normal conditions vary between about –4 ‰ to 1 ‰ in $\delta^{18}O$ and –1 ‰ and 3 ‰ $\delta^{13}C$ (Veizer, 1983; Morse and Mackenzie, 1990).

With few exceptions, trace element concentrations of dull and non–luminescent samples from venerid and pectinid valves are similar to those in pristine biogenic aragonite and calcite respectively, while samples of uncertain affinity, polychaete annelids, echinoids and cirripeds show at least partially altered carbonate. Figure 4.3 shows the samples distributed by $^{87}Sr/^{86}Sr$ age versus depth. $^{40}Ar/^{39}Ar$ ages and other main features of the AND–2A current age model are also shown (Acton et al., 2008). At the time the age model was constructed, pectinid sample 4–1 (11.67 Ma at 144 mbsf) helped corroborate an Ar–Ar age of 11.39 Ma at about 128 mbsf. Sample 4–2 was analyzed later and produced a slightly younger age. This variation increases the error somewhat, but further reaffirms the age model at that depth. Pectinid samples 7 and 11–3, and venerid sample 15 turned out to be also in close agreement with the age model. However, samples 11–1 and 11–2 and all other venerid samples (i.e., samples 9, 10 and 15–4) produced less radiogenic than anticipated $^{87}Sr/^{86}Sr$ corresponding with older than expected ages. With the exception of sample 16–1 taken from an echinoid fragments, and sample 8–2,

probably a cirriped, all samples with high concentration of Mn and Fe also produced higher than expected $^{87}Sr/^{86}Sr$ ages.

4.5. Discussion

Among pectinids, only samples 4–3, 6 and 13 were judged to be substantially altered. Sample 6 was not positively identified and could belong to a different taxon. Sample 4–3 was taken from the outer layer of the shell. Elemental chemistry of subsamples 8–1 and 8–2 indicates marginal alteration and their age estimate is probably not reliable. At the same time, relatively high Mg and Sr contents suggest these estimates may not be adequate, but this is not quantifiable. Sample 8, a very small, highly luminescent fragment, may be a cirriped piece. Though from a different stratigraphic level, sample 19, an unequivocal cirriped fragment, shows elemental composition and luminescence more akin to sample 8 than the rest of the pecten samples (Table 4.1).

Sample 11–3 has a Sr isotope ratio interpreted to reflect seawater composition at the time of precipitation, while samples 11–1 and 11–2 are significantly lighter. These subsamples, however, come from different material types present within sample 11. Fragment size precludes discriminating if these belong to different taxa or if they come from different parts of the same bivalve, but they look different enough to suspect a different taxonomic origin. Subsample 3 was taken from a thin, white fragment exhibiting vitreous luster reminiscent of calcite, while subsamples 1 and 2 came from fragments that were buff, thick and dull, with a discernable ribbed outer layer and a crystalline middle layer as were present in venerid samples 9 and 10. The elemental composition of subsamples 11–1 and 11–2 is very similar to that of venerids, and these are probably aragonite samples, not calcite. This observation is further supported by the $^{87}Sr/^{86}Sr$ results.

A similar observation can be made for subsample 15–1, the only venerid that produced a reasonable age estimate. Sample 15 also has 2 types of skeletal material. The description of subsample 11–3 is entirely appropriate for subsample 15–1; 15–4, on the

other hand, was taken from the middle layer of a typical venerid fragment. Given the appearance and elemental chemistry, it is evident that sample 11–3 came from a venerid while sample 15–1 is a pectinid fragment. It follows that the Sr isotopic composition is characteristically different for the different bivalves in the core. All calcitic pecten samples have $^{87}Sr/^{86}Sr$ values that are close to the original seawater composition at the time of precipitation, while all aragonitic Veneridae samples have lower than expected Sr isotopic compositions. Pecten samples 4, 7, 11–3, 15–1 and 14 are providing reasonable Sr age constrains for AND–2A.

Echinoid sample 16–3 and 18 produced $^{87}Sr/^{86}Sr$ ages in accord with the age model. These samples have a slightly higher Mn content, potentially normal for the specific individuals, but a very high Fe concentration. A maximum Fe/Ca of about 24 mmol/mol have been reported in echinoidal stereoms growing in heavy–metal polluted areas (e.g., Warnau et al., 1998). Fe/Ca in the samples analyzed is up to 15 times larger. The proper ages of some of the subsamples suggests that the alteration is localized and that efforts to draw material from the non–luminescent sectors of the skeleton may have been successful. It is doubtful that Fe can be incorporated into high magnesian calcite in such large amounts.

4.5.1. Oxygen isotopes

The limited oxygen isotope measurements further stress the chemical contrast between the two bivalvia families recovered from AND–2A, and help provide preliminary estimates of the marine climate contrast in time (between ~16.5 and ~11 Ma) and space (between local and global conditions) through simple scenarios of temperature and freshwater input. Assuming samples 4, 7, 9 and 10 are indeed pristine and represent conditions at the time of crystallization, the expected δ_w at the time of precipitation can be calculated assuming the bivalves were growing their shells at the published average deep–ocean Mg–temperature at 11 and 16–16.5 Ma (Lear et al., 2000). These values can then be compared to the published average δ_w to draw conclusion about the local

conditions at the times of interest. The Kim and O'Neil (1997) temperature dependent calcite to water fractionation relationship was used for samples 4 and 7 and Grossmand and Ku (1986) paleotemperature equation for aragonitic samples 9 and 10.

Both these equations are widely used and are, if nothing else, a sound tool for comparison with other studies. Analytical uncertainties associated with carbonate $\delta^{18}O$ determination do not surpass 0.5 ºC, and mollusks species specific fractionation is a minor concern. The development of a Mg/Ca global temperature curve requires the assessment of several important problems, among them are: 1) that Mg/Ca species specific differences are understood and corrected, 2) that primary Mg/Ca composition preservation is demonstrated, 3) that the variation of Mg/Ca in seawater during the Cenozoic is known, and 4) that a reliable calibration to calculate the temperature is adopted. Though all these issues were properly addressed in Lear et al.(2000) and their estimates constitute a satisfactory working model, some points more than others still hold some degree of uncertainty, and the final Mg/Ca record used for comparison is a low resolution profile where temperature extremes are not registered.

Covariant curves of temperature, benthic $\delta^{18}O$ and δ_w presented in Lear et al. (2000) (Figure 4.5) suggest that sample 4 should reflect somewhat cooler conditions than samples 7, 9 and 10. At 16–16.5 Ma estimated deep–ocean temperature is about 6.2 °C and δ_w is –0.75 ‰. This time interval coincides with the ending of a warming trend, and occurs shortly before a rapid ice accumulation event in the late Early Miocene (Lear et al., 2000, p. 270; Lewis et al., 2007). Modeling sample 7 calcite $\delta^{18}O$ at marine temperatures between 5 and 7 °C requires a δ_w between –0.1 ‰, and 0.4 ‰, a range not too far removed from the global δ_w estimate of –0.75 ‰. This suggests that local temperature and δ_w were probably close to deep–sea averages at the time. The difference in δ_w can be accommodated by sea–water temperature that is no more than 4 ºC colder than the deep–sea average. The likely combined effects of increased δ_w and reduced temperature would indicate conditions relatively close to world averages.

On the other hand, modeling sample 4 at marine temperatures between 3 °C and 5 °C, based on Lear et al. (2000) 4.6 °C deep–sea temperature estimate at 11 Ma, requires a δ_w between 2 ‰, and 2.5 ‰, when the world average is estimated at –0.41 ‰. This result suggests that both temperature and δ_w probably diverge considerably from the world average at the time. In fact, the large temperature reduction that would be necessary to precipitate sample 4 in waters with δ_w close to the deep–sea average (i.e., some 11 ºC of temperature drop) suggests that an important portion of this difference is attributable to ice accumulation. Cooling and in particular continental and sea–ice accumulation were affecting McMurdo Sound around 11 Ma.

In contrast, samples 9 and 10 require δ_w between –6 ‰, and –9 ‰ to satisfy temperature constraints. This is a very different scenario than the one suggested by pectinid sample 7. Aragonite samples are slightly older, recovered deeper in the core. The time elapsed between the precipitation of samples 9 and 10 and that of sample 7, 0.5 to 0.7 Ma based on the core's age model, may suffice to consolidate local changes. Important freshwater inputs could explain these estimates. For example, δ_w between –6 ‰ and –9 ‰ can be obtained by mixing 66 ‰ to 72 % seawater, δ_w = –0.75 ‰ with glacial meltwater, $\delta^{18}O$ = –30 ‰. This is a rather conservative estimate of meltwater's oxygen isotopic composition with respect to modern Antarctica's ice average $\delta^{18}O$, but probably reasonable considering the smaller ice accumulations that presumably existed there at the time. Salinity of a mix 70% seawater –30% meltwater is about 24 psu. Although Veneridae is a predominantly marine family (O'foighil, D., 2008, pers. comm.) this salinity is within the ecological limits of modern living Veneridae (e.g., *M. mercenaria*). This result suggests a significant source of freshwater close to AND–2A before 16 Ma. Recently, geomorphologic and sedimentologic evidence of large volumes of fast–flowing subglacial meltwaters discharges from the Dry Valleys into the Ross Sea during the middle Miocene was presented by Lewis et al. (2006). The particular episodes studied by the cited authors are more recent than 16.5 Ma (i.e., between 12 and 14 Ma),

but their observations and conclusions highlight the plausibility of similar episodic large discharges of meltwater occurring into McMurdo Sound at an earlier time. Further sampling for oxygen isotope analyses at other levels to reinforce and refine these results is necessary.

4.5.2. Sr isotopes

The brackish water that could explain the oxygen isotopic values of samples 9 and 10, even if the mix is modeled with meltwater less than –30 ‰ $\delta^{18}O$ allowing for greater proportions of seawater, makes reconciliation of high Sr concentrations in the venerids problematic. Using a maximum Sr/Ca equivalent to that of modern seawater, the calculated Sr distribution coefficients (D_{Sr} = [mSr/mCa]Aragonite/[mSr^{2+}/mCa^{2+}] seawater) consistent with the measured concentrations are in average 1.2 (min 0.4, max 2.0). This is in good agreement with published values applicable to inorganic and most skeletal aragonite (Veizer, 1983; Morse and Mackenzie, 1990). Mollusks, however, discriminate against Sr incorporation. The D_{Sr} required to produce the measured Sr concentrations in aragonite from brackish waters should be even higher. Although enrichment at this level is not unfeasible in recent bivalves, it is unclear what physico–chemical (i.e., temperature, pressure and cation complexing), metabolic or kinetic factors could facilitate this larger distribution coefficient.

Sr is contributed to the ocean by freshwater and hydrothermal fluid interactions with the lithosphere, and a simple mixing model can help establish the feasibility of the rock sources required to produce a local solution with the measured $^{87}Sr/^{86}Sr$. In the analyzed core, and more precisely, in LSU 7 from where the venerid samples were recovered, volcanogenic components are volumetrically important. In general, volcanism in the Antarctica plate is dominated by alkaline basalts (Kyle, 1990). The McMurdo volcanic group, which encompasses all volcanic rocks in the western Ross Embayment, contains the largest volumes of felsic and probably basaltic volcanic rocks on the entire Antarctic plate, and is the closest and possibly most important volcanic source to AND–

2A. Within this group, the Erebus volcanic province is in immediate proximity to the drill hole. Although most of Erebus volcanism is younger than about 7 Ma, oldest ages between 15 and 19 Ma have been reported for this province (Kyle, 1990).

Broadly, age appropriate volcanic sources in the western Ross Embayment range from a few ppm Sr in felsic rocks to about 1,700 ppm in mafic ones, with an average close to 700 ppm (Kyle, 1990; Rocholl et al., 1995; Rocchi et al., 1998; Rocchi et al., 2002), not remarkably high. $^{87}Sr/^{86}Sr$ in these rocks varies roughly between 0.7030 and 0.7050. This is in agreement with the 0.704 average used by Faure and Mensing (2005) for Mesozoic and Cenozoic volcanic rocks. Aragonite $^{87}Sr/^{86}Sr$ varies between 0.7079 and 0.7085, very close to the average isotope ratio of carbonate rocks. Modeling $^{87}Sr/^{86}Sr$ using average volcanic rocks, v= 0.7040, marine carbonates, m= 0.7080 and igneous crystalline rocks s= 0.720, the observed aragonite Sr isotope composition requires a volcanic input of up to 0.75. The average $^{87}Sr/^{86}Sr$ from older Paleozoic igneous rocks in northern Victoria Land, about 0.710 (Rocchi et al., 1998), would suggest that this is probably a good estimate to use in the three component mixing model because Sr isotope ratio derived from Precambrian crystalline rocks may be absent as an immediate Sr source adjacent to McMurdo Sound. However, that would reduce the volcanic input maximum to just 0.25 to 0.35, which is unlikely. A 0.75 volcanic input requires basically no contribution from carbonate rocks, and supports East Antarctica provenance of the heavier $^{87}Sr/^{86}Sr$ (Appendix 4.2).

Even though the above exercise shows the potential to develop local $^{87}Sr/^{86}Sr$ in fluids, it equally applies to global seawater Sr isotopic composition and does not explain the anomalous Sr concentrations and isotopic values of the venerids. Because Sr signature is contrasting along taxonomic lines, the lifestyles of the bivalves may offer an explanation. In general, modern pectinids and venerids are both suspension feeders, but while pectinids are epifaunal, venerids are infaunal siphonate. Modifications at the water–sediment interface can potentially exist and be reflected only in bivalves with siphons

at this level. The carbon isotopic composition, which also helps discern the bivalves' families, gives some support to this idea. In deed Venerids show a more negative $\delta^{13}C$ suggesting a possible ^{12}C rich DIC interstitial water source. Nevertheless, the possibility of alteration or co–precipitation of a Sr–rich phase within the aragonite shell that could account for the anomalous isotopic compositions and concentrations respectively cannot be discarded or confirmed.

4.6. Conclusions

Reliable Sr ages are obtained from well preserved fossil samples recovered from AND–2A, in particular from calcitic bivalves. Pectinid samples help to further establish age control at 144.05 , 366.8 , and 430.6 mbsf in accord with the core's age model (Acton et al., 2008). CL serves to preliminarily assess diagenetic alteration of carbonate fossils, but may not suffice to understand samples with more complex chemical alteration. With the exception of echinoid fragments, samples with high concentrations of Mn and Fe produced higher than expected $^{87}Sr/^{86}Sr$ ages in relation to the core's age model.

Aragonite samples appear pristine, but Sr ages resulted in older estimates than are reasonably possible and were not useful to improve the chronostratigraphic control of the core. Basic calculations using preliminary oxygen isotope determinations confirm that different paleoenvironmental conditions existed around 16 and 11 Ma. Global marine climate seems to be better represented in Antarctica in the late Early Miocene (Burdigalian–Langhian), while cooling and continental and sea ice accumulation may have controlled local marine conditions in the early Late Miocene (Serravalian–Tortonian).

Oxygen isotope compositions of the venerid samples also suggest that the AND–2A area was subject to abundant and/or substantially depleted meltwater input shortly before local cooler conditions prevailed at ~ 16 Ma. Further assessment is necessary to satisfactorily explain the anomalously high Sr content of some aragonites which also possess unexpectedly low $^{87}Sr/^{86}Sr$ values. Reconciliation of these observations requires

either that alteration be unequivocally demonstrated or that a secondary, high–Sr phase be present within the skeletal carbonates, providing unreasonable concentrations and isotopic age estimates.

Acknowledgements

The ANDRILL project is a multinational collaboration between the Antarctic programmes of Germany, Italy, New Zealand and the United States. Antarctica New Zealand is the project operator and developed the drilling system in collaboration with A. Pyne. Antarctica New Zealand supported the drilling team at Scott Base; Raytheon Polar Services Corporation supported the science team at McMurdo Station and the Crary Science and Engineering Laboratory. The ANDRILL Science Management Office at the University of Nebraska–Lincoln provided science planning and operational support. The scientific studies are jointly supported by the US National Science Foundation, the New Zealand Foundation for Research Science and Technology and the Royal Society of New Zealand Marsden Fund, the Italian Antarctic Research Programme, the German Research Foundation and the Alfred Wegener Institute for Polar and Marine Research.

We thank Ted Huston and Lora Wingate for technical help, and Diarmaid O'foighil, Youxue Zhang and the reviewers for their pertinent, detailed and enriching comments. ISMAR scientific contribution n. 1613.

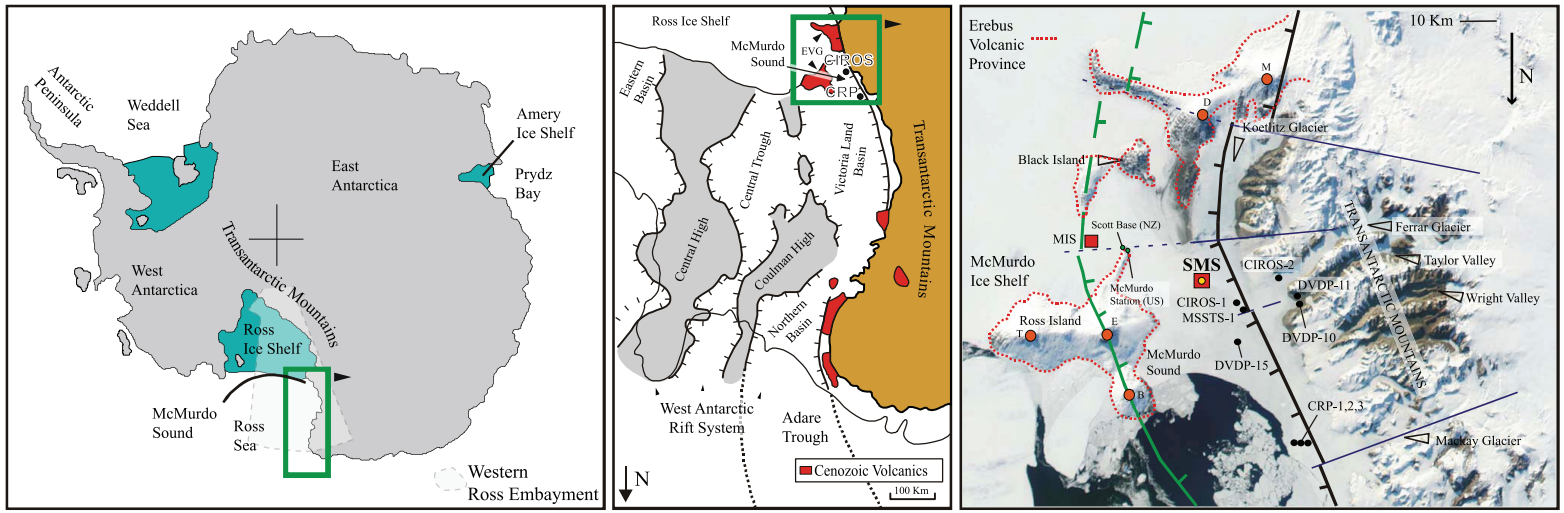

Figure 4.1. Location map. McMurdo Sound is part of the western Ross Sea Embayment, adjacent to the Ross Ice Shelf and the Transantarctic Mountains. Volcanic centres: B – Mount Bird, EVG – Erebus Volcanic Province, E – Mount Erebus, D – Mount Discovery, M – Mount Morning, T – Mount Terror. ANDRILL MIS (McMurdo Ice Shelf) and SMS (Southern McMurdo Sound) drillholes and previous stratigraphic drill holes (CIROS - Cenozoic Investigations in the Western Ross Sea, MSSTS - McMurdo Sound Sediment and Tectonic Studies, DVDP - Dry Valley Drilling Project, CRP - Cape Roberts Project) are indicated. Samples used in this study were recovered from the SMS drill site, core AND-2A. Map modified from Harwood et al.(2005)

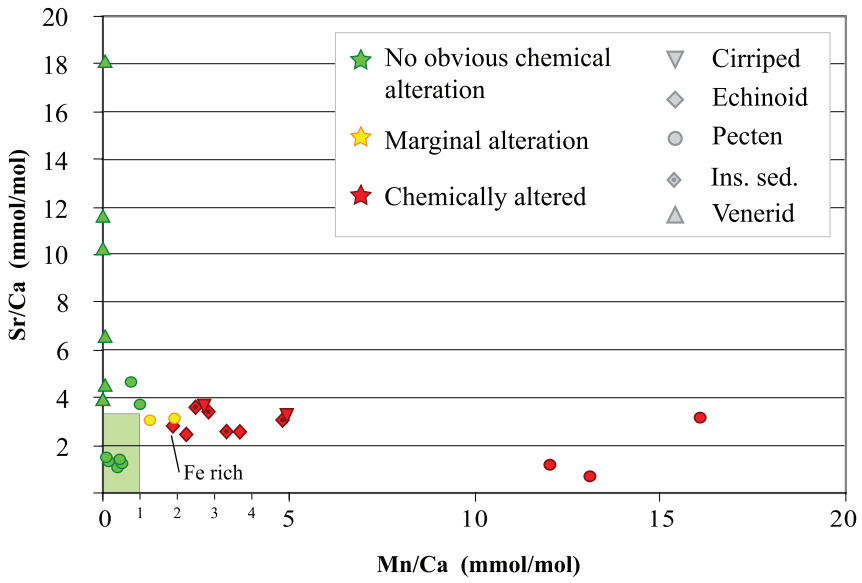

Figure 4.2. Sr vs Mn in samples with Mn/Ca ≤ 20 mmol/mol. Higher values of Sr are always associated with very low Mn – Fe content. The shaded area indicates normal values for recent, unaltered bivalves. Ins. sed. – indeterminate taxonomic affiliation.

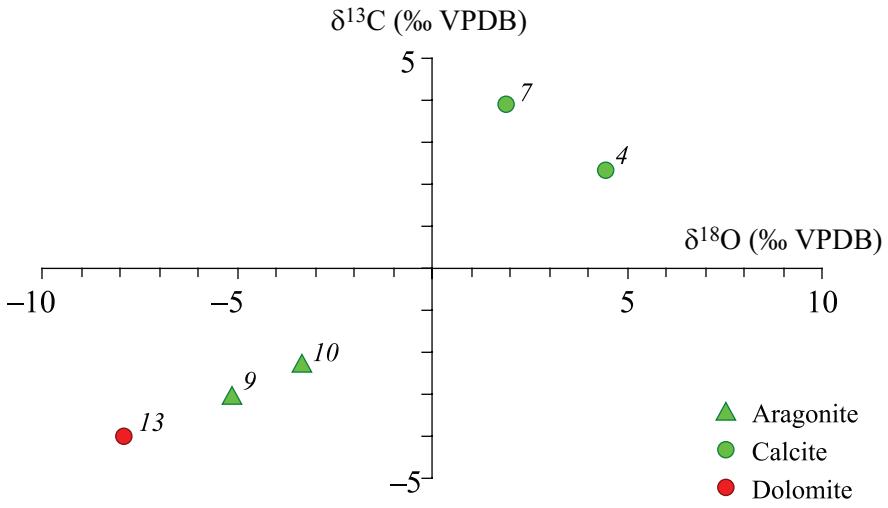

Figure 4.3. Oxygen and carbon isotopes of unaltered calcite and aragonite samples (green symbols). Also shown is dolomitized sample 13 (red circle). Color code as in figure 4.2. The 2 bivalve families belong to clearly distinguishable populations.

Figure 4.4. Samples plotted according to $^{87}Sr/^{86}Sr$ age vs. depth. Chemical alteration and fragment type are identified as indicated by the legend. $^{40}Ar/^{39}Ar$ determinations (blue squares) and other points defined by AND-2A age model (Acton et al., 2008) are shown (black crosses) along with an approximate sedimentation rate (dotted line). Potential hiatuses are indicated as wavy lines. The number of hiatuses does not represent realistic estimates. Note the aragonite samples overestimate the age model

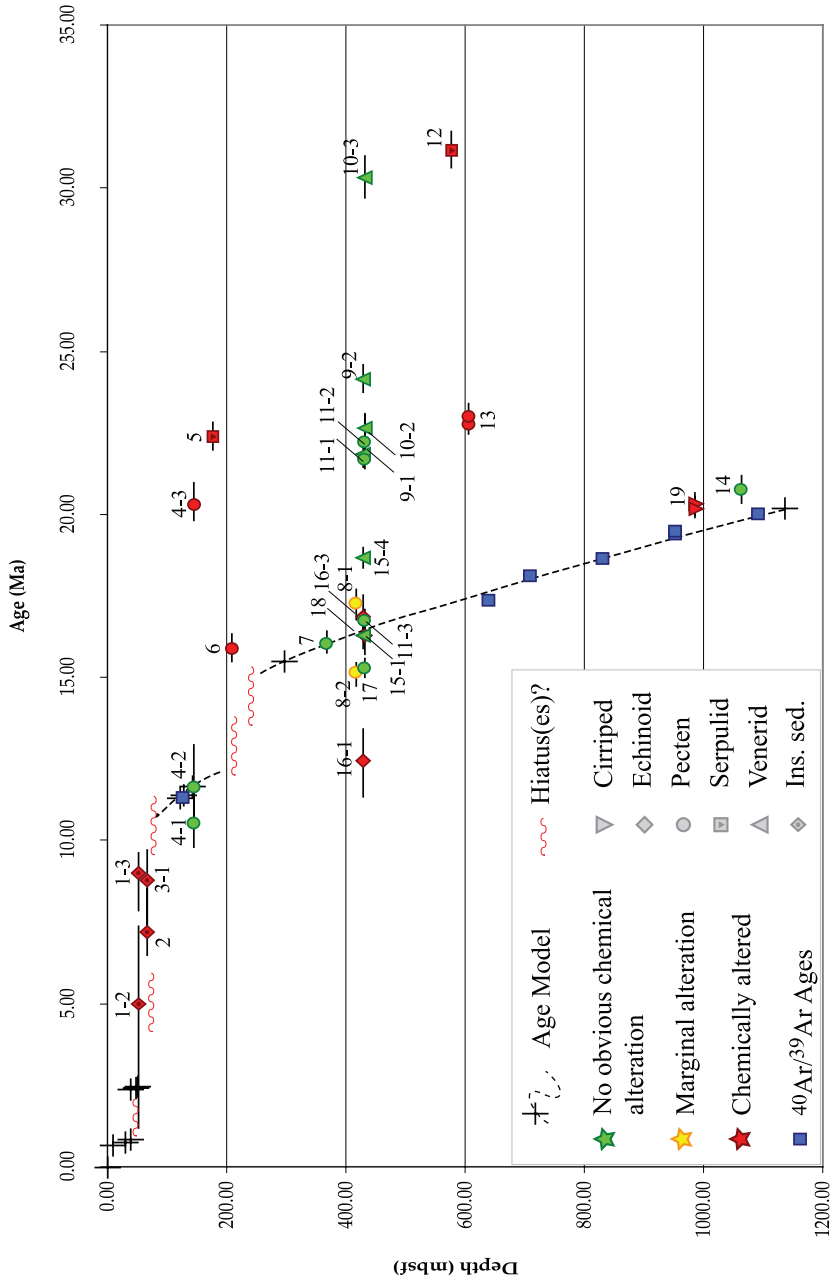
Age (Ma)
0.00
5.00
10.00
15.00
20.00
25.00
30.00
35.00
Depth (mbsf)
0.00
200.00
400.00
600.00
800.00
1000.00
1200.00
Age Model
Hiatus(es)?
No obvious chemical alteration
Marginal alteration
Chemically altered
$^{40}Ar/^{39}Ar$ Ages
Cirriped
Echinoid
Pecten
Serpulid
Venerid
Ins. sed.
1-2
1-3
2
3-1
4-1
4-2
4-3
5
6
7
8-1
8-2
9-1
9-2
10-2
10-3
11-1
11-2
11-3
12
13
14
15-1
15-4
16-1
16-3
17
18
19

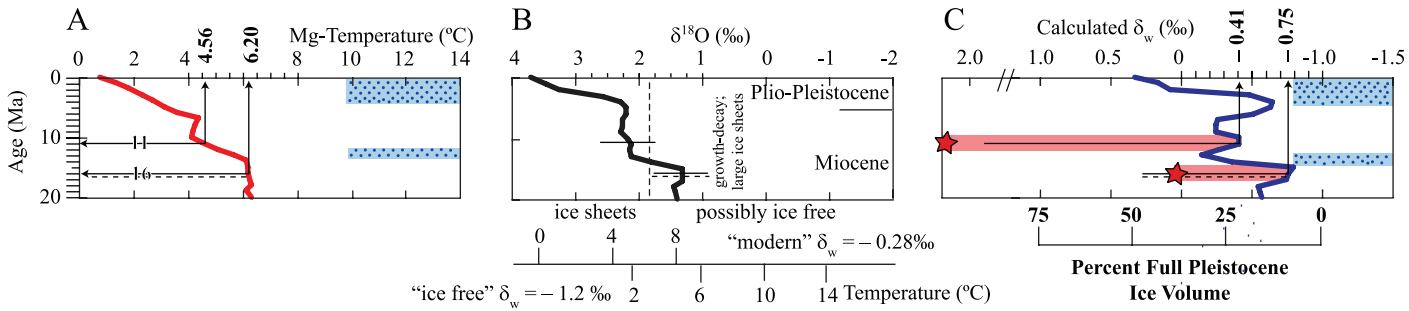

Figure 4.5. A. Lear et al. (2000) Mg temperature record for the past 20 Ma. Estimates at 11, 16 and 16.5 Ma are indicated with arrows and the temperature values highlighted in bold characters. Blue sections represent times of major ice growth. B. Benthic $\delta^{18}O$ record from Miller et al.(1987). Their proposed limit of large scale ice-sheets also shown (vertical dashed line). It is suggested that at 16.5-16.0 Ma, ice sheets may have been small or absent. C. δ_w variation estimated from temperature and benthic $\delta^{18}O$ from A and B and interpreted as ice volume. Major ice-sheet expansions are indicated again with blue-dotted areas. Estimated δ_w for the times of interest are indicated in bold characters. Percentages of Pliocene full ice volume from Dwyer et al. (1995).The highlighted temperature values from Lear et al. (2000) and the measured $\delta^{18}O$ of samples 4, 7, 9 and 10 were used to calculate δ_w. Red stars shown in frame C represent general δ_w results for calcite samples 4 (~11 Ma) and 7 (~16 Ma). The differences to Lear et al. (2000) δ_w calculations are an indication of the local climate divergence from global averages. Modified from Lear et al. (2000), Figure 1, p. 270.

Table 4.1. AND-2A analyzed shell samples. Columns from left to right: sample depth, lithostratigraphic unit, in-house sample identification, general field description, subsamples identification, subsample general description, elemental chemistry, cathodoluminescence (B-bright, D-dull, N-nonluminescent, X-uncharacteristic luminescence), and Sr isotope compositions, and carbon and oxygen isotope compositions

Depth (mbsf)	LSU	In-House ID	Field Information	Chem ID	Comment	Mg/Ca	Sr/Ca	Mn/Ca	Fe/Ca	CL	$^{87}Sr/^{86}Sr$ ±	$\delta^{13}C$ $\delta^{18}O$ (VPDB)
						(mmol/mol)						
53.51-53.52	**2**	1	Indeterminate macrofossil fragment (cirriped?)	1-2	Crystalline area	**17.7**	**2.58**	3.3	**1.1**	**B**	**0.709 8.6E-5**	—
				1-3	Chalky area in the shape of chambers	**16.1**	**3.08**	4.9	4.0	**B**	**0.709 1.0E-5**	
67.13-67.15	**2**	2	Indeterminate macrofossil, chalky	2	Chalky material similar to sample 3	**9.64**	3.58	2.5	**1.6**	**B**	**0.709 1.7E-5**	—
67.56-67.59	**2**	3	Indeterminate macrofossil, chalky	3-1	Chalky, flaky zone	**9.40**	3.44	2.8	**1.8**	**B**	**0.709 1.8E-5**	—
144.03-144.06	**4**	4	Indeterminate macrofossil (probably a bivalve)	4-1	Crystalline middle layer	**11.7**	4.58	**0.8**	**0.0**	**D**	**0.709 2.0E-5**	
				4-2	Chalky inner layer - towards the ventral edge	**13.1**	3.64	**1.0**	**0.0**	**D**	**0.709 1.7E-5**	**2.32 4.49**
				4-3	Crystalline outer layer	**34.0**	3.18	16.1	24.0	**D**	**0.708 2.5E-5**	
175.41-175.43	**4**	5	Serpulid tubes relatively well preserved	5	Inner surface of the tube	331	**2.02**	83.0	321.0	**B**	**0.708 2.0E-5**	—
208.96-208.99	**4**	6	Pectinid fragments. Indeterminate bivalve? Fragment	6	Surface from the cleanest corner. Exterior milled away	**13.0**	**1.20**	12.0	6.6	**D**	**0.709 2.0E-5**	—
366.80-366.85	**7**	7	Well preserved, articulated *Adamussium?* sp.	7	Surface - thin shell	**9.13**	**1.20**	**0.5**	4.8	**D**	**0.709 1.3E-5**	**3.88 1.88**
416.78-416.79	**7**	8	Indeterminate bivalve fragment, thick (pectinid?)	8-1	Chalky outer layer	**15.5**	3.08	1.3	4.0	**B**	**0.709 2.4E-5**	—
				8-2	Crystalline section	**16.6**	3.16	1.9	4.5	**B**	**0.709 1.2E-5**	
429.28-429.30	**7**	9	Veneridae sp. 1, well preserved sliced	9-1	Chalky very soft outer layer	**1.85**	11.6	**0.0**	**0.0**	**N**	**0.708 1.9E-5**	
				9-2	Crystalline inner layer	**0.78**	10.3	**0.0**	**0.0**	**N**	**0.708 1.3E-5**	**-3.10 -5.13**
430.49-430.51	**7**	10	Veneridae sp. 1, well preserved, sectioned	10-2	Middle layer, slightly darker, translucent	**2.48**	3.95	**0.0**	**0.0**	**N**	**0.708 1.8E-5**	**-2.34 -3.31**
				10-3	Inner layer, lighter, opaque	**1.78**	18.1	**0.0**	**0.0**	**N**	**0.708 1.2E-5**	
430.54-430.68	**7**	11	Costate pectinid, articulated; well preserved	11-1	Inner layer crystalline-looking shell	**1.74**	4.50	**0.0**	**0.0**	**D**	**0.708 1.5E-5**	
				11-2	Outer ribbed layer in crystalline shell	**1.56**	6.61	**0.0**	**0.0**	**D**	**0.708 3.9E-5**	—
				11-3	Surface of the white,thin, vitreous piece	**3.08**	**1.25**	**0.2**	**0.0**	**D**	**0.709 1.3E-5**	
576.29-576.32	**8**	12	Serpulid tubes	12	Inner surface of the tube	856	**1.19**	32.7	772.8	**B**	**0.708 1.0E-5**	—
605.61-605.66	**8**	13	*Costate pectinid*, well preserved shell, sliced	13-1	Outer ribbed surface	733	**0.65**	13.1	307.0	**X**	**0.708 1.2E-5**	—
				13-2	Inner surface	1412	**1.01**	28.1	1123.0	**X**	**0.708 1.0E-5**	
1063.71-1063.73	**14**	14	*Adamussium* cf. *alanbeui,* well preserved, with umbo, sliced	14	Surface - very soft	**2.46**	**1.06**	**0.4**	**1.1**	**N**	**0.708 1.3E-5**	—
429.98-430.00	**7**	15	Veneridae sp.	15-1	Surface of vitreous-looking piece (not venerid-like)	**2.89**	**1.42**	**0.1**	**0.2**	**N**	**0.709 1.9E-5**	—
				15-4	Inner (middle?) layer	**0.76**	3.92	**-0.0**	**0.0**	**N**	**0.709 1.9E-5**	
429.98-430.00	**7**	16	Echinoid fragments	16-1	Mamelon	**152**	**2.78**	1.9	63.5	**D**	**0.709 1.4E-5**	—
				16-3	Sterom plate outer surface	**310**	**2.57**	3.7	215.0	**B/N/D**	**0.709 3.5E-5**	
430.54-430.68	**7**	17	Pectinid	17-1	Surface - luminescent	**9.50**	**1.35**	**0.5**	5.7	**B**	**0.709 1.0E-5**	—
430.54-430.68	**7**	18	Echinoid fragments	18-1	Mamelon	**106**	**2.50**	2.2	31.7	**D**	**0.709 3.0E-5**	—
986.01-986.02	**12**	19	Cirriped fragment	19-2	Inner layer (Inside fracture, non-luminescent)	**14.8**	3.68	2.7	6.6	**N**	**0.708 1.0E-5**	—
				19-3	Inner smooth suface	**44.6**	3.34	4.9	13.6	**B**	**0.708 1.0E-5**	

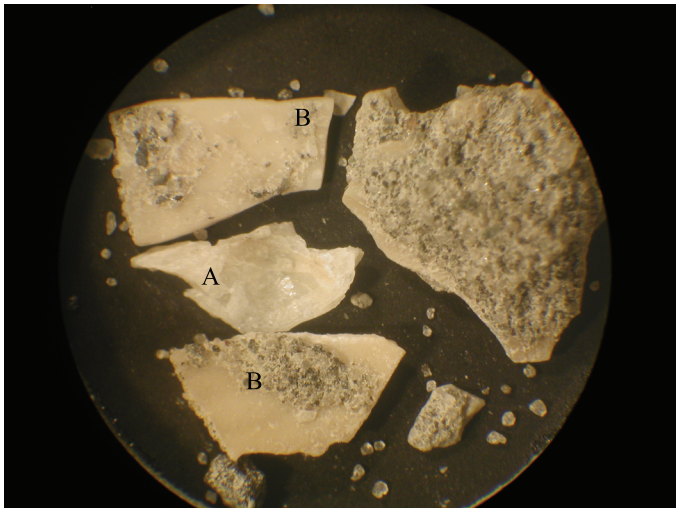

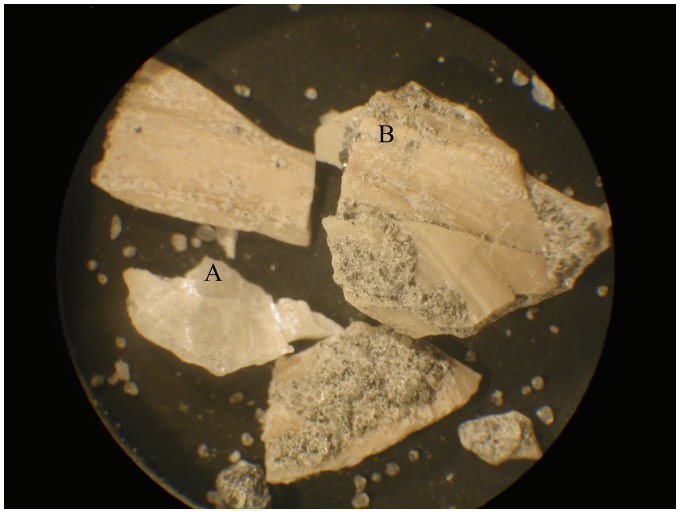

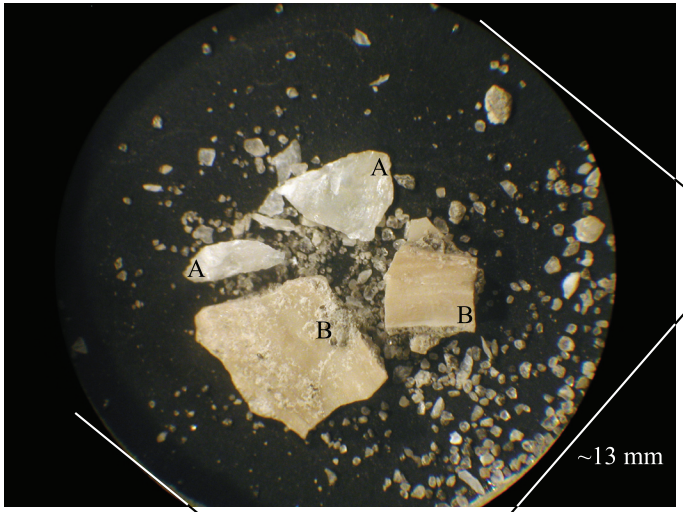

Pictures of sample 11 when it was received. The 2 pictures at the top show the anverse and reverse of the same fragments.

Subsamples 11-1 and 11-2 were taken from fragments such as the ones here labelled B. Subsample 11-3 was taken from a piece similar to the ones labelled A.

The same can be observed in sample 15.

Appendix 4.1

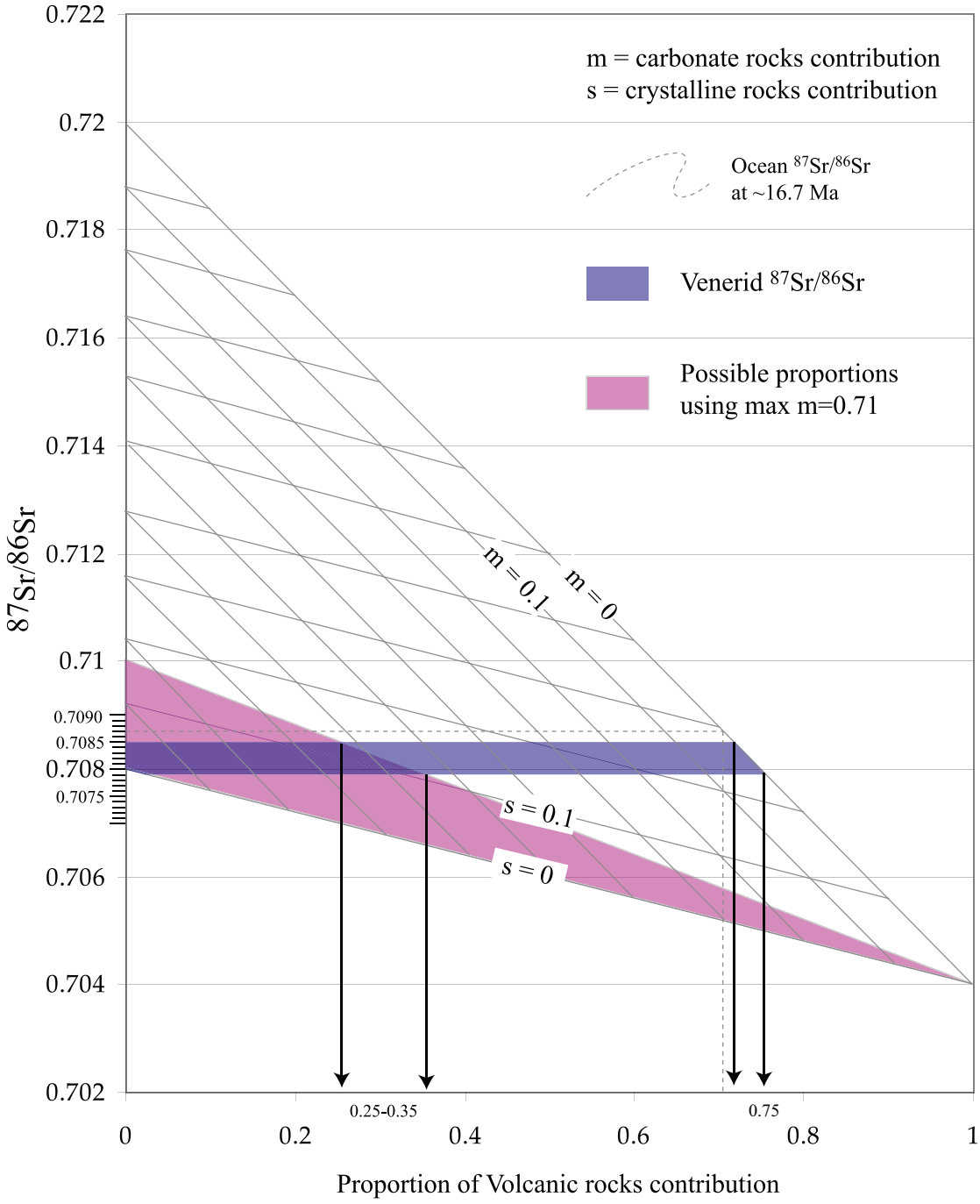

Appendix 4.2. Mixing model of seawater Sr isotope compositions

References

Acton, G., Crampton, J., Di Vincenzo, G., Fielding, C.G., Florindo, F., Hannah, M.J., Harwood, D.M., Ishman, S.E., Johnson, K., Jovane, L., Levy, R.H., Lum, B., Marcano, M.C., Mukasa, S.B., Ohneiser, C., Olney, M., Riesselman, C., Sagnotti, L., Stefano, C., Strada, E., Taviani, M., Tuzzi, E., Verosub, K.L., Wilson, G.S., and Zattin, M., 2008. Preliminary Integrated chronostratigraphy of the AND-2A core, ANDRILL Southern McMurdo Sound Project Antarctica, *in* Harwood, D.M., Florindo, F., Talarico, F., and Levy, R.H., eds., Studies from the ANDRILL, Southern McMurdo Sound Project, Antarctica, Terra Antarctica, *in press*.

Alley, R.B., Anandakrishnan, S., and Jung, P., 2001. Stochastic resonance in the North Atlantic. Paleoceanography, 16 (2): 190-198.

Augustin, L., Barbante, C., Barnes, P.R.F., Marc Barnola, J., Bigler, M., Castellano, E., Cattani, O., Chappellaz, J., Dahl-Jensen, D., Delmonte, B., Dreyfus, G., Durand, G., Falourd, S., Fischer, H., Fluckiger, J., Hansson, M.E., Huybrechts, P., Jugie, G., Johnsen, S.J., Jouzel, J., Kaufmann, P., Kipfstuhl, J., Lambert, F., Lipenkov, V.Y., Littot, G.C., Longinelli, A., Lorrain, R., Maggi, V., Masson-Delmotte, V., Miller, H., Mulvaney, R., Oerlemans, J., Oerter, H., Orombelli, G., Parrenin, F., Peel, D.A., Petit, J.-R., Raynaud, D., Ritz, C., Ruth, U., Schwander, J., Siegenthaler, U., Souchez, R., Stauffer, B., Peder Steffensen, J., Stenni, B., Stocker, T.F., Tabacco, I.E., Udisti, R., van de Wal, R.S.W., van den Broeke, M., Weiss, J., Wilhelms, F., Winther, J.-G., Wolff, E.W., and Zucchelli, M., 2004. Eight glacial cycles from an Antarctic ice core. Nature, 429 (6992): 623-628.

Barbin, V., 2000. Cathodoluminescence of carbonate shells: biochemical vs diagenetic process, *in* Pagel, M., Barbin, V., Blanc, P., and Ohnenstetter, D., eds., Cathodoluminescence in Geosciences, Springer, Berlin: 303-330.

Barnola, J.M., Raynaud, D., Korotkevich, Y.S., and Lorius, C., 1987. Vostok ice core provides 160,000-year record of atmospheric CO_2. Nature, 329 (6138): 408-414.

Billups, K., and Schrag, D.P., 2003. Application of benthic foraminiferal Mg/Ca ratios to questions of Cenozoic climate change. Earth and Planetary Science Letters, 209: 181-195.

Bornhold, B.D., and Milliman, J.D., 1973. Generic environmental control of carbonate mineralogy in serpulid (Polychaete) tubes. The Journal of Geology, 81: 363-373.

Brand, U., and Veizer, J., 1980. Chemical diagenesis of a multicomponent carbonate system 1: Trace Elements. Journal of Sedimentary Petrology, 50: 1219-1236.

Carpenter, S.J., and Lohmann, K.C., 1992. Sr/Mg ratios of modern marine calcite: Empirical indicators of ocean chemistry and precipitation rate. Geochimica et Cosmochimica Acta, 56 (5): 1837-1849.

Cronin, T.M., and Dowsett, H.J., 1993. PRISM; warm climates of the Pliocene. GeoTimes, 38 (11): 17-19.

Crowley, T.J., 1991. Modeling pliocene warmth. Quaternary Science Reviews, 10 (2-3): 275-282.

Crowley, T.J., and Berner, R.A., 2001. CO_2 and climate change. Science, 292 (5518): 870-872.

Cubasch, U., Meehl, G.A., Boer, G.J., Stouffer, R.J., Dix, M., Noda, A., Senior, C.A., Raper, S., and Yap, K.S., 2001. Projections of future climate change, *in* Houghton,

J.T., Ding, Y., Griggs, D.J., Noguer, M., van der Linden, P.J., Dai, X., Maskell, K., and Johnson, C.A., eds., Climate Change 2001: The Scientific Basis. Contribution of Working Group I to the Third Assessment Report of the Intergovernmental Panel on Climate Change, Cambridge University Press, Cambridge: 527-578.

DeConto, R.M., and Pollard, D., 2003a. A coupled climate-ice sheet modeling approach to the Early Cenozoic history of the Antarctic ice sheet. Palaeogeography, Palaeoclimatology, Palaeoecology, 198 (1-2): 39-52.

—, 2003b. Rapid Cenozoic glaciation of Antarctica induced by declining atmospheric CO_2. Nature, 421 (6920): 245-249.

Dowsett, H.J., Barron, J.A., Poore, R.Z., Thompson, R.S., Cronin, T.M., Ishman, S.E., and Willard, D.A., 1999. Middle Pliocene paleoenvironmental reconstruction; PRISM2. 0196-1497, USGS.

Dwyer, G.S., Cronin, T.M., Baker, P.A., Raymo, M.E., Buzas, J.S., and Correge, T., 1995. North Atlantic deepwater temperature change during Late Pliocene and Late Quaternary climatic cycles. Science, 270: 1347-1351.

Faure, G., and Mensing, T., 2005. Isotopes. Principles and applications. John Wiley & Sons, 897 p.

Fielding, C.G., Atkins, C.B., Basset, K.N., Browne, G.H., Dunbar, G.B., Field, B.D., Frank, T.D., Krissek, L.A., Panter, K.S., Passchier, S., Pekar, S.F., Sandroni, S., and Talarico, F., 2008. Sedimentology and stratigraphy of the AND-2A core, ANDRILL Southern McMurdo Sound Project, Antarctica, *in* Harwood, D.M., Florindo, F., Talarico, F., and Levy, R.H., eds., Studies from the ANDRILL, Southern McMurdo Sound Project, Antarctica, Terra Antarctica, *in press*.

Florindo, F., Harwood, D.M., Talarico, F., and Levy, R.H., 2008. Background to the ANDRILL Southern McMurdo Sound Project, Antarctica, *in* Harwood, D.M., Florindo, F., Talarico, F., and Levy, R.H., eds., Studies from the ANDRILL, Southern McMurdo Sound Project, Antarctica, Terra Antarctica, *in press*.

Gillett, N.P., Stone, D.A., Stott, P.A., Nozawa, T., Karpechko, A.Y., Hegerl, G.C., Wehner, M.F., and Jones, P.D., 2008. Attribution of polar warming to human influence. Nature Geosci, 1 (11): 750-754.

Grossman, E.L., and Ku, T.-L., 1986. Oxygen and carbon isotope fractionation in biogenic aragonite; temperature effects. Chemical Geology; Isotope Geoscience Section, 59 (1): 59-74.

Haq, B.U., Hardenbol, J., and Vail, P.R., 1987. Chronology of fluctuating sea levels since the Triassic. Science, 235 (4793): 1156-1167.

Harwood, D.M., Florindo, F., Levy, R.H., Fielding, C.G., Pekar, S.F., and Speece, M.A., 2005. ANDRILL Southern McMurdo Sound Project Scientific Prospectus. *in*. ANDRILL SMO Contribution No. 5. 5, Lincoln, 29 p.

Harwood, D.M., and Webb, P.N., 1998. Glacial transport of diatoms in the Antarctic Sirius Group; Pliocene refrigerator. GSA Today, 8 (4): 4-8.

Howarth, R.J., and McArthur, J.M., 1997. Statistics for strontium isotope stratigraphy. A robust LOWESS fit to marine Sr-isotope curve for 0 - 206 Ma, with look-up tables for the derivation of numerical age. Journal of Geology, 105: 441-456.

IPCC, 2001. Climate Change 2001: The Scientific Basis. Contribution of Working Group I to the Third Assessment Report of the Intergovernmental Panel on Climate

Change. Cambridge University Press, Cambridge, United Kingdom and New York 881 p.
—, 2007. Climate Change 2007: The Physical Science Basis. Contribution of Working Group I to the Fourth Assessment Report of the Intergovernmental Panel on Climate Change. Cambridge University Press, Cambridge, United Kingdom and New York, 996 p.
Kennett, J.P., and Hodell, D.A., 1995. Stability or instability of Antarctic ice sheets during warm climates of the Pliocene? GSA Today, 5 (1): 1-13, 22.
Kim, S.-T., and O'Neil, J.R., 1997. Equilibrium and nonequilibrium oxygen isotope effects in synthetic carbonates. Geochimica et Cosmochimica Acta, 61 (16): 3461-3475.
Kyle, P.R., 1990. McMurdo Volcanic Group, western Ross Embayment; introduction, *in* LeMasurier, W.E., Thomson, J.W., Baker, P.E., Kyle, P.R., Rowley, P.D., Smellie, J.L., and Verwoerd, W.J., eds., Volcanoes of the Antarctic Plate and Southern oceans. Antarctic Research Series, 48: 19-25.
Lear, C.H., Elderfield, H., and Wilson, P.A., 2000. Cenozoic Deep-Sea temperatures and global ice volumes from Mg/Ca in benthic foraminiferal calcite. Science, 287: 269-272.
Lear, C.H., Rosenthal, Y., and Slowey, N., 2002. Benthic foraminiferal Mg/Ca-paleothermometry; a revised core-top calibration. Geochimica et Cosmochimica Acta, 66 (19): 3375-3387.
Lewis, A.R., Marchant, D.R., Ashworth, A.C., Hemming, S.R., and Machlus, M.L., 2007. Major middle Miocene global climate change: Evidence from East Antarctica and the Transantarctic Mountains. GSA Bulletin, 119 (11/12): 1449-1461.
Lewis, A.R., Marchant, D.R., Kowalewski, D.E., Baldwin, S.L., and Webb, L.E., 2006. The age and origin of the Labyrinth, western Dry Valleys, Antarctica: evidence for extensive middle Miocene subglacial floods and freshwater discharge to the Southern Ocean. Geology, 34 (7): 513-516.
Machel, H.G., 2000. Application of cathodoluminescence to carbonate diagenesis., *in* Pagel, M., Barbin, V., Blanc, P., and Ohnenstetter, D., eds., Cathodoluminescence in Geosciences, Springer, Berlin: 271-302.
Mackenzie, F.T., Bischoff, W.D., Bishop, F.C., Loijens, M., Schoonmaker, J., and Wollast, R., 1983. Magnesian calcites: low temperature occurrence, solubility and solid solution behavior. Reviews in Mineralogy, 11: 97-144.
McArthur, J.M., Howarth, R.J., and Bailey, T.R., 2001. Strontium isotope stratigraphy: LOWESS Version 3. Best-fit line to the marine Sr-isotope curve for 0 to 509 Ma and accompanying look-up table for deriving numerical age. Look-up table Version 4:08/04. Journal of Geology, 109: 155-169.
McKay, R.M., Barrett, P.J., Harper, M.A., and Hannah, M.J., 2008. Atmospheric transport and concentration of diatoms in surficial and glacial sediments of the Allan Hills, Transantarctic Mountains. Palaeogeography, Palaeoclimatology, Palaeoecology, 260 (1-2): 168-183.
Meehl, G.A., Stocker, T.F., Collins, W.D., Friedlingstein, P., Gaye, A.T., Gregory, J.M., Kitoh, A., Knutti, R., Murphy, J.M., Noda, A., Raper, S.C.B., Watterson, I.G., Weaver, A.J., and Zhao, Z.-C., 2007. Projections of future climate change,

in Solomon, S., Qin, D., Manning, M., Chen, Z., Marquis, M., Averyt, K.B., Tignor, M., and Miller, H.L., eds., Climate Change 2001: The Scientific Basis. Contribution of Working Group I to the Third Assessment Report of the Intergovernmental Panel on Climate Change, Cambridge University Press, Cambridge: 527-578.

Miller, K.G., Fairbanks, R.G., and Mountain, G.S., 1987. Tertiary oxygen isotope synthesis, sea level history, and continental margin erosion. Palaeogeoceanography, 2 (1): 1-19.

Miller, M.F., and Mabin, M.C.G., 1998. Antarctic Neogene landscapes; in the refrigerator or in the deep freeze? GSA Today, 8 (4): 1-8.

Milliman, J.D., 1974. Marine carbonates, Recent Sedimentary Carbonates, 1, Springer-Verlag, Berlin: 373.

Morse, J.W., and Mackenzie, F.T., 1990. Geochemistry of sedimentary carbonates. Elsevier, Amsterdam, 707 p.

Mukasa, S.B., Shervais, J.W., Wilshier, H.G., and Nielson, J.E., 1991. Intrinsic Nd, Pb, and Sr isotopic heterogeneities exhibited by the Lherz Peridotite massif, French Pyrenees. J. Petrol. Spec. Lith. Issue: 117-134.

Murphy, L., Warnke, D.A., Andersson, C., Channell, J., and Stoner, J., 2002. History of ice rafting at South Atlantic ODP Site 177-1092 during the Gauss and Late Gilbert Chrons. Palaeogeoceanography, Palaeoclimatology, Palaeoecology, 182: 183-196.

Parkinson, C.L., and Cavalieri, D.J., 2008. Arctic sea ice variability and trends, 1979-2006. J. Geophys. Res., 113 (C07003).

Pekar, S.F., and DeConto, R.M., 2006. High-resolution ice-volume estimates for the early Miocene: Evidence for a dynamic ice sheet in Antarctica. Palaeogeography, Palaeoclimatology, Palaeoecology, 231 (1-2): 101-109.

Petit, J.R., Jouzel, J., Raynaud, D., Barkov, N.I., Barnola, J.M., Basile, I., Bender, M., Chappellaz, J., Davis, M., Delaygue, G., Delmotte, M., Kotlyakov, V.M., Legrand, M., Lipenkov, V.Y., Lorius, C., Pepin, L., Ritz, C., Saltzmann, E., and Stievenard, M., 1999. Climate and atmospheric history of the past 420,000 years from the Vostok ice core, Antarctica. Nature, 399 (6735): 429-436.

Popp, B.N., Podosek, F.A., Brannon, J.C., and Pier, J., 1986. $^{87}Sr/^{86}Sr$ ratios in Permo-Carboniferous seawater from the analyses of well-preserved brachiopod shells. Geochimica et Cosmochimica Acta, 50: 1321-1328.

Raymo, M.E., Lisiecki, L.E., and Nisancioglu, K.H., 2006. Plio-Pleistocene ice volume, Antarctic climate, and the global $\delta^{18}O$ record. Science, 313: 492-495.

Rocchi, S., Amienti, P., D'Orazio, M., Tonarini, S., Wijbrans, J.R., and Di Vincenzo, G., 2002. Cenozoic magmatism in the western Ross Embayment: Role of mantle plume versus plate dynamics in the development of the West Antarctic Rift System. Journal of Geophysical Research, 107 (B9): 2195.

Rocchi, S., Tonarini, S., Armienti, P., Innocenti, F., and Manetti, P., 1998. Geochemical and isotopic structure of the early Paleozoic active margin of Gondwana in northern Victoria Land, Antarctica. Tectonophysics, 284: 261-281.

Rocholl, A., Stein, M., Molzahn, M., Hart, S.R., and Worner, G., 1995. Geochemical evolution of rift magmas by progressive tapping of a stratified mantle source beneath the Ross Sea Rift, Northern Victoria Land, Antarctica. Earth and

Planetary Science Letters, 131: 207-224.
Rosenthal, Y., Field, M.P., and Sherrell, R.M., 1999. Precise determination of element/calcium ratios in calcareous samples using sector field inductively coupled plasma mass spectrometry. Analytical Chemistry, 71: 3248-3253.
Taviani, M., Hannah, M.J., Harwood, D.M., Ishman, S.E., Johnson, K., Olney, M., Riesselman, C., Tuzzi, E., Askin, R., Beu, A.G., Blair, S., Cantarelli, V., Ceregato, A., Corrado, S., Mohr, B., Nielsen, S.H.H., Persico, D., Petrushak, S., Raine, J.I., and Warny, S., 2008. Paleontological characterization; an analysis of the AND-2A core, ANDRILL Southern McMurdo Sound Project Antarctica, *in* Harwood, D.M., Florindo, F., Talarico, F., and Levy, R.H., eds., Studies from the ANDRILL, Southern McMurdo Sound Project, Antarctica, Terra Antarctica, *in press*.
Veizer, J., 1983. Trace elements and isotopes in sedimentary carbonates. Reviews in Mineralogy, 11: 265-299.
Veizer, J., Godderis, Y., and Francois, L.M., 2000. Evidence for decoupling of atmospheric CO_2 and global climate during the Phanerozoic eon. Nature, 408 (6813): 698-701.
Warnau, M., Biondo, R., Temara, A., Bouquegneau, J.-M., Jangoux, M., and Dubois, P., 1998. Distribution of heavy metals in the echinoid Paracentrotus lividus from the Mediterranean Posidonia oceanica ecosystem: seasonal and geographical variations. Journal of Sea Research, 39 (3-4): 267-280.
Webb, P.N., and Harwood, D.M., 1991. Late Cenozoic Glacial History of the Ross Embayment, Antarctica. Quaternary Science Reviews, 10: 215-223.
Webb, P.N., Harwood, D.M., McKelvey, B.C., Mercer, J.H., and Stott, L.D., 1984. Cenozoic marine sedimentation and ice-volume variation on the East Antarctic Craton. Geology 12 (5): 287-291.
Zachos, J., Pagani, M., Sloan, L., Thomas, E., and Billups, K., 2001. Trends, rhythms, and aberrations in global climate 65 Ma to present. Science, 292 (5517): 686-693.

CHAPTER 5

Sr isotope systematics of aragonite shell fragments and pore water from an ANDRILL core, Southern McMurdo Sound, Antarctica

Abstract

Biogenic material recovered from ANDRILL (ANtarctic Geological DRILLing program) Southern McMurdo Sound project core AND–2A was analyzed to solve discrepancies observed in previous Sr isotope determinations. Initial attempts to apply $^{87}Sr/^{86}Sr$ stratigraphy to the shells from the core produced mixed results. Well–preserved calcitic shell fragments yielded accurate ages, while seemingly unaltered aragonite shells invariably produced older than expected ages. Additional analyses of the aragonite shells and $^{87}Sr/^{86}Sr$ compositions of pore water are presented here. X–ray microdiffractions confirmed that only aragonite is present in the shells. In addition, electron microprobe elemental mapping revealed that Sr concentration in aragonite shells defines growth bands in the inner layer, suggesting original incorporation of Sr as a function of seasonal change. Venerid outer layers, however, have anomalously high Sr concentrations. If primary, these concentrations could only be controlled by changes in the aragonite Sr distribution coefficient as a function of crystal growth. However, oxygen isotope compositions and Sr concentrations from pore water can be used to model outer layer compositions reasonably well. The high correlation observed between $\delta^{18}O–\delta^{13}C$ is more reasonably explained by alteration of the outer layer, which is consistently more depleted in ^{18}O and ^{13}C than the inner layer. Pore water $^{87}Sr/^{86}Sr$ is in general agreement with the core's age model only at the aragonite–bearing interval. This limited concurrence

suggests that $^{87}Sr/^{86}Sr$ disequilibrium between pore water and the carbonates is the rule rather than the exception in the core. The $^{87}Sr/^{86}Sr$ values, which cannot be attributed to equilibration with modified pore waters, may represent original, though currently unexplained anomalies tentatively associated to water–sediment microenvironment modifications and infaunal life habit of the venerid bivalves. However, they are most likely the result of early diagenetic alteration as suggested by pore water oxygen isotope compositions and Sr concentrations, even in the absence of a definite paragenesis.

Keywords

Sr–87/Sr–86; O–18/O–16; Bivalvia; Venerida; Pore water; Miocene; McMurdo Ice Shelf.

5.1. Introduction

Cenozoic climate has been characterized, and in large measure determined, by ice sheet dynamics. Antarctica, in particular, due to its size and topography has driven or modulated global climate during the Cenozoic (Kennett, 1977; 1982; DeConto et al., 2007). Imminent climate change (Cubasch et al., 2001; Meehl et al., 2007) demands a better understanding of the potential consequences of ice sheet responses to increased temperatures. In this context, stratigraphic records of Antarctica's margin are an invaluable source of information to clarify ice sheet evolution and improve model predictions with better proxy data.

The ANDRILL (ANtarctic Geological DRILLing) program is a multinational joint effort to drill Antarctica's margin in search of Cenozoic stratigraphic records to study variation in ice sheets and obtain a better understanding of polar climate evolution (Harwood et al., 2005; Harwood et al., 2006; Harwood et al., 2009). ANDRILL's second field campaign, the Southern McMurdo Sound (SMS) project, collected core AND–2A during the austral summer of 2007 at 77.758141 ºS, 165.276765 ºE (Figure 5.1). Specific

goals of this project included: 1) improve chronostratigraphic control, 2) document melt–water discharge events from the Dry Valleys of the Transantarctic Mountains, and 3) evaluate the persistence of polar conditions in Antarctica over the past 15 million years.

The core presented several macrofossil–bearing intervals that were sampled in part to assess the aforementioned objectives using Sr and O isotopes. Because the residence time of Sr in seawater is considerably longer than its mixing time and because Sr is not fractionated by near–surface physico–chemical processes, Sr isotopic composition of seawater at any one time is homogeneous and a reflection of global rock distribution, proportion and weathering intensity (Graustein, 1989; Faure and Mensing, 2005). Sr is incorporated into carbonate materials without fractionation, such that $^{87}Sr/^{86}Sr$ ratios of unaltered marine carbonates are routinely compared to the well established secular variation of Sr isotopic composition of seawater (Hess et al., 1986; Howarth and McArthur, 1997; McArthur et al., 2001) to provide chronostratigraphic control. Similarly, well preserved samples can be used to estimate Sr sources and to model mixing and weathering mechanisms. In contrast, oxygen isotopes are incorporated into molluscan carbonates at an equilibrium fractionation with respect to seawater (Epstein et al., 1953; Wefer and Berger, 1991). Given that this fractionation is a predictable function of temperature at equilibrium, shell oxygen isotope compositions can be traced back to temperatures if the $\delta^{18}O$ value of the water can be estimated with some confidence. In consequence, $\delta^{18}O$ of well–preserved carbonate materials can provide climate constraints based on its dependence on water temperature and freshwater influx.

Previous work on venerid and pectinid shells from the macrofossil–rich intervals of core AND–2A showed marginal or no evidence of diagenetic alteration. $^{87}Sr/^{86}Sr$ compositions of unaltered calcite fragments provided additional chronostratigraphic control to the core (Acton et al., 2008). In contrast to calcite fragments, Sr isotope compositions of the aragonitic venerid shells were lower than expected in all samples resulting in older than reasonable $^{87}Sr/^{86}Sr$ ages, while the Sr concentration was higher

than that observed in modern bivalves. Based on the lack of chemical and optical evidence for alteration, oxygen isotope data were also used to compare local marine climate conditions to global averages at about 16 and 11 Ma (Marcano et al., 2009). Given the significance of environmental or diagenetic interpretations reliant on AND–2A samples, and considering that the aragonite anomalous Sr compositions were not unequivocally explained using basic Sr isotope mass balance calculations, these samples are further explored here using more detailed techniques, and are evaluated against new Sr data from the core's pore water. Unlike biogenic carbonates, interstitial fluids in AND–2A appear to be highly modified as suggested by initial chemical analyses of pore water and fracture filling cements (Gui, 2009; Frank and Gui, *in press*). Here, the Sr concentrations and isotope compositions of AND–2A pore water are explored and related to the results from shell studies.

Pursuing this problem is relevant to understand possible unique paleoenvironmental or paleoecological conditions during Antarctica's Neogene, or conversely, to explore unforeseen diagenetic pathways in a distinctive postdepositional environment. Disregarding the Sr behavior observed in these samples as unspecific alteration without providing further assessment or working hypotheses, closes this opportunity. Furthermore, as will be described in the following section, AND–2A anomalous results are not an isolated occurrence and may relate to regional processes associated with Antarctica's unique climate.

5.2. Sr compositions in biogenic material from other Antarctic cores

Sr isotope ratios measured in aragonitic bivalves recovered from site 270, leg 28 of the Deep Sea Drilling Project (DSDP), southeastern portion of the Ross Sea (77.4413 º S, 178.503 º W) and hole 1 of the Cenozoic investigations of the Western Ross Sea (CIROS–1) off Ferrar Glacier in McMurdo Sound (77.581872 ºS, 164.498859 ºE; Barrera, 1989) produced ages consistent with biostratigraphic estimates. Similarly, several aragonitic bivalve samples from the Cape Roberts Project (CRP-1, CRP-2/2A,

and CRP-3), drilled about 65 km north of CIROS–1 (77.009 ºS, 163.755 ºE), produced Sr ages consistent with $^{40}Ar/^{39}Ar$ isotopic ages and diatoms biostratigraphic results (Lavelle, 1998, 2000, 2001). Identification, description and criteria to rule out alteration or transport in the studies above vary widely, and it is not clear whether all aragonitic shells were venerids.

Shells from the first ANDRILL core recovered in McMurdo Sound (AND-1B, MIS - McMurdo Ice Sheet Project, Naish et al., 2007) also produced ages, based on Sr isotope compositions, with some ambiguities (Wilson et al., 2007). The mineralogy and degree of alteration of these fragments were only visually discerned, as was the case for the CRP project. Within the uncertainty of shell fragments identification, the bivalves appear to be consistently associated with the lowest $^{87}Sr/^{86}Sr$ values, while other macrofossils produced ages closer to the core's age model. Mineralogy was not specified, and therefore it is uncertain whether the older ages are associated with aragonitic bivalves only, as was the case in the AND–2A core. Wilson et al. (2007) ruled out local $^{87}Sr/^{86}Sr$ water compositions associated with glacial outwash and shell material recycling as possible causes of the spurious ages. They concluded that the most likely cause of the age discrepancy was contamination by matrix sediments. Results continued to be equivocal after several cycles of HCl etching of the shell fragments, which suggests that $^{87}Sr/^{86}Sr$ compositions were probably intrinsic and not the product of contamination. Partial equilibration with pore waters was proposed as an alternative cause of anomalous $^{87}Sr/^{86}Sr$ compositions but this hypothesis was not tested.

The $^{87}Sr/^{86}Sr$ compositions of bivalve shells positively identified as aragonite reported from site 739, leg 119 of the Ocean Drilling Project (ODP), in Prydz Bay, Antarctica (75.0818 ºS, 67.285 ºE) also produced unexpected ages (Thierstein et al., 1991). In this case, the Sr isotope ages were younger (latest Early Oligocene–earliest Miocene) than the aragonite–bearing stratigraphic units (latest Eocene–earliest Oligocene). Pore waters from the same depths of the aragonite–bearing diamictites were

analyzed for Sr concentration and isotopic compositions. Sr concentrations were between 1.5 and 2 times that of modern seawater, and Sr isotope ratios were among the most radiogenic ever recoded by the ODP and the DSDP. Thierstein et al. (1991) calculated that aragonite Sr isotope compositions would require either 90% freshwater initial contribution, or 10 to 17% postdepositional incorporation of Sr from the current pore water. They also calculated that pore water compositions could be reasonably derived from altered continental detritus, but the apparent pristine aragonite of the macrofossil shells remained puzzling and in demand of further investigation.

5.3. Methods and results

Previous analyses to identify and discriminate alteration effects on these and other selected macrofossil fragments are described in Marcano et al. (2009). Here, we focus on AND-2A venerid samples recovered between 429.28 m and 430.51 m below seafloor (mbsf) identified as in–house samples number 9, 10, 11-1, 15-2 and 15-3. Each valve's outer and inner layer could be clearly recognized in most fragments. These layers were sampled separately for the chemical analyses, but relatively large sample sizes were required for conventional powder X–ray diffraction technique used by Marcano et al. (2009). Results could not account for the presence of small localized alteration products or differences within the layers.

Powder X–ray microdiffraction (PXRD) was used in this study to reconfirm mineralogy without sample homogenization. PXRD patterns were collected on a Rigaku R-AXIS SPIDER diffractometer with an imaging plate detector using graphite monochromated Cu-Kα radiation (1.5406 Å) at ambient temperature. Whole fragments of venerid shell exhibiting both outer and inner layers were used. The sample is mounted on a cryoloop with paratone N oil for analysis at room temperature, and the diffractogram obtained from sections of samples where both layers occupied approximate equal volumes. To avoid preferred orientation, images were collected for 5 minutes while rotating the sample about the φ–axis at 10° s^{-1} and oscillating ω between 120° and 180°

at 1° s^{-1}, with ψ set at 45° (see Appendix 5.1 for a diagram of sample orientation). These were integrated with a 0.05° step size with the AreaMax2 software package. Powder patterns were processed in Jade Plus3 to calculate peak positions and intensities. The Jade software package developed by Materials Data Inc. (MDI) supports and provides access to comprehensive XRD databases such as the Powder Diffraction Files (PDF2 and 4), produced by the International Center for the Diffraction Data (ICDD). The suggested match was exclusively aragonite, with both layers contributing equally to the result.

Electron microprobe elemental mapping (Figure 5.2) was done to localize areas of anomalous Sr concentration in the shell. The X–ray mapping was carried out on a cross section of a shell fragment (sample 10) using wavelength–dispersive (WLD) spectrometry in a Cameca SX–100 electron probe microanalyzer (EPMA). The backscattered electron (BSE) image suggests that the mineralogy of the inner and outer layers of the venerid fragment is uniform. Instead of occurring in isolate phases, Sr is highly and evenly concentrated in the prismatic outer layers of the shells, while it concentrates only along well defined bands in the crystallographic homogeneous inner layers. To avoid precision limitations imposed by the analytical time necessary to quantify the entire Sr map, concentrations were measured along 3 transects, 270 μm in length each, along the cross section of the fragment. Data were collected from 3 spectrometers with a detection limit of 270 ppm and analytical precision of 0.03 wt %. Beam diameter was adjusted to 5, 2 and <0.5 μm with stepsize varying from 5 to 2 μm, producing a total of 245 measurements (Appendix 5.2). Increased Sr concentration corresponds to the outer layer and the bands observed in the compositional map. Samples strictly within the outer prismatic layer average 2.3 ± 0.4 wt % Sr, or 4.5 ± 0.6 mole % $SrCO_3$ (n=15, error is 2σ), a concentration about 5 times that of the inner layer bands (0.5 ± 0.2 wt % Sr or 1.0 ± 0.4 mole % $SrCO_3$, n=43, error is 2s). These high–Sr bands in turn have about twice the background Sr concentration of the inner layer (0.3 ± 0.1wt %, 0.5 ± 0.2 mole % $SrCO_3$, n=184, error is 2σ).

Sr concentrations were determined on a Perkin Elmer Optima 3300 DV inductively coupled plasma–optical emission spectrometer (ICP–OES) using 10–point calibration curves. Ba, Ca, K, and Mg are also reported, although pore water chemistry was measured on–ice and discussed elsewhere (Panter et al., *in press*). One High–Purity® standard solution (Trace Metals in Drinking Water) and one in–house standard indicated that accuracy of the chemical analyses was ±5% or better for Sr and Ca, ±10% or better for Mg, and ±18% or better for K and Ba (Table 5.1). ICP–OES determinations are in agreement with on–ice measurements within the precision reported here for K and Mg, except for the Mg determination at 545.06 mbsf where the discrepancy between measurements is close to 30%. Sr concentration varies from between 1.5 and about 84.4 ppm at 779.74 mbsf; Ca varies from 174 to 4136 ppm. Behavior of Sr and Ca downcore is very similar decreasing in the upper 60 meters to their respective minima (~2 and ~185 ppm) and increasing thereafter. They diverge between c. 336 and 545 mbsf, where Ca decreases while Sr continues to increase. In contrast, Mg starts to increase below 30 mbsf and continues to do so until about 545 mbsf when it decreases to the deepest sample at 963.49 mbsf (Table 5.1, Figure 5.3–A). In general, relative to Ca, Mg concentration decreases below ~300 mbsf while the Sr to Ca relation remains unchanged (Figure 5.3–B and –C). These relations, however, are more variable when considered at depth. In detail, Mg is contributed to pore water in excess of Ca in the shallower section of the core to a maximum at 43.75 mbsf. A rapid decrease occurs from this depth to ~120 mbsf, which is followed by relatively stable ratios down to ~960 mbsf. Sr/Ca trend is opposite to Mg/Ca in the upper ~120 m of the core. Below this depth, Sr/Ca is more variable peaking at 545.06 mbsf and then decreasing to values close to modern seawater in the deeper pore water samples (Figure 5.4).

Sr concentrations were used to determine initial pore water sample size for $^{87}Sr/^{86}Sr$ determinations. 2.5N HCl was added to the residues after complete pore water evaporation. Sr was then separated using column chromatography (Mukasa et al., 1991).

Samples were dried to a solid, treated with a drop of 14N HNO_3, redried, and loaded on a single Re filament. Sr was loaded with 0.1% H_3PO_4 and $TaClO_4$ solution. $^{87}Sr/^{86}Sr$ measurements were done on a VG Sector multi–collector thermal ionization mass spectrometer (TIMS). Sr isotope composition was corrected for mass-fractionation using $^{86}Sr/^{88}Sr = 0.1194$. The repeated analyses of NBS-987 standard (n=3) gave an average $^{87}Sr/^{86}Sr = 0.710252 \pm 10$. Total blanks averaged 0.35 ng for Sr, which are negligible (Table 5.1).

Pore–water Sr isotope compositions in the upper ~200 m of the core show large deviations from the core's age model (Figure 5.5). Close to the core's top, pore water $^{87}Sr/^{86}Sr$ is well below modern seawater values (0.70807 ± 15). From this depth to ~235 mbsf, Sr isotope compositions increase to their maximum (0.71022 ± 15 at 73.18 mbsf) and then decrease to values close to those predicted by the core's age model (0.70889 ± 15 at 235.71 mbsf) where they remain relatively stable to a depth of ~620 mbsf. Pore water $^{87}Sr/^{86}Sr$ drops to its lowest values at 779.74 mbsf (0.70692 ± 15) and finally increases to the deepest pore water measured at ~960 mbsf to values still below those corresponding to the age model (0.70802 ± 15).

5.4. Discussion

5.4.1. Aragonite preservation

Although thin bivalve shells are classified among the least reliable materials to preserve seawater Sr isotope ratios (Smalley et al., 1994), it is also true that aragonite is easily altered shortly after deposition (Bathurst, 1975; Brand and Veizer, 1980), such that shells that retain this mineralogy are presumed pristine and expected to preserve their original chemical composition. The absence of cathodoluminescence along with high Sr and low Fe and Mn concentrations reported for AND–2A venerid shells recovered around 430 mbsf, were initial indications of limited or no diagenetic alteration (Marcano et al., 2009). In this study, the aragonite composition of these samples has once again been confirmed by microdiffraction. Because only very small volumes of uncrushed sample

are needed for this technique and both outer and inner layer contributed equally to the diffraction, no doubt remains about the uniform mineralogy of the shell.

In a number of previous studies, Sr incorporation into molluscan aragonite has been directly and inversely correlated to temperature, and also to growth rate and age (Stecher et al., 1996; Hart and Blusztajn, 1998; Dutton et al., 2002; Gillikin et al., 2005; Freitas et al., 2006; Surge and Walker, 2006; Elliot et al., 2009). No unique or conclusive relation has been established, and as suggested by some (e.g., Gillikin et al., 2005; Bailey and Lear, 2006), controls on Sr incorporation into bivalve shells in particular may even be species specific. Regardless of the cause, controlling factors of Sr incorporation to skeletal aragonite vary as the carbonate is incrementally added to the shell. Therefore, a record of growth is produced and should be evident in the shell's Sr distribution. It is reasonable to conclude that the concentration contrast along the bands observed within the inner layer and asymptotic to the outer layer of the venerid fragments from AND–2A is the result of aragonite accretion through time as Sr incorporation fluctuates in response to changing conditions (Figure 5.2). These bands are growth bands, and as such, good evidence of precipitation by the living bivalve.

However, the Sr concentrations of the outer layer and, to a lesser degree, of the Sr–rich bands of the inner layer are anomalously high compared to modern bivalves as was indicated before by the Sr/Ca determined by ICP–MS and again confirmed in this study by detailed electron microprobe analysis. Modern mollusks in general discriminate against skeletal Sr incorporation, and their Sr content is usually less than ~4,000 ppm or 0.77 mole% $SrCO_3$ (Kinsman, 1969; Veizer, 1983; Morse and Mackenzie, 1990). In contrast, most modern aragonitic cements contain between 1 and 2 wt% $SrCO_3$ (~1.2 and 2.3 mole% $SrCO_3$), although inorganic aragonite with up to 14 mole% $SrCO_3$ has been reported from hot spring deposits (Morse and Mackenzie, 1990). This unusual Sr content suggests that recrystallization of the outer layer, a neomorphic process in which the mineral remains the same after reaction (Folk, 1965; Bathurst, 1975), could

have occurred. Although this process is primarily described in calcite, no mineralogical restriction has been made explicitly.

Recrystallization can involve changes in crystal shape, volume, or lattice orientation (Bathurst, 1975). The prismatic structure observed in the Sr–rich outer layer of samples is common in modern aragonite bivalves. The possible preservation of the original crystalline microstructure, however, is not enough to discard the presence of a secondary carbonate given that the crystal form can also persist through mineralogical stabilization when the diagenetic reaction takes place through migrating solution films that allow chemical changes to occur at the grain boundaries, without developing porosity (Kinsman, 1969; Maliva, 2000). Although authigenic aragonite has not been described in AND–2A, Wada and Okada (1989) described aragonite cements at a variety of depths in the CIROS–1 core, which was drilled less than 30 km away from the locality for this study (Figure 5.1). This may or may not be indicative of conditions conducive to aragonite precipitation in AND–2A given that subsurface environments can change quickly and at close range (Bathurst, 1975; Aller, 1982).

General conditions favorable to carbonate precipitation from the pore water exist along the entire core (i.e., very high alkalinity). Knowledge of the specific saturation state of the current pore fluids, however, is not useful given the disequilibrium between pore water and shell aragonite shown by Sr isotopes and the limited scale and localized nature of the potential recrystallization process. Calculated aragonite $\delta^{18}O$ values (between –10.3 and –11.0 ‰) using oxygen isotope compositions determined in current pore water and borehole temperatures at the level of the aragonite–bearing interval, about –10 ‰ and between 21 and 24 ºC, respectively (Frank and Gui, *in press;* Wonik et al., *in press*) are at least 2 ‰ lower than the lowest $\delta^{18}O$ measured in the venerid shell outer layer (–8.4 ‰) and up to 9.5 ‰ lower than the most positive $\delta^{18}O$ value (–1.5 ‰). These estimates were calculated using the Grossman and Ku (1986) corrected paleotemperature equation, which is in good agreement with relations based on theoretical estimates of water–

aragonite oxygen fractionation (e.g., Kim et al., 2007).

The modeled $\delta^{18}O$ values show disequilibrium between the aragonitic shells and the pore water for the conditions of the core today. However, using lower temperatures, it is possible to replicate the measured aragonite $^{18}O/^{16}O$. This scenario requires alteration to occur earlier in the burial history of the samples without further re–equilibration with pore water in spite of increasing temperature. In the first 50 m of the core from the top, temperatures increase from ~ 0 to 5 ºC, while water $\delta^{18}O$ decreases from modern seawater values of ~ –1 ‰ to about –10 ‰ (Frank and Gui, *in press;* Wonik et al., *in press*). Assuming linear changes with depth for both parameters in the first 50 m of the core, aragonite $\delta^{18}O$ precipitating in this interval would have compositions between ~3.5 and –6 ‰. Under stable conditions with respect to temperature and pore water $\delta^{18}O$, maximum alteration could have occurred when the sample was ~200 mbsf. This is good indication that parts of the shell could have been subjected to early alteration. Mg and Ca behavior below ~600 mbsf is probably associated with dolomitization and more pervasive alteration downcore as suggested by Mg–rich samples reported earlier.

A simple non–thermodynamic calculation using a Sr partition coefficient of 1.13 (calculated by interpolating to 24 ºC the values of the distribution coefficient calculated by Kinsman and Holland (1969) at 16 and 80 ºC), suggests the Sr concentrations of aragonite cement precipitating from modern pore water at the level of interest, where Sr/Ca could potentially vary between 8 mmol/mol and 14 mmol/mol (Figure 5.4), should be between 9 mmol/mol and 16 mmol/mol. Sr/Ca in the aragonite shells vary anywhere from 4 mmol/mol to 18 mmol/mol (Marcano et al., 2009). There are limitations associated to this calculation, in particular when considering AND–2A pore water's high ionic strength. Nevertheless, higher aragonite Sr concentrations can certainly be modeled using the pore water Sr instead of that in average seawater.

Though recrystallization without mineralogical change probably occurred, a satisfactory diagenetic process to explain it and further physical evidence of its

occurrence are both difficult to produce. The original aragonitic outer shell material must have been dissolved to once more precipitate as aragonite. Carbonate cement compositions are in part controlled by the mineralogy of the particles present in the sediment (Walter, 1986), and although in this case cementation *sensu stricto* did not occur, it illustrates the plausibility of primary mineralogy controlling diagenetic phases. Unless conditions exist that inhibit calcite precipitation, the more thermodynamically stable calcite crystals will tend to precipitate from fluids saturated with respect to aragonite. Aragonite and high–magnesian calcite, the common skeletal carbonate materials to precipitate in shallow environments, are in metastable equilibrium with seawater and will tend to recrystallize to calcite in the early diagenetic environment (inversion of Folk (1965), polymorphic transformation of Bathurst (1975)). Although the presence of ions in the pore fluids influences mineral equilibria, and the free energies of formation of pure aragonite and pure calcite are close enough that small changes in the fluid can impact their equilibria (Morse and MacKenzie, 1990; Bathurst, 1975), it is difficult to explain fluid changes across migrating films so that aragonite is dissolved and reprecipitated as the film advances. Even if kinetic processes supersede thermodynamic controls of solution–precipitation (as is common in natural carbonates), it is unclear why diagenetic stabilization should increase Sr concentration. Not surprisingly, diagnostic physical products of this potential recrystallization without mineralogical change were absent in petrographic and SEM analyses of AND–2A samples. As Bathurst (1975) observed, demonstrated diagenetic carbonate fabrics that occur without mineralogical transformation are rare, and the petrographic evidence offered to support them require sometimes belief "amounting to missionary fervour".

AND–2A aragonite shells are characterized by low Mn and Fe concentrations, an otherwise good indicator for lack of extensive diagenetic alteration. However, the low Mn and Fe concentrations may be a reflection of their absence in the diagenetic environment, probably an indication of conditions sufficiently oxidizing to prevent reduction of

oxides and hydroxides. Abundant iron–rich oxidizing phases and the near absence of organic matter support this possibility. In addition, Mn and Fe share structural affinity to the trigonal calcite, not the orthogonal aragonite. This alone may have prevented their incorporation into the secondary carbonate, even if present in the sediment after the death of the bivalves. Slow recrystallization may have also prevented inclusion of Mn and Fe in aragonite (Morse and Mackenzie, 1990).

Assuming for the moment that the anomalous Sr concentrations of the shell aragonite can be achieved as described, and that recrystallization occurred and was limited largely to the outer layer, crystal structure may have played a role in promoting chemical changes. Solubility can be influenced by grain properties and mineral structure differences typically exist between bivalve layers. According to Walter and Morse (1985), thermodynamically more stable carbonate phases can in some cases dissolve faster than more stable ones due to differences in microstructural complexity. Consequently, it is possible that original contrast in crystalline structure translates into a stability gradient between the bivalve layers, which could result in selective or localized diagenetic stabilization.

The alteration scenarios discussed above are based mainly on the excessive Sr concentration of the outer layer, which in itself is not a diagenetic indicator. Conversely, this compositional contrast could be primary. Modern aragonite specimens, however, do not distinctly illustrate this proposition. Elliot et al. (2009) obtained similar average Sr/Ca from different layers of modern *Tridacna gigas* specimens, though the inner layers showed higher variability. Neither average nor variability differences could be distinguished between the Sr/Ca ratios from the prismatic outer layer and the cross–lamellar inner layer of *Mercenaria campechiensis* from the Gulf Coast in Florida (salinity between 19 psu and 36 psu), although Sr concentration behavior with respect to $\delta^{18}O$ differed between layers (Surge and Walker, 2006). Takesue et al. (2008) found significant differences in several cation–to–Ca ratios as a function of the aragonite crystal structure

in the estuarine bivalve *Corbula amurensis*, with the notable exceptions of Sr and Na. The shell used to do the latter analysis grew in waters with maximum salinity of 28.5 psu. Interestingly, Foster et al. (2009) studying the marine cold water bivalve *Arctica islandica* found significant Sr/Ca differences between samples from the axis of maximum growth and those from transects parallel to it, as well as between and within aragonite prisms from the umbo and the outer shell. They concluded that changes in shell architecture were a likely candidate to control Sr incorporation through Sr distribution coefficient changes associated with differences in crystal growth. Their analyses were not designed to sample different crystal structures, but the differences they observed keep open the possibility of structure mediated Sr incorporation in some aragonitic bivalves, possibly an indirect consequence of growth rate contrast.

As pointed out by Marcano et al. (2009), calculated non–thermodynamic Sr partition coefficients (K_{Sr}) for aragonite between 0.4 and 2 are necessary to obtain the measured Sr concentrations in AND–2A shells if these were precipitating from normal modern seawater. Inorganic precipitation of aragonite has been used to calculate the temperature–dependent partition of Sr in aragonite. These experiments have produced relatively consistent K_{Sr} values close to 1 for temperatures <100 ºC (Kinsman and Holland, 1969; Dietzel et al., 2003; Gaetani and Cohen, 2006). All of these calculations imply that the Sr/Ca in aragonite should be very close to the Sr/Ca in the fluid from which it precipitates. However, Bathurst (1975) in analyzing the calculations of Kinsman and Holland (1969), noted the large uncertainties involved. For instance, according to him, if uncertainties are taken into consideration the predicted Sr concentration of inorganic aragonite precipitating from a known fluid at a fixed temperature could vary by more than 3,500 ppm. Moreover, Gaetani and Cohen (2006) pointed out the large discrepancy between the values based on experimental precipitation and their theoretical calculations. Both their theoretical approaches return considerably lower distribution coefficients, which are directly instead of inversely correlated to temperature (Figure

5.6). The authors suggest that aragonites that conform to a partition coefficient close to 1 are actually strongly enriched in Sr relative to the expected equilibrium concentrations, which should be between 0.5 mmol/mol and 1 mmol/mol for temperatures from 15 ºC to 75 ºC. Early on, Lowenstam (1964a; 1964b) noted than Sr/Ca in Annelida, Arthropoda, Bryozoa, Cnidaria, Polyplacophora, Tunicates and several algae were similar to that of seawater. This has been interpreted to result from lower taxa's inability to exert control over the mineralogy of their tests. Some of these organisms are reef builders, which are fast growers pressured by space competition and presumably lack the evolutive ability to control shell chemistry (Stanley and Hardie, 1998). In contrast, the equilibrium ratios calculated by Gaetani and Cohen (2006) are relatively close to the typically low Sr/Ca found in aragonite precipitated by some molluscan classes (including the Pelecipoda) which diverge considerably from seawater and are presumed to be the product of higher taxa control over shell chemistry. This contradiction suggests that the incorporation of Sr in aragonite particularly in biogenic aragonite, is a complex process not yet fully understood.

A primary origin of aragonitic shells from AND–2A is supported by evidence such as the presence of primary growth bands in the shells and the lack of $^{87}Sr/^{86}Sr$ equilibrium between the shells and the ambient pore water. The difficulties associated with physically documenting and chemically explaining potential diagenetic changes in the outer layer of AND–2A venerids and the uncertainties in the partition coefficient of Sr in aragonite further suggest lack of alteration. Nevertheless, the extreme outer layer Sr concentration is difficult to reconcile with precipitation by a living bivalve and with the fresh water input required to explain the more negative $\delta^{18}O$ measured in the outer layer.

5.4.2. Pore water $^{87}Sr/^{86}Sr$

Excluding a relatively small deviation at 545.06 mbsf, pore waters $^{87}Sr/^{86}Sr$ are within the core's age model range between c. 336 and 620 mbsf (Figure 5.5). This section includes the aragonite bearing interval at ~430 mbsf. At all other depths pore–water Sr

isotope compositions diverge substantially from the core's age model. Unlike pore water, $^{87}Sr/^{86}Sr$ ratios of unaltered calcite shell fragments were in agreement with the age model in the aragonite–bearing interval (366.83 mbsf) and also above and below (144.05 and 986.02 mbsf). Although pore water may appear to have maintained its original Sr isotope composition at the aragonite–bearing level, this is probably not the case.

Carbonate Sr isotopes require high water–to–rock ratios (on the order of 10^3) to equilibrate with fluids unless these are brines. In that case equilibration can occur at considerably lower water to rock ratios (~10), similar to those of oxygen during freshwater diagenesis (Banner and Hanson, 1990). AND–2A pore water is highly saline, increasing linearly at a rate of about 30 psu per 100 m depth and stabilizing below ~500 mbsf to salinities between 150 and 200 in the practical salinity scale (Frank and Gui, *in press*). Alkalinity is also high (maxximum ~55 mM). Equilibration is expected to occur at a fast pace, even at the slow rates that should characterize subsurface fluid flow and in spite of the potential fluid circulation restrictions that volcanic sediments could impose at certain levels as has been suggested to occur in other areas (Anderson, 1973).

For brines in particular, appropriate chemical models to describe mineral solubility in subsurface conditions are lacking, and non-equilibrium processes are probably the norm (Morse and Mackenzie, 1990). Nevertheless, given the observed carbonate–pore water isotopic contrasts, the highly modified chemistry of AND–2A pore water and the age of the stratigraphic column, late modification or substitution of the pore water probably occurred in this area, which is located only a few tens of kilometers from the coast. Pore water compositions of the DSDP leg 28 sites 270 to 273 in the continental shelf of the Ross Sea, for example, are very different from AND–2A fluids. Maximum alkalinity reported in Leg 28 is 25 meq/kg, though it remains mostly below 10 meq/kg, while salinity drops with depth from normal marine to a minimum of ~27 psu (Mann and Gieskes, 1975). They also reported a slight Sr concentration increase downcore possibly associated with aragonite dissolution. Sr concentration in AND–2A decreases

in the uppermost part of the core (Figure 5.4). The unusual Sr isotopic composition of AND–2A pore water is also evident through the Elderfield and Gieskes (1982) study that summarized Sr concentration and isotopic composition trends for 37 DSDP holes with latitudinal distribution between 0.5 and 69.9 º (Median = 31.53 º lat). In contrast to AND-2A, overall pore water isotopic compositions in all analyzed drill–holes decrease with depth from normal or close to normal modern marine values in the upper 10 mbsf, to a minimum of 0.70490. $^{87}Sr/^{86}Sr$ significantly greater than that of modern seawater were not measured in any of the more than 160 pore water data sets included in this study.

The current pore water $^{87}Sr/^{86}Sr$ compositions appear not to be only the direct result of reactions with volcanic glass. All through AND-2A volcanic alteration products are found in close proximity to unaltered glass (Fielding et al., *in press*). Given the reactive nature of volcanic material, the presence of unaltered grains may in part indicate that some of the alteration products originated at the sedimentary source instead of the subsurface. Sr isotope compositions of pore water are inadequate to explain the anomalous $^{87}Sr/^{86}Sr$ in AND–2A aragonites and give support to the parautochtonous origin of the pore water.

5.4.3. Shell isotopic compositions

Calcite pectinids and aragonite venerids at ~430 mbsf have contrasting oxygen and carbon isotope compositions (Figure 5.7). While all measured calcites at ~430 mbsf (n=3) produced very similar $\delta^{18}O$ and $\delta^{13}C$ values, aragonites did not. Scenarios of aragonite $\delta^{18}O$ equilibration with pore water were already posed and discussed when addressing aragonite preservation, and they showed that localized early alteration and stabilization probably occurred. The $\delta^{18}O$ contrast between the venerid inner layers at 430 mbsf (~16 Ma) and younger calcite compositions (~11 Ma) was interpreted as the product of seawater–freshwater mixing (Marcano, 2009). At a temperature of 6.2 ºC (Lear et al., 2000) and using oxygen isotope compositions of –0.75 and –30 ‰ for seawater and freshwater, respectively, the measured aragonite $\delta^{18}O$ values would have precipitated

from fluids that were 63 to 92 % seawater. At a temperature of 2 ºC the proportion of seawater required diminishes by just ~ 4 %.

The carbon isotope composition of the shell is a function of the isotopic composition of the bicarbonate from where it forms, which in turns reflect the incorporation of organic and inorganic carbon, as well as metabolic fractionation. Variations in carbon isotopic composition indicate in part changes in productivity in a direction that is a function of depth or microhabitat conditions (Grossman and Ku, 1986; Hoefs, 1997) and it is difficult to predict or estimate. Although metabolic CO_2 appears to have limited influence in molluscan carbonate (McConnaughey and Gillikin, 2008), it is unlikely that C can be incorporated into biogenic carbonate exclusively reflecting hydrological conditions (i.e., without vital effects). The $\delta^{13}C$ difference between calcite and aragonite was argued to reflect in part contrasting life styles between the pectinid and venerid bivalves (Marcano et al., 2009).

Considerable differences exist in both oxygen and carbon isotope values between outer and inner layers. Values in outer layers are more negative than those from corresponding inner layers. Bivalve shell layers are formed from different pallial fluid sources along different areas of the mantle (Moore, 1969; McConnaughey and Gillikin, 2008), and adjacent points from different layers do not necessarily form at the same time. This discrepancy may be exacerbated by rapid growth. Primary intrashell contrast in $\delta^{13}C$ is common, but in $\delta^{18}O$, though reported (e.g., Elliot et al., 2009), is small or absent (Surge and Walker, 2006). While $\delta^{18}O$ comparisons between layers in most studies are based on long, usually multiyear data from complete valves, the mm–size fragments analyzed here provide data from a single point. The $\delta^{18}O$ contrast between the layers is better explained as the product of localized alteration.

The high correlation between $\delta^{18}O$ and $\delta^{13}C$ and its similarity with such relation observed in corals (Gonzalez and Lohmann, 1985; McConnaughey, 1989b, 1989a) could be argued to represent disequilibrium precipitation in contrast to the equilibrium

fractionation that characterizes most modern mollusks (Epstein et al., 1953; Grossman and Ku, 1986). A fairly good correlation between $\delta^{18}O$ and $\delta^{13}C$ have been reported for modern *M. mercenaria* (Elliot et al., 2003), and departures from established oxygen isotope equilibrium fractionation of aragonite exist in other clams (Carré et al., 2005), which suggests disequilibrium precipitation in aragonite bivalves is possible. Kinetic effects probably associated with periods of rapid growth are the main cause of disequilibrium and likely a consequence of bivalves seasonal growth. Though the similarity with the slope derived from the coral data is intriguing, this possibility is rather speculative and cannot be tested.

Modern biogenic and non–biogenic calcium carbonate Sr isotope compositions are indistinguishable from the homogenized seawater $^{87}Sr/^{86}Sr$ value (Faure and Mensing, 2005). As expressed earlier, it is expected that unaltered ancient carbonates reflect seawater $^{87}Sr/^{86}Sr$ at the time of precipitation. Given the infaunal life mode of venerids, the development of microenvironments close to the water–sediment interface where Sr (and as mentioned before, C) could be sufficiently modified by reaction with volcanic material before incorporation to venerid shells may be a reasonable explanation for the shell $^{87}Sr/^{86}Sr$. At the same time, such water–sediment interface fluid modifications and their impact on infaunal bivalves require further investigation.

5.5. Conclusion

Aragonite shell fragments recovered from ANDRILL AND–2A core in Southern McMurdo Sound, Antarctica, have preserved original mineralogy as shown by detailed PXRD and further suggested by the presence of increased Sr concentration along growth bands in the inner layer of the shells. Sr concentration in the outer layer, however, is anomalously high, and Sr isotope composition of all subsamples is less radiogenic than expected. Within the uncertainties associated with the incorporation of Sr into aragonite, the observed high–Sr concentrations of the shells can be explained using AND–2A pore water Sr concentration and a reasonable partition coefficient. Alteration is more

conclusively suggested by the persistent depletion in ^{18}O of outer layers compared to the inner layers and the plausible shell $\delta^{18}O$ values calculated using core temperatures and fluid $\delta^{18}O$. The Sr isotope discrepancies were not resolved when comparing the aragonite composition to the core's pore water $^{87}Sr/^{86}Sr$. The latter is highly modified, differs from pore water of the Ross Sea shelf and from the average of ~160 pore water compositions reported by Elderfield and Gieskes (1982), and is not in equilibrium with AND–2A carbonates. Together, these observations suggest that the anomalous Sr concentrations and isotope compositions observed in the aragonite bivalves of AND–2A are probably the result of partial alteration of some areas of the shells that were originally more susceptible to diagenesis.

Acknowledgements

We are very thankful to Carl Henderson and Lora Wingate, and also to Anja Schleicher, Antek G. Wong–Foy, Sara Worsham and Lindsay Shuller for their technical support. Many thanks also to Adam Matzger, Rod Ewing, Marcus Johnson, Jamie Gleason and Glenn Gaetani for sharing their expertise. NSF grant #EAR-991135. The ANDRILL project is a multinational collaboration between the Antarctic programmes of Germany, Italy, New Zealand and the United States. Antarctica New Zealand is the project operator and developed the drilling system in collaboration with A. Pyne. Antarctica New Zealand supported the drilling team at Scott Base; Raytheon Polar Services Corporation supported the science team at McMurdo Station and the Crary Science and Engineering Laboratory. The ANDRILL Science Management Office at the University of Nebraska-Lincoln provided science planning and operational support. The scientific studies are jointly supported by the US National Science Foundation, the New Zealand Foundation for Research Science and Technology and the Royal Society of New Zealand Marsden Fund, the Italian Antarctic Research Programme, the German Research Foundation and the Alfred Wegener Institute for Polar and Marine Research.

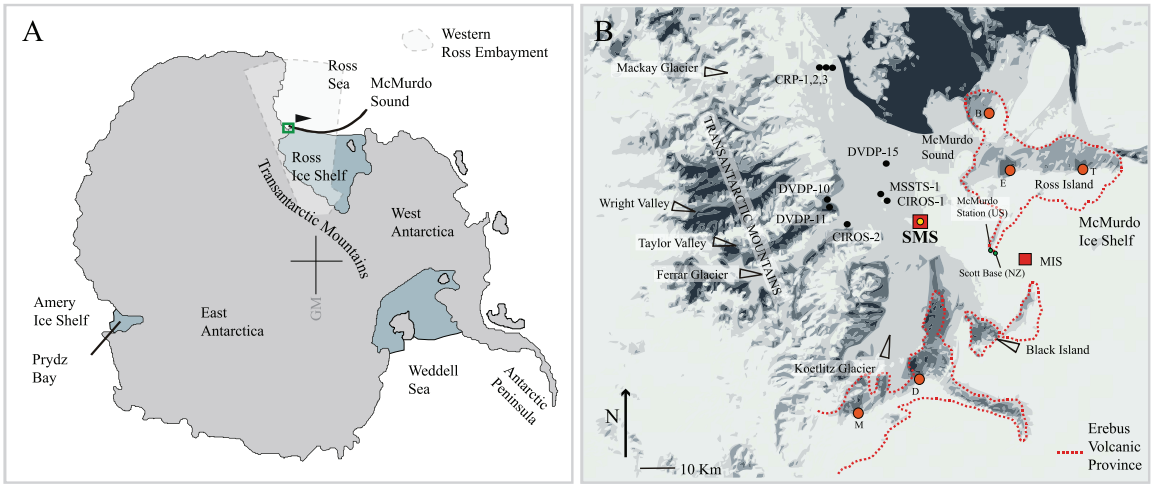

Figure 5.1. Location map. A. McMurdo Sound at the edge of the Ross Ice Shelf, Antarctica. B. ANDRILL SMS (Southern McMurdo Sound) and MIS (McMurdo Ice Shelf) drill–holes location in Southern McMurdo Sound (squares). CRP – Cape Roberts Project; DVDP – Dry Valley Drilling Project; MSSTS – McMurdo Sound Sediment and Tectonic Study; CIROS – Cenozoic Investigations of the Ross Sea. Dotted line demarks the Erebus volcanic province; B – Mount Bird; E – Mount Erebus; T – Mount Terror; M – Mount Morning; D – Mount Discovery. Modified from Harwood et al., (2005).

Figure 5.2. Sr compositional map over background BSE image (visible at the edges). Scale bar applies to both images. Two of the three measured compositional profiles are superimposed on the elemental map. Measurement locations are shown as points along the abscissa. Profile A: beam diameter 2 μm, sample spacing 2 μm. Profile B: beam diameter 0.5 μm, sample spacing 5 μm.

BSE 15 kV
Sr Lα 10 kV
200 μm
wt % Sr
A
B

Figure 5.3. A. Concentrations of Mg^{2+}, Sr^{2+}, and Ca^{2+} in AND–2A pore water centered to a zero mean and scaled to unit standard deviations. Sr^{2+} and Ca^{2+} concentration co–vary, while Mg^{2+} deviates from this pattern near the top of the core. B. Mg^{2+} to Ca^{2+} correlation. Depth is indicated by both sample symbol diameter and color map. Data fitted to a quadratic polynomial function using the least squares method, R^2=0.88. C. $Sr^{2+}$to Ca^{2+} correlation. Depth indicated as in B. Linear least square fit, R^2=0.96.

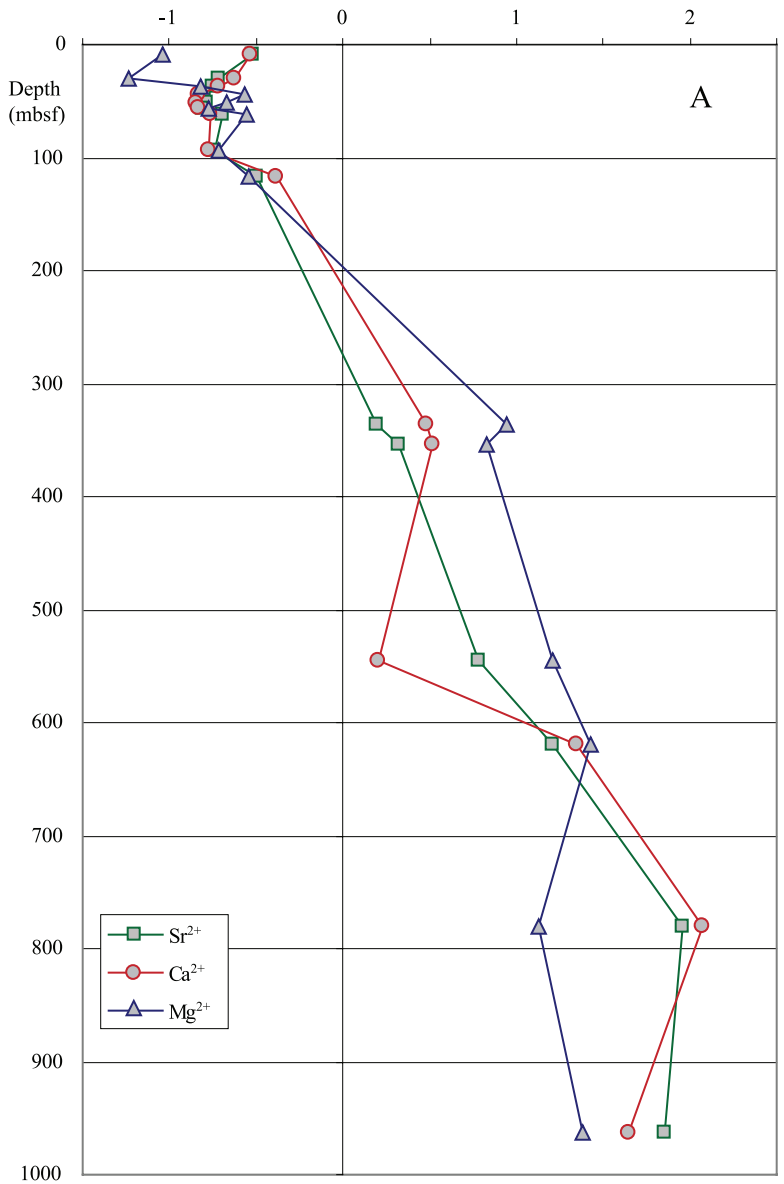
A
Depth
(mbsf)
-1
0
1
2
0
100
200
300
400
500
600
700
800
900
1000
Sr2+
Ca2+
Mg2+

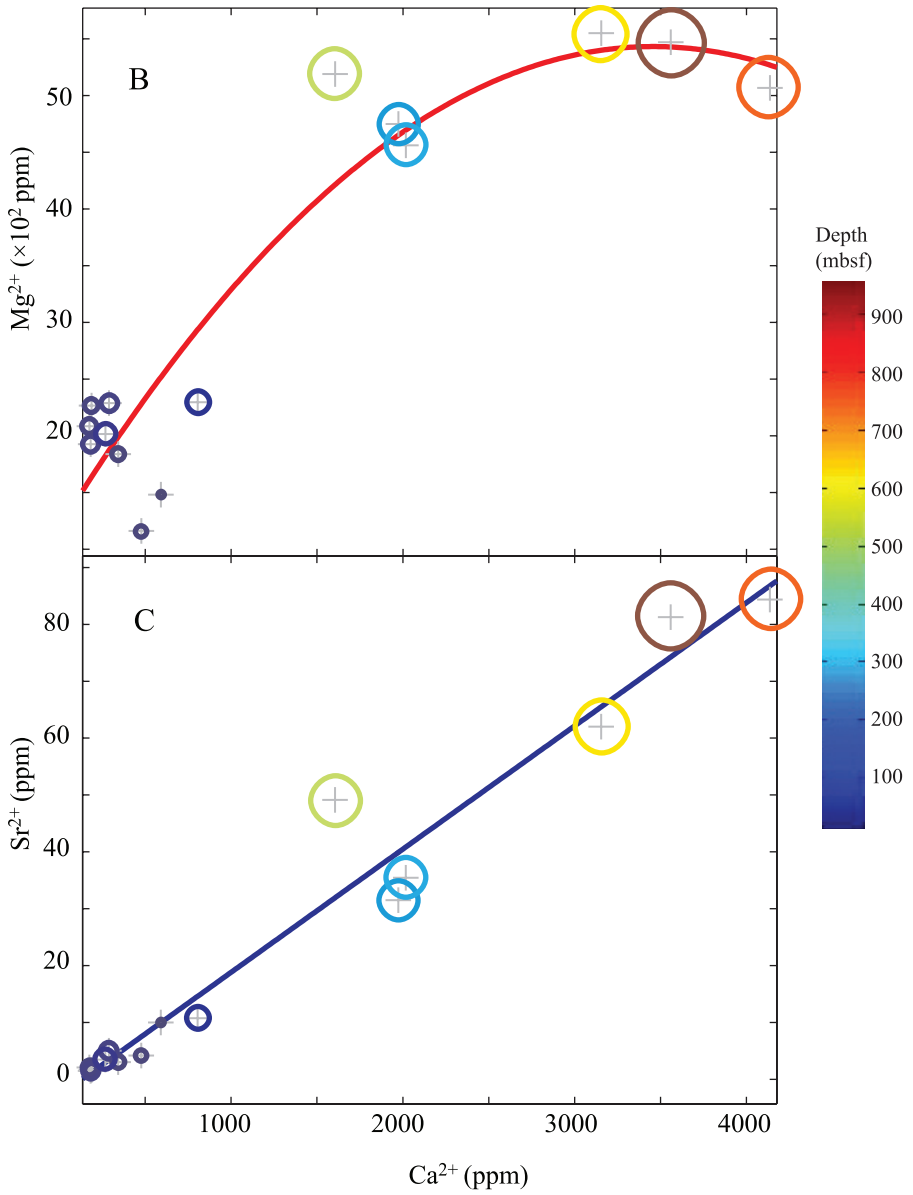
B
C
Mg2+ (×102 ppm)
Sr2+ (ppm)
Ca2+ (ppm)
Depth
(mbsf)
1000
2000
3000
4000
100
200
300
400
500
600
700
800
900

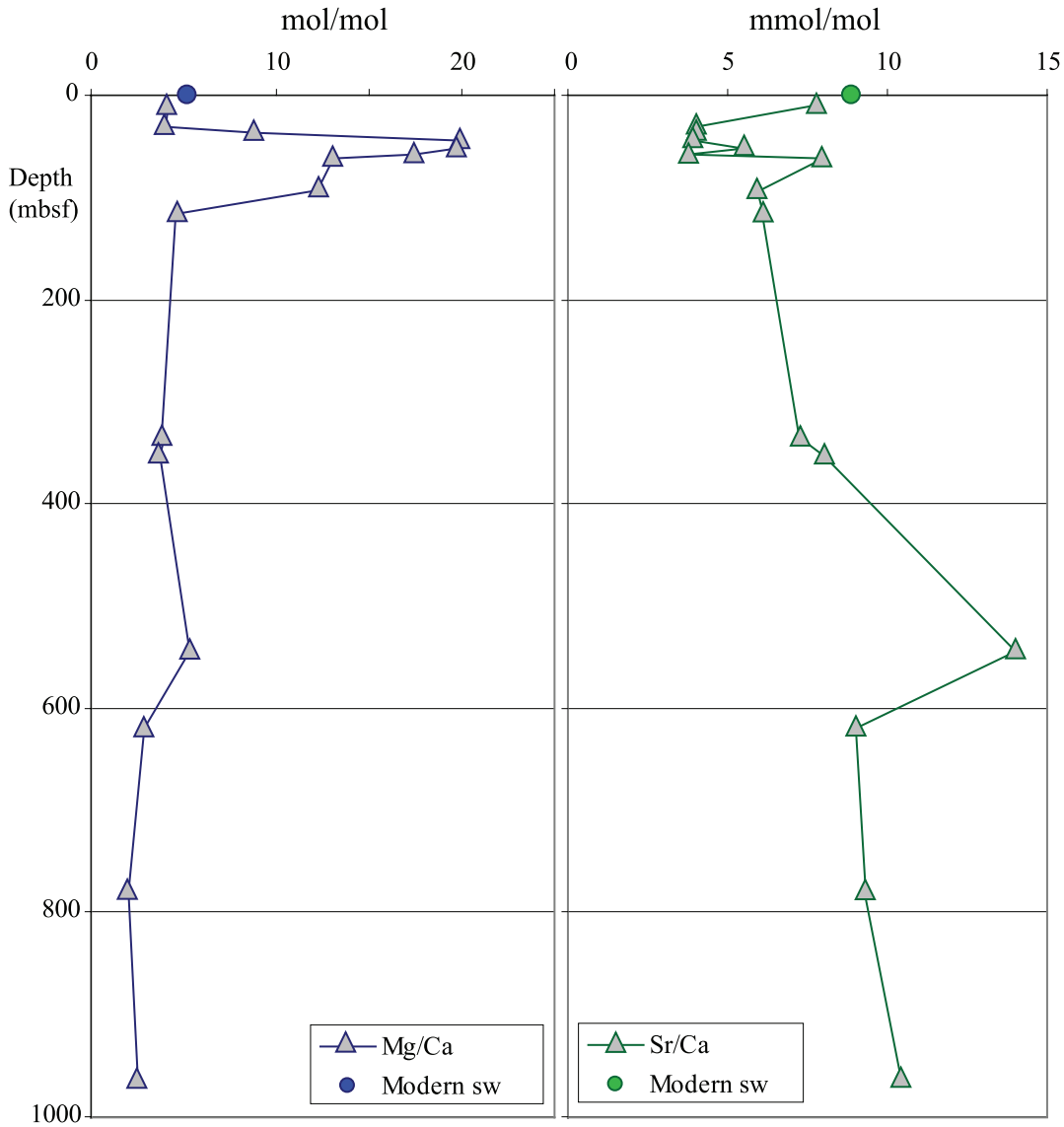

Figure 5.4. Mg^{2+}/Ca^{2+} and Sr^{2+}/Ca^{2+} variation with depth.

Figure 5.5. Sr isotope compositions of pore water (blue diamonds) and previously analyzed carbonate samples (Marcano et al., 2009). Green symbols are samples with no clear indications of alteration. Yellow symbols are samples marginally altered. Circles: pectinid samples (calcite). Triangles: venerid samples (aragonite). Black open circles: AND–2A age model data. Overall age range is indicated by the grey vertical band. Modern seawater $^{87}Sr/^{86}Sr$ value indicated by a blue circle at 0 m depth.

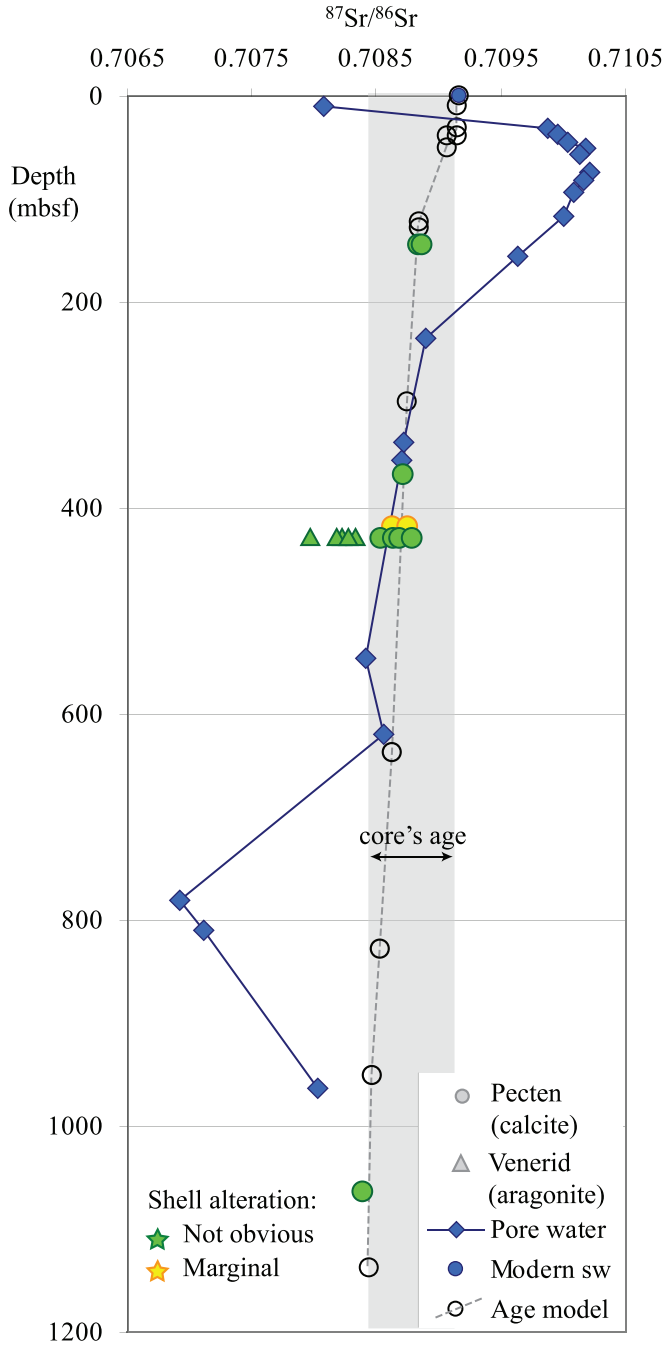
$^{87}Sr/^{86}Sr$
0.7065
0.7075
0.7085
0.7095
0.7105
0
200
400
600
800
1000
1200
Depth
(mbsf)
core's age
Shell alteration:
Not obvious
Marginal
Pecten
(calcite)
Venerid
(aragonite)
Pore water
Modern sw
Age model

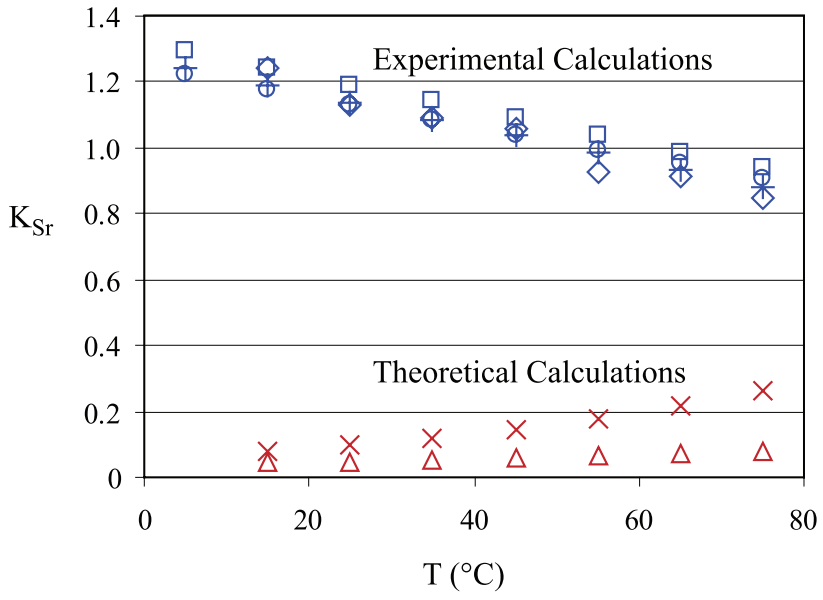

Figure 5.6. Aragonite Sr distribution coefficients versus temperature. K_{Sr} calculated from experimental precipitation of aragonites are from Kinsmand and Holland (1969) (circles), Dietzel et al. (2003) (squares and crosses), and Gaetani and Cohen (2006) (diamonds). Theoretical calculations Gaetani and Cohen (2006), from thermodynamics (crosses) and from the lattice strain equation (triangles). Modified from Gaetani and Cohen (2006).

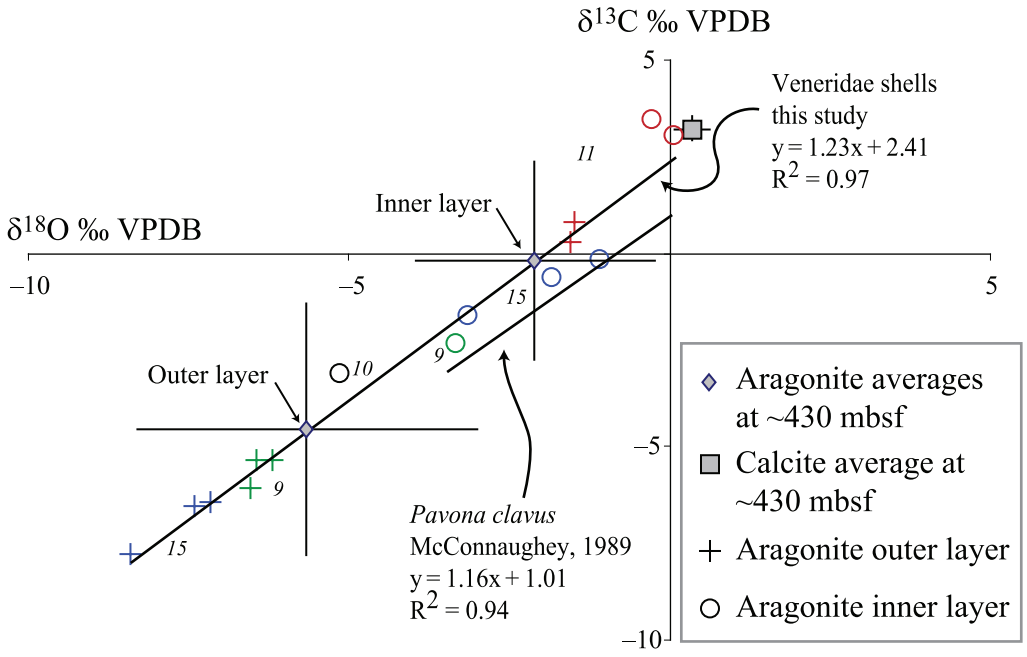

Figure 5.7. Oxygen and carbon isotope compositions of AND–2A bivalve samples. Open squares: pectinid samples (calcite). Open circles and crosses: venerids' inner and outer layer samples respectively (aragonite). In–house sample identification in italics. Linear fits calculated to all aragonite data and to the tropical coral *Pavona clavus* data from McConnaughey (1989).

Table 5.1

Chemical compositions of AND-2A pore water

In-house ID		Depth (mbsf)	ppm					mmol/mol	mol/mol
			Ba	Ca	K	Mg	Sr	Sr/Ca	Mg/Ca
PW	1	9.67-9.72	BDL[a]	590.71	1070.38	1481.34	10.01	7.75	4.13
PW	2-1	30.09-30.15	BDL	477.21	549.60	1161.31	4.17	4.00	4.01
PW	3-1	37.41-37.46	BDL	342.93	559.53	1839.13	3.04	4.06	8.84
PW	4	43.72-43.77	BDL	187.02	708.77	2266.84	1.62	3.97	19.98
PW	5	51.30-51.35	BDL	174.67	602.01	2085.34	2.09	5.48	19.68
PW	6	57.21-57.26	BDL	181.94	578.97	1927.02	1.50	3.76	17.46
PW	7	62.66-62.71	BDL	289.18	779.41	2289.23	5.03	7.95	13.05
PW	10-1	92.97-93.03	BDL	268.23	572.65	2015.55	3.47	5.91	12.39
PW	11	116.22-116-27	BDL	805.60	621.22	2297.04	10.75	6.11	4.70
PW	14-1	336.18-336.28	BDL	1973.06	1873.25	4749.58	31.51	7.31	3.97
PW	15	353.53-353.63	BDL	2017.07	1945.29	4561.63	35.44	8.04	3.73
PW	16	545.01-545.11	0.22	1604.87	2209.72	5190.41	49.12	14.00	5.33
PW	17	619.35-619.45	0.31	3154.36	3312.98	5551.51	62.00	8.99	2.90
PW	18	779.69-779.79	0.22	4136.57	1375.33	5068.06	84.37	9.33	2.02
PW	20	963.44-963.54	0.27	3558.58	1425.83	5471.54	81.29	10.45	2.53

[a] **BDL - Below detection limit.**

Accuracy better than ±5% for Sr and Ca, ±10% for Mg, and ±18% for Ba.

References

Acton, G., Crampton, J., Di Vincenzo, G., Fielding, C.G., Florindo, F., Hannah, M.J., Harwood, D.M., Ishman, S.E., Johnson, K., Jovane, L., Levy, R.H., Lum, B., Marcano, M.C., Mukasa, S.B., Ohneiser, C., Olney, M., Riesselman, C., Sagnotti, L., Stefano, C., Strada, E., Taviani, M., Tuzzi, E., Verosub, K.L., Wilson, G.S., and Zattin, M., 2008. Preliminary Integrated chronostratigraphy of the AND-2A core, ANDRILL Southern McMurdo Sound Project Antarctica. *In* Harwood, D.M., Florindo, F*., et al.*, eds., Studies from the ANDRILL, Southern McMurdo Sound Project, Antarctica, Terra Antarctica, *in press*.

Anderson, T.F., 1973. Oxygen and carbon isotope compositions of altered carbonate from the western Pacific, core 53, Deep Sea Drilling Project. Marine Geology, 15: 169-180.

Bailey, T.R., and Lear, C.H., 2006. Testing the effect of carbonate saturation of the Sr/Ca of biogenic aragonite: a case study from the River Ehen, Cumbria, UK. Geochemistry, Geophysics, Geosystems, 7 (3).

Banner, J.L., and Hanson, G.N., 1990. Calculation of simultaneous isotopic and trace element variations during water-rock interaction with applications to carbonate diagenesis. Geochimica et Cosmochimica Acta, 54: 3123-3137.

Barrera, E., 1989. Strontium isotope ages. *In* Barrett, P.J., ed., Antarctic Cenozoic history from the CIROS-1 drillhole, McMurdo Sound, Volume 245, DSIR Bulletin: 151-152.

Bathurst, R.G.C., 1975. Carbonate sediments and their diagenesis. Elsevier, Amsterdam, 593 p.

Birchfield, G.E., Weertman, J., and Lunde, A., 1982. A model study of the role of high-altitude topography in the climatic response of orbital insolation anomalies. Journal of the Atmospheric Sciences, 39 (1): 71-87.

Brand, U., and Veizer, J., 1980. Chemical diagenesis of a multicomponent carbonate system 1: Trace Elements. Journal of Sedimentary Petrology, 50: 1219-1236.

Carré, M., Bentaleb, I., Blamart, D., Ogle, N., Cardenas, F., Zevallos, S., Kalin, R.M., Ortilieb, L., and Fontugne, M., 2005. Stable isotopes and sclerochronology of the bivalve *Mesodesma donacium*: potential application to Peruvian paleoceanographic reconstructions. Palaeogeography, Palaeoclimatology, Palaeoecology, 228: 4-25.

Cubasch, U., Meehl, G.A., Boer, G.J., Stouffer, R.J., Dix, M., Noda, A., Senior, C.A., Raper, S., and Yap, K.S., 2001. Projections of future climate change. *In* Houghton, J.T., Ding, Y*., et al.*, eds., Climate Change 2001: The Scientific Basis. Contribution of Working Group I to the Third Assessment Report of the Intergovernmental Panel on Climate Change, Cambridge University Press, Cambridge: 527-578.

DeConto, R., Pollard, D., and Harwood, D.M., 2007. Sea ice feedback and Cenozoic evolution of Antarctic climate and ice sheets. Palaeogeoceanography, 22.

Dietzel, M., Gussone, N., and Eisenhauer, A., 2003. Co-precipitation of Sr^{2+} and Ba^{2+} with aragonite by membrane diffusion of CO_2 between 10 and 50 ºC. Chemical Geology, 203: 139-151.

Dutton, A., Lohmann, K.C., and Zinsmeister, W.J., 2002. Stable isotope and

minor elements proxies for Eocene climate of Seymour Island, Antarctica. Palaeogeoceanography, 17 (2): 1016.
Elderfield, H., and Gieskes, J.M., 1982. Sr isotopes in interstitial waters of Deep Sea Drilling Project cores. Nature, 300: 493-497.
Elliot, M., Welsh, K., Chicott, C., McCulloch, M., Chappell, J., and Ayling, B., 2009. Profiles of trace elements and stable isotopes derived from giant long-lived *Tridacta gigas* bivalves: potential applications in paleoclimate studies. Palaeogeography, Palaeoclimatology, Palaeoecology, 280: 132-142.
Elliot, M.B., deMenocal, B.K.L., and Howe, S.S., 2003. Environmental controls on the stable isotopic composition of *Mercenaria mercenaria*. Potential application to paleoenvironmental studies. Geochem., Geophys. Geosyst., 4 (7): 1056.
Epstein, S., Buchsbaum, R., Lowenstam, H.A., and Urey, H.C., 1953. Revised carbonate-water isotopic temperature scale. Geological Society of America Bulletin, 64 (11): 1316-1326.
Faure, G., and Mensing, T., 2005. Isotopes. Principles and applications. John Wiley & Sons, 897 p.
Fielding, C.G., Atkins, C.B., Basset, K.N., Browne, G.H., Dunbar, G.B., Field, B.D., Frank, T.D., Krissek, L.A., Panter, K.S., Passchier, S., Pekar, S.F., Sandroni, S., and Talarico, F., *in press*. Sedimentology and stratigraphy of the AND-2A core, ANDRILL Southern McMurdo Sound Project, Antarctica. *In* Harwood, D.M., Florindo, F*., et al.*, eds., Studies from the ANDRILL, Southern McMurdo Sound Project, Antarctica, Terra Antarctica, *in press*.
Folk, R., 1965. Some aspects of recrystallization in ancient limestones. Society of Economic Paleontologists and Mineralogists, spec. pub. 13: 14-48.
Foster, L., Allison, N., Finch, A.A., and Andersson, C., 2009. Strontium distribution in the shell of the aragonite bivalve *Arctica islandica*. Geochemistry, Geophysics, Geosystems, 10 (3).
Frank, T.D., and Gui, Z., *in press*. Cryogenic origin for brine in the subsurface of southern McMurdo Sound, Antarctica. Geology.
Freitas, P.S., Clarke, L.J., Kennedy, H., Richardson, C.A., and Abrantes, F., 2006. Environmental and biological controls on elemental (Mg/Ca, Sr/Ca and Mn/Ca) ratios in shells of the king scallop *Pecten maximus*. Geochimica et Cosmochimica Acta, 70: 5119-5133.
Gaetani, G.A., and Cohen, A.L., 2006. Element partitioning during precipitation of aragonite from seawater: a framework for understanding paleoproxies. Geochimica et Cosmochimica Acta, 70: 4617-4634.
Gillikin, D.P., Lorrain, A., Navez, J., Taylor, J.W., André, L., Keppens, E., Baeyens, W., and Dehairs, F., 2005. Strong biological controls on Sr/Ca rations in aragonitic marine bivalve shells. Geochemistry, Geophysics, Geosystems, 6 (5): 16 p.
Gonzalez, L., and Lohmann, K.C., 1985. Carbon and oxygen isotopic composition of Holocene reefal carbonates. Geology, 13: 811-814.
Graustein, W.C., 1989. $^{87}Sr/^{86}Sr$ ratios measure the sources and flow of strontium in terrestrial ecosystems. *In* Rundel, P.W., Ehleringer, J.R*., et al.*, eds., Ecological Studies, Volume 68: 491-512.
Grossman, E.L., and Ku, T.-L., 1986. Oxygen and carbon isotope fractionation in

biogenic aragonite; temperature effects. Chemical Geology; Isotope Geoscience Section, 59 (1): 59-74.
Gui, Z., 2009. Origin of brines in Neogene sediments of the Ross Sea, Antarctica: AND-2A Core, ANDRILL, Southern McMurdo Sound Project, M.S. thesis: Lincoln, University of Nebraska. 51 p.
Hart, S.R., and Blusztajn, J., 1998. Clams as recorders of ocean ridge volcanism and hydrothermal vent field activity. Science, 280: 883-886.
Harwood, D.M., Florindo, F., Levy, R.H., Fielding, C.G., Pekar, S.F., and Speece, M.A., 2005. ANDRILL Southern McMurdo Sound Project Scientific Prospectus. *In* ANDRILL SMO Contribution No. 5, Lincoln, 29 p.
Harwood, D.M., Florindo, F., Talarico, F., Levy, R.H., Kuhn, G., Naish, T., Niessen, F., Powell, R., Pyne, A., and Wilson, G.S., 2009. Antarctic drilling recovers stratigraphic records from the continental margin. EOS, Transactions, American Geophysical Union, 90 (11).
Harwood, D.M., Levy, R.H., Cowie, J., Florindo, F., Naish, T., Powell, R., and Pyne, A., 2006. Deep drilling with the ANDRILL program in Antarctica. Scientific Drilling, (3): 43-45.
Hess, J., Bender, M., and Schilling, J.-G., 1986. Evolution of the ratio of Strontium-87 to Strontium-86 in seawater from Cretaceous to Present1. Science, 231 (4741): 979-984.
Hoefs, J., 1997. Stable Isotope Geochemistry. Springer, Berlin; New York, 201 p. p.
Howarth, R.J., and McArthur, J.M., 1997. Statistics for strontium isotope stratigraphy. A robust LOWESS fit to marine Sr-isotope curve for 0 - 206 Ma, with look-up tables for the derivation of numerical age. Journal of Geology, 105: 441-456.
Kennett, J.P., 1977. Cenozoic evolution of Antarctic glaciation, the circum-Antarctic Ocean, and their impact on global paleoceonography. J. Geophys. Res., 82 (27): 3843-3860.
Kim, S.-T., O'Neil, J.R., Hillaire-Marcel, C., and Mucci, A., 2007. Oxygen isotope fractionation between synthetic aragonite and water: influence of temperature and Mg^{+2} concentration. Geochemica et Cosmochimica Acta, 71: 4704-4715.
Kinsman, D., 1969. Interpretations of Sr^{2+} concentrations in carbonate minerals and rocks. Journal of Sedimentary Petrology, 39 (2): 486-508.
Kinsman, D., and Holland, H.D., 1969. The co-precipitations of cations with $CaCO_3$ - IV. The co-precipitation of Sr^{2+} with aragonite between 16º and 96º C. Geochimica et Cosmochimica Acta, 33: 1-17.
Lavelle, M., 1998. Strontium-isotope stratigraphy of the CRP-1 drillhole, Ross Sea, Antarctica. Terra Antarctica, 5 (3): 691-696.
—, 2000. Strontium isotope stratigraphy and age model for CRP-2/2A, Victoria Land Basin, Antarctica. Terra Antarctica, 7 (4): 611-619.
—, 2001. Strontium isotope stratigraphy for CRP-3, Victoria Land Basin, Antarctica. Terra Antarctica, 8 (4): 593-597.
Lear, C.H., Elderfield, H., and Wilson, P.A., 2000. Cenozoic Deep-Sea temperatures and global ice volumes from Mg/Ca in benthic foraminiferal calcite. Science, 287: 269-272.
Lowenstam, H.A., 1964a. Coexisting calcites and aragonites from skeletal carbonates

of marine organisms and their strontium and magnesium contents, *in*, Recent researches in the fields of hydrosphere, atmosphere and nuclear geochemistry. V. Sugawara Festival, Tokyo: 373-404 p.

—, 1964b. Sr/Ca ratio of skeletal aragonites from the recent marine biota at Palau and from fossil gastropods. *In* Craig, Harmen*, et al.*, eds., Isotopic and Cosmic Chemistry, Amsterdam.

Mann, R., and Gieskes, J.M., 1975. Interstitial waters studies, Leg 28. *In* Hayes, D.E., Frakes, L.A.*, et al.*, eds., Initial reports of the Deep Sea Drilling Project, Volume 28, U. S. Government Printing Office, Washington: 805-814.

Marcano, M.C., Mukasa, S., Lohmann, K.C., Stefano, C., Taviani, M., and Andronikov, A., 2009. Chronostratigraphic and paleoenvironmental constraints derived from the $^{87}Sr/^{86}Sr$ and $\delta^{18}O$ signal of Miocene bivalves, Southern McMurdo Sound, Antarctica. Global and Planetary Change, (Special Issue: Antarctic Cryosphere).

McArthur, J.M., Howarth, R.J., and Bailey, T.R., 2001. Strontium isotope stratigraphy: LOWESS Version 3. Best-fit line to the marine Sr-isotope curve for 0 to 509 Ma and accompanying look-up table for deriving numerical age. Look-up table Version 4:08/04. Journal of Geology, 109: 155-169.

McConnaughey, T., 1989a. ^{13}C and ^{18}O isotopic disequilibrium in biological carbonates: I. Patterns. Geochimica et Cosmochimica Acta, 53: 151-162.

—, 1989b. ^{13}C and ^{18}O isotopic disequilibrium in biological carbonates: II. In vitro simulation of kinetic isotope effects. Geochimica et Cosmochimica Acta, 53: 163-171.

McConnaughey, T., and Gillikin, D.P., 2008. Carbon isotopes in mollusks shell carbonates. Geo-Marine Letters, 28: 287-299.

Meehl, G.A., Stocker, T.F., Collins, W.D., Friedlingstein, P., Gaye, A.T., Gregory, J.M., Kitoh, A., Knutti, R., Murphy, J.M., Noda, A., Raper, S.C.B., Watterson, I.G., Weaver, A.J., and Zhao, Z.-C., 2007. Projections of future climate change. *In* Solomon, S., Qin, D*., et al.*, eds., Climate Change 2001: The Scientific Basis. Contribution of Working Group I to the Third Assessment Report of the Intergovernmental Panel on Climate Change, Cambridge University Press, Cambridge: 527-578.

Moore, R.C., 1969. Treatise on invertebrate paleontology. Part N. Vols 1, 2. No3. Mollusca 6 Bivalvia, The Geological Society of America, Laurence, 951 p.

Morse, J.W., and Mackenzie, F.T., 1990. Geochemistry of sedimentary carbonates. Elsevier, Amsterdam, 707 p.

Mukasa, S.B., Shervais, J.W., Wilshier, H.G., and Nielson, J.E., 1991. Intrinsic Nd, Pb, and Sr isotopic heterogeneities exhibited by the Lherz Peridotite massif, French Pyrenees. J. Petrol. Spec. Lith. Issue: 117-134.

Naish, T., Powell, R., Levy, R.H., Henrys, S., Krissek, L.A., Niessen, F., Pompilio, M., Scherer, R., Wilson, G.S., and Team, t.A.-M.S., 2007. Synthesis of the initial scientific results of the MIS project (AND-1B core), Victoria Land Basin, Antarctica. Terra Antarctica, 14 (3): 317-327.

Panter, K.S., Talarico, F., Basset, K.N., Del Carlo, P., Field, B.D., Frank, T.D., Hoffmann, S., Kuhn, G., Sandroni, S., Taviani, M., Bracciali, L., Cornamusini, G., von Eynatten, H., Rocchi, S., and Team, t.A.-S.S., *in press*. Petrology and

geochemistry of the AND-2A core, ANDRILL Southern McMurdo Sound Project, Antarctica. *In* Florindo, F., Harwood, D.M.*, et al.*, eds., Studies from the ANDRILL, Southern McMurdo Sound Project, Antarctica, Terra Antarctica.

Smalley, C., Higgins, A.C., Howarth, R.J., Nicholson, H., Jones, C.E., Swinburne, N.H.M., and Bessa, J., 1994. Seawater Sr isotope variations through time: a procedure for constructing a reference curve to date and correlate marine sedimentary rocks. Geology, 22: 431-434.

Stanley, S.M., and Hardie, L., 1998. Secular oscillations in the carbonate mineralogy of reef-building and sediment-producing organisms driven by tectonically forced shifts in seawater chemistry. Palaeogeography, Palaeoclimatology, Palaeoecology, 144: 3-19.

Stecher, H.A., Krantz, D.E., Lord, C.J., Luther, G.W., and Bock, K.W., 1996. Profiles of strontium and barium in *Mercenaria mercenaria* and *Spisula solidissima* shells. Geochimica et Cosmochimica Acta, 60 (18): 3445-3456.

Surge, D., and Walker, K.J., 2006. Geochemical variation in microstructural shell layers of the southern quahog (*Mercenaria campechiensis*): implications for reconstructing seasonality. Palaeogeography, Palaeoclimatology, Palaeoecology, 237: 182-190.

Takesue, R.K., Bacon, C.R., and Thompson, J.K., 2008. Influences of organic matter and calcification rate on trace elements in aragonitic estuarine bivalves shells. Geochimica et Cosmochimica Acta, 72: 5431-5445.

Thierstein, H.R., Macdougall, J.D., Martin, E.E., Larsen, B., Barron, J.A., and Baldauf, J., 1991. Age determinations of Paleogene diamictites from Prydz Bay (Site 739), Antarctica, using Sr isotopes of mollusks and biostratigraphy of microfossils (diatoms and coccoliths). *In* Barron, J.A., Larsen, B.*, et al.*, eds., Proc. ODP, Sci. Results, Volume 119, College Station, TX (Ocean Drilling Program): 742-745.

Veizer, J., 1983. Trace elements and isotopes in sedimentary carbonates. Reviews in Mineralogy, 11: 265-299.

Wada, H., and Okada, H., 1989. Carbonate isotopes. *In* Barrett, P.J., ed., Antarctic Cenozoic history from the CIROS-1 drillhole, McMurdo Sound, Volume 245, DSIR Bulletin: 195-200.

Walter, L.M., 1986. Relative efficiency of carbonate dissolution and precipitation during diagenesis, a progress report of the role of solution chemistry. *In* Gautier, D.L., ed. Special Publication Society of Economic Paleontologists and Mineralogists. V. 38, 1-11 p.

Walter, L.M., and Morse, J.W., 1985. The dissolution kinetics of shallow marine carbonates in seawater: a laboratory study. Geochimica et Cosmochimica Acta, 49: 1503-1513.

Wefer, G., and Berger, W.H., 1991. Isotope paleontology: growth and composition of extant calcareous species. Marine Geology, 100 (1-4): 207-248.

Wilson, G.S., Levy, R.H., Browne, G.H., Cody, R., Dunbar, N., Florindo, F., Henrys, S., Graham, I., McIntosh, W.C., McKay, R.M., Naish, T., Ohneiser, C., Powell, R., Ross, J., Sagnotti, L., Scherer, R., Sjunneskog, C., Strong, C.P., Taviani, M., Winter, D., and Team, t.A.-M.S., 2007. Preliminary integrated chronostratigraphy of the AND-1B core, ANDRILL McMurdo Ice Shelf Project, Antarctica. Terra

Antarctica, 14 (3): 297-316.
Wonik, T., Grelle, T., Hardwerger, D., Jarrard, R.D., McKee, A., Patterson, T., Paulsen, T., Pierdominici, S., Schmitt, D.R., Schroder, H., Speece, M.A., Wilson, T., and Team, t.A.-S.S., *in press*. Downhole measurements in the AND-2A borehole, ANDRILL Southern McMurdo Sound Project, Antarctica. *In* Florindo, F., Harwood, D.M.*, et al.*, eds., Studies from the ANDRILL, Southern McMurdo Sound Project, Antarctica, Volume 15, Terra Antarctica.

CHAPTER 6

Conclusion

Oxygen isotope records from several contemporaneous taxa better represent the marine environment and show complexities that are not expressed by individuals alone. Because shell calcification occurs at different times for each taxon due to the contrasting ecological limits of each species, oxygen isotope analysis of an array of individuals from the same environment provides a better account of their shared marine climate. Applying relatively straightforward strategies, the oxygen isotope records of a biocenosis led to the following conclusions: 1) relatively small changes in δ_w may impact fractionation calculations. This means that δ_w approximations in paleoenvironmental studies require careful consideration; 2) both equilibrium precipitation and precipitation at a departure from equilibrium are plausible in modern environments. Given that equilibrium precipitation is the basis of paleoenvironmental reconstructions, this strategy should be useful to test initial assumptions in fossil samples. Assuming equilibrium precipitation in mollusks may not be always appropriate, and departures from it surely exist in the fossil record as they do today; 3) lower than published precipitation temperature thresholds occur locally. Acclimation may be responsible for shifts in these values. This suggests that applying modern analogs' temperature thresholds to ancient samples may be problematic; 4) summer growth retardation occurs despite the lack of evidence from the shape of the $\delta^{18}O$ data suggesting that intra–annual growth analysis should be pursued in fossil samples. Such analysis must start with objective time assignment to $\delta^{18}O$ vs. distance profiles; 5) lowest and highest possible temperatures are produced by different

taxa. In spite of the complexities associated with multiple materials and sample strategies, paleotemperature range is better approximated using several fossil taxa.

Taking a step further to improve the use of bivalve $\delta^{18}O$ in paleoenvironmental interpretations, modern shell carbonate $\delta^{18}O$ was modeled at a regional scale incorporating salinity influences to characterize shallow water marine climates. This exercise produced the following conclusions: 1) relatively long–term temperature variability along the North American east coast can be characterized by sinusoid fits; 2) salinity variability, on the other hand, is difficult to describe regionally. Although salinity drops appear to be seasonally controlled, the noise in the data is too large to describe the populations using best–fit sinusoids or probability density functions of any kind; 3) seasonal and local changes in $\delta^{18}O$–salinity relations are relevant to accurately predict $\delta^{18}O$ values of shallow marine environments. It follows that δ_w variation should also be important when interpreting past marine environments; 4) salinity variation complicates temperature interpretations in temperate marine climates. The influence of salinity variation must be incorporated to paleoenvironmental studies instead of being artificially confined by assuming a static δ_w; 5) seasonal variation of bivalve shell $\delta^{18}O$ is shown to be relevant in discriminating between tropical and temperate marine climates. Variation in summer is larger than in winter in inner and outer tropical marine climates and the opposite is true in warm and cool temperate regions. Distinction between these broad climate regimes should help improve paleoenvironmental interpretations of fossil communities.

Analyses of bivalve fragments recovered from ANDRILL's core AND–2A, Southern McMurdo Sound, Antarctica, helped improve age control at several depths using $^{87}Sr/^{86}Sr$ while $\delta^{18}O$ provided initial constraints to local marine climate during the Miocene. Contrasts in preservation imposed challenges to further paleoenvironmental interpretations but provided an opportunity to explore unusual Sr concentrations and isotopic compositions in shell aragonite. The following conclusions were drawn from

the work on biogenic carbonates from AND–2A: 1) Antarctica's bottom waters were closer to global seawater temperature averages in the late Early Miocene (Burdigalian-Langhian) than in the early Late Miocene (Serravalian-Tortonian); 2) at ~11 Ma cooling and continental and sea ice accumulation may have controlled local marine conditions in Southern McMurdo Sound; 3) aragonite shell fragments have preserved their original mineralogy as shown by detailed PXRD and further suggested by the presence of growth bands in the inner layer of the shells; 4) the anomalously high Sr concentration of the outer layer can be relatively well explained using AND–2A pore water Sr concentration and a reasonable partition coefficient. This suggests that post–depositional processes are responsible for the anomalous Sr observed in aragonite shells; 5) the variability in the concentration values of aragonite are explained by partial alteration of the shells. Some areas of the shells were originally more susceptible to diagenesis. This alteration potential contrast is probably associated to the correlation between crystal structure and growth rates; 6) alteration is more conclusively suggested by the outer layers' persistent depletion in ^{18}O compared to the inner layers and the plausible shell $\delta^{18}O$ values calculated using core temperatures and fluid $\delta^{18}O$; 7) disequilibrium between biogenic carbonates and pore water Sr isotope compositions and the substantial contrast in $^{87}Sr/^{86}Sr$ with respect to other pore water in the Ross Sea shelf support a para–authoctonous origin of the fluids present in AND–2A today.

APPENDIX 1

Research Proposal

Mid-Pliocene $\delta^{18}O$ and Mg/Ca paleotemperatures from the western North Atlantic Ocean: the prelude to northern hemisphere glaciation

Introduction

Interactions among the various components of the climate system are diverse and complex. While definite climate variability has been captured within historical boundaries, this timeframe is insufficient to recognize, evaluate, or predict changes. A better understanding of the climate system comes only from an examination of its behavior in the geologic past, where a much longer record and wider range of possible behaviors allows us to place present-day conditions into context. Imminent short-term effects of the remarkable increase in anthropogenic CO_2 during the last century, for example, becomes apparent when examining the final ~ 400 ka record of the Vostok ice-core from East Antarctica (Barnola *et al.*, 1987; Petit *et al.*, 1999). Even though some research suggests decoupling between global temperature trends and atmospheric greenhouse gases concentration at longer time scales (Veizer et al., 2000), the Vostok and similar ice-core records leave no question about the covariant behavior of these two factors in the short run, and the immediacy of future climate warming (see Crowley and Berner, 2001; Lynas, 2004). Still, the extent of warming and its effect on other climate components remains unclear.

The uncertain consequences of impending warmth have compelled scientists to focus on earlier warm periods in the Earth's history for insight about our future. Extreme warm intervals such as the Cretaceous and early Eocene may not be useful analogs for

the immediate future given that boundary conditions were quite different then. The mid-Pliocene, however, may be particularly suitable as a window into the more immediate future of our climate for several reasons. First, tectonic configuration, and probably greenhouse gas concentration are comparable to today. Secondly, because it is so recent, the evidence of climate change can be more reliably extracted from the sedimentary record since well-preserved sediments and microfossils from this time allow us to reconstruct climate with more confidence than studies of more distant times. Third, initial indications are that the mid-Pliocene was a time of relative warmth in comparison to today, just prior to the onset of northern hemisphere glaciations. Understanding this transition is relevant to estimate future climate response. Thus, it seems reasonable to explore climate records from this time. In addition, several recognized and potentially climate-significant events occurred during the mid-Pliocene (e.g., the final closure of the Central American seaway, CAS). These offer the opportunity to evaluate their impact on oceanic and atmospheric circulation.

Reconstructing Ancient Climate

Past climate can be qualitatively evaluated using direct evidence such as the nature, distribution and changes through time of climate-sensitive lithologies and fossils. A variety of statistical approaches have been developed in an effort to make more robust correlations between past and present faunal assemblages (see Parrish, 1998 for an extended review of paleoclimatic indicators). The value of these techniques is considerable, but commonly impaired by poor preservation and uncertainties on the degree to which modern faunas offer analogs to ancient ones. Alternatively, oxygen isotope ratios from marine carbonates are strong indicators of environmental change. Foraminifera $\delta^{18}O$ values from deep-sea cores have become the standard proxy with which to evaluate climate behavior (Shackleton, 1976; Shackleton et al., 1984; Mix, 1987). While complications arise due to the combined influences of temperature and global ice volume on the $\delta^{18}O$ signal from marine carbonates, the measure has been

used with much success. Deep marine $\delta^{18}O$ records are remarkably similar to the correspondent air temperature estimates from ice-cores (Petit et al., 1999; Shackleton, 2000). Detailed $\delta^{18}O$ profiles can reveal not only when the Earth's climate was warm or cold, but also the finer-scale details of climate variability and the nature of transitions between climate extremes. At a scale of 10^3 - 10^4 years, for example, warming events appear very rapid, while cooling seems to be much more gradual (Maslin et al., 2001), warm periods exhibit less variability (Draut et al., 2003), and, as shown in recent records, climate appears capable of rapid switches between stable modes (Alley et al., 2001).

Benthic foraminifera $\delta^{18}O$ variability has been explained by changes in ice volume (Shackleton, 1967), in both ice volume and temperature (e.g., Zachos et al., 2001; Oerlemans, 2004), or in deep sea water temperature, which in turn represents high latitude sea surface temperature (Emiliani, 1955; Savin, 1977). Considered in its totality, the Cenozoic marine $\delta^{18}O$ is probably a true mixed signal. For shorter periods within the Tertiary, however, other evidence may assist to credibly explain the signal as mainly the product of one factor or the other. Planktonic $\delta^{18}O$ may or may not represent temperature conditions of the upper ocean. Not only because of the mixed signal problem already discussed which affects equally surface water dwellers, but also because of imprecise knowledge of calcification depths. Covariant changes in planktonic and benthic $\delta^{18}O$ can be regarded as caused by global changes in ocean isotopic composition (Shackleton, 1967; Prell, 1984). Temperature changes, on the other hand, could affect populations separately producing diverging signals. Both records are commonly used in combination, and the interpretation is usually supported by several other concurrent observations.

Calcium carbonate from other marine organisms is similarly used to assess climate. Mollusk shells, particularly from bivalves, have proven useful in assessing environmental conditions and seasonality (Jones et al., 1983; Jones and Quitmyer, 1996; Goodwin et al., 2003; Ivany et al., 2003). The amplitude of intraannual variation recorded in shells is a valuable indicator of temperature range, although these data demand

caution on face values interpretation for a number of reasons particularly if they come from marginal marine environments where the influence of salinity can be significant (e.g.,Ivany et al., 2004).

Pliocene Climate

Efforts have been made to characterize the climate of the Pliocene (Berggren et al., 1995) and to generate reliable paleoenvironmental reconstructions of its warmer intervals (Dowsett et al., 1994; Barron et al., 1996; Dowsett et al., 1999; Draut et al., 2003).The early and middle Pliocene includes probably the warmest spells in the past 7 Ma (Zubakov and Borzenkova, 1988). The early Pliocene (~ 5.3 – 3.5 Ma) was a time of relative warmth (Poore and Sloan, 1996) and low ice volume. Sedimentology, micropaleontology, and isotope geochemistry, all show little evidence for Northern Hemisphere glaciation before 3.2 Ma (Raymo, 1994). Deep-sea core $\delta^{18}O$ and concurrent ice rafted detritus (IRD) firmly place the initiation of intense glaciation in the northern Hemisphere at 2.5 – 2.4 Ma (Shackleton et al., 1984; Raymo, 1994; Hay et al., 2002), and the final stretch of the Pliocene witnessed the beginning of the high-amplitude, high-frequency glacial-interglacial regime characteristic of the Quaternary.

Here, I focus on the middle Pliocene, an informal and variably defined interval roughly between 4.5 and 2.5 Ma. The period between 4.4 and 3.3 Ma is known as the mid-Pliocene Climatic Optimum (Zubakov and Borzenkova, 1988). More recently, stratigraphic and faunal studies have also suggested a period of sustained warmth around 3 Ma (e.g., Dowsett and Cronin, 1990; Willard et al., 1993). CO_2 concentration reached twice pre-industrial levels (Budyko, 1982; Crowley, 1991), and eustatic sea level was higher by up to 60 m in comparison to the Modern (Haq et al., 1987). Global warmth and high sea-level presumably led to substantial melting of the Antarctica ice sheet (e.g., Webb et al., 1984). The Pliocene Research, Interpretations, and Synoptic Mapping project (PRISM -- Dowsett et al., 1999; Dowsett, 2004) applied multiple proxies to the interval between 3.29 - 2.97 Ma to reconstruct sea surface temperatures and continental

climate. Mainly relying on the application of factor analytic transfer functions, modern analog technique (MAT), and semiquantitative comparison of mid-Pliocene foraminifera, diatoms, and ostracods to modern fauna, they further substantiate a period of widespread mid-Pliocene warmth. This period is characterized by a Northern Hemisphere ice cap restricted to Greenland, a seasonally ice-free Artic Ocean, sea-level higher than today by about 25 m, and warmer sea surface temperatures (SST) at high latitudes (e.g., by up to 7 degrees in the eastern North Atlantic). Continental areas experienced higher humidity and northward expansion of warm-climate species (Thompson and Fleming, 1996). A 3 Ma warm scenario has been successfully reproduced using general circulation models with twice the present atmospheric levels (PAL) of CO_2 (Crowley, 1991), providing a plausible cause for warming.

Questions have emerged, however, about the specific nature of the mid-Pliocene global warmth (i.e., its extent and intensity). A number of other studies show conflicting evidence for warmth, and some in fact suggest cooling instead. Although the non-covariance between planktonic and benthic records suggests a lack of long-lasting ice increase at this time (Prell, 1984), the deep marine $\delta^{18}O$ and IRD records suggest that small ice sheets developed in the northern hemisphere around 3 Ma (Raymo, 1994). Zubakov and Borzenkova (1988) maintain that the inferred ice growth is recorded in the stratigraphy of sub-aerial and marine sections in the Black Sea. The marine record also suggests that at mid-latitudes warming was not significant. High-resolution benthic $\delta^{18}O$ from ODP site 607 (41° N - 33° W) in the central North Atlantic is a good example. The record between 3.1 and 2.9 Ma produced a maximum $\delta^{18}O$ value of 3.1‰, only slightly less than the average Holocene value of about 3.2‰ (Raymo, 1994). Taken exclusively as a temperature signature, these data suggest the warmest deep water at about ~3 Ma was only 0.3 °C warmer than today (Erez and Luz, 1983). The full isotope change from the alleged warmth to the initial glacial conditions (i.e., 0.3‰ from 3.1 to 2.70 Ma), requires cooling by only 1.3 °C. If this signal is attributed entirely to ice volume, sea

level in the mid-Pliocene must have been ~10 m above that of today. This estimate entails net melting of the Antarctica ice sheet between then and now since only 5 m of sea level change would occur if the modern, and presumably larger, Greenland ice cap were to melt completely. Melting in Antarctica during the mid-Pliocene is controversial (see below). Surprisingly, analytical transfer functions applied to planktonic foraminifera assemblages of site 607 (Coates et al., 1992; Dowsett et al., 1996) indicate an equally small but opposite change in SST between the Pliocene and today.

More recently, Draut et al., (2003) estimated mid-Pliocene SST and sea level from high-resolution planktonic and benthic $\delta^{18}O$ records in the eastern North Atlantic ODP site 981 (55° N – 14° W). For a short interval around 3.2 Ma, just prior to the above studies, they recognized a relatively warm interval but concluded that sea level was no more than 5 m above present-day and that SST were only 1.2 °C warmer than today (in contrast to the ~7 °C suggested by Dowsett and Poore, 1991). Based on their $\delta^{18}O$ record, the interval in which they focused encompasses the warmest and least variable of the last 3.3 Ma (figure 1) suggesting that, at a first approximation, the globally warm mid-Pliocene interpreted by the PRISM project may not be confirmed by isotope data. ODP site 981 is a high-latitude site and should exhibit greater sensitivity to climate variation, as this region is directly affected by the influx of warm water from the western boundary current. A greater climate response is also expected here during warmer periods given the probable decrease in meridional temperature gradient while low latitude temperatures are basically maintained.

This work, as well as world over deep-ocean oxygen isotope profiles, calls into question the proposal of a much warmer mid-Pliocene interval. The recently published LR04 benthic $\delta^{18}O$ stack by Lisiecki and Raymo (2005) provides a good summary of the deep-ocean signal for the past 5.3 Ma. The stack was created using information from over 57 sites, the majority of them in the Atlantic Ocean, and includes around 38,000 individual $\delta^{18}O$ measurements. The correlation technique maximized the signal-to-noise

ratio. The resulting age uncertainty between 4 and 3 Ma is on the order of 15 ky, and the mean standard error on the delta values is 0.06‰. According to the authors, the stack is an excellent paleoceanographic type section for the Pliocene-Pleistocene, and accurately reflects changes in global climate. Figure 2 shows a spliced section of the resulting stack between 4.0 and 2.7 Ma that, again, falls short of showing any significant $\delta^{18}O$ decrease around 3 Ma. Figure 3 is a simple sketch of the differences between these numbers and the value at 0 ka. The areas where these differences are positive, negative or neutral are highlighted, and further emphasize the lack of significant higher $\delta^{18}O$ values at 3 Ma.

Other related studies also fail to support a global mid-Pliocene temperature increase around 3 Ma. Lear et al., (2003), used a multiproxy approach that included paleothermometry to assess relative timing of emergence of the Panamá isthmus, changes in Atlantic circulation, global cooling and ice sheet growth. They failed to perceive any indication of warming during the Pliocene, and instead suggest continuous cooling by ~ 3.5 °C from 5 Ma to today. Additionally, substantial ice cap reduction in the Southern Hemisphere, an important endorsement to global warmth during the mid-Pliocene, is questioned by evidence that rejects extensive post-Miocene melting (e.g., Kennett and Hodell, 1995- for a review on this controversy see Miller and Mabin, 1988). Even a small retreat of Antarctica ice sheet would produce large amounts of IRD that are simply absent at this time (Joseph et al., 2002). Lastly, the proposed 2x elevation in mid-Pliocene CO_2 invoked as a cause for warmth has been challenged using $\delta^{13}C$ of marine organic carbon (Raymo and Rau, 1992; Raymo et al., 1996) and stomata density of fossil leaves (Burgh et al., 1993; Kurschner et al., 1996), both of which find maximum Pliocene CO_2 concentration only 35% above pre-industrial levels. These two very different proxies call into question the 2 x CO_2 PAL scenario, and suggest that further exploration of mid-Pliocene conditions is warranted.

In summary, while the beginning and end of the Pliocene are reasonably well understood, the mid-Pliocene transition from generally warmer conditions into a glacial-

interglacial world clearly presents some ambiguities. Conflicting evidence calling for much warmer, slightly warmer, or measurably cooler conditions during same interval of time (see Figure 4) emphasizes the importance of continued work on this transition so as to better understand the workings of the climate system right before locking into glacial mode. Below, I outline proposed research to constrain mid-Pliocene climate change using multiple proxies in onshore and offshore sections of the central US Atlantic Coastal Plain. This region is particularly sensitive as it is influenced by meridional heat transport of the Atlantic Ocean western boundary current, a likely propeller of changes in the Northern Hemisphere during the Neogene. In addition, faunal data (discussed below) from this region lends support to claims for a mid-Pliocene warm interval. The oxygen isotopic signature and independent temperature estimates are, however, lacking. These should clarify climate characteristics in this region during the mid-Pliocene, and help understand its repercussions in the North Atlantic region.

Western North Atlantic Ocean data sources

Offshore

ODP site 603 (35° N, 70° W) on the upper continental rise off Cape Hatteras, had the goal of sampling a complete Jurassic to present section that would provide a detailed record of all sedimentary processes associated to the opening of the Atlantic Ocean. Full penetration and coring was not achieved in site 603. Yet hole 603C, drilled in 4643 m of water, recovered a remarkably complete Pliocene to present section, unparalleled by any of the many neighboring sites. The length of sediments cored (366 m) consists of an almost continuous 115-m-thick, mid-Pliocene hemipelagic claystone. Judging from the available photographs and comments contained in the Initial Reports volume, these sediments are basically undisturbed. The location of the site away from the slope, and the available seismic profiles showing numerous, well-defined, and continuous reflectors, suggest this section is not structurally repeated.

Position and nature of its Pliocene section, makes this site an ideal target for

isotopic studies at 3 Ma. Figure 5 shows site 603 along with surface currents and other important features of the modern north Atlantic. Existing oceanographic mechanisms in the North Atlantic started operating after the initiation of the Central American Seaway closure, between 4 – 3 Ma (e.g., Raymo et al., 1992; Burton et al., 1997), although there is record of North Atlantic Deep Water (NADP) formation since the Miocene (e.g., Roth et al., 2000). Temperature and speed of the western boundary current (i.e., Gulfstream) along with NADW production, directly relate to climate change (Raymo et al., 1996; Driscoll and Haug, 1998). Variations in the isotopic composition of foraminiferal calcite recovered from areas affected by surface and deep currents in the North Atlantic can be the result of larger climatic changes. 603C sediments and forams are important in assessing the extent and prominence of a warm spell during the mid-Pliocene.

Foraminifera recovered in 603C core catchers (fraction > 177 μm) are mostly planktonic with a few calcareous benthic, moderately well preserved, (van Hinte et al., 1987). Preservation worsens with increasing depth, particularly below core 27 (latest early Pliocene). Poore (1991), in his census of cores 2-19 (fraction >149 μm), indicates that forams were subject to severe dissolution based on etching of tests, presence of fragments, and high abundance of benthic forms (i.e., planktonic to benthic ratios vary from 4 to 49 in mid-Pliocene cores included in his study). Genera *Globigerinoides sp*. and *Globigerina sp*. make up close to half the planktonic present in cores 10, and 14-19. Information on abundance and diversity may not be completely reliable due to potential dissolution, although the most abundant species are also some of the most susceptible to dissolution, for example, *G. ruber* and *G. sacculifer* (e.g., Coulbourn et al., 1980). Isotopic signature in well-preserved specimens, however, should not offer major problems. Detailed isotopic studies of this collection were never carried out.

Ganssen (1987) analyzed 14 samples of well-preserved *Globigerinoides obliquus* within this interval. His profile shows an increase in oxygen isotopic composition in 2 steps (see Figure 6). From about 3.7 to 3.5 Ma, and again around 3 Ma. Few samples

were used in this preliminary study. Interpretation based on isotopic signature changes gathered from such a small amount of data should be considered tentative at best. This figure also includes the result of bulk sediment analyses of 33 samples from cores 10 to 27 carried out to construct a better preliminary picture of the isotopic signature expected from a more detailed sampling. Most values between 2.9 and 3.9 Ma, cluster around 0.2 - 0.8 ‰. Two noticeable jumps of about 2 ‰ occur close to 3.19 and ~3 Ma to the maximum and minimum values of the profile respectively (i.e., 2.5 and –1.3 ‰). Since it is difficult to tell these variations represent actual changes in the isotopic composition of the microfauna or changes in the proportion of the sediment components, two additional data sets are included in this figure to try to establish such correlation. The first is the planktonic to benthic ratio in the available cores analyzed by Poore (1991), which gives an indication of dissolution changes. The second is the reported abundance of calcareous nannoplankton through the entire interval based on the analysis of 38 smear slides (van Hinte et al., 1987). Coccoliths comprise a large fraction of the samples and may be introducing a surface temperature bias in the isotopic signature. No consistent variation is observed between the isotope profiles and either one of these data. Even though the samples used to produce the different curves in this figure are not exactly the same, they provide an adequate picture of the components general behavior. We can argue the $\delta^{18}O$ minimum at ~ 3 Ma may represent a real isotopic shift susceptible to interpretation in terms of changing environmental conditions. This peak reinforces a minimum in the published planktonic data, not the case at ~3.2 Ma. Toning down the shortfalls of lacking a better dissolution estimate, these very coarse preliminary numbers are encouraging and hints potential in the proposed study.

Onshore

Pliocene units outcrop along the North American east coast, from Florida to New Jersey. These well-studied, open marine and richly fossiliferous deposits mainly representing sea-level high stands, are particularly appropriate to evaluate Pliocene

paleoenvironmental and paleoceanographic conditions along the western Atlantic. Marine units include the Pinecrest Beds of the Tamiami Formation in Florida, the Duplin and Raysor Formations in Georgia, North Carolina and South Carolina, and the Yorktown and Chowan River Formation in North Carolina and Virginia, among others. Some units, especially in Florida, are characterized by near-shore facies more susceptible to the influence of local extreme conditions. The Plio-Pleistocene units outcropping in the Carolinas and Virginia largely conform a series of overlapping depositional wedges, thinning to the West. They filled adjacent basins divided by tectonic highs that were covered by thin sediment veneers only during maximum transgressions (e.g., Ward et al., 1991).

Figure 7 shows a generalized stratigraphic correlation for the mid-Atlantic coastal plain along with their approximate outcrop areas in Virginia, North Carolina and South Carolina. The figure includes only marine units more appropriate for assessing a representative mid-Pliocene climate through paleoenvironmental studies. Florida mid-Pliocene units, with facies indicative of near-shore environments and potentially reflecting extreme saline and temperature conditions are excluded, and will not be dealt with any further. The correlation table is modified from the sea level changes and climate fluctuations figure published by Ward et al., (1991), based on planktonic foraminifer zones, radiometric determinations, and coast migration assessment resolved against global sea-level and oxygen isotope curves from deep-sea cores. The map is based on the extent of the units published by the same authors. Although not precise, ages are reasonably well constrained.

Qualitative studies based on the biogeographic distribution of different faunal groups present in these units (e.g., Hazel, 1971; Ward and Blackwelder, 1980; Gibson, 1983; Snyder et al., 1983; Hazel, 1988; Snyder et al., 2001), as well as quantitative estimates based on factor analytical transfer functions in ostracods and foraminifera (e.g., Cronin and Dowsett, 1990; Dowsett and Wiggs, 1992) have provided insight into the

environmental conditions on the mid-Atlantic coast during the Pliocene. Results of these studies are discussed below and summarized in Figure 8.

Hazel (1988), given the strong correlation of ostracoda with temperature, used distributional data of species and temperature on the modern Atlantic shelf to determine marine paleoclimates during the deposition of Pliocene and early Pleistocene units in Virginia and North Carolina. Results indicate that the Yorktown Formation was deposited in a warm temperate to subtropical marine climate, with summer highs increasing up in section. Hazel considers the closure of the Panamá isthmus and subsequent intensification of the Gulf Stream to be the cause of the Yorktown warming trend. Temperatures for the overlying Chowan River Formation are suggested to be even higher.

Cronin and Dowsett (1990) applied an ostracod transfer function to samples recovered from Pliocene units along the east coast from ~27 to ~38° N. They concluded marine Pliocene inner-shelf climates between 35-38° N were significantly warmer than today during both summer and winter. Between 33-35° N, marine climates were some 3 to 4 degrees warmer than to the North in summer, but about the same in winter, with thermal gradients less steep than today. Finally, between 27-28° N, summer and winter temperature were both about 2 degrees warmer than between 33-35° N. Marine climate for the Pliocene along the east coast is described as subtropical.

Cronin (1991), as part of the PRISM project, developed and applied another ostracod transfer function to several stratigraphic sections from Panamá to Iceland, getting basically the same numeric results than those obtained by Cronin and Dowsett (1990) for the mid-Atlantic section. From 3.5 to 3.0 Ma, a stronger Gulf Stream and North Atlantic Drift may have influenced the North Atlantic and the Arctic too. He concludes that meridional temperature gradients were less steep during the mid-Pliocene than today or the Pleistocene. Tropical and subtropical shelf waters were as warm as or cooler than today with outer shelf waters slightly cooler probably due to upwelling. The shelf area north of Cape Hatteras was affected by warm water.

Dowsett and Wiggs (1992) studied planktonic foraminifera of the Yorktown Formation in Virginia. The most common specimen is Globigerina bulloides, abundant today in the North Atlantic (mean surface water temperatures of 5-15 °C and salinities between 34 and 35 psu). Based on its presence others have suggested the unit was deposited in cool waters (Snyder et al., 1983; Gibson, 1983). Dowsett and Wiggs argue that the common occurrence of Globigerinoides and Neogloboquadrina (warm-low salinity species) in the upper members of the Yorktown Formation suggests mean temperatures greater than 20 °C. The oldest Sunken Meadow Member may represent cooler conditions although only one sample of this unit was analyzed. Applying a planktonic foraminifer transfer function developed for the North Atlantic (Dowsett and Poore, 1990; Dowsett, 1991) to the Yorktown assemblage, they suggest SST 3 to 5 °C warmer than today during winter, with summer temperatures unchanged. These estimates are in agreement with the results Dowsett and Poore (1991) obtained for Hole 603 off shore Cape Hatteras. The temperature estimates indicate reduced seasonality, probably due to northward migration of the sub-tropical gyre.

Snyder et al., (2001) sampled benthic foraminifera in Pliocene sections of North Carolina and conclude there is no unique indication of increasing depth or temperature. The nature of the studied assemblages and the notorious lack of resistant warm benthic forms do not support warmer temperatures in this section. Paleoenvironment and paleobathymety are consistent with other faunal groups, but not so paleotemperatures. Nonetheless, the authors conclude that there is not sufficient evidence to challenge other Pliocene mid-latitudinal higher temperature estimates, and presume that localized conditions might have overprinted the larger climatic signal, although paleogeographic reconstructions for the units studied (see for example Ward et al., 1991 and Petuch, 2004) position the sampling area some 50 km off-shore.

Krantz (1990) used young scallop isotope profiles to produce paleotemperature estimates. For the Yorktown Formation he interprets marine climate varying from mild

and warm temperate to marginally subtropical. The author considers the mollusk isotope data confirms an apparent warming through the Chowan River Formation to subtropical marine climate as proposed by Hazel (1971) based on ostracoda biostratigraphy, but finds no evidence of extremely high temperatures. Krantz's paleotemperature estimates for James City Formation diverge significantly from previous estimates probably due to alteration or partial records. The author concludes all temperature estimates, with the exception of James City and the upper section of the Chowan River Formation, are in excellent agreement with estimates based on ostracods assemblages.

Summarizing the above observations, mollusk and ostracod faunal assemblages of the Yorktown Formation indicate open marine and warm-temperate conditions with bottom water temperatures between 14 and 22 °C (Ward and Blackwelder, 1980; Hazel, 1988; Cronin and Dowsett, 1990). Transfer functions developed for the Western Atlantic suggest winter SST of 3 to 5 degrees warmer than, and summer temperatures comparable to, modern values. Scallop isotope profiles, although interpreted as warm temperate marine climate, invariably suggest winter temperatures bellow 10 °C, inconsistent with this classification. The most abundant species of planktonic foraminifera, *Globigerina bulloides*, is a temperate surface water dweller, and recent assessment of benthic forms does not support an increase in temperature through the Yorktown section.

The differences in interpreted temperature ranges through faunal studies warrant the use of oxygen isotopes to further substantiate these results.

Proposed research

The preceding sections show a number of problems with mid-Pliocene climate interpretations, namely: 1) inherent limitations of paleoecological studies (Poag, 1981) widely used to suggest increased warmth during the mid-Pliocene; 2) incomplete isotopic data available to corroborate or contradict the interpreted warmth; 3) lack of independent temperature estimates for Atlantic Coastal Plain marine units; 4) disagreement drawn from detailed deep-sea benthic and planktonic isotopic profiles previously explained,

and 5) lack of definite support for mid-Pliocene global warmth from greenhouse gases concentration and ice-sheet melting.

I intend to improve and diversify the proxy record in the Atlantic Coastal Plain to better understand climate in this sensitive area shortly before the initiation of Northern Hemisphere Glaciations. I plan to generate isotopic and relevant elemental data from the same marine units that produced the faunal assemblages suggestive of prominent warmth at ~3 Ma, and from additional correlative deeper deposits. The goal is to discern to the largest possible extent the composition and temperature signals in the carbonate isotopic signature, through Mg paelothermometry and the use of other non-paleoecological evidence. These results, negotiated with the former faunal interpretations will serve to assess (1) mid-latitude marine climates off-shore and in the shelf based on temperature and seasonality estimates, (2) nature of the western boundary current at the time based on the referred temperature estimates, and shallow and deep water column contrasts, and (3) regional character of the mid-Pliocene climate based on the new evidence and interpretations. This approach will enrich substantially the available data, and will help resolve standing discrepancies. Finally, the production of a high-resolution isotopic profile in mid-latitudes may become an additional resource to further explore potential response to orbital parameters or other periodic forcing.

Objectives

The proposed research has the following direct goals:

1) using the continuous mid-Pliocene high recovery section of the DSDP Leg 93, Hole 603C, located 434 Km east of Cape Hatteras:

1.1) produce a high-resolution planktonic and possibly benthic oxygen-carbon isotope profiles from cores 14 to 27;

1.2) Mg/Ca ratio from appropriate benthic foraminifera if available;

1.3) analyze and explain the high-resolution profiles in terms of local oceanographic characteristics, and how these concern regional water mass dynamics,

2) using Atlantic Coastal Plain marine units deposited between 4 and 3 Ma ago that outcrop in Virginia, North Carolina and South Carolina:

2.1) produce oxygen and carbon isotope profiles of appropriate benthic and planktonic foraminifera from outcrop and core samples;

2.2) generate an independent temperature record using Mg/Ca ratios in ostracods and possibly benthic foraminifera;

2.3) produce high-resolution bivalve isotope profiles across intervals of increased change to characterize shelf marine climates through seasonality assessment;

2.4) analyze the general and detailed profiles, and interpret them in terms of local marine climate. Relate these results to previous estimates of temperature and seasonality based on faunal assemblages. Assess differences and/or similarities and their consequence for regional climate interpretations.

Once offshore and onshore data has been independently analyzed, I intend to distill the former results into a basic picture of ocean climate and circulation for a restricted latitudinal band during the mid-Pliocene. Environmental changes in preparation to the onset of Northern hemisphere glaciations, although not clear, are surely present in the Atlantic at this time. Both records will extend for no more than 1 Ma, facilitating correlation between the two areas. The goal is to:

1) discriminate the contributing factors to the local signals on the basis of my previous results, and additional constrains imposed by regional, non-paleoecological models (e.g., Bintanja et al., 2005);

2) establish the degree of covariance between residual benthic and planktonic profiles within, and across study areas and what it means for global conditions;

3) reflect on agreements and discrepancies between faunal data and isotope profiles, and what it means in terms of proxy use, and local vs. regional scope in climatic interpretations.

4) finally, integrate all previous results and analyses to conclude on mid-Pliocene

climate warmth.

A critical issue that needs to be addressed for this last stage is the accuracy of age determinations and, in consequence, of the proposed correlation. Isotope based correlation is a possibility, although some of the independence in the interpretation is lost to the assumption of instantaneous correlative isotopic changes. Other sources of error affecting all the stages of the project, and potential problems with the data, as well as their impact on subsequent interpretations, will be continually discussed.

General plan of work

Sample acquisition:

DSDP- Site 603, Hole C

Drilled 434 Km east of Cape Hatteras in 4643 m of water, includes a nearly complete high sedimentation rate section of the Pliocene. Cores 14 to 27 comprise about 1.2 Ma (from ~4.0 to ~2.8 Ma). This interval goes from 106.8 m to 241.2 m, a total of approximately 134.4 m, with an average sedimentation rate of one centimeter per century (10.4 cm/10^3 years, Canninga et al., 1987). These cores will be the main target to produce a preliminary intermediate-resolution isotope profile using a sampling density of 1 per section for a total of 89 samples.

I intend to resample the critical interval around 3 Ma at a higher resolution of 7 samples per section, approximately one every 20 cm. The higher resolution profile will include 3 to 4 cores, a total of 126 to 168 samples each representing about 2000 years of sedimentation.

Species

Planktonic foraminifera will include the ones in the preliminary studies, abundant in Poore (1991), and likely to produce good and informative isotopic records. *Globigerinoides rubber* (pink) (d'Orbigny) and *Globigerinoides sacculifer* (Brady) should provide the highest possible temperature estimates, since both species are reported to record summer temperatures (*G. rubber* has shown to have a constant fractionation that

can be accounted for). *Globigerina bulloides* (d'Orbigny) has been reported to variably deviate from equilibrium, but may help discern productivity patterns. It is also one of the species identified in mid-Pliocene Coastal Plain units, and may prove helpful during the final stages of the research. *Globigerinoides obliquus* (Bolli) was used by Ganssen (1987) and will also be a target. Benthic are about 10 times less abundant than planktonic, and are not identified. *Uvigerina sp*., should be a target, probably present in 603C, since is also found in site 604.

Mid-Atlantic coastal plain units

There are many paleontological studies based on mid-Pliocene foraminifera of the central coastal plain of North America, in particular from the Yorktown Formation. Many of these samples should be available through appropriately directed requests. These would include collections of planktonic and benthic foraminifera, ostracods and bivalves. The collaboration with USGS experts, extensively familiar with the biogeographic studies and the area's stratigraphy, will be of great benefit in the acquisition of samples from these units. Field collection can be organized if collections turn out to be unavailable or material should appear insufficient. Figure 9 shows some of the localities used in previous publications along with the approximate outcropping limits of the Yorktown members, Duplin and Raysor Formations. Additionally Ward and Blackwelder (1990) provide 91 Yorktown localities with reference to USGS 7 ½ min quadrants.

Species

Published faunal charts and plates of the microfaunal content of the Yorktown formation suggests we should focus on the following taxa:

Planktonic. Globigerina bulloides (d'Orbigny), Neogloboquadrina acostaensis (Blow), *N. humerosa* (Takayanagi and Saito).

Benthic. Uvigerina spp., Cibicides sp.

Ostracods. Loxoconcha spp.

Bivalves. Spisula sp., Mercenaria sp.

Paleothermometry studies have usually been applied to deep-water forms of ostracods (e.g., *Krithe spp*.). However, some work has been done on *Loxoconcha*, a marine/estuarine genus common in the Yorktown sediments. These can be used to experiment with an independent paleotemperature signal.

Selected bivalve genera are known to produce high-quality seasonal records.

Procedures

Some samples may need a complete routine micropaleontologic preparation (i.e. disaggregate, wet sieve for appropriate fractions, dry, and hand-pick) to obtain the target specimens. Presumably, there will be samples requiring only the final steps.

Appropriate inspection and cleaning protocols should be applied to the selected foraminifera and ostracods to avoid contamination from sediment or secondary calcite. Same care will be taken before sectioning and sampling the bivalves. If fitting, XRD and SEM analyses will be considered in diagenetic altered or contaminated suspects.

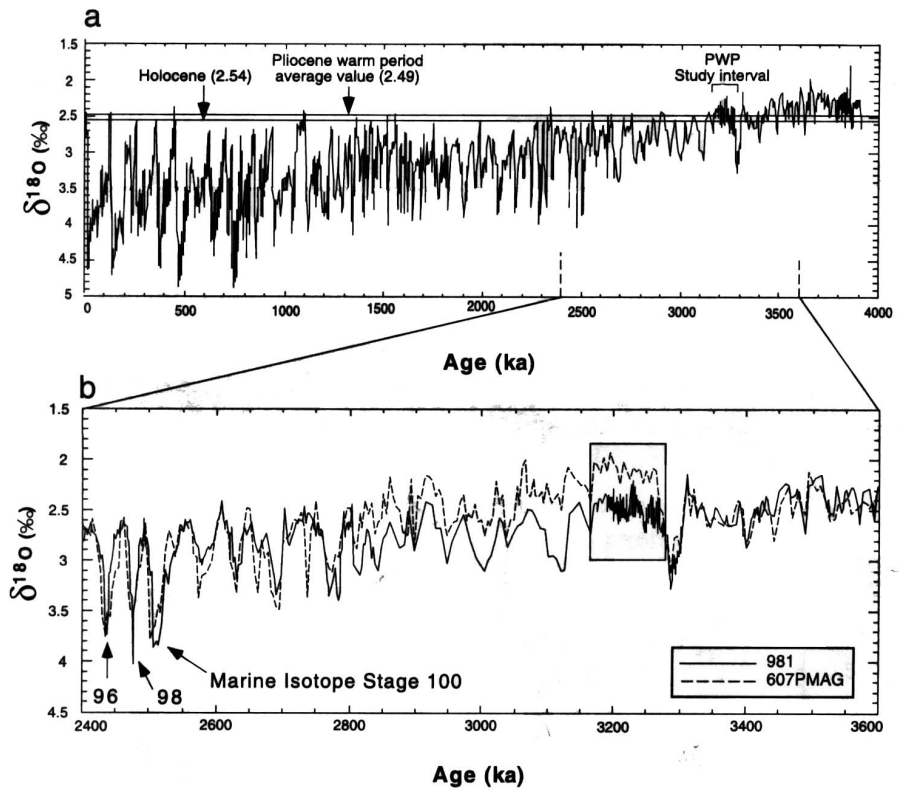

Figure 1

Profile taken from Draut et al., 2003. The upper panel shows the composite *C. wuellerstorfi* profile from sites 980 and 981. Horizontal lines show the average values for the Holocene and the mid-Pliocene section studied by these authors, which is detailed in the panel below. The difference between these two averages is 0.5‰. Lower values are observed only before 3.2 Ma.

In the lower panel, a similar profile obtained for site 607 is superimposed to the 981 profile where, again, $\delta^{18}O$ increases after 3.2 Ma. In site 607 profile, however, a noticeable average change occurs at ~ 3.28 Ma.

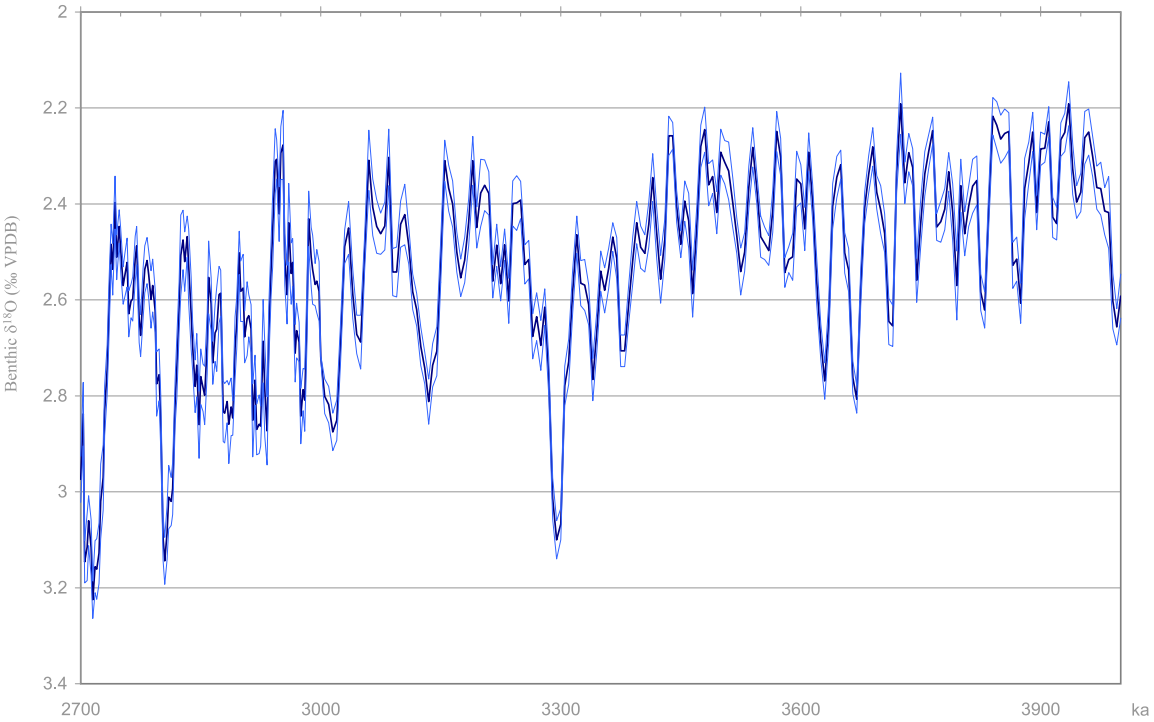

Figure 2

LR04 benthic $\delta^{18}O$ stack by Lisiecki and Raymo (2005) provides a good summary of the deep-ocean signal for the past 5.3 Ma. This figure ties together 2 sections with differing resolutions. From 2.7 to 3 Ma the interval size is 2.5 ka, and the mean number of data points per interval is 16.5. From 3 to 4 Ma, the interval size is 5 ka with an average of 15.5 points per interval. The construction of the stack is graphic and in consequence, independent of time. The age model applied by the authors is based on a simple ice volume model and considering sedimentation rate of the individual 57 cores used as changes in the average linear sedimentation rate are minimized.nthic $\delta^{18}O$ stack by Lisiecki and Raymo (2005) provides a good summary of the deep-ocean signal for the past 5.3 Ma. This figure ties together 2 sections with differing resolutions. From 2.7 to 3 Ma the interval size is 2.5 ka, and the mean number of data points per interval is 16.5. From 3 to 4 Ma, the interval size is 5 ka with an average of 15.5 points per interval. The construction of the stack is graphic and in consequence, independent of time. The age model applied by the authors is based on a simple ice volume model and considering sedimentation rate of the individual 57 cores used LR04 benthic $\delta^{18}O$ stack by Lisiecki and Raymo (2005) provides a good summary of the deep-ocean signal for the past 5.3 Ma. This figure ties together 2 sections with differing resolutions. From 2.7 to 3 Ma the interval size is 2.5 ka, and the mean number of data points per interval is 16.5. From

3 to 4 Ma, the interval size is 5 ka with an average of 15.5 points per interval. The construction of the stack is graphic and in consequence, independent of time. The age model applied by the authors is based on a simple ice volume model and considering sedimentation rate of the individual 57 cores used as changes in the average linear sedimentation rate are minimized.

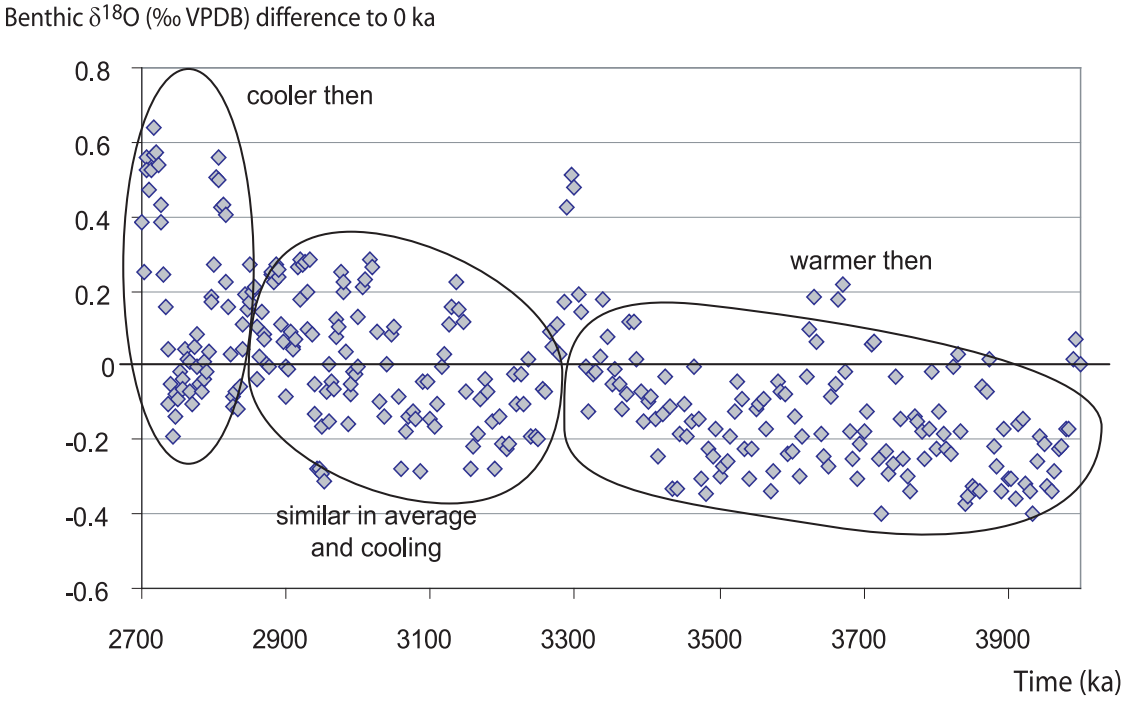

Figure 3
Benthic $\delta^{18}O$ differences to modern value for the section of the stack represented in part a (i.e., at time 0 ka). Three areas are distinguished through visual inspection of point density with respect to the reference value. From 4 to about 3.3 Ma isotopic signature is in general heavier. Points are approximately equally distributed above and below modern composition around 3 Ma but showing an overall cooling tendency. Around 2.7 Ma, most points are above zero, indicating in general a heavier isotopic signature at the time.

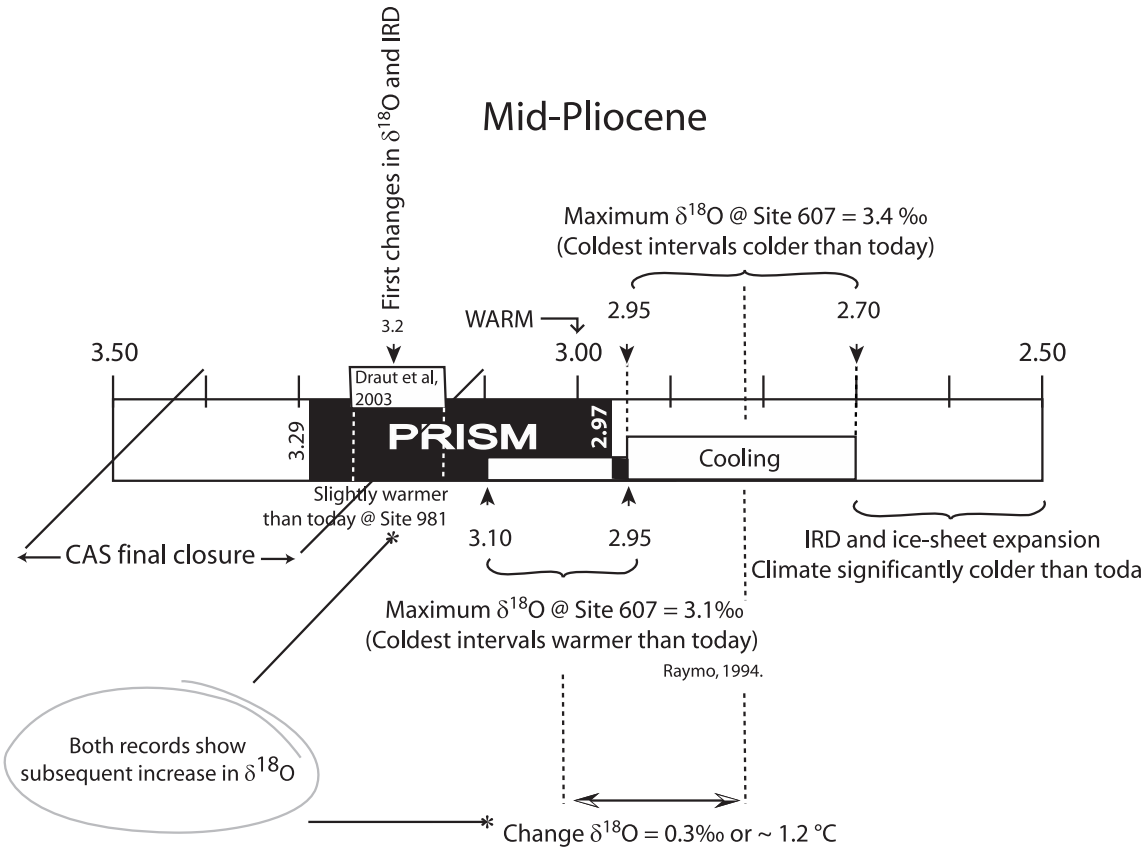

Figure 4

Mid-Pliocene climate outline including time span and main climate related result conveyed by the studies referred in the text. Deep-water temperature change suggested by the difference in $\delta^{18}O$ averages between the interval 3.10 - 2.95 Ma and 2.95 - 2.70 Ma, were calculated using the relation derive by Eres and Luz (1983) from benthic foraminifera.

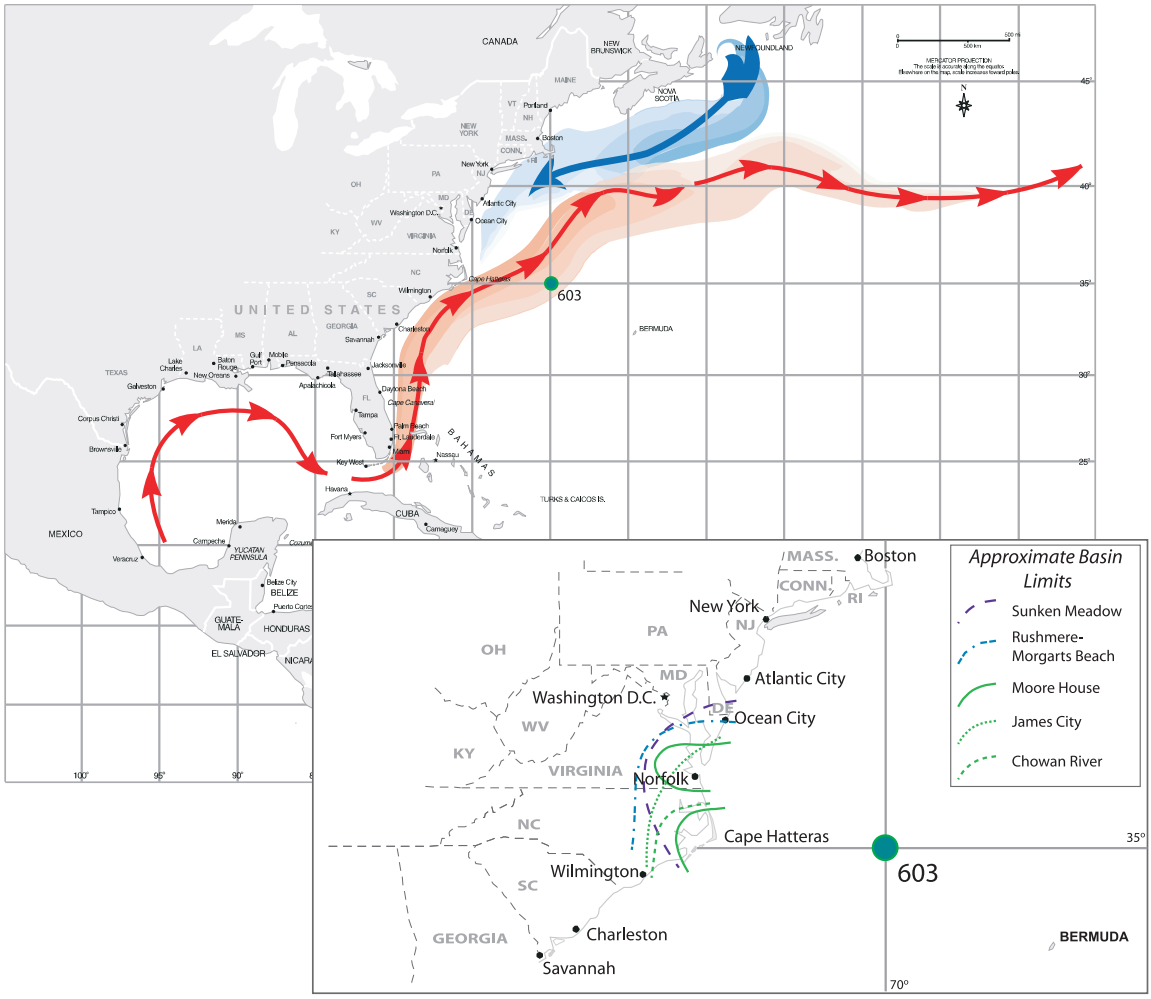

Figure 5

Map showing the eastern North Atlantic Ocean, main surface and deep currents affecting the area today, and location of DSDP site 603. The inset shows the approximate location of some of the Pliocene-Pleistocene basins after Krantz (1990).

Figure 6
Site 603C $\delta^{18}O$ profiles. The planktonic data is from Ganssen (1987).
The upper section includes data from Globigerinoides ruber (triangles - 4 samples recovered from cores 10, 11, 14, and 15). The rest of the points were measured on Globigerinoides obliquus (diamonds - cores 11, 13-18, and 20-27). The second profile (squares) is the isotopic composition of bulk sediment samples from cores 10 to 27, with the exception of core 12 (no recovery). The shadowed section approximately encloses the PRISM time frame. On the right axis an approximate time scale has been obtained by extrapolating using available sample ages. The histogram in the upper right section of the diagram represents planktonic to benthic ratios available only for the uppermost section of the graph (from Poore, 1991). The continuous line shows the volume percent of calcareous nannoplankton from 38 smear slides analyses (van Hinte et al., 1987), and the broken line the percent of CaCO3 . See text for discussion.

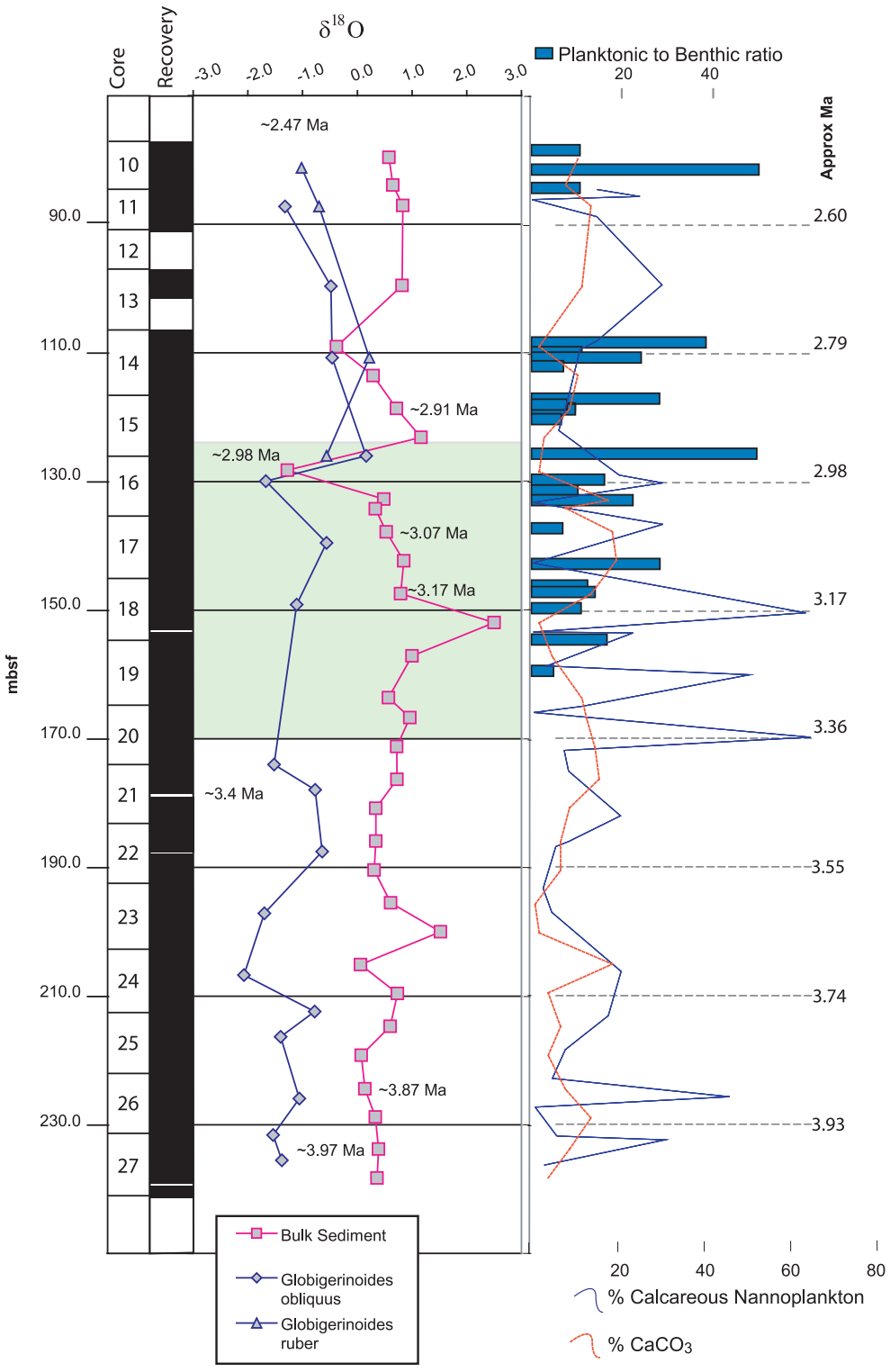
Core
Recovery
δ18O
-3.0
-2.0
-1.0
0.0
1.0
2.0
3.0
Planktonic to Benthic ratio
20
40
Approx Ma
mbsf
90.0
110.0
130.0
150.0
170.0
190.0
210.0
230.0
10
11
12
13
14
15
16
17
18
19
20
21
22
23
24
25
26
27
~2.47 Ma
~2.91 Ma
~2.98 Ma
~3.07 Ma
~3.17 Ma
~3.4 Ma
~3.87 Ma
~3.97 Ma
2.60
2.79
2.98
3.17
3.36
3.55
3.74
3.93
Bulk Sediment
Globigerinoides obliquus
Globigerinoides ruber
20
40
60
80
% Calcareous Nannoplankton
% CaCO3

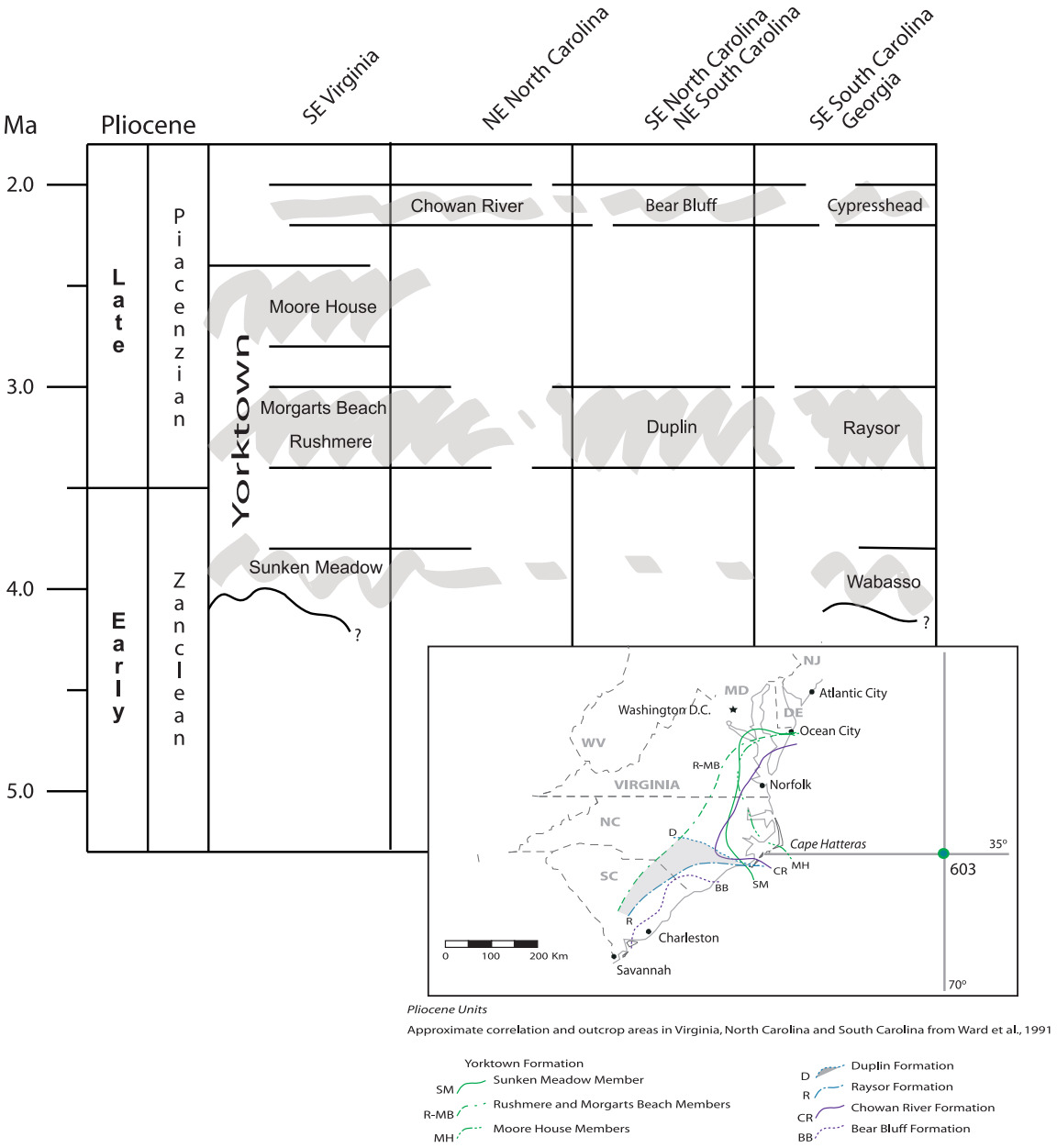

Figure 7

Generalized stratigraphic correlation of mid-Atlantic marine units during the Pliocene and approximate outcrop areas. In the inset only relevant units to the paleoclimatic interpretations have been included. Based on the correlation and maps published by Ward et al., (1991).

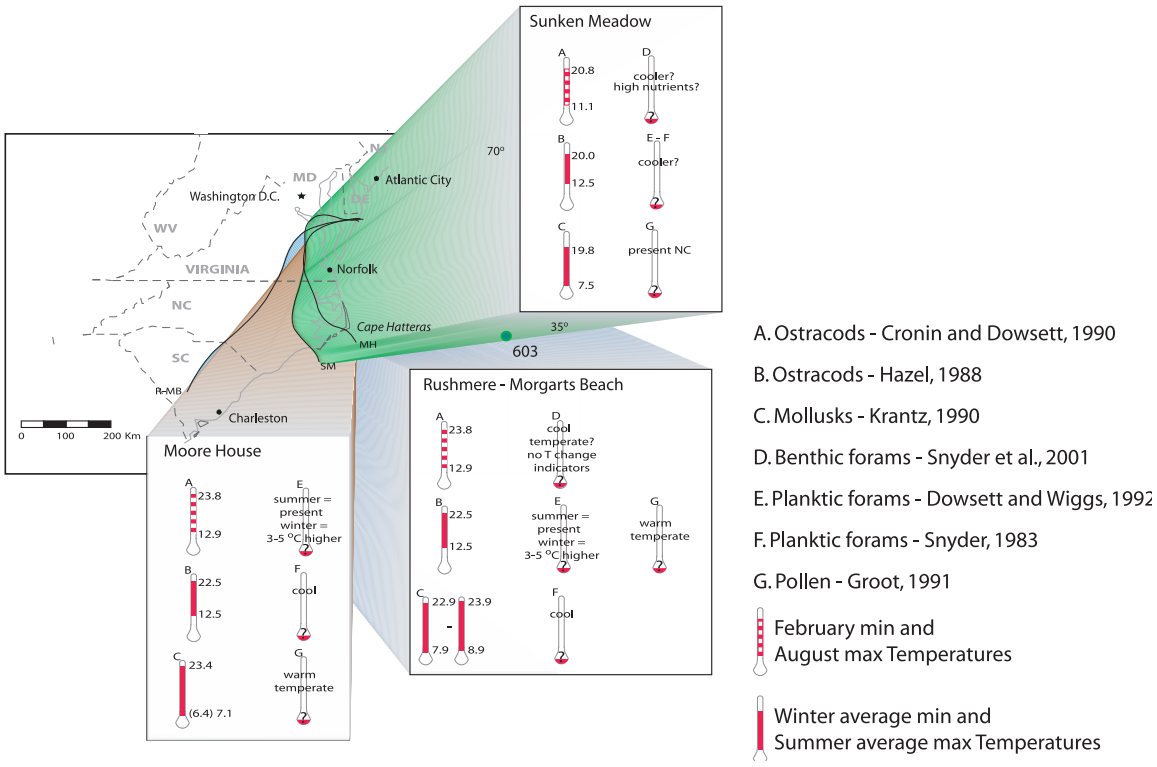

Figure 8

Paleoenvironmental interpretations and outcrop extension of the Yorktown Formation members. Sea water temperature estimates are shown for each member and in association with their correspondent outcrop areas after Ward et al. (1991). Temperatures represent averages or max/min as indicated. Units are presented in chronological order clockwise from the top. Modern average sst for the adjacent area is 10.11 ^{o}C in February, and 25.93 ^{o}C in August (Reynolds and Smith, 1995).

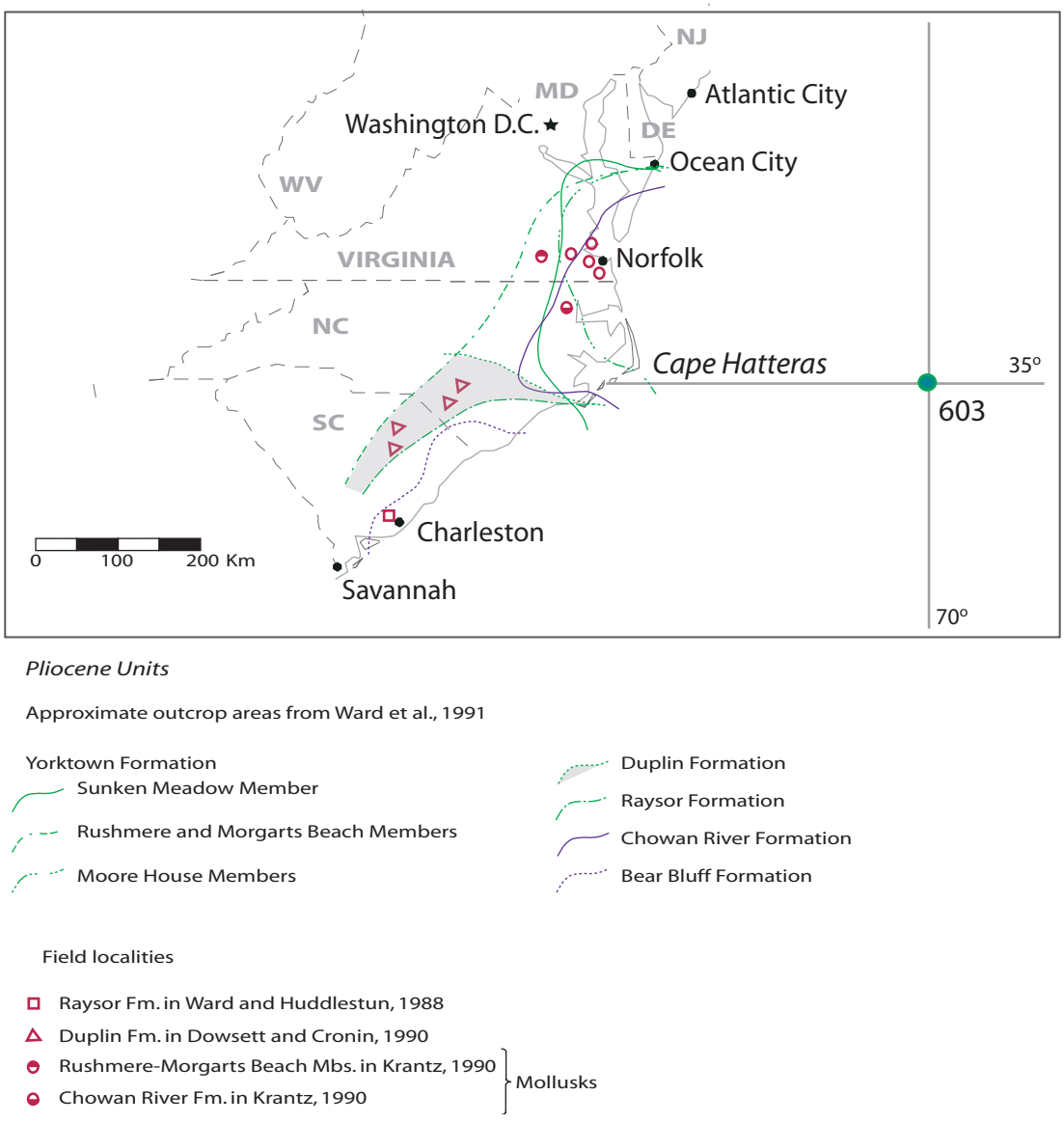

Figure 9

Location of sample sites from sources discussed in the text. In addition, there are 91 sample sites described and located in Ward and Blackwelder (1990).

References

Alley, R. B., S. Anandakrishnan, et al. (2001). "Stochastic resonance in the North Atlantic." Paleoceanography **16**(2): 190-198.

Augustin, L., C. Barbante, et al. (2004). "Eight glacial cycles from an Antarctic ice core." Nature **429**(6992): 623-628.

Barnola, J. M., D. Raynaud, et al. (1987). "Vostok ice core provides 160,000-year record of atmospheric CO (sub 2)." Nature (London) **329**(6138): 408-414.

Barron, J. A., T. M. Cronin, et al. (1996). Middle Pliocene paleoenvironments of the Northern Hemisphere; Paleoclimate and evolution, with emphasis on human origins. Symposium on Paleoclimate and evolution, Airlie, VA, United States (USA), Yale University Press, New Haven, CT, United States (USA).

Berggren, W. A., D. V. Kent, et al. (1995). "A revised Cenozoic geochronology and chronostratigraphy." Special Publication - SEPM (Society for Sedimentary Geology) **54**: 129-212.

Bintanja, R., R. S. W. van de Wal, et al. (2005). "Modelled atmospheric temperatures and global sea levels over the past million years." **437**(7055): 125-128.

Budyko, M. I. (1982). "The Earth's climate; past and future." International Geophysics Series **29**: 309.

Burgh, J. V. D., H. Visscher, et al. (1993). "Paleoatmospheric Signatures in Neogene Fossil Leaves." Science **260**(5115): 1788-1790.

Burton, K. W., L. Hongfei, et al. (1997). "Closure of the Central American Isthmus and its effect on deep-water formation in the North Atlantic." Nature (London) **386**(6623): 382-385.

Canninga, G., J. D. A. Zijderveld, et al. (1987). "Late Cenozoic magnetostratigraphy of deep Sea Drilling Project Hole 603C, Leg 93, on the North American continental rise off Cape Hatteras." Initial reports of the Deep Sea Drilling Project covering Leg 93 of the cruises of the drilling vessel Glomar Challenger, Norfolk, Virginia, to Norfolk, Virginia, May-June, 1983 **93**(1-2): 839-848.

Coates, A. G., J. B. C. Jackson, et al. (1992). "Closure of the Isthmus of Panama; the near-shore marine record of Costa Rica and western Panama." Geological Society of America Bulletin **104**(7): 814-828.

Coulbourn, W. T., F. L. Parker, et al. (1980). "Faunal and solution patterns of planktonic foraminifera in surface sediments of the North Pacific." Marine Micropaleontology **5**(4): 329-399.

Cronin, T. M. (1991). "Pliocene shallow water paleoceanography of the North Atlantic Ocean based on marine ostracodes; Pliocene climates." American Geophysical Union, 1990 spring meeting, Baltimore, MD, United States, May 29-June 1, 1990 Quaternary Science Reviews **10**(2-3): 175-188.

Cronin, T. M. and H. J. Dowsett (1990). "A quantitative micropaleontologic method for shallow marine paleoclimatology; application to Pliocene deposits of the western North Atlantic Ocean." Marine Micropaleontology **16**(1-2): 117-147.

Crowley, T. J. (1991). "Modeling pliocene warmth." Quaternary Science Reviews **10**(2-3): 275-282.

Crowley, T. J. and R. A. Berner (2001). "CO (sub 2) and climate change." Science **292**(5518): 870-872.
Dowsett, H., J. Barron, et al. (1996). "Middle Pliocene sea surface temperatures: a global reconstruction." Marine Micropaleontology **27**(1-4): 13-25.
Dowsett, H., R. Thompson, et al. (1994). "Joint investigations of the Middle Pliocene climate I: PRISM paleoenvironmental reconstructions." Global and Planetary Change **9**(3-4): 169-195.
Dowsett, H. J. (1991). "The development of a long-range foraminifer transfer function and application to the late Pleistocene North Atlantic climatic extremes." Paleoceanography **6**(2): 259-273.
Dowsett, H. J. (2004). Bracketing Mid-Pliocene Sea Surface Temperature: Maximum and Minimum Possible Warming. Data series (Geological Survey (U.S.)) ; 114. U. S. G. Survey. Reston, Va. : U.S. Geological Survey, 2004. **2004**.
Dowsett, H. J., J. A. Barron, et al. (1999). Middle Pliocene paleoenvironmental reconstruction; PRISM2. United States (USA). **OF 99-0535**.
Dowsett, H. J. and T. M. Cronin (1990). "High eustatic sea level during the middle Pliocene; evidence from the Southeastern U.S. Atlantic Coastal Plain; with Suppl. Data 90-13." Geology (Boulder) **18**(5): 435-438.
Dowsett, H. J. and R. Z. Poore (1990). "A new planktic foraminifer transfer function for estimating Pliocene-Holocene paleoceanographic conditions in the North Atlantic." Marine Micropaleontology **16**(1-2): 1-23.
Dowsett, H. J. and R. Z. Poore (1991). "Pliocene sea surface temperatures of the North Atlantic Ocean at 3.0 Ma; Pliocene climates." American Geophysical Union, 1990 spring meeting, Baltimore, MD, United States, May 29-June 1, 1990 Quaternary Science Reviews **10**(2-3): 189-204.
Dowsett, H. J. and L. B. Wiggs (1992). "Planktonic foraminiferal assemblage of the Yorktown Formation, Virginia, USA." Micropaleontology **38**(1): 75-86.
Draut, A. E., M. E. Raymo, et al. (2003). "Climate stability during the Pliocene warm period." Paleoceanography **18**(4): 1078.
Driscoll, N. W. and G. H. Haug (1998). "A Short Circuit in Thermohaline Circulation: A Cause for Northern Hemisphere Glaciation?" Science **282**(5388): 436-438.
Emiliani, C. (1955). "Pleistocene temperatures." Journal of Geology **63**(6): 538-578.
Erez, J. and B. Luz (1983). "Experimental paleotemperature equation for planktonic foraminifera." Geochimica et Cosmochimica Acta **47**(6): 1025-1031.
Ganssen, G. (1987). "Late Cenozoic stable isotopic stratigraphy, Deep Sea Drilling Project sites 603 and 604, Northeast American continental rise." Initial reports of the Deep Sea Drilling Project covering Leg 93 of the cruises of the drilling vessel Glomar Challenger, Norfolk, Virginia, to Norfolk, Virginia, May-June, 1983 **93**(1-2): 997-1002.
Gibson, T. G. (1983). "Key foraminifera from upper Oligocene to lower Pleistocene strata of the central Atlantic Coastal Plain; Geology and paleontology of the Lee Creek Mine, North Carolina; I." Smithsonian Contributions to Paleobiology **53**: 355-453.
Goodwin, D. H., B. R. Schoene, et al. (2003). "Resolution and fidelity of oxygen isotopes as paleotemperature proxies in bivalve mollusk shells; models and observations."

Palaios **18**(2): 110-125.
Haq, B. U., J. Hardenbol, et al. (1987). "Chronology of fluctuating sea levels since the Triassic." Science **235**(4793): 1156-1167.
Hay, W. W., E. Soeding, et al. (2002). "The late Cenozoic uplift; climate change paradox." International Journal of Earth Sciences **91**(5): 746-774.
Hazel, J. E. (1971). Ostracode biostratigraphy of the Yorktown Formation (upper Miocene and lower Pliocene) of Virginia and North Carolina. United States (USA), U. S. Geological Survey, Reston, VA, United States (USA). **P 0704 U. S. Geological Survey Professional Paper:** 13.
Hazel, J. E. (1988). Determining late Neogene and Quaternary palaeoclimates and palaeotemperature regimes using ostracods. Ostracoda in the earth sciences. P. De Deckker, J.-P. Colin and J.-P. Peypouquet. Netherlands (NLD), Elsevier, Amsterdam, Netherlands (NLD).
Ivany, L. C., B. H. Wilkinson, et al. (2003). "Using stable isotopic data to resolve rate and duration of growth throughout ontogeny; an example from the surf clam, Spisula solidissima." Palaios **18**(2): 126-137.
Ivany, L. C., B. H. Wilkinson, et al. (2004). "INTRA-ANNUAL ISOTOPIC VARIATION IN VENERICARDIA BIVALVES: IMPLICATIONS FOR EARLY EOCENE TEMPERATURE, SEASONALITY, AND SALINITY ON THE U.S. GULF COAST." Journal of Sedimentary Research **74**(1): 7-19.
Jones, D. S. and I. R. Quitmyer (1996). "Marking time with bivalve shells; oxygen isotopes and season of annual increment formation; Skeletal records of ecologic change." Palaios **11**(4): 340-346.
Jones, D. S., D. F. Williams, et al. (1983). "Combined stable isotope-growth increment sclerochronology in modern and fossil bivalve molluscs; The Geological Society of America, 96th annual meeting." The Geological Society of America, 96th annual meeting, Indianapolis, IN, United States, Oct. 31-Nov. 3, 1983 Abstracts with Programs - Geological Society of America **15**(6): 605.
Joseph, L. H., D. K. Rea, et al. (2002). "Antarctic environmental variability since the late Miocene: ODP Site 745, the East Kerguelen sediment drift." Earth and Planetary Science Letters **201**(1): 127-142.
Kennett, J. P. and D. A. Hodell (1995). "Stability or instability of Antarctic ice sheets during warm climates of the Pliocene?" GSA Today **5**(1): 1-13, 22.
Krantz, D. E. (1990). "Mollusk-isotope records of Plio-Pleistocene marine paleoclimate, U. S. Middle Atlantic Coastal Plain." Palaios **5**(4): 317-335.
Kurschner, W. M., J. Van der Burgh, et al. (1996). "Oak leaves as biosensors of late Neogene and early Pleistocene paleoatmospheric CO (sub 2) concentrations; Climates and climate variability of the Pliocene." Marine Micropaleontology **27**(1-4): 299-312.
Lear, C. H., Y. Rosenthal, et al. (2003). "The closing of a seaway; ocean water masses and global climate change." Earth and Planetary Science Letters **210**(3-4): 425-436.
Lisiecki, L. E. and M. E. Raymo (2005). "A Pliocene-Pleistocene stack of 57 globally distributed benthic d18O records." Palaeogeography **20**: PA 1003.
Lynas, M. (2004). "Warning from a warming world - Mark Lynas gives an account of

his three-year journey across five continents in search of evidence of the effects of global warming." the Royal Geographical Society magazine (May 2004) 51 (5 pages).
Maslin, M., D. Sedov, et al. (2001). Synthesis of the nature and causes of rapid climate transitions during the Quaternary. The Oceans and Rapid Climate Change: past, present, and future. A. G. Union. **126**.
Miller, M. F. p. and M. C. G. p. Mabin (1998). "Antarctic Neogene landscapes; in the refrigerator or in the deep freeze?" GSA Today **8**(4): 1-8.
Mix, A. C. (1987). The oxygen-isotope record of glaciation. North America and adjacent oceans during the last deglaciation. W. F. Ruddiman and H. E. Wright, Jr. United States (USA), Geol. Soc. Am., Boulder, CO, United States (USA).
Oerlemans, J. (2004). "Correcting the Cenozoic delta (super 18) O deep-sea temperature record for Antarctic ice volume." Palaeogeography, Palaeoclimatology, Palaeoecology **208**(3-4): 195-205.
Parrish, J. T. (1998). Interpreting Pre-Quaternary Climate from the Geologic Record. New York, Columbia University Press.
Petit, J. R., J. Jouzel, et al. (1999). "Climate and atmospheric history of the past 420,000 years from the Vostok ice core, Antarctica." Nature (London) **399**(6735): 429-436.
Petuch, E. J. (2004). Cenozoic seas: the view from eastern North America. Boca Raton, CRC Press.
Poag, C. W. (1981). Ecologic atlas of benthic foraminifera of the Gulf of Mexico. United States (USA), Mar. Sci. Int., Woods Hole, MA, United States (USA).
Poore, R. Z. and L. C. Sloan (1996). "Introduction Climates and Climate Variability of the Pliocene." Marine Micropaleontology **27**(1-4): 1-2.
Prell, W. L. (1984). "Covariance patterns of foraminiferal delta (super 18) O; an evaluation of Pliocene ice volume changes near 3.2 million years ago." Science **226**(4675): 692-694.
Raymo, M. E. (1994). "The initiation of Northern Hemisphere glaciation." Annual Review of Earth and Planetary Sciences **22**: 353-383.
Raymo, M. E., B. Grant, et al. (1996). "Mid-Pliocene warmth; stronger greenhouse and stronger conveyor." Marine Micropaleontology **27**(1-4): 313-326.
Raymo, M. E., B. Grant, et al. (1996). "Mid-Pliocene warmth; stronger greenhouse and stronger conveyor; Climates and climate variability of the Pliocene." Marine Micropaleontology **27**(1-4): 313-326.
Raymo, M. E., D. Hodell, et al. (1992). "Response of deep ocean circulation to initiation of Northern Hemisphere glaciation (3-2 Ma)." Paleoceanography **7**(5): 645-672.
Raymo, M. E. and G. Rau (1992). "Plio-Pleistocene atmospheric CO (sub 2) levels inferred from POM delta (super 13) C at DSDP Site 607; AGU 1992 fall meeting [modified]." American Geophysical Union 1992 fall meeting, San Francisco, CA, United States, Dec. 7-11, 1992
EOS, Transactions, American Geophysical Union **73**(43): 95-96.
Roth, J. M., A. W. Droxler, et al. (2000). "The Caribbean carbonate crash at the middle to late Miocene transition; linkage to the establishment of the modern global ocean conveyor; Proceedings of the Ocean Drilling Program, scientific results, Caribbean Ocean history and the Cretaceous/Tertiary boundary event; covering

Leg 165 of the cruises of the drilling vessel JOIDES Resolution, Miami, Florida, to San Juan Puerto Rico, sites 998-1002, 19 December 1995-17 February 1996." Proceedings of the Ocean Drilling Program, Scientific Results **165**: 249-273.

Savin, S. M. (1977). "The history of the Earth's surface temperature during the past 100 million years." Annual Review of Earth and Planetary Sciences **5**: 319-355.

Shackleton, N. (1967). "Oxygen isotope analyses and pleistocene temperatures re-assessed." Nature (London) **215**(5096): 15-17.

Shackleton, N. J. (1976). "Oxygen isotope evidence relating to the end of the last interglacial at the substage 5e to 5d transition about 115,000 years ago." Abstracts with Programs - Geological Society of America **8**(6): 1099-1100.

Shackleton, N. J. (2000). "The 100,000-year ice-age cycle identified and found to lag temperature, carbon dioxide, and orbital eccentricity." Science **289**(5486): 1897-1902.

Shackleton, N. J., J. Blackman, et al. (1984). "Oxygen isotope calibration of the onset of ice-rafting and history of glaciation in the North Atlantic region." Nature (London) **307**(5952): 620-623.

Snyder, S. W., L. L. Mauger, et al. (1983). "Planktonic foraminifera and biostratigraphy of the Yorktown Formation, Lee Creek Mine; Geology and paleontology of the Lee Creek Mine, North Carolina; I." Smithsonian Contributions to Paleobiology **53**: 455-481.

Snyder, S. W., L. L. Mauger, et al. (2001). "Benthic Foraminifera and paleoecology of the Pliocene Yorktown and Chowan River formations, Lee Creek Mine, North Carolina, USA." Journal of Foraminiferal Research **31**(3): 244-274.

Thompson, R. S. and R. F. Fleming (1996). "Middle Pliocene vegetation; reconstructions, paleoclimatic inferences, and boundary conditions for climate modeling; Climates and climate variability of the Pliocene." Marine Micropaleontology **27**(1-4): 27-49.

van Hinte, J. E., S. W. Wise, Jr., et al. (1987). "Site 603." Initial reports of the Deep Sea Drilling Project covering Leg 93 of the cruises of the drilling vessel Glomar Challenger, Norfolk, Virginia, to Norfolk, Virginia, May-June, 1983 **93**(1-2): 25-276.

Veizer, J., Y. Godderis, et al. (2000). "Evidence for decoupling of atmospheric CO2 and global climate during the Phanerozoic eon." Nature **408**(6813): 698-701.

Ward, L. W., R. H. Bailey, et al. (1991). Pliocene and early Pleistocene stratigraphy, depositional history, and molluscan paleobiogeography of the coastal plain. The geology of the Carolinas; Carolina Geological Society fiftieth anniversary volume. J. W. Horton, Jr and V. A. Zullo. United States (USA), Univ. Tenn. Press, Knoxville, TN, United States (USA).

Ward, L. W. and B. W. Blackwelder (1980). Stratigraphic revision of upper Miocene and lower Pliocene beds of the Chesapeake Group, middle Atlantic Coastal Plain. United States (USA), U. S. Geological Survey, Reston, VA, United States (USA). **B 1482-D. U. S. Geological Survey Bulletin:** D1-D61.

Webb, P. N., D. M. Harwood, et al. (1984). "Cenozoic marine sedimentation and ice-volume variation on the East Antarctic Craton." Geology (Boulder) **12**(5): 287-291.

Willard, D. A., T. M. Cronin, et al. (1993). "Terrestrial and marine records of climatic and environmental changes during the Pliocene in subtropical Florida." Geology **21**(8): 679-682.

Zachos, J., M. Pagani, et al. (2001). "Trends, rhythms, and aberrations in global climate 65 Ma to present; Paleoclimate; Earth's variable climatic past." Science **292**(5517): 686-693.

Zubakov, V. A. and I. I. Borzenkova (1988). "Pliocene palaeoclimates: Past climates as possible analogues of mid-twenty-first century climate." Palaeogeography, Palaeoclimatology, Palaeoecology **65**(1-2): 35-49.

Appendix 2 - Stable Isotope Data

ID	ID	min.	Sample	DATE	TIME	line/#	δ13C (KIS)	±	δ18O (KIS)	±	δ13C (VPDB)	δ18O (VPDB)	Max P	Error? (!)	Comments
Fmth-02-Ech	spn-1-1	HMg cc	1-G81	4/12/03	13:12:10	A / 3	4.15	0.00	2.52	0.03	**0.36**	**-1.84**	670		Primary spine proximal (including base, milled ring and collar)
Fmth-02-Ech	spn-1-2	HMg cc	2-G81	4/12/03	13:43:04	B / 3	5.23	0.01	2.81	0.01	**1.46**	**-1.51**	526		Primary spine medial shaft - cortex
Fmth-02-Ech	spn-2-1a	HMg cc	4-G81	4/12/03	14:47:00	B / 4	2.18	0.02	1.57	0.04	**-1.60**	**-2.75**	242		Primary spine base
Fmth-02-Ech	spn-2-1b	HMg cc	5-G81	4/12/03	15:21:04	A / 5	5.00	0.01	3.19	0.04	**1.21**	**-1.17**	703		Primary spine collar
Fmth-02-Ech	spn-2-2	HMg cc	6-G81	4/12/03	15:52:19	B / 5	5.28	0.02	2.98	0.01	**1.52**	**-1.34**	721		Primary spine medial shaft - cortex
Fmth-02-Ech	spn-2-3	HMg cc	7-G81	4/12/03	16:23:05	A / 6	4.26	0.01	2.30	0.03	**0.46**	**-2.06**	325		Primary spine distal shaft -- cortex
Fmth-02-Ech	spn-3-1	HMg cc	8-G81	4/12/03	16:57:15	B / 6	5.10	0.03	2.81	0.04	**1.33**	**-1.51**	1203		Primary spine collar
Fmth-02-Ech	spn-3-2	HMg cc	9-G81	4/12/03	17:28:34	A / 7	5.23	0.02	2.66	0.04	**1.44**	**-1.70**	773		Primary spine medial shaft -- cortex
Fmth-02-Ech	spn-3-3	HMg cc	10-G81	4/12/03	18:00:56	B / 7	4.80	0.01	2.42	0.02	**1.03**	**-1.90**	495		Primary spine distal shaft -- cortex
Fmth-02-Ech	A-tth-1	HMg cc	11-G81	4/12/03	18:35:29	A / 8	2.09	0.01	1.61	0.03	**-1.71**	**-2.74**	1169		Pyramid -- Ribbed surface
Fmth-02-Ech	A-tth-2	HMg cc	12-G81	4/12/03	19:08:28	B / 8	2.26	0.02	1.47	0.04	**-1.52**	**-2.85**	237		Pyramid -- Wall parallel to ribbed surface
Fmth-02-Ech	B-tth-3	HMg cc	13-G81	4/12/03	19:40:57	A / 9	2.71	0.01	2.13	0.03	**-1.10**	**-2.22**	799		Pyramid -- Lower section
Fmth-02-Ech	C-tth-1	HMg cc	14-G81	4/12/03	20:14:23	B / 9	2.31	0.02	1.62	0.01	**-1.47**	**-2.70**	893		Pyramid -- Ribbed surface
Fmth-02-Ech	C-tth-2	HMg cc	15-G81	4/12/03	20:44:57	A / 10	2.35	0.01	1.27	0.02	**-1.45**	**-3.08**	355		Pyramid -- Parallel wall
Fmth-02-Ech	C-tth-3a	HMg cc	16-G81	4/12/03	21:20:10	B / 10	2.55	0.02	1.95	0.02	**-1.24**	**-2.37**	452		Pyramid -- Around groove in the lower section
Fmth-02-Ech	C-tth-3b	HMg cc	17-G81	4/12/03	21:56:11	A / 11	3.08	0.02	2.13	0.04	**-0.72**	**-2.22**	275		Pyramid -- Very tip on the lower section
Fmth-02-Ech	bdy-1	HMg cc	18-G81	4/12/03	22:30:53	B / 11	1.70	0.01	2.15	0.05	**-2.08**	**-2.17**	1573	!	Auricles -- perignathic girdle (lowermost pieces (3))
Fmth-02-Ech	bdy-2	HMg cc	19-G81	4/12/03	23:02:41	A / 12	1.56	0.03	2.02	0.02	**-2.24**	**-2.34**	628		Ambulacral area low -- poriferous zone
Fmth-02-Ech	bdy-3	HMg cc	20-G81	4/12/03	23:37:52	B / 12	2.97	0.01	2.17	0.01	**-0.81**	**-2.15**	453		Ambulacral area middle -- poriferous zone
Fmth-02-Ech	bdy-4	HMg cc	21-G81	4/13/03	0:24:27	A / 14	3.24	0.02	2.19	0.03	**-0.56**	**-2.16**	761		Ambulacral area high -- poriferous zone
Fmth-02-Ech	bdy-5	HMg cc	22-G81	4/13/03	11:38:41	B / 14	2.53	0.01	1.57	0.02	**-1.25**	**-2.75**	361		Ambulacral area low -- interporiferous zone
Fmth-02-Ech	bdy-6	HMg cc	23-G81	4/22/03	10:05:58	B / 22	3.35	0.01	1.60	0.03	**-0.43**	**-2.73**	418		Ambulacral area middle -- interporiferous zone
Fmth-02-Ech	bdy-7	HMg cc	24-G81	4/13/03	12:46:27	B / 15	4.25	0.01	2.01	0.02	**0.48**	**-2.31**	348		Ambulacral area high -- interporiferous zone
Fmth-02-Ech	bdy-11	HMg cc	28-G81	4/15/03	11:47:28	B / 11	3.31	0.01	1.19	0.02	**-0.47**	**-3.13**	398		Mamelon in middle interambulacral plate
Fmth-02-Ech	bdy-12	HMg cc	30-G81	4/15/03	11:13:44	A / 13	3.98	0.01	1.23	0.04	**0.18**	**-3.12**	297		Mamelon in higher interambulacral plate
Fmth-02-Ech	bdy-10	HMg cc	27-G81	4/14/03	18:59:37	B / 8	2.55	0.03	1.27	0.07	**-1.23**	**-3.05**	167	!	Mamelon in lower interambulacral plate
Fmth-02-Ech	bdy-11a	HMg cc	29-G81	4/13/03	11:03:59	A / 18	3.84	0.03	1.76	0.05	**0.04**	**-2.60**	658		Previous middle interambulacral plate -- base of plate (boss)
Fmth-02-Ech	bdy-8	HMg cc	25-G81	4/14/03	19:33:49	A / 9	2.28	0.01	1.80	0.04	**-1.52**	**-2.56**	296		Interambulacral plate
Fmth-02-Ech	bdy-13	HMg cc	31-G81	4/13/03	12:13:36	A / 19	3.03	0.02	1.99	0.05	**-0.77**	**-2.36**	774		Posterior genital plate
Fmth-02-Ech	bdy-9	HMg cc	26-G81	4/13/03	13:52:12	B / 16	3.28	0.02	2.12	0.05	**-0.50**	**-2.20**	598		Interambulacral plate
Fmth-02-Alg	1	HMg cc	32-G81	4/14/03	14:37:51	A / 5	5.51	0.02	2.93	0.03	**1.72**	**-1.42**	1159		
Fmth-02-Alg	2	HMg cc	33-G81	4/13/03	13:22:36	A / 20	5.01	0.01	2.71	0.02	**1.22**	**-1.65**	939		
Fmth-02-Alg	3	HMg cc	34-G81	4/14/03	15:30:27	B / 5	5.16	0.03	2.54	0.04	**1.39**	**-1.79**	730		
Fmth-02-Alg	4	HMg cc	35-G81	4/13/03	14:26:25	A / 21	4.66	0.02	2.90	0.03	**0.87**	**-1.45**	1749	!	Right before dark band
Fmth-02-Alg	5	HMg cc	36-G81	4/14/03	16:02:02	A / 6	5.03	0.02	2.15	0.01	**1.24**	**-2.21**	1889	!	
Fmth-02-Alg	6	HMg cc	37-G81	4/14/03	18:25:44	A / 8	5.10	0.01	2.58	0.05	**1.31**	**-1.78**	1819	!	
Fmth-02-Alg	7	HMg cc	38-G81	4/14/03	16:40:36	B / 6	4.88	0.01	2.84	0.04	**1.11**	**-1.49**	567		
Fmth-02-Alg	8	HMg cc	39-G81	4/14/03	17:50:06	B / 7	5.04	0.02	3.38	0.03	**1.27**	**-0.94**	732		
Fmth-02-Alg	9	HMg cc	40-G81	4/14/03	17:14:26	A / 7	5.34	0.01	2.86	0.01	**1.55**	**-1.50**	1999	!	
Fmth-02-Ech	spn-1-3	HMg cc	3-G81	4/12/03	14:14:17	A / 4	2.11	0.11	-3.24	0.19	**-1.69**	**-7.59**	115	!	Primary spine distal shaft -- cortex (mostly glue - small)

ID	ID	min.	Sample	DATE	TIME	line/#	δ13C (KIS)	±	δ18O (KIS)	±	δ13C (VPDB)	δ18O (VPDB)	Max P	Error? (!)	Comments
Fmth-02-Crl	1-1	arag	1-G54	5/4/03	13:22:45	A / 3	-1.30	0.01	0.71	0.02	**-5.12**	**-3.64**	373		For samples 1-24, the amount of CaCO3 may be as small as 1/3. A lot of epoxy.
Fmth-02-Crl	1-2	arag	2-G54	5/4/03	13:54:25	B / 3	2.39	0.02	2.38	0.05	**-1.39**	**-1.95**	241		
Fmth-02-Crl	1-3	arag	3-G54	5/4/03	14:25:30	A / 4	3.41	0.02	2.76	0.01	**-0.39**	**-1.60**	279		
Fmth-02-Crl	1-4	arag	4-G54	5/4/03	14:58:37	B / 4	3.89	0.01	2.74	0.02	**0.12**	**-1.58**	387		
Fmth-02-Crl	2-1	arag	5-G54	5/4/03	15:31:44	A / 5	2.25	0.02	2.07	0.08	**-1.55**	**-2.28**	250	!	
Fmth-02-Crl	2-3	arag	7-G54	5/4/03	16:35:07	A / 6	1.48	0.01	1.50	0.02	**-2.33**	**-2.85**	1019		Pieces
Fmth-02-Crl	3-1	arag	8-G54	5/4/03	17:07:45	B / 6	1.79	0.02	1.73	0.06	**-2.00**	**-2.59**	202	!	
Fmth-02-Crl	3-2	arag	9-G54	5/4/03	17:41:20	A / 7	1.12	0.03	1.50	0.12	**-2.69**	**-2.85**	217	!	
Fmth-02-Crl	3-4	arag	11-G54	5/15/03	16:38:21	B / 7	2.36	0.02	2.29	0.05	**-1.42**	**-2.03**	262		
Fmth-02-Crl	4-1	arag	12-G54	5/15/03	11:32:18	A / 3	1.82	0.02	1.82	0.05	**-1.99**	**-2.54**	203	!	
Fmth-02-Crl	4-2	arag	13-G54	5/14/03	8:20:15	B / 7	0.06	0.02	1.23	0.03	**-3.73**	**-3.09**	322		
Fmth-02-Crl	4-2	arag	13-G54	5/15/03	16:05:44	A / 8	0.83	0.01	1.53	0.03	**-2.98**	**-2.82**	473		
Fmth-02-Crl	4-3	arag	14-G54	5/15/03	12:05:06	B / 3	3.17	0.03	2.76	0.04	**-0.61**	**-1.56**	229		
Fmth-02-Crl	4-4	arag	15-G54	5/15/03	18:07:16	B / 8	4.00	0.03	2.90	0.04	**0.23**	**-1.42**	271		
Fmth-02-Crl	4-4	arag	15-G54	5/14/03	9:52:30	A / 8	3.57	0.03	2.79	0.02	**-0.23**	**-1.57**	284		
Fmth-02-Crl	5-1	arag	16-G54	5/15/03	12:37:18	A / 4	0.11	0.02	1.48	0.02	**-3.70**	**-2.88**	939		
Fmth-02-Crl	5-2	arag	17-G54	5/15/03	17:34:33	A / 11	2.28	0.03	2.05	0.02	**-1.52**	**-2.31**	357		
Fmth-02-Crl	6-1	arag	19-G54	5/15/03	22:10:58	B / 11	0.71	0.02	1.69	0.03	**-3.08**	**-2.64**	611		
Fmth-02-Crl	6-3	arag	21-G54	5/14/03	10:25:32	B / 8	1.98	0.03	2.14	0.03	**-1.81**	**-2.18**	257		
Fmth-02-Srp	1	cc	22-G54	5/15/03	13:46:10	A / 5	-0.54	0.03	2.90	0.05	**-4.36**	**-1.45**	610		
Fmth-02-Srp	2	cc	23-G54	5/17/03	21:46:49	A / 14	-0.87	0.03	3.07	0.05	**-4.69**	**-1.29**	705		
Fmth-02-Srp	3	cc	24-G54	5/15/03	14:17:55	B / 5	1.99	0.01	2.73	0.02	**-1.79**	**-1.59**	500		
Fmth-02-Scllp	A3	cc	27-G54	5/22/03	7:30:40	B / 17	4.89	0.02	4.27	0.03	**1.12**	**-0.05**	390		
Fmth-02-Scllp	A5	cc	29-G54	5/16/03	1:01:55	B / 15	4.97	0.01	4.43	0.02	**1.20**	**0.11**	293		
Fmth-02-Scllp	A6	cc	30-G54	5/15/03	14:49:17	A / 6	4.74	0.02	3.54	0.04	**0.95**	**-0.82**	208		
Fmth-02-Scllp	B3	cc	33-G54	5/16/03	1:46:32	B / 16	5.23	0.02	6.36	0.03	**1.46**	**2.05**	321		
Fmth-02-Scllp	B4	cc	34-G54	5/15/03	15:21:57	B / 6	5.23	0.02	6.09	0.03	**1.46**	**1.78**	293		
Fmth-02-Scllp	B6	cc	36-G54	5/17/03	18:21:52	A / 10	4.64	0.04	3.33	0.08	**0.84**	**-1.03**	198	!	
Fmth-02-Scllp	B7	cc	37-G54	5/16/03	2:30:08	B / 17	4.60	0.02	2.74	0.03	**0.83**	**-1.58**	351		
Fmth-02-Scllp	B9	cc	39-G54	5/18/03	0:13:19	A / 18	4.46	0.02	2.41	0.03	**0.67**	**-1.95**	387		

ID	ID	min.	Sample	DATE	TIME	line/#	δ13C (KIS)	±	δ18O (KIS)	±	δ13C (VPDB)	δ18O (VPDB)	Max P	Error? (!)	Comments
Fmth-02-Sc-dt	1	cc	1-J2	6/16/03	13:04:33	A / 3	4.72	0.02	4.05	0.05	**0.92**	**-0.23**	701	!	Each sample is an individual growth band.
Fmth-02-Sc-dt	5	cc	5-J2	6/16/03	13:37:21	B / 3	4.64	0.01	3.42	0.02	**0.88**	**-0.85**	290		
Fmth-02-Sc-dt	10	cc	10-J2	6/16/03	14:11:08	A / 4	4.62	0.01	3.41	0.05	**0.82**	**-0.87**	506		
Fmth-02-Sc-dt	14	cc	14-J2	7/29/03	4:05:44	B / 15	4.62	0.00	3.48	0.02	**0.85**	**-0.79**	487		adjacent
Fmth-02-Sc-dt	20	cc	20-J2	6/16/03	15:18:19	A / 5	4.71	0.05	3.69	0.07	**0.90**	**-0.59**	629	!	
Fmth-02-Sc-dt	25	cc	25-J2	6/16/03	15:51:34	B / 5	4.57	0.01	3.17	0.05	**0.80**	**-1.10**	234	!	
Fmth-02-Sc-dt	30	cc	30-J2	6/16/03	16:25:18	A / 6	4.69	0.01	3.13	0.01	**0.88**	**-1.15**	271		
Fmth-02-Sc-dt	35	cc	35-J2	6/16/03	16:59:08	B / 6	4.57	0.01	3.09	0.03	**0.81**	**-1.18**	502		
Fmth-02-Sc-dt	40	cc	40-J2	6/16/03	17:32:47	A / 7	4.48	0.01	2.98	0.03	**0.67**	**-1.30**	285		Not very well developed. In some sections it looks like a part of 39
Fmth-02-Sc-dt	41	cc	1-G73	6/16/03	18:07:39	B / 7	4.54	0.02	2.94	0.01	**0.77**	**-1.33**	608		
Fmth-02-Sc-dt	45	cc	5-G73	6/16/03	18:44:15	A / 8	4.39	0.03	3.08	0.06	**0.58**	**-1.19**	581	!	
Fmth-02-Sc-dt	50	cc	10-G73	6/16/03	19:17:31	B / 8	4.20	0.01	2.60	0.03	**0.44**	**-1.67**	377		
Fmth-02-Sc-dt	55	cc	15-G73	6/16/03	19:52:35	A / 9	4.50	0.01	2.31	0.02	**0.69**	**-1.97**	423		
Fmth-02-Sc-dt	60	cc	20-G73	6/16/03	20:26:22	B / 9	4.46	0.02	2.17	0.01	**0.70**	**-2.09**	301		
Fmth-02-Sc-dt	65	cc	25-G73	6/16/03	21:00:58	A / 10	4.61	0.02	2.23	0.03	**0.80**	**-2.04**	217		Not well developed in some sections. Took it as a growth band anyway.
Fmth-02-Sc-dt	70	cc	30-G73	6/16/03	21:34:51	B / 10	4.44	0.02	1.89	0.02	**0.67**	**-2.38**	298		
Fmth-02-Sc-dt	75	cc	35-G73	6/16/03	22:09:17	A / 11	4.55	0.04	2.05	0.05	**0.74**	**-2.22**	220	!	
Fmth-02-Sc-dt	80	cc	40-G73	6/16/03	22:42:52	B / 11	4.60	0.01	2.51	0.04	**0.83**	**-1.75**	283		
Fmth-02-Sc-dt	81	cc	1-G84	6/16/03	23:17:39	A / 12	4.58	0.01	2.31	0.03	**0.77**	**-1.96**	280		
Fmth-02-Sc-dt	85	cc	5-G84	6/16/03	23:51:27	B / 12	4.65	0.01	2.51	0.01	**0.88**	**-1.76**	265		
Fmth-02-Sc-dt	90	cc	10-G84	6/17/03	1:42:30	A / 14	4.76	0.01	2.37	0.02	**0.96**	**-1.90**	437		And around here too
Fmth-02-Sc-dt	95	cc	15-G84	6/17/03	2:18:36	B / 14	4.76	0.01	2.26	0.05	**1.00**	**-2.01**	290	!	
Fmth-02-Sc-dt	100	cc	20-G84	6/17/03	2:56:41	A / 15	4.61	0.01	2.49	0.02	**0.80**	**-1.79**	252		
Fmth-02-Sc-dt	105	cc	25-G84	6/17/03	3:30:15	B / 15	4.73	0.01	2.83	0.02	**0.97**	**-1.44**	246		
Fmth-02-Sc-dt	109	cc	29-G84	7/29/03	2:18:31	A / 14	4.75	0.02	3.15	0.02	**0.94**	**-1.12**	248		adjacent
Fmth-02-Sc-dt	116 a	cc	36-G84	7/29/03	2:52:21	B / 14	4.73	0.01	3.72	0.02	**0.97**	**-0.55**	422		adjacent
Fmth-02-Sc-dt	118	cc	39-G84	7/29/03	3:32:10	A / 15	4.72	0.02	3.49	0.05	**0.91**	**-0.79**	231		adjacent
Fmth-02-Sc-dt	120	cc	1-G80	6/17/03	9:14:04	B / 17	4.84	0.04	4.40	0.02	**1.07**	**0.13**	197		probably okay despite low yield--I'd run an adjacent to check
Fmth-02-Sc-dt	125	cc	6-G80	7/28/03	22:55:12	A / 11	5.07	0.02	4.61	0.02	**1.27**	**0.33**	463		
Fmth-02-Sc-dt	129	cc	10-G80	6/17/03	10:25:31	B / 18	5.20	0.01	5.07	0.04	**1.43**	**0.80**	235		
Fmth-02-Sc-dt	134	cc	15-G80	6/17/03	11:01:39	A / 19	5.31	0.02	6.73	0.04	**1.51**	**2.44**	259		Right before the juvenile-adult break
Fmth-02-Sc-dt	140	cc	21-G80	7/28/03	23:28:28	B / 11	5.18	0.02	5.10	0.06	**1.41**	**0.83**	191	!	
Fmth-02-Sc-dt	144	cc	25-G80	6/17/03	12:13:32	A / 20	5.01	0.01	4.90	0.05	**1.21**	**0.62**	223	!	
Fmth-02-Sc-dt	149	cc	30-G80	6/17/03	12:49:22	B / 20	4.86	0.02	4.35	0.03	**1.10**	**0.08**	242		
Fmth-02-Sc-dt	153	cc	34-G80	7/29/03	0:01:16	A / 12	4.56	0.04	3.26	0.05	**0.75**	**-1.02**	168		

ID	ID	min.	Sample	DATE	TIME	line/#	δ13C (KIS)	±	δ18O (KIS)	±	δ13C (VPDB)	δ18O (VPDB)	Max P	Error? (!)	
Fmth-02-Mrc	1	arag	1-G81	7/19/03	18:30:38	B / 17	5.42	0.01	1.77	0.02	**1.65**	**-2.50**	497		Bottom clear (obvious) white
Fmth-02-Mrc	**2**	arag	2-G53	6/27/03	16:56:03	B / 3	4.49	0.04	2.03	0.02	**0.72**	**-2.24**	191		First clear dark line
Fmth-02-Mrc	3	arag	3-G53	6/27/03	17:28:46	A / 4	5.20	0.01	1.81	0.06	**1.40**	**-2.46**	206		White - no clear bands, in between dark
Fmth-02-Mrc	**4**	arag	4-G53	6/27/03	18:02:24	B / 4	4.81	0.02	1.96	0.03	**1.04**	**-2.31**	185		Second clear dark line
Fmth-02-Mrc	5	arag	5-G53	6/27/03	18:35:04	A / 5	5.19	0.03	2.82	0.07	**1.39**	**-1.45**	190		White - no clear bands
Fmth-02-Mrc	6	arag	2-G81	7/19/03	17:55:18	A / 18	5.32	0.02	2.88	0.02	**1.52**	**-1.40**	412		White
Fmth-02-Mrc	**7**	arag	7-G53	6/27/03	19:40:13	A / 6	4.40	0.02	4.22	0.11	**0.59**	**-0.06**	194		Third clear dark line
Fmth-02-Mrc	8	arag	8-G53	6/27/03	20:13:35	B / 6	4.77	0.05	4.32	0.06	**1.01**	**0.05**	176		White - no clear bands
Fmth-02-Mrc	9	arag	9-G53	6/27/03	20:46:09	A / 7	4.55	0.01	2.91	0.06	**0.74**	**-1.36**	230		White
Fmth-02-Mrc	10	arag	10-G53	6/27/03	21:19:18	B / 7	5.02	0.02	2.37	0.01	**1.26**	**-1.90**	194		White
Fmth-02-Mrc	**11**	arag	11-G53	6/27/03	21:51:34	A / 8	4.06	0.01	1.58	0.04	**0.24**	**-2.69**	245		Dark
Fmth-02-Mrc	12	arag	12-G53	6/27/03	22:24:38	B / 8	3.82	0.02	1.51	0.03	**0.06**	**-2.76**	260		White
Fmth-02-Mrc	**13**	arag	13-G53	6/27/03	22:57:15	A / 9	3.10	0.01	1.33	0.02	**-0.73**	**-2.94**	253		Dark
Fmth-02-Mrc	14	arag	14-G53	6/27/03	23:30:28	B / 9	4.68	0.02	2.36	0.03	**0.91**	**-1.91**	218		White
Fmth-02-Mrc	15	arag	15-G53	6/28/03	0:02:50	A / 10	4.47	0.04	3.29	0.03	**0.66**	**-0.99**	222		White
Fmth-02-Mrc	**16**	arag	16-G53	6/28/03	0:36:00	B / 10	3.26	0.03	4.22	0.08	**-0.50**	**-0.05**	169		Dark
Fmth-02-Mrc	17	arag	6-G81	7/19/03	20:18:04	A / 20	4.03	0.01	2.41	0.02	**0.22**	**-1.86**	492		White
Fmth-02-Mrc	18	arag	18-G53	6/28/03	1:42:45	B / 11	3.81	0.01	1.64	0.04	**0.05**	**-2.63**	251		White
Fmth-02-Mrc	**19**	arag	19-G53	6/28/03	2:15:59	A / 12	3.87	0.01	1.00	0.02	**0.06**	**-3.27**	308		Darker diffuse area
Fmth-02-Mrc	20	arag	20-G53	6/28/03	2:49:26	B / 12	3.67	0.03	1.46	0.02	**-0.09**	**-2.81**	271		White
Fmth-02-Mrc	21	arag	21-G53	6/28/03	4:29:39	A / 14	3.44	0.03	1.87	0.04	**-0.38**	**-2.40**	266		White
Fmth-02-Mrc	**22**	arag	22-G53	6/28/03	5:02:44	B / 14	1.88	0.03	2.96	0.02	**-1.88**	**-1.31**	263		Dark
Fmth-02-Mrc	23	arag	23-G53	6/28/03	5:42:03	A / 15	2.35	0.02	2.99	0.03	**-1.48**	**-1.29**	285		White
Fmth-02-Mrc	24	arag	24-G53	6/28/03	6:14:27	B / 15	2.81	0.01	-0.17	0.01	-0.95	-4.44	433		White
Fmth-02-Mrc	25	arag	25-G53	6/28/03	6:53:58	A / 16	2.35	0.02	2.02	0.02	-1.48	-2.26	338		White
Fmth-02-Mrc	30	arag	30-G53	6/28/03	7:26:51	B / 16	2.41	0.02	1.10	0.02	-1.35	-3.17	261		Dark area, banding visible. Darker as it goes further away. Taken ~100microns
Fmth-02-Mrc	35	arag	35-G53	6/28/03	8:01:12	A / 17	3.47	0.02	2.93	0.04	-0.34	-1.34	295		
Fmth-02-Mrc	**40**	arag	40-G53	6/28/03	8:33:48	B / 17	2.47	0.02	1.01	0.03	-1.29	-3.26	241		
Fmth-02-Mrc	**45**	arag	5-J1	6/28/03	9:07:36	A / 18	2.72	0.02	1.69	0.02	-1.11	-2.59	650		
Fmth-02-Mrc	48	arag	8-J1	6/28/03	9:39:37	B / 18	4.49	0.01	2.59	0.02	0.73	-1.68	291		White
Fmth-02-Mrc	**49**	arag	9-J1	6/28/03	10:23:39	A / 19	3.09	0.03	3.07	0.07	-0.73	-1.21	602		Begining dark
Fmth-02-Mrc	**50**	arag	10-J1	6/28/03	10:53:50	B / 19	3.45	0.02	1.03	0.03	-0.31	-3.24	298		Middle dark
Fmth-02-Mrc	51	arag	7-G81	7/19/03	22:04:34	B / 20	5.89	0.03	2.86	0.05	2.12	-1.41	608		
Fmth-02-Mrc	**52**	arag	12-J1	7/11/03	15:53:48	B / 4	2.82	0.02	2.31	0.04	-0.94	-1.96	270		Dark
Fmth-02-Mrc	*53*	arag	13-J1	6/28/03	12:31:30	A / 21	3.44	0.01	1.30	0.03	-0.38	-2.97	402		Dark
Fmth-02-Mrc	*54*	arag	14-J1	7/12/03	13:34:33	B / 8	2.07	0.02	0.70	0.02	-1.68	-3.57	384		Band white-dark
Fmth-02-Mrc	*55*	arag	15-J1	6/28/03	13:14:24	A / 22	2.96	0.01	1.86	0.03	-0.86	-2.42	294		Band white-dark
Fmth-02-Mrc	*56*	arag	16-J1	7/11/03	16:25:35	A / 5	3.76	0.02	1.12	0.04	-0.06	-3.15	543		Band white-dark
Fmth-02-Mrc	**57**	arag	17-J1	6/28/03	13:58:45	A / 23	0.38	0.01	1.47	0.01	-3.47	-2.80	341		Dark
Fmth-02-Mrc	58	arag	18-J1	7/12/03	15:12:40	A / 8	3.42	0.02	1.32	0.04	-0.40	-2.96	264		Light
Fmth-02-Mrc	**59**	arag	19-J1	7/11/03	16:58:30	B / 5	-0.09	0.01	1.73	0.04	-3.84	-2.54	338		Dark
Fmth-02-Mrc	60	arag	20-J1	7/12/03	16:18:27	A / 9	0.09	0.02	2.09	0.01	-3.76	-2.18	416		Light -very edge

ANDRILL core AND–2A pore water Sr isotope compositions

Depth (mbsf)	$^{87}Sr/^{86}Sr$	Error
9.70	0.70807	1.1×10^{-05}
30.12	0.70987	1.0×10^{-05}
37.44	0.70996	1.0×10^{-05}
43.75	0.71003	1.1×10^{-05}
51.33	0.71018	1.7×10^{-05}
57.24	0.71012	1.5×10^{-05}
73.18	0.71022	1.0×10^{-05}
81.06	0.71017	1.0×10^{-05}
93.00	0.71009	1.3×10^{-05}
116.25	0.71001	1.0×10^{-05}
155.79	0.70963	1.0×10^{-05}
235.71	0.70889	1.0×10^{-05}
336.23	0.70872	1.2×10^{-05}
353.58	0.70870	1.1×10^{-05}
545.06	0.70842	1.0×10^{-05}
619.4	0.70855	1.0×10^{-05}
779.74	0.70692	1.0×10^{-05}
809.89	0.70711	1.0×10^{-05}
963.49	0.70802	1.0×10^{-05}

Chapter 2

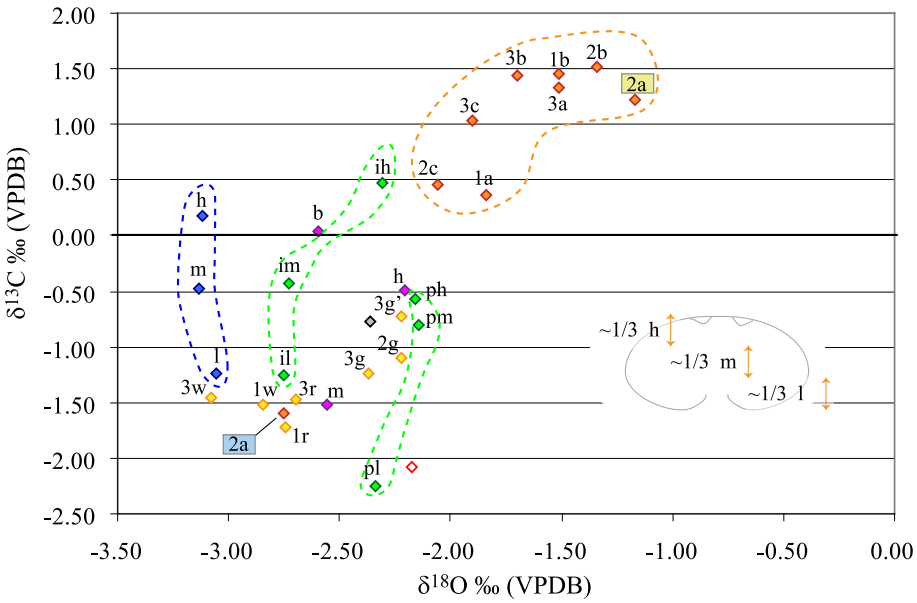

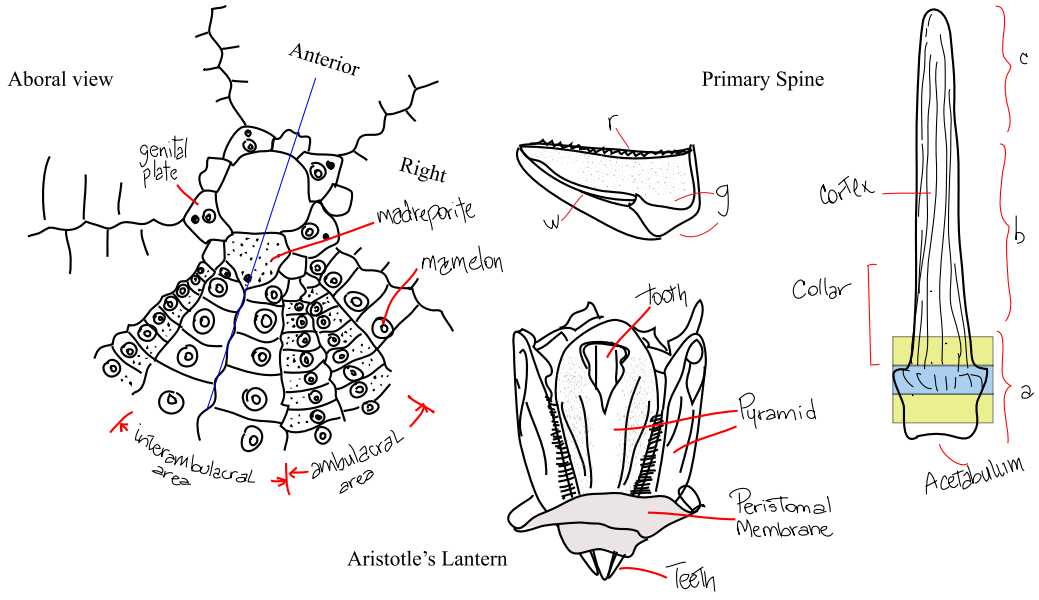

Sampling scheme and detailed isotope results for the echinoids sampled.

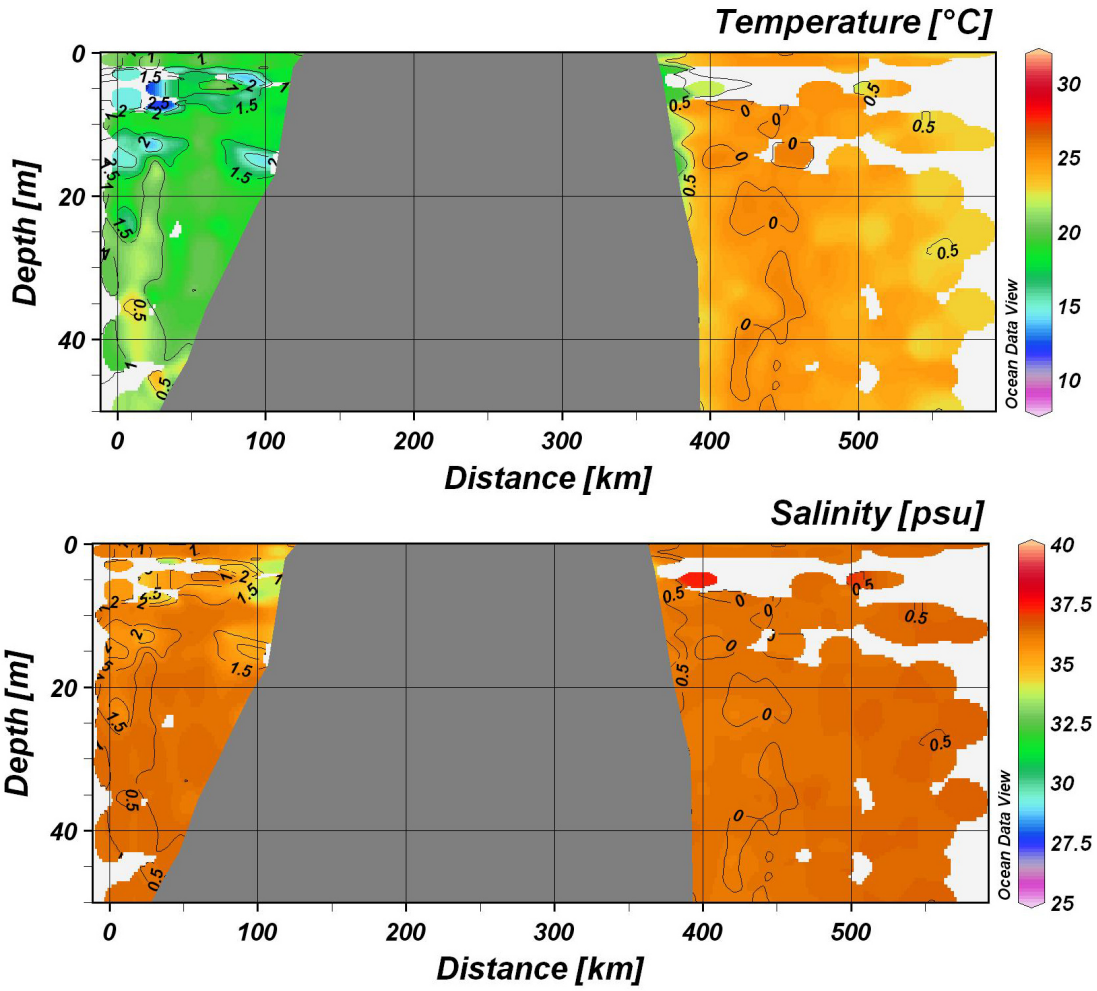

Zone 1 Average cross sections for winter months (DJF). Color maps to the right correspond to temperature and salinity, respectively. Contours are aragonite $\delta^{18}O$ values in both sections.

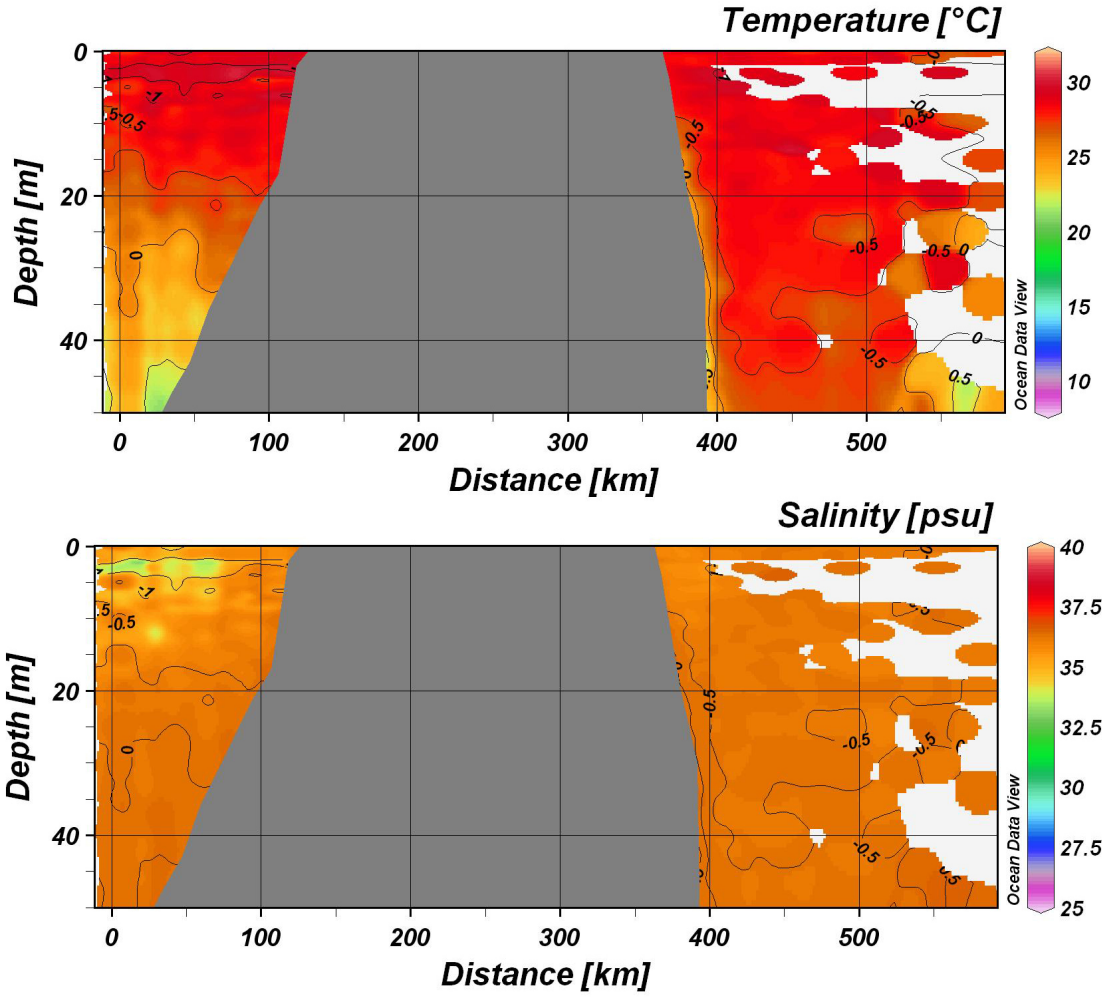

Zone 1 Average cross sections for summer months (JJA). Color maps to the right correspond to temperature and salinity, respectively. Contours are aragonite $\delta^{18}O$ values in both sections.

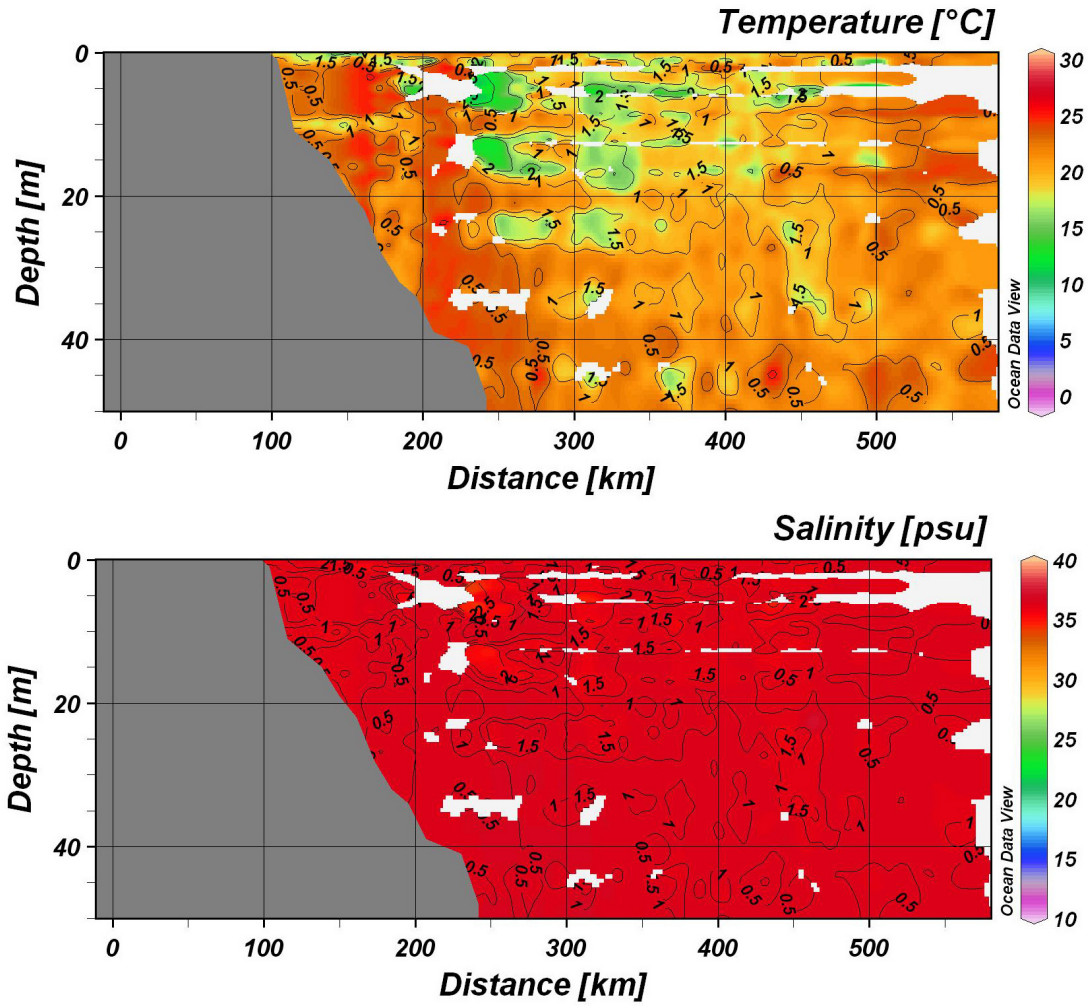

Zone 2 Average cross sections for winter months (DJF). Color maps to the right correspond to temperature and salinity, respectively. Contours are aragonite $\delta^{18}O$ values in both sections.

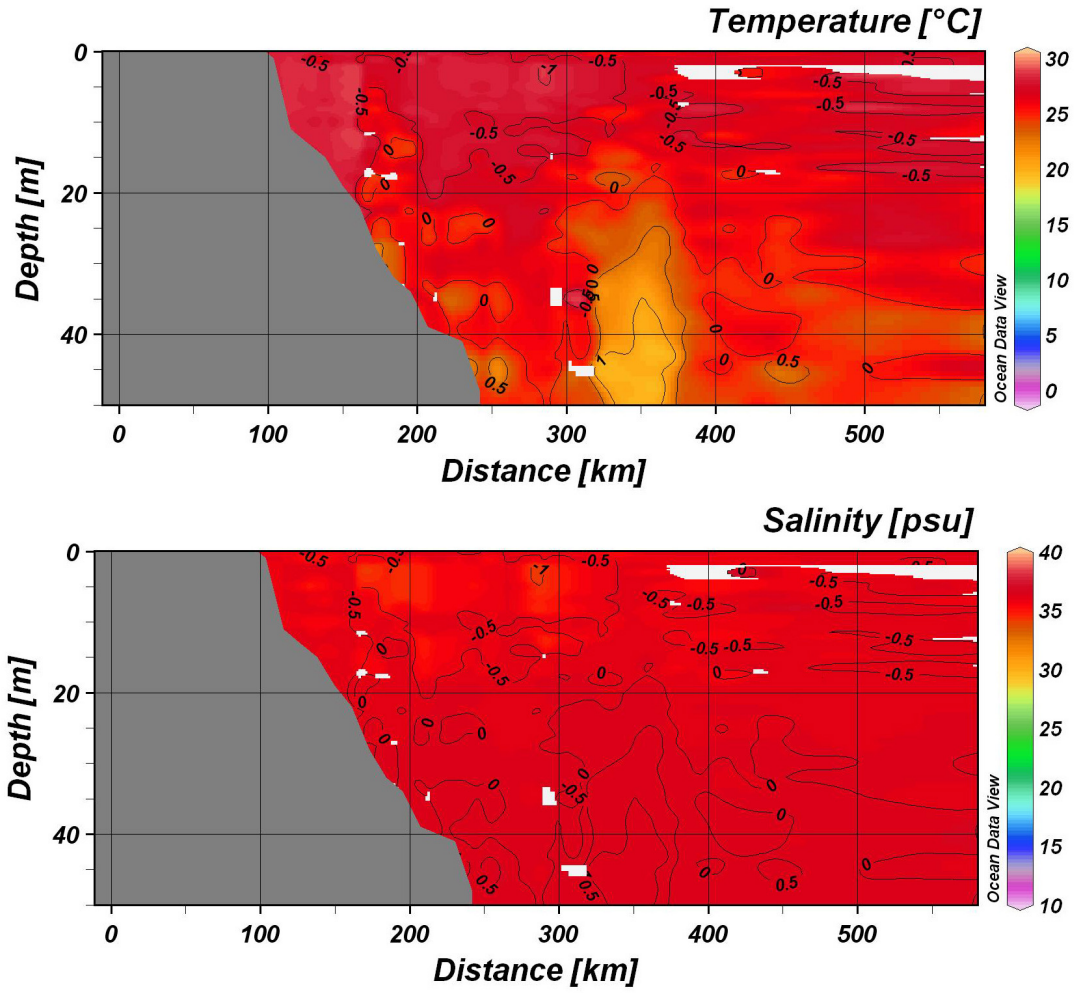

Zone 2 Average cross sections for summer months (JJA). Color maps to the right correspond to temperature and salinity, respectively. Contours are aragonite $\delta^{18}O$ values in both sections.

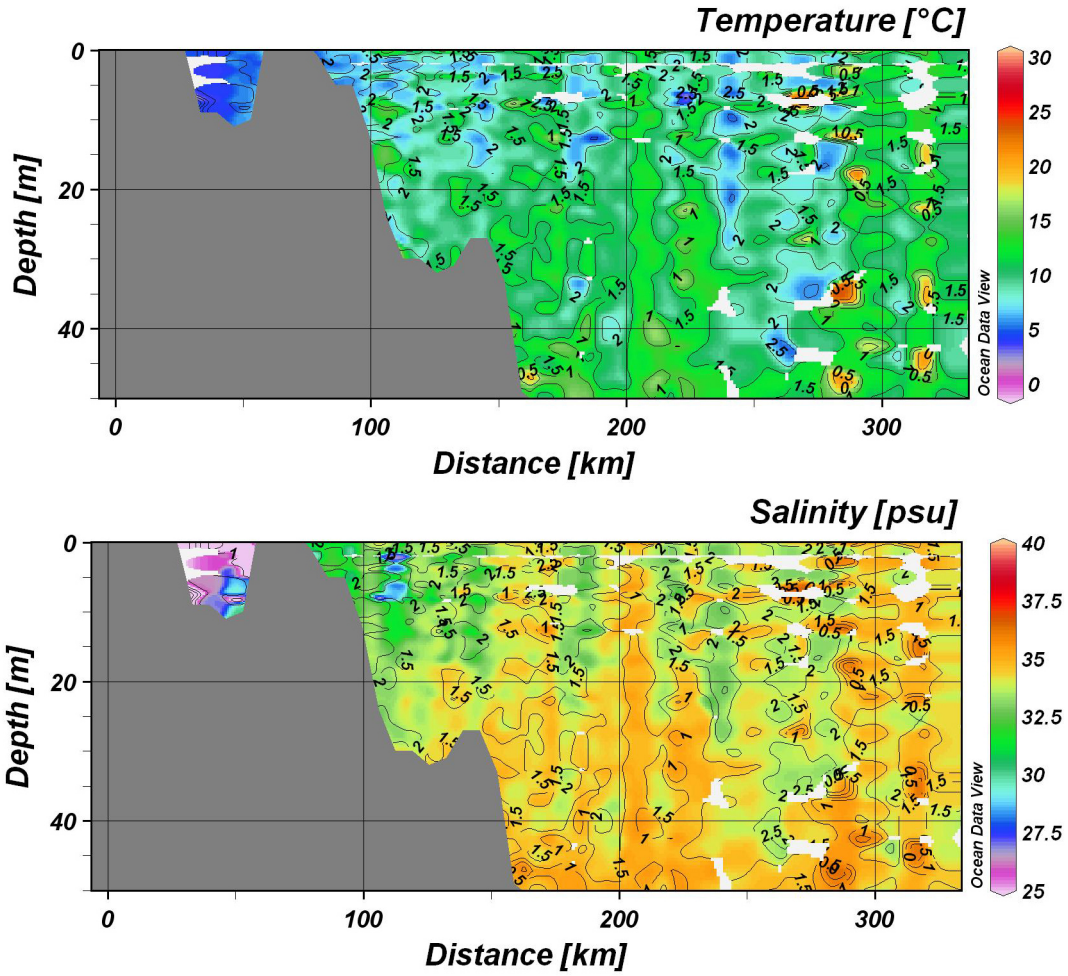

Zone 3 Average cross sections for winter months (DJF). Color maps to the right correspond to temperature and salinity, respectively. Contours are aragonite $\delta^{18}O$ values in both sections.

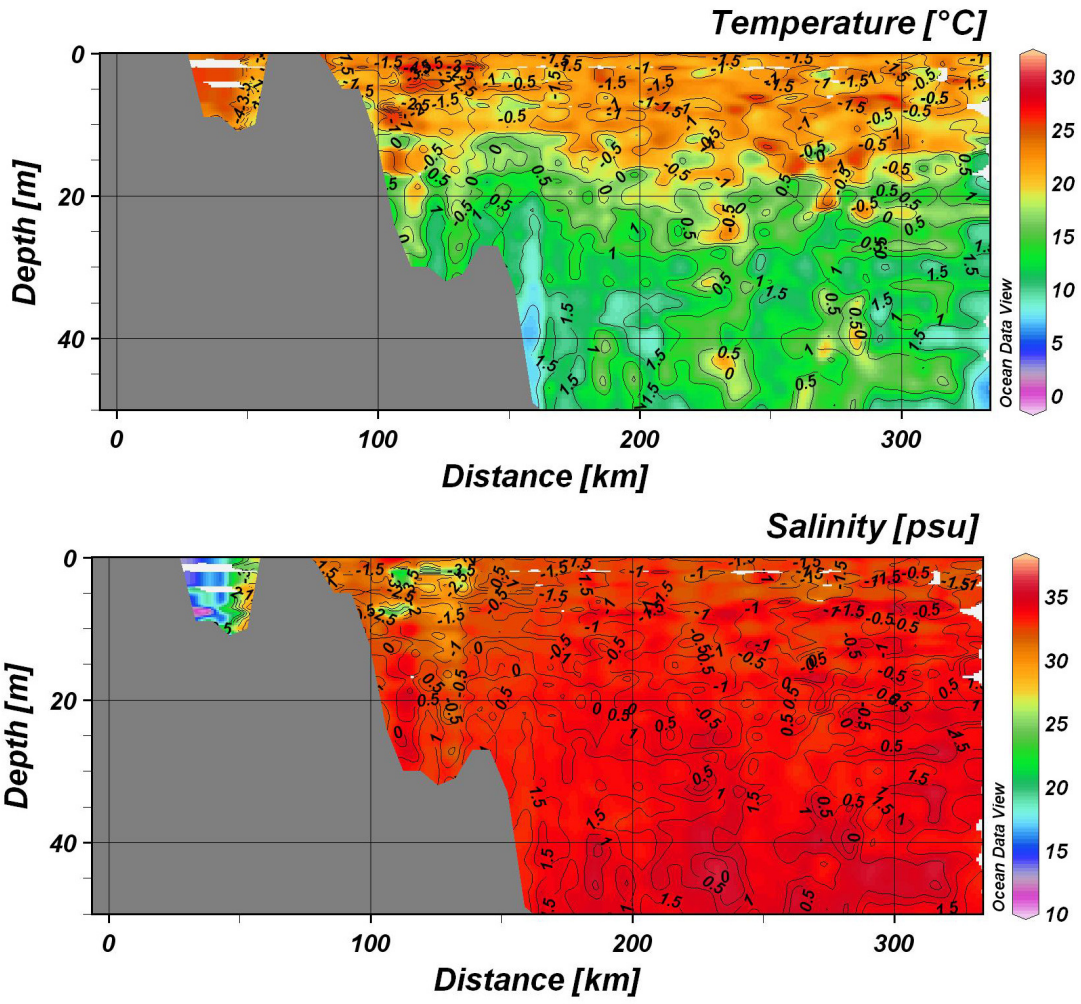

Zone 3 Average cross sections for summer months (JJA). Color maps to the right correspond to temperature and salinity, respectively. Contours are aragonite $\delta^{18}O$ values in both sections.

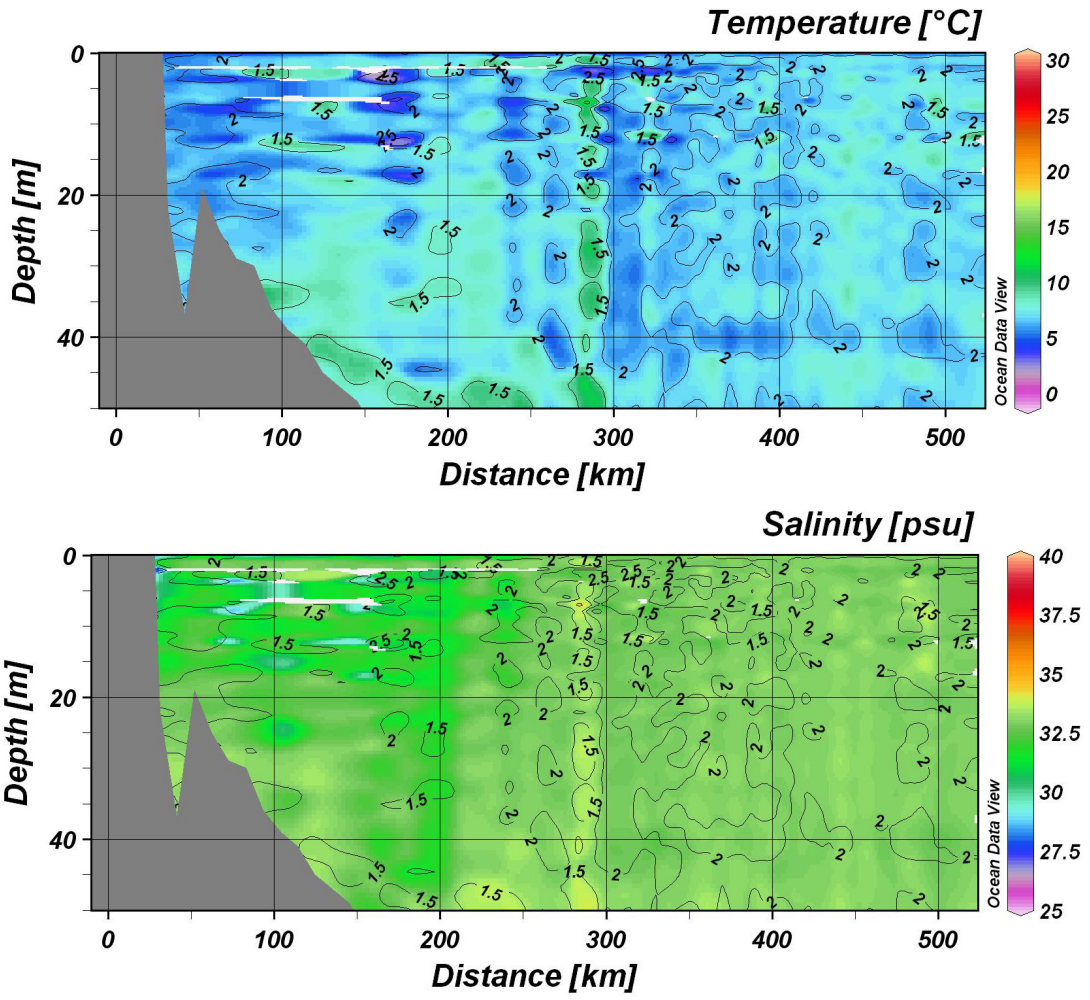

Zone 4 Average cross sections for winter months (DJF). Color maps to the right correspond to temperature and salinity, respectively. Contours are aragonite $\delta^{18}O$ values in both sections.

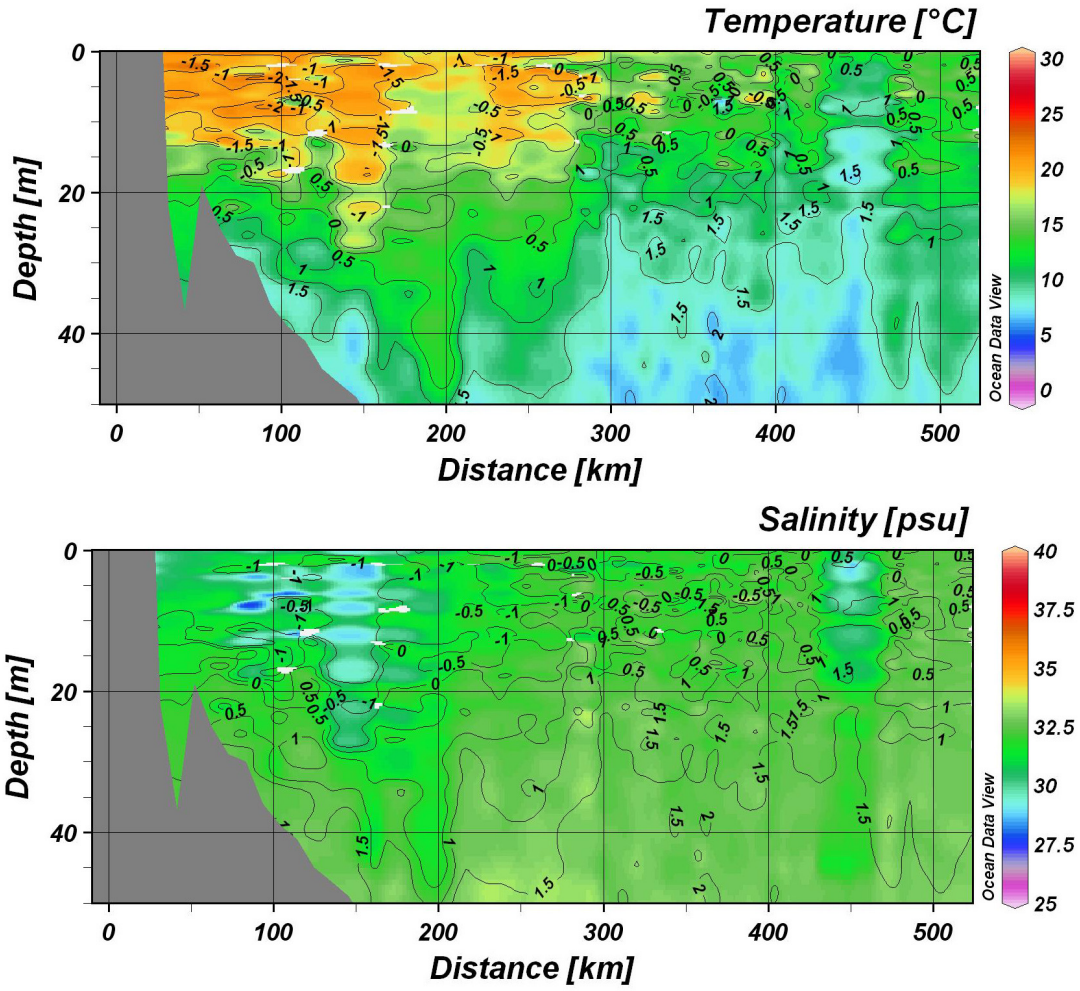

Zone 4 Average cross sections for summer months (JJA). Color maps to the right correspond to temperature and salinity, respectively. Contours are aragonite $\delta^{18}O$ values in both sections.